2014

Coordinating Stem Cell Behavior in the Hair Follicle

Chiung-Ying Chang

COORDINATING STEM CELL BEHAVIOR IN THE HAIR FOLLICLE

A Thesis Presented to the Faculty of

The Rockefeller University

in Partial Fulfillment of the Requirements for

the degree of Doctor of Philosophy

by

Chiung-Ying Chang

June 2014

COORDINATING STEM CELL BEHAVIOR IN THE HAIR FOLLICLE

Chiung-Ying Chang, Ph.D.
The Rockefeller University 2014

Tissue stem cells perform important functions throughout an organism's life. They generate new cells to replenish cells that are lost during normal wear and tear or in response to acute injury. Remarkably, hair follicles naturally undergo repetitive cycles of regeneration and degeneration, a process that is accomplished with the support of stem cells within the hair follicles. It is this feature that makes this miniorgan an attractive model system to study stem cell biology.

Interestingly, hair follicle is home to two distinct stem cell populations: epithelial hair follicle stem cells (HFSCs), which contribute to the formation of hair shafts, and melanocyte stem cells (McSCs), which contribute to hair pigmentation. During the hair cycle, HFSCs and McSCs work in harmony to generate a pigmented hair. However, little is known about the inter-stem-cell crosstalk governing this intricate coordination.

To identify candidate transcription factors that specify HFSCs in mouse, the gene expression profiles of the HFSCs residing in the bulge of hair follicles versus the epithelial basal cells outside the bulge were compared. One of the "molecular signature" genes being upregulated in the HFSCs is nuclear factor I/B (*Nfib*). Embryonic ablation of *Nfib* revealed that *Nfib* is required for the hair follicle morphogenesis and hair follicle-mediated re-epithelization during wound repair.

Meanwhile, to address the function of *Nfib* in established HFSCs, I conditionally induced *Nfib* ablation in the adult HFSCs. Interestingly, I found that the ablation of *Nfib* in the adult HFSCs did not perturb the HFSC maintenance, as the growth of hair follicles

and the hair cycle proceeded relatively normally. Instead, and even more unexpected, NFIB loss in the HFSCs promoted the proliferation and precocious differentiation of their nearby McSCs. These findings provide new insights into how McSC and HFSC behaviors maintain reliance upon cooperative factors within the hair follicle and how this might be uncoupled in injury, stress and disease states.

ACKNOWLEDGEMENTS

The past 5 years in graduate school for me has been a time of intellectual and personal growth that cannot be achieved without support from a lot of people. At first, I would like to express my special appreciation and thanks to my advisor, Elaine Fuchs. She has been encouraging, supportive, and generous with guidance and advices. She allowed me the freedom to try, to fail, and to explore my interests, while she was always available and made time to discuss with me when thoughts and inputs from her were needed. She sets a high standard for the practice of science that has inspired me and encouraged me to do so.

I am also grateful to be able to work in a great and exciting lab environment during graduate school that Elaine has created. I would like to thank all the past and present people in the Fuchs Lab who I have worked with. They were not just inspiring scientists but also fun to work with. In particular, I would like to thank Xuan Wang, who mentored me during my rotation, for helping me get started in the lab. I thank Ya-Chieh Hsu, Brice Keyes and Ting Chen for providing me very helpful inputs on my projects and, more importantly, for being supportive and good friends during graduate school. They were generous in sharing with me their personal philosophy that made me a better person. Daily conversions with them were so joyful and positive that always made me feel better when I got frustrated and felt lost in the lab. I thank Scott Williams for providing me a lot of constructs and helping me design lentiviral vectors for *in vivo Edn2* overexpression that was an important part of my work. I thank Hilda Amalia Pasolli for analyzing my samples and contributing exceptional electron microscopy images in my thesis. I thank Markus Schober, Irina Matos and Evan Heller for their kindness in keeping

the microscopes functioning smoothly and training me to handle microscope properly. I thank Peter Chi for showing me how to do sorting and helping me get familiar with the lab as we were working in the same bay. I thank Naoki Oshimori, Maria Genander and Wen-Hui Lien for sharing with me their unpublished transcriptional profiling data. My thesis was made possible by virtue of the contribution from Geraldine Guasch who initiated *Nfib* project in the lab.

In addition, I am grateful to all the staff in the lab, particularly Lisa Polak, Nicole Stokes, Dan Oristian and Angelie Aldeguer for managing my mouse lines, teaching me how to handle mice and providing me essential technical supports in skin grafting and lentiviral injection and many other experiments. I thank Ellen Wong for providing high-quality antibodies and being a great lunch mate. I thank Maria Nikolova for showing me how to culture keratinocytes and making this lab run efficiently. June Racelis was always very patient with me and showed me how to conduct *in situ* hybridization. I thank Peter Janki for being very supportive and a great friend, and Sophia Chai for assistance in lentivirus preparation.

I also would like to acknowledge the graduate program and all the staff at the Dean's Office of Rockefeller for supporting my studies. I thank my thesis committee members, Sandy Simon and C. David Allis, as well as my external examiner Alexandra Joyner for their suggestions, commitment of time, and help in preparing this thesis and for their supports in helping me move on to the next step. I also thank Leslie Vosshall for allowing me to do my first rotation in her lab to explore neuroscience and fly genetics.

The supports from resource centers at Rockefeller were indispensable in my works. In particular, I thank Svetlana Mazel, Lily Li, Stanka Semova, Selam Tadesse at

Flow Cytometry Resource Center for helping me isolating cells by FACS. I thank Scott Dewell at Genomics for assistance in high throughput DNA sequencing analysis. I thank Bio-Imaging center for assistance in confocal microscopes and thank Comparative Bioscience Center for husbandry care of mice. RNA-seq was conducted with support from Genomics Resources at Weill Cornell Medical College.

I thank collaborators Olivier Elemento and Jenny Giannopoulou for conducting bioinformatics analyses in my thesis. I am grateful to Richard Gronostajski for providing *Nfib* mice and Vincent Hearing for melanocyte antibodies.

Finally and most importantly, I am deeply indebted to my family for their support and encouragement, without which I would have not been able to complete my studies.

TABLE OF CONTENTS

Chapter 1: Introduction……..……1

Development of epidermis and hair follicles…….3

Hair cycle……...9

Hair follicle stem cells..……..10

Bulge hair follicle stem cells vs. hair germ cells..……12

Molecular regulation of hair follicle stem cell behavior……..13

Skin pigmentation……..16

Melanin synthesis…….…….…….…….…….…….…….……..18

The origin of melanocytes ……20

Molecular basis of melanocyte development…….25

A central mediator in melanocyte development: MITF……...….25

Wnt signaling……..…30

Kit signaling……..31

Edn signaling…….....34

Melanocyte stem cells in hair follicles……..….38

Activation of melanocyte stem cells……..39

Quiescence of melanocyte stem cells……41

Survival of melanocyte stem cells…….43

The coupling of epithelial-melanocyte stem cell behaviors…….45

Chapter 2: Characterization of NFIB's function during skin development……..48

Introduction……49

Results

NFIB is enriched in the bulge and the ORS of hair follicles……52

Loss of NFIB delays epidermal development……55

Loss of NFIB impedes hair follicle induction and morphogenesis……56

Hair follicle stem cell precursors cannot maintain SOX9 expression upon NFIB loss……..…64

NFIB acts downstream of NOG/BMP signaling……66

Discussion……..69

Materials and Methods……..……..73

Chapter 3: The role of nuclear factor I/B in coordinating epithelial-melanocyte stem cell behavior in the hair follicle…….……...……..78

Introduction…….……...……79

Results

*NFIB is expressed in hair follicle stem cells but not in melanocytes…..…*80

*Postnatal ablation of Nfib does not perturb hair cycle or follicle architecture…….……...*81

*NFIB loss disrupts the stem cell synchrony within the hair follicle..…….*86

*Premature transfer of pigment promotes apoptotic cell death of hair follicle stem cells in the NFIB-deficient hair follicles…...….....*93

*RNA-seq and ChIP-seq analyses identify endothelin 2 (Edn2) as a direct NFIB-regulated gene……..*97

*Up-regulation of Edn2 in skin induces hyperpigmentation……*110

Discussion……112

Materials and Methods……114

Chapter 4: Summary and Perspectives……126

The importance of stem cells in tissue morphogenesis..…..……128

Stem cell quiescence……..…..……132

Implications beyond the hair follicle……...137

References……...……182

LIST OF FIGURES

1-1. Architecture of mouse skin……..4
1-2. Illustration of neurulation……..……..5
1-3. Hair follicle morphogenesis and hair cycle. ……..……7
1-4. Melanosome maturation……..……...19
1-5. Molecular basis involved in melanocyte development…….……..27
1-6. Pigmentation in hair follicles…….…….46
2-1. NFIB is enriched in the ORS and the bulge of hair follicles…..…….54
2-2. Co-localization of NFIB with HFSC markers……...55
2-3. Epidermal stratification is delayed upon NFIB loss…..……57
2-4. Disruption of *Nfib* reduces hair follicle density during embryonic stage…….…..58
2-5. Loss of NFIB impedes hair follicle morphogenesis……...60
2-6. NFIB loss specifically in epidermal cells results in delayed hair coat formation…..61
2-7. Hair follicle morphogenesis is retarded upon NFIB loss …..……62
2-8. NFIB loss results in reduced transient-amplifying matrix population……...63
2-9. Expression of HFSC markers in *Nfib* cKO hair follicles…..……...65
2-10. NFIB is required for hair follicle-mediated re-epithelization upon wounding…..…67
2-11. NFIB level is regulated by NOG/BMP signaling…..……68
3-1. NFIB is not expressed in melanocytes…..……82
3-2. Two inducible-Cre lines used in this study to ablate *Nfib* in hair follicles…..……84
3-3. Conditional *Nfib* targeting in HFSCs does not perturb hair growth and cycle. …….85
3-4. NFIB loss enhances McSC self-renewal and perturbs McSC activity……..,87
3-5. Ectopic differentiation of McSCs induced by NFIB loss occurs from late catagen...90
3-6. Schematic summary of melanocyte behavior upon NFIB loss…..…….92
3-7. Hyperpigmentation in the dermis of aged *Sox9-CreER*/*Nfib* cKO skin…..……..94
3-8. Ultrastructure of *Nfib* cKO hair follicles……...95
3-9. Apoptosis and proliferation of *Nfib* cKO HFSCs…..……96
3-10. Isolation of bulge and HG HFSCs from *K15-CrePGR*/*Nfib* cKO skins for RNA-seq analysis…..……...……98
3-11. Pathway analysis of RNA-seq results…..……..100
3-12. NFIB expression in mutants lacking major signaling pathways…..……...102

3-13. Immunoprecipitation with NFIB antibody…..……103
3-14. Genomic distributions of NFIB ChIP-seq peaks and motif analysis……..104
3-15. Identification of direct NFIB target genes in HFSCs…..……106
3-16. RNA-seq and ChIP-seq analyses identify *Edn2* as a direct NFIB-regulated gene……..……..107
3-17. Inhibition of Kit signaling reduces McSC differentiation upon NFIB loss……109
3-18. Up-regulation of *Edn2* induces hyperpigmentation in skin…..……111
3-19. Inhibition of Edn signaling reduces precocious melanocyte differentiation in *Nfib* cKO hair follicles……..……112
4-1. NFIX expression pattern in hair follicles…..……...131

LIST OF TABLES

2-1. *Nfib* enrichment in the hair follicle from microarray analyses……..50

3-1. Gene list from RNA-seq analysis of bulge/HG HFSCs from *K15-CrePGR/Nfib* cKO and heterozygous (WT) skins……...…140

3-2. Gene list from NFIB ChIP-seq analysis……...165

LIST OF ABBREVIATIONS

ChIP	Chromatin immunoprecipitation
cKO	Conditional knockout
DP	Dermal papilla
EdU	5-ethynyl-2'-deoxyuridine
EGFP	Enhanced green fluorescent protein
FACS	Fluorescence-activated cell sorting
HFSCs	Hair follicle stem cells
Het	Heterozygous
HG	Hair germ
IP	Immunoprecipitation
IRS	Inner root sheath
KO	Knockout
LRCs	Label-retaining cells
LV	Lentiviral vector
McSCs	Melanocytes stem cells
ORS	Outer root sheath
qPCR	Quantitative polymerase chain reaction
RFP	Red fluorescent protein
RNA-seq	RNA-sequencing
TA	Transit-amplifying
rtTA	Reverse tetracycline-controlled transactivator
r.t.	Room temperature
TRE	Tetracycline response element
WS	Waardenburg syndrome
WT	Wild type
YFP	Yellow Fluorescent Protein

Chapter 1:

Introduction

Stem cells perform important functions for living organisms throughout their lives. They are distinguished from other cell types by their self-renewing ability to retain stem cell identity, and capability to differentiate into tissue specific types of cells. Throughout an organisms' life, tissue stem cells can generate new cells to replenish cells that are lost during injury or normal wear and tear. Given their unique regenerative capacity, understanding the molecular basis of stem cell specification and maintenance offers new potentials for improving the treatment for diseases and wounds.

Hair is one of the defining characteristics of mammals. Hair is not only important for thermal regulation in animals, but also aids in sensing the environment, and with specific color patterns, can facilitate social interactions. Remarkably, the hair follicle, a structure cyclically generating a hair shaft, naturally undergoes repetitive regeneration and degeneration, a process that is accomplished with the support of stem cells within hair follicles. It is this feature and the synchrony of hair follicles in young mice that make this miniorgan a favorable model system to study stem cell biology. Interestingly, there are two populations of stem cells sharing a residence in hair follicles: hair follicle stem cells (HFSCs), which produce the progeny that form the follicular structure and hair shaft; and melanocyte stem cells (McSCs), which are responsible for generating the mature melanocytes that transfer pigment to hair shaft cells. They coordinate their activities during each hair cycle to grow pigmented hair.

In this chapter, I summarize recent studies of individual stem cell populations within hair follicles and discuss the importance of coordinating stem cell behaviors for tissue regeneration. Beginning with a description of the epithelium and hair follicle development, I focus on a historical summary of HFSC identification and the regulation

of HFSC characteristics. Then, I turn the focus to the melanocyte lineage, describing the origin of melanocytes, molecular basis of melanocyte development and recent studies of McSC regulation. Finally, I discuss how two stem cell populations synchronize their behaviors during the hair cycle.

Development of the epidermis and hair follicles

The outermost part of skin is called the epidermis, a stratified squamous epithelium, which provides a protective barrier against dehydration, scratches and environmental attacks such as pathogen infection. Underlying the epidermis is connective tissue dermis, which is separated from the epidermis by a basement membrane; underlying the dermis is the subcutis, which is composed of adipocytes for fat storage (Fig. 1-1a). Growing downward into the dermis and even the subcutis, specific areas of mammal epidermis also give rise to several appendages including sweat glands, hair follicles and their associated sebaceous glands (Fig. 1-1a). Notably, in contrast to human skin covered with very abundant sweat glands for thermoregulation, mouse and non-primate mammal skin have limited sweat glands and are dominated instead by the presence of hair follicles.

Developmentally, the epidermis is derived from ectoderm, which is formed during gastrulation. Further, the ectoderm is divided into three domains as a consequence of neural induction occurring around embryonic (E) 8.5 (Fig. 1-2a). During neurulation, central ectodermal tissue is thickened and becomes neural plate, which gives rise to brain and spinal cord of an organism. Lying next to the neural plate is neural plate border, which becomes neural crest, and non-neural ectoderm, which develops into the epidermis

(Chapter 3 in (Gilbert, 2010)).

The epidermis appears first as a single layer structure by E9.5. From E14.5, its thickness is expanded to become a four-layered stratified squamous epithelium, which is completed around E17.5 (Fig. 1-2b) (reviewed in (Blanpain and Fuchs, 2006)). As development proceeds, proliferative basal cells gradually weaken their adhesion to the basement membrane, exiting their residence and moving upward to further differentiate

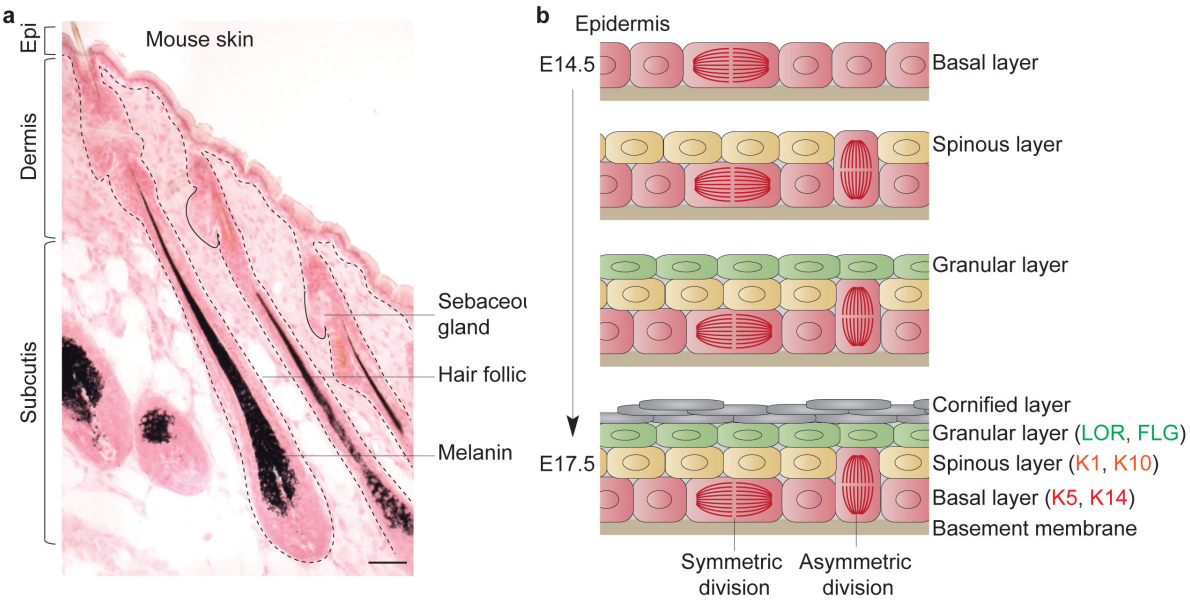

Figure 1-1. Architecture of mouse skin. a, Cross-section views of mouse dorsal skin. Mammalian skin consists of three major layers: the epidermis, the dermis and the subcutis. The epidermis gives rise to several appendages including hair follicles and their associated sebaceous glands. Melanins, present only in hair follicles of mouse dorsal skin, were detected by *Fontana-Masson* silver staining followed by Nuclear Fast Red. Scale bars: 25μm. **b,** Epidermal stratification. During skin development, the epidermis appears first as a single layer (basal layer), which resides on the basement membrane and cells in which divide symmetrically to support the expansion of skin surface. During epidermal stratification, about 70% of proliferative basal cells undergo asymmetric division to establish differentiated cell layers sequentially including the spinous layer, granular layer and cornified layer. Individual layer can be identified by the presence of specific proteins. After stratification, basal cells still constantly proliferate and supply new cells into differentiated layers to support long-term skin renewal and wound healing.

into suprabasal spinous cells and later granular cells. Interestingly, the stratification can also be achieved through asymmetric division, by which basal cells orient their mitotic plane of cell cleavage perpendicularly to the basement membrane and place one daughter cell in the upper layer (Lechler and Fuchs, 2005).

Along the path, epidermal cells (keratinocytes) switch their gene expression profiles to fulfill differentiation. Basal layer keratinocytes express two markers keratin 5 (*Krt5*; *K5*) and keratin 14 (*K14)*, and as they exit, they downregulate these keratins and express genes encoding keratin 1 (*K1*) and keratin 10 (*K10*). When this spinous layer

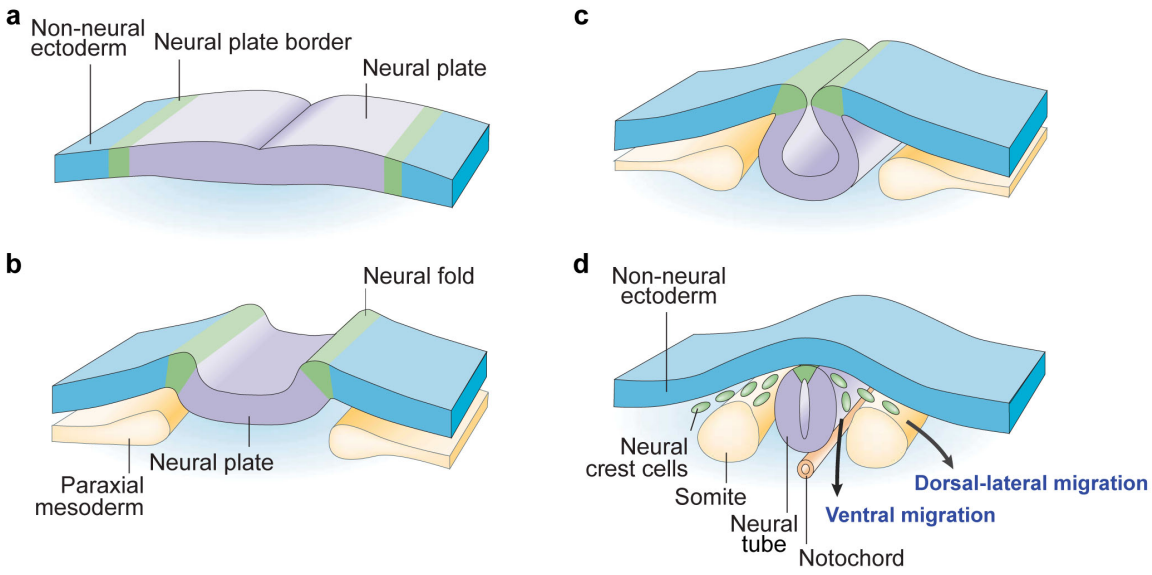

Figure 1-2. Illustration of neurulation. a, The ectoderm is divided into three domains during neurulation including neural plate (purple), neural plate border (green) and non-neural ectoderm (blue). **b-c,** Two sides of the neural plate borders (green) elevate and fuse with each other (neural fold), causing the neural plate to roll into a neural tube separated from non-neural ectoderm. **d,** Soon after, neural crest cells derived from neural plate borders delaminate from the neural tube, migrating either dorsal-laterally to become melanocytes or ventrally to differentiate into neurons, Schwann cells and many other cell types. Neural tube further gives rise to brain and spinal cord, and non-neural ectoderm further becomes the epidermis. Figures are modified from Gammill and Bronner-Fraser, 2003.

differentiates further, loricrin (*Lor*) and filaggrin (*Flg*) are induced as the granular layer forms (Fig. 1-2b). When granular cells terminally differentiate, transcriptional and metabolic activities cease, organelles are lost and cells die when they reach the cornified layer (or called stratum corneum). These dead squames are sacs of crosslinked proteins that are sealed by lipids at the skin surface to constitute a protective barrier. Throughout life, the dead keratinocytes in the cornified layer are constantly shed and replaced by new cells generated by basal cells from the bottom layer, which are epidermal stem cells. They stay undifferentiated during epidermal stratification and maintain their stemness in adult to accomplish the renewal of the skin surface.

Besides epidermis, embryonic epidermal cells also give rise to hair follicles and their associated sebaceous glands (Fig. 1-1a and 1-3a) (reviewed in (Paus et al., 1999)). The mouse hair coat consists of four different pelage hair types named guard, awl, auchene, and zigzag hairs, which are formed in consecutive waves during embryogenesis and completed by early postnatal life (Schlake, 2007). The hair follicles of primary or guard hairs appear first at E14.5, followed by secondary awl and auchene follicle induction at E16.5, and finally zigzag hair follicles at ~E18.5 (reviewed in (Schmidt-Ullrich and Paus, 2005)). Hair follicle induction depends on a series of reciprocal communications between the epithelium and underlying mesenchyme. At the beginning of the follicle formation, signals from dermal cells are thought to initiate epidermal invagination, generating a bud-like structure called hair placode (Fig. 1-3a) (Hardy, 1992).

Figure 1-3. Hair follicle morphogenesis and hair cycle. **a,** Hair follicle morphogenesis. Hair follicles are formed during embryonic stage. The reciprocal interactions between epidermal and dermal cells drive epidermal invagination to form a placode concomitant with the aggregation of dermal cells, called dermal condensate. Cells in the placode proliferate and the placode elongates to become a hair germ and subsequently a hair peg, which warps the dermal papilla (DP). Melanoblasts in the epidermis migrate into hair follicles. The DP acts as a signal center to induce the differentiation of melanoblast to become differentiated melanocytes (red) as well as the differentiation of transit-amplifying matrix cells to form differentiated hair layers including hair shaft, inner root sheath (IRS) and companion layer surrounded by outer root sheath (ORS). Keratinocytes in the upper region of hair germ/peg are $SOX9^{+}$ and stay undifferentiated as HFSC precursors, and melanoblasts there become melanocyte stem cells (McSCs; green). Around one week after birth, the formation of hair follicles is completed and hair shafts start coming out of skin surface. By P16, it enters the destructive phase (catagen), in which the lower portion of hair follicles is degenerated and the DP is dragged upward to stay attached to the base of degenerating hair follicles. **b,** Hair cycle. After catagen, hair follicles, which have two major regions including the bulge and the secondary hair germ (HG), go into the resting phase (telogen). When activated by signals from the DP in early anagen, $CD34^{+}$ bulge HFSCs and and HG cells proliferate to generate a new hair follicle. The old hair shaft in the bulge, called the club hair, might stay there or sometimes detach from the new hair follicle, the process called exogen. After 2-3 weeks of anagen, hair follicles enter catagen/telogen again. SG: sebaceous gland.

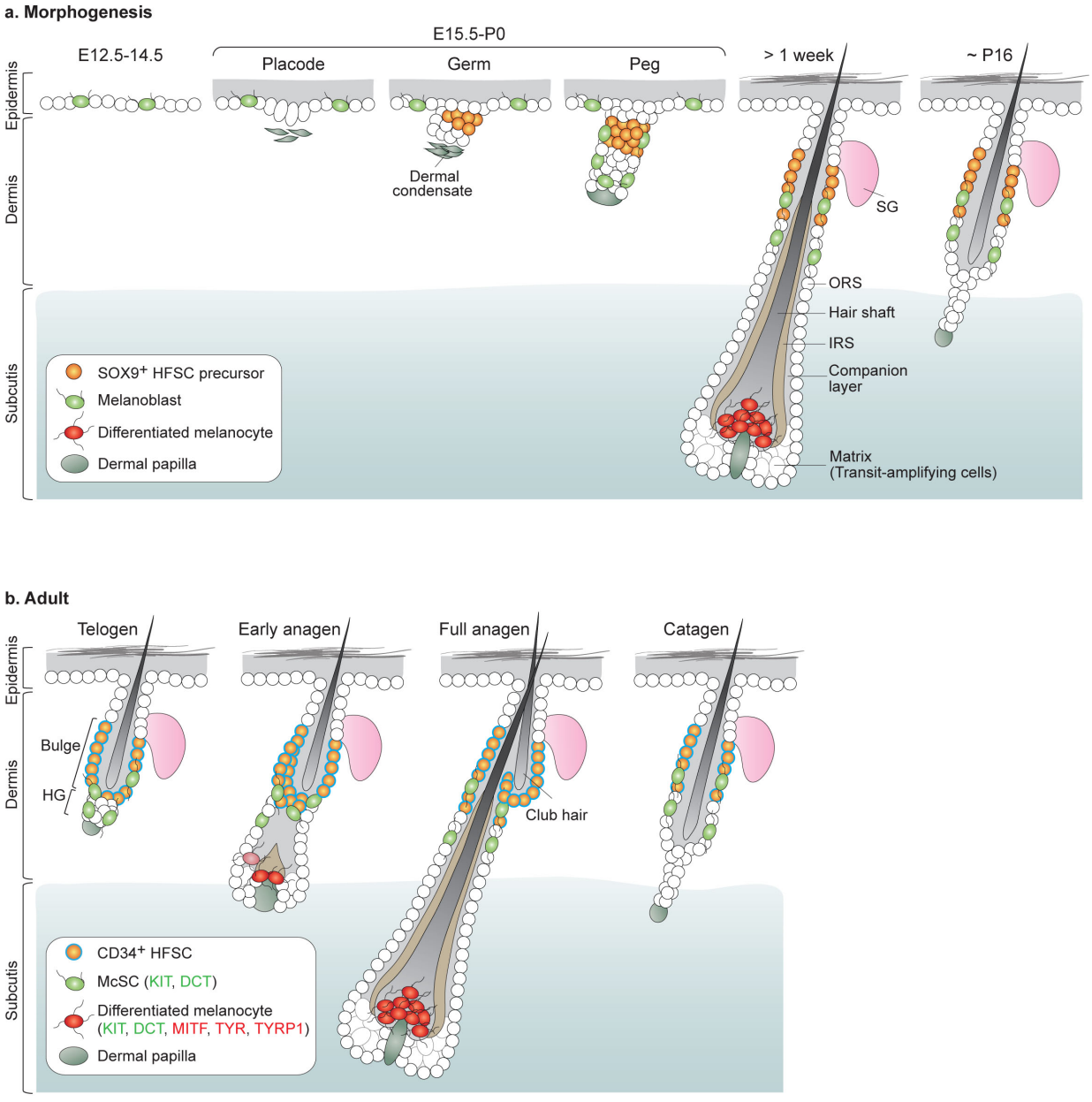
a. Morphogenesis
E12.5-14.5
E15.5-P0
Placode
Germ
Peg
> 1 week
~ P16
Epidermis
Dermis
Subcutis
Dermal condensate
SG
ORS
Hair shaft
IRS
Companion layer
Matrix (Transit-amplifying cells)
SOX9+ HFSC precursor
Melanoblast
Differentiated melanocyte
Dermal papilla
b. Adult
Telogen
Early anagen
Full anagen
Catagen
Bulge
HG
Club hair
CD34+ HFSC
McSC (KIT, DCT)
Differentiated melanocyte (KIT, DCT, MITF, TYR, TYRP1)
Dermal papilla

Soon thereafter, further signal interactions between the hair placode and a local aggregation of fibroblasts (dermal condensate) directly below guide the elongation of placode forming the hair germ. Regional variations in proliferation rate appear in the hair germ as it grows. Low-proliferative cells in the upper region of follicles become SOX9 positive and are specified as the precursors of hair follicle stem cells (HFSCs) (Nowak et al., 2008) (Fig. 1-3a). Conversely, cells in the high-proliferative region in the leading edge give rise to the hair matrix, which gradually wraps around the dermal condensate and then forms a mature dermal papilla (DP). The DP acts as a signal center to instruct nearby matrix cells to proliferate and further differentiate into a three-layered central hair shaft (cuticle, cortex, medulla), a three-layered inner root sheath (IRS; Henle, Huxley, cuticle) and a companion layer (Fig. 1-3a) (Hardy, 1992). The outer layer is called outer root sheath (ORS), which is contiguous with the basal layer of the epidermis and is surrounded externally by the basement membrane. Postnatally, hair follicles keep growing and reach maturation with maximal length around one week after birth, the time when the hair shaft starts extruding out of skin surface.

Hair cycle

Following morphogenesis, hair follicles undergo cyclic degeneration and regeneration throughout the life of the animal. There are four major phases in the hair cycle: the growth phase (anagen), the destructive phase (catagen), the resting phase (telogen) and the shedding phase (exogen) (reviewed in (Müller-Röver et al., 2001)) (Fig. 1-3b). As morphogenesis is completed, matrix cells remain proliferative to fuel the growth of hair shaft for another 7-9 days until ~postnatal (P) 16, when hair follicles enter

the destructive catagen phase. In catagen, the lower two-third or cycling portion of hair follicle rapidly degenerates in 2-3 days owing to the cells there undergoing apoptosis. At the same time, the DP is unwrapped from the matrix, dragged upward to keep attached with the surviving region of the hair follicle. Thus, the upper, permanent region of hair follicle survives through catagen and subsequently enters the dormant telogen phase, in which follicle cells remain mitotically quiescent until the beginning of next hair growth. In the following anagen, a new hair follicle is formed next to the original hair follicle, in which the old hair shaft (named club hair) sits in a silo-like structure separated from the anagen portion. Quite frequently, when the new hair follicle grows, club hairs shed off and the process is called exogen (Milner et al., 2002).

In mice, hair follicles rest in telogen for one to two days in the first hair cycle, while with additional hair cycles, they stay in telogen progressively longer, from weeks to months accompanied with more asynchronous activation pattern of hair follicles. Conversely, the duration of anagen is relatively consistent, which lasts 2-3 weeks resulting in the growth of 1cm-long hair in mouse. Thus, the periodic cycling of hair regeneration renews the mouse hair coat, implicating the existence of stem cells to fuel the regenerative process.

Hair follicle stem cells

Hair follicle stem cells (HFSCs) reside within a discrete microenvironment, which is the permanent, bulge structure of the hair follicle that remains after degeneration in catagen (Fig. 1-3b) (Cotsarelis et al., 1990; Tumbar et al., 2004). Specified during morphogenesis, the cells located in the upper ORS stay undifferentiated during hair

growth, and they escape from apoptosis in catagen, becoming HFSCs in adults (Nowak et al., 2008) (Fig. 1-3a). Throughout most of the resting phase of the hair cycle, they stay quiescence; while in response to activating signals released from the DP at the onset of anagen, HFSCs become proliferative to support hair growth. Notably, only in a rather short period of early anagen do they enter the cell cycle and perform a limited number of divisions (average ~3 times); nevertheless, they produce and supply sufficient number of new cells to the matrix, in which transit-amplifying or progenitor cells proliferate intensively throughout anagen to generate hair shaft and other differentiated layers within the follicles (Sotiropoulou et al., 2008; Waghmare et al., 2008; Zhang et al., 2009). Besides contributing to hair growth, HFSCs are multipotent and engaging in multiple lineages including sebaceous gland (Horsley et al., 2006; Oshima et al., 2001) and surface epidermis (Ito et al., 2005; Taylor et al., 2000a; Tumbar et al., 2004) when recruited to help in wound repair.

Given their slow cycling nature, HFSCs were first identified by nucleotide pulse-chase experiments. When radioactive thymidines were given to the mice (pulse), they were incorporated into DNA during cell division. Once labeled, cells in the bulge that cycle slowly retained the markers over an extended period of time (chase) and were identified as label-retaining cells (LRCs), which are distinguished from other rapidly-proliferating cells that constantly dilute out the label during cell division (Cotsarelis et al., 1990). Evidence from subsequent experiments using a second pulse of nucleotide analogue to trace bulge LRC fate revealed their ability to proliferate and contribute to follicle regeneration, a feature of stem cells (Taylor et al., 2000b). The hypothesis was further strengthened when new markers and methods were developed for the purification

and characterization of this population. Those included an *in vivo* pulse chase system coupled with doxycycline-inducible GFP-tagged histone labeling (*Tet-Off-H2B-GFP*) (Tumbar et al., 2004), *K15* promoter-mediated fluorescent protein expression in the bulge (Morris et al., 2004), and identification of antibodies recognizing bulge cell surface markers CD34 and α6-Integrin (Blanpain et al., 2004; Trempus et al., 2003). All these methods were compatible with fluorescence-activated cell sorting (FACS) for isolating bulge cells, making it possible to study the molecular basis specifying their unique features. In addition, the *Tet-Off-H2B-GFP* mouse carrying strong labeling signals permitted monitoring of the LRC behaviors. Besides forming new hair follicles, bulge LRCs also contribute to repairing the epidermis in response to wounding (Tumbar et al., 2004).

Bulge hair follicle stem cells vs. hair germ cells

There is a group of cells lying at the base of resting (telogen) hair follicle between the bulge and the signal center DP, The region is called the hair germ (HG), sometimes called secondary HG to distinguish from primary HG formed during morphogenesis (Fig. 1-3b). Monitoring the relationship of bulge HFSCs and HG cells reveals that HG cells, staying in closee proximity to the DP, act as the first responders to DP signals to fuel the initiating stage of hair growth, which is then further maintained by the activation of bulge stem cells as a second step of this process (Greco et al., 2009; Panteleyev et al., 2001). Like bulge stem cells, HG cells are quiescent throughout most of the resting phase of the hair cycle; during the transition from telogen to anagen, HG cells become proliferative while the timing of their activation is earlier than bulge HFSCs. *In vitro*, HG cells also proliferate sooner but surprisingly display a shorter-lived potential than bulge stem cells.

Molecularly, bulge HFSCs and HG cells can be separated by cell surface marker CD34, which is expressed in the bulge but not HG, while they also share the expression of genes that are essential for bulge HFSC function including *Lhx2*, *Sox9* and *Tcf3* {Greco:2009ik}.

Thus, it is tempting to speculate that the cells in the HG, a transient structure of the hair follicle, act as progenitors contributing quickly and largely to the transit amplifying pool of matrix cells that maintain contact with the DP in the mature hair follicle and that fuel the production of the hair shaft and its channel (IRS). By contrast, bulge HFSCs, which are activated later and are used more sparingly to extend the ORS, are thought to serve as long-term HFSCs (Rompolas et al., 2013), which not only sustains hair growth but also renew themselves to generate a new bulge and HG during each hair cycle (Hsu et al., 2011a).

Molecular regulation of hair follicle stem cell behavior

Stem cell activation relies on a series of activating signals counterbalancing inhibitory cues from the niche. In the long period of rest in telogen, high levels of bone morphogenetic protein (BMP) signals are critical for maintaining HFSCs in a quiescent state. When activated upon ligand binding, BMP receptors induce phosphorylation of mediators SMAD1, 5 and 8 (pSMAD1/5/8), which are recognized as the sign of BMP activation. Further, pSMAD1/5/8 forms a complex with their partner SMAD4 and translocate to the nucleus, where they act as transcription factors to modulate gene expression (reviewed in (Shi and Massagué, 2003)). During telogen, bulge and HG cells display nuclear pSMAD1/5/8 signals (Andl et al., 2004; Zhang et al., 2006), which is

accompanied by the upregulation of their targets inhibitor of DNA binding (*Id*) genes revealed in HFSC transcriptional profiles (Morris et al., 2004; Tumbar et al., 2004). Consistent with the notion that BMP activation promotes quiescence, *BMP receptor*-deficient hair follicles fail to stay in telogen because mutant HFSCs lose dormancy and begin to proliferate rapidly (Kobielak et al., 2007; Zhang et al., 2006). Complicating the phenotype, these abnormally activated stem cells, however, cannot generate a proper follicular structure. They are further blocked in terminal differentiation stages, suggesting that BMP signaling has additional roles in hair shaft differentiation of the normal hair matrix (Andl et al., 2004; Kobielak et al., 2003; Kulessa et al., 2000).

By the transition of telogen to anagen, while there are still abundant BMP ligands coming from numerous sources within the bulge and also exterior dermal environment (Blanpain et al., 2004; Hsu et al., 2011a; Plikus et al., 2008; Zhang et al., 2006), the DP lying beneath the HG augments the secretion of antagonist noggin (NOG), which overrides BMP's ability of inhibiting HFSC activation to induce hair growth. (Botchkarev et al., 2001; Kulessa et al., 2000; Zhang et al., 2006). In concert with BMP inhibition at the onset of anagen, upregulated within the DP are several other activating cues including FGF7 (Greco et al., 2009) and TGF-β factors (Oshimori and Fuchs, 2012), accompanied with the activation of Wnt signaling in the HG (Celso et al., 2004; Greco et al., 2009; Lowry et al., 2005; Rendl et al., 2005; Van Mater et al., 2003).

Following a two-step model for HFSC activation, the first responders to receive and react to those positive regulators are HG cells, which drive the initiation of hair growth. Soon after, bulge stem cells are activated to further sustain the hair growth (Greco et al., 2009). This raises an interesting question: what signals activate bulge

HFSCs that stay one-step away from the DP? It is still an open question in regard to the direct activating signals acting on the bulge stem cells. Possibly, bulge stem cells also respond to the DP signals yet in a rather distant manner than HG cells. It has also been proposed that in a paracrine fashion, DP-activated HG cells further pass down secondary activating cues back to the bulge as factors such as sonic hedgehog (*Shh*) appear when the HG is active and enlarged to become the matrix (Jaks et al., 2008; Panteleyev et al., 2001; Xiong et al., 2013). It is also possible that besides the DP, HFSC activation relies on other uncharacterized niche components surrounding hair follicles such as the dermis and subcutis (Festa et al., 2011; Plikus et al., 2008).

Within the nucleus, several transcription factors have also been found to be involved in bulge regulation. For instance, NFATc1, which is enriched in telogen bulge, is required for maintaining HFSC quiescence (Horsley et al., 2008). Following BMP inhibition, *Nfatc1* is down regulated during the onset of anagen, suggesting its inhibitory role in HFSC activation. Loss of function studies supported the notion, since hair follicles losing *Nfatc1* are not able to stay in telogen, owing to the ectopic expression of positive cell cycle regulator *Cdk4*. Meanwhile, *Lhx2*-deficient hair follicles also lose quiescence and constantly re-enter the hair cycle (Folgueras et al., 2013; Rhee et al., 2006). Surprisingly however, and in contrast to *Nfatc1* loss, *Lhx2* loss results in HFSCs differentiating to become sebocytes. Additionally, although many HFSC transcription factors and other signature genes have been identified through the development of new purification methods and high-throughput sequencing techniques (Lien et al., 2011), the functions of most of these genes are still uncharacterized, and the links between extracellular signals and intrinsic factors also await to be uncovered.

Skin pigmentation

Animal skins also display diverse color patterns and the coloration plays an essential role in the basic pursuits of life including survival and reproduction. For instance, some animals use cryptic colors and patterns to escape predators by blending into particular natural background (camouflage), while some animals defend themselves by displaying very bright coloration as warning signals. On the other hand, some animals use coloration to increase mating success by exhibiting attractive patterns to gain potential mates' attentions. For humans, pigments not only contribute to skin coloration, but also provide protection against UV-induced DNA damage. As skin is directly exposed to high levels of sunlight, melanin can absorb UV or neutralize UV-induced reactive oxygen species (ROS), preventing the accumulation of DNA mutations in skin cells and reducing the incidence of skin cancers.

Interestingly, different cell types are involved in generating pigments in different species. In *Drosophila melanogaster*, epithelial cells are responsible for producing pigments and creating pigmented cuticles in a cell-autonomous manner. In vertebrates, more specialized cells are used to produce pigments. In cold-blooded animals such as fish and amphibians, chromatophores can generate colorful pigments and they can further change body patterns rapidly by aggregating or dispersing pigments within them.

Mammalian skins have chromatophore-like cells called melanocytes. Notably, different from cold-blooded animals, pigmentation in mammals is determined in a rather non-cell-autonomous way, in which melanocytes tightly interact with epidermal cells. In human, melanocytes reside in the basal layer of epidermis and intermingle with keratinocytes, where they produce pigments and transfer them to nearby keratinocytes to

impart color to the epidermis (Fig. 1-1b). In both human and mouse, melanocytes also reside in the bulb of mature hair follicles and work in harmony with matrix cells to transfer pigment to the differentiating hair cells (Fig. 1-1a). Interestingly, the number of melanocytes in human skin types is relatively constant in such a way that one melanocyte interacts with approximately 36 keratinocytes to form an epidermal-melanin unit (Fitzpatrick and Breathnach, 1963). Thus, color heterogeneity between different ethnic groups or even between different regions of skin from the same individual largely originates from varied pigment-producing activities of individual melanocytes (reviewed in Costin and Hearing, 2007). In response to stimuli such as UV, melanocytes increase pigment production, which is mediated by the activation of α-melanocyte-stimulating hormone (α-MSH)-induced cAMP/CREB pathway in melanocytes (Cui et al., 2007; D'Orazio et al., 2006).

Surprisingly, melanocyte distributions are distinct in different parts of the skin. For instance, in the dorsal skin or most of the hairy regions of the mouse, melanocytes are present in hair follicles and are absent in surface epidermis. By contrast, melanocytes are in both compartments of non-hairy skin of ear and tail. Also, their territory is not limited to only one organ but they are also present in the eye, some internal organs and the inner ear (Colombo et al., 2011). Notably, eye pigmentation does not simply rely on melanocytes in uvea (pigmented layer of the eye). Retinal pigment epithelium (RPE) cells, which are specialized epithelial cells providing visual acuity, can also synthesize melanin to provide for photoprotection against UV-induced damage to the most bared region of our body.

Melanin synthesis

Melanins, the basic unit of pigmentation, are the polymerized derivatives of the amino acid tyrosine after a series of oxidation reactions (Hearing and Tsukamoto, 1991; Hearing, 2011). Classified by their structures, there are two major types of melanins including black/brown eumelanins and pheomelanins with yellow or red color. In general, most of hairs contain a mixture of melanins while the proportion of the two different melanins determine a wide spectrum of hair/skin colors.

In both melanocytes and eye RPE cells, melanins are synthesized in a specialized structure called melanosomes, which is a type of lysosome-related organelle with its contents derived from early endosomes (reviewed in Raposo and Marks, 2007). The process of melanosome formation and maturation can be divided into four stages according to their morphology and pigment density (Fig. 1-4). Melanosomes at the first two stages lack pigments but the structural component---premelanosome protein (PMEL), which is sorted into immature melanosomes to form scaffold fibrils completed by stage 2. Once the fibrous scaffolds are fully formed, melanin-synthesizing enzymes such as tyrosinase (TYR), tyrosinase-related protein1 (TYRP1) and dopachrome tautomerase (DCT or called TYRP2) are targeted to melanosomes, in which they convert tyrosine to melanin. Synthesized melanins are deposited onto the fibrils resulting in fibril thickening and darkening at stage 3; then, the fibrils become completely covered by melanins when melanosomes are mature at stage 4. In epidermal and hair follicle melanocytes, mature melanosomes are then delivered along microtubules to dendritic dips where they are transferred to surrounding keratinocytes, while RPE cells keep the melanosomes for themselves. The process of how melanocytes transfer melanosomes to keratinocytes is

unclear. Some hypotheses have been proposed that melanosome transfer could be mediated by exocytosis, cytophagocytosis, fusion and membrane vesicle transport (Yamaguchi and Hearing, 2009).

Besides ubiquitous components from late endosomes or lysosomes, melanosomes harbor numerous melanocyte-specific genes for enzymes and structural components, which when mutated cause albinism in humans or coat-color defect in animals (reviewed in Hirobe, 2011). For instance, *albino* mice have white hair coats owing to the mutations in *Tyr*, which encodes the most essential enzyme during pigment production; *Tyrp1* and *Dct* mutations result in brown and diluted hair coats. Meanwhile, color switches between dark and red/fair is controlled by signal peptide α-MSH, which binds to receptor MC1R

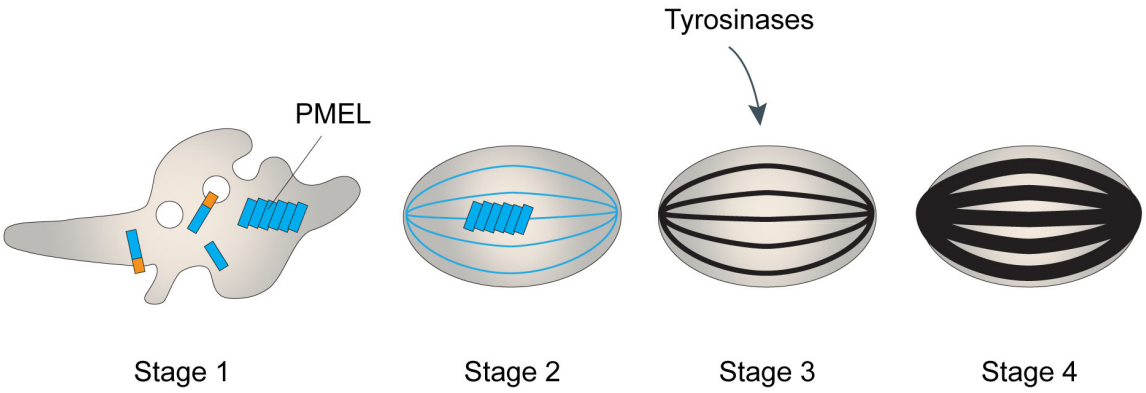

Figure 1-4. Melanosome maturation. Melanosomes (grey color) are derived from early endosomes accumulated with melanocyte-specific protein, PMEL. PMEL is a transmembrane protein, which is further cleaved by proprotein convertase in melanosomes (stage 1). As a result, the luminal fragment of PMEL dissociates from the membrane and forms melanosomal fibrils, completed in stage 2. As melanin-synthesizing enzymes such as tyrosinase and tyrosinase-related proteins are targeted to maturing melanosomes (stage 3), melanins are deposited onto the fibrils promoting the maturation of melanosomes (stage 4).

displayed on melanocyte cell surface (Burchill et al., 1989; Robbins et al., 1993; Valverde et al., 1995). Inducing cAMP/CREB pathway, α-MSH signals increase tyrosinase activity and its level to promote dark eumelanin production (Bertolotto et al., 1998; 1996; Price et al., 1998b). Notably, melanocytes with pigment-producing defects retain relatively normal morphology and are still present in skin and hair follicles, suggesting that melanin content is not essential for melanocyte development and maintenance.

The origin of melanocytes

Melanocytes are derivatives of neural crest cells, a population of multipotent cells that develop from ectoderm but are unique to the vertebrate embryo (Rawles, 1947) (Fig. 1-2d). A single neural crest cell can differentiate into any of several cell types, and the cell fate choice is dependent on its location in the embryo. The cranial neural crest gives rise to the majority of the bone and cartilage of the head and face, as well as to nerve ganglia, smooth muscle, connective tissue and melanocytes. The cardiac neural crest contributes to heart development by forming the aorticopulmonary septum and conotruncal cushions. The vagal and sacral neural crest becomes mainly enteric ganglia of the gut. The trunk neural crest cells give rise to neurons and glia of the peripheral nervous system, to secretory cells of adrenal medulla and to most of the melanocytes in skin.

In 1868, embryologist Wilhelm His first described the neural crest as a "*Zwischenstrang*," a band of particular material lying between the epidermis and the neural tube (Hörstadius, 1950) (Fig. 1-2d). In the early phase of neural development, the

ectoderm is specified by inductive signals and divided into three regions: non-neural ectoderm, which becomes the epidermis; neural plate, which forms the neural tube and further gives rise to central nervous system; and two border regions between non-neural ectoderm and neural plate, which are called the neural plate borders and are the origin of neural crest (Fig. 1-2a). In harmony with the folding of the neural plate during neurulation, the neural plate borders arise to form the neural folds, which further fuse with each other to become neural crest as part of the dorsal region of the neural tube lying beneath non-neural ectoderm (Fig.1-2b-d).

Complex signaling pathways and transcriptional networks are involved in the induction of the neural crest (Gammill and Bronner-Fraser, 2003; Knecht and Bronner-Fraser, 2002). Studies done in *Xenopus laevis* have revealed a model: the diffusion of BMPs (bone morphogenetic proteins) and their antagonists create a gradient of BMP activity across ectoderm, so that high BMP activity specifies non-neural ectoderm; low activity specifies neural plate; and intermediate signals specifies neural plate borders (Wilson and Hemmati-Brivanlou, 1997). However, BMPs alone are not sufficient to induce neural crest formation and segregate it from the neural and non-neural ectoderm. It requires further inputs as secondary signals from adjacent non-neural ectoderm or underlying mesoderm, including WNTs (García-Castro et al., 2002; Mayor et al., 1997), and FGFs (Fibroblast growth factors) (LaBonne and Bronner-Fraser, 1998; Mayor et al., 1997; Monsoro-Burq et al., 2003). Driving the neural crest induction, these extracellular signals further lead to transcription cascades within neural crest cells to upregulate specific transcription factors (Meulemans and Bronner-Fraser, 2004). Those factors include Slug/Snail (Nieto et al., 1994), FoxD3 (Dottori et al., 2001; Kos et al., 2001;

Sasai et al., 2001), Sox10 (Dutton et al., 2001), and Sox9 (Spokony et al., 2002), which specify neural crest cells and segregate them from the neural tube cells.

The neural crest is a transient structure. The cells in the neural crest have the potential to migrate and enter new locations to become tissue-specific cell types. Soon after the structure forms or even before the neural tube is closed fully by E8.5, neural crest cells detach from the neural tube through undergoing epithelial-mesenchymal transformation, the process that allows them to detach from neuroepithelium and migrate into the cell-free space between the surface ectoderm, neural tube and somite (Fig. 1-2d) (Erickson and Weston, 1983; Serbedzija et al., 1990; Sternberg and Kimber, 1986b; 1986a). On the migration trajectory, neural crest cells are exposed to a variety of instructive signals that guide them to adopt specific cell fates. For instance, migratory neural crest cells in the trunk region either enter a dorsal-lateral migration pathway to become melanocytes, or migrate ventrally to become neurons, glial Schwann cells and other cell types.

In addition to inducing neural crest formation, the transcription factor FOXD3 was found to play a critical role in migration of neural crest cells (Kos et al., 2001). Expressed in undifferentiated early migratory neural crest cells as a neural crest specifier, *FoxD3* is later down regulated in melanocyte precursors (melanoblasts) as they go into the dorsal-lateral pathway, while its level remains high in cells entering the ventral pathway. Loss- and gain-of-function studies have further revealed its function in lineage specification: down-regulation of *FoxD3* in nascent neural crest cells promotes the expansion of melanocyte lineage at the expense of neural/glial lineages; conversely, neural crest cells with ectopic *FoxD3* lose the freedom and only follow the ventral

pathway. Probing deeper into the mechanism, further studies have showed that FOXD3 represses the melanocyte lineage at least partly through inhibiting the expression of *Mitf*, which encodes a master transcription factor in melanogenesis (Thomas and Erickson, 2009).

The final destination for most of dorsal-lateral migrating melanoblasts is skin. Entering the skin dermis from E11.5, melanoblasts further migrate upward to cross the basement membrane and penetrate into epidermis by E12.5 (Fig. 1-3a). As the epidermis starts invaginating to form hair follicles around E15.5, melanoblasts in the epidermis gradually migrate toward the hair follicles where they complete maturation to become pigment-producing melanocytes. While most of melanoblasts still linger in the epidermis of mouse at birth, the number of epidermal melanoblasts significantly decreases postnatally by P4 (Hirobe, 1984). In adult mice, melanocytes are rarely seen in the epidermis and are only seen in hair follicles of dorsal/hairy skin. However, it is still not clear what the signals are that attract melanoblasts to migrate from the epidermis into the hair follicles. The existence of attractive signals from developing hair follicles has been proposed since 1947 and is evident by transplantation experiments (Rawles, 1947). When a part of mouse neural crest was transplanted into chick peritoneum, melanocytes scattered randomly if the hair follicles were absent in the graft. Comparatively, melanocytes can find their way to hair follicles and were observed chiefly in follicles when they were simultaneously developing in the graft, although the development of melanocyte and hair follicle seems to go on separately and independently.

Although it has been widely accepted that melanocytes are derived from the neural crest cells migrating in the dorsal-lateral pathway during development, recent

studies have showed unexpectedly that Schwann cells associated with the nerves are another source of melanocytes (Adameyko et al., 2009). As some neural crest cells in the ventral pathway become Schwann cell precursors during development, Schwann cell precursors can differentiate not only into mature Schwann cells but also into melanocytes. Lineage-tracing experiments showed that Schwann cell precursors migrate along the extending nerves, at the end of the nerves that project toward the skin. Some of the Schwann cells detach from the nerves, populate the cutaneous area, and contribute to a substantial number of melanocytes in hair follicles.

Interestingly, myelinating Schwann cells in adult skin still maintain the potential to differentiate into melanocytes when they lose contact with the nerves (Adameyko et al., 2009), although the mechanism is unclear if mature Schwann cells directly trans-differentiate into melanocytes or undergo de-differentiation process back to neural crest cell-like state. Also, it is not clear how the fate choices in Schwann cells are controlled. Although nerve-derived neuregulin 1 can promote Schwann cell precursor adopting glial fate and IGF1/PDGF produced by Schwann cells act in opposing manner to favor melanocyte differentiation (Adameyko et al., 2009), it is unknown if similar mechanisms occur in adult after nerve damage. In addition, it is also not clear if the melanocytes from two different sources contribute equally to skin pigmentation, although some evidence points to melanoblasts in the dorsal-lateral pathway contributing little to adult skin melanocytes (around 5-10%) since their number decreases shortly after migration is initiated (Adameyko et al., 2009). Further elucidation about the relationship between melanocytes and glial cells is important and it might provide insights into the mechanism of abnormal pigmentation happening in conjunction with neurological disorders such as

neurofibromatosis and nerve sheath tumor.

Molecular basis of melanocyte development

Before genomics and the gene-targeting era, we learned the function of individual loci through analyzing the phenotypes of spontaneous or mutagen-induced mutants. As organisms lacking melanocytes are in general viable, mutations affecting pigmentation or hair coat color are easily noticed and isolated. So far in mouse, more than 350 loci have been associated with coloration (http://www.espcr.org/micemut/#cloned). Approximately half of the loci are cloned and analyzed at the molecular level, and a plethora of pigmentation enzymes, transcription factors and signaling pathways required for melanogenesis have been identified and mostly their functions are conserved between human and mouse.

A central mediator in melanocyte development: MITF

MITF is a master transcription factor in melanocytes that controls their development and pigment production (Levy et al., 2006). MITF is a basic-helix-loop-helix leucine zipper (bHLH-Zip) transcription factor belonging to Myc supergene family (Hodgkinson et al., 1993; Hughes et al., 1993). During melanocyte development, MITF is the earliest marker appearing in committed melanoblasts when they are on the migratory trajectory toward the skin around E10-11 (Nakayama et al., 1998; Opdecamp et al., 1997). In *Mitf*-null embryos, neural crest cells are not able to differentiate into melanoblasts judged by the absence of DCT^+ or KIT^+ cells, which instead appear subsequent to MITF appearance in WT embryos (Steel et al., 1992). Thus, loss of *Mitf*

results in white hair coat phenotype in conjunction with complete lack of melanocytes in mutant mice (Nakayama et al., 1998; Opdecamp et al., 1997). The importance of *Mitf* in melanocyte development was further highlighted by the study showing that ectopic expression of *Mitf* is sufficient to convert embryonic fibroblasts (NIH3T3 cells) into cells with characteristics of melanocytes (Tachibana et al., 1996), suggesting that MITF is a master transcription factor to specify melanocyte cell fate.

Many MITF target genes have been identified, revealing its function in controlling many aspects of melanocyte behaviors including differentiation, proliferation and survival (Fig. 1-5). Through binding to specific E-box elements (CACGTG or CATGTG) in their promoters, MITF controls melanin production by regulating the expression of three major melanin biosynthesis-required enzymes including TYR, TYRP1 and DCT (Hemesath et al., 1994; Lowings et al., 1992). Other melanosomal proteins such as PMEL17, MLANA (Du et al., 2003), OA1/GRP143 (Vetrini et al., 2004) are also shown to be transcriptionally regulated by MITF as well as differentiation-involved signaling proteins including MC1R (Adachi et al., 2000) and ENDRB (Sato-Jin et al., 2008). Therefore, the involvement of MITF in promoting melanosome formation places MITF as an important factor not only during development to facilitate pigment-free precursors to become fully functional pigment-producing melanocytes, but also in adult to increase melanocyte activity during sun-tanning (Cui et al., 2007; D'Orazio et al., 2006; Price et al., 1998b). Upon UV exposure, *Mitf* is upregulated in skin melanocytes leading to increased melanin production and skin hyperpigmentation.

Given that failure in upregulating differentiation genes cannot account for the complete lack of pigment cells in MITF-deficient mutants (Nakayama et al., 1998),

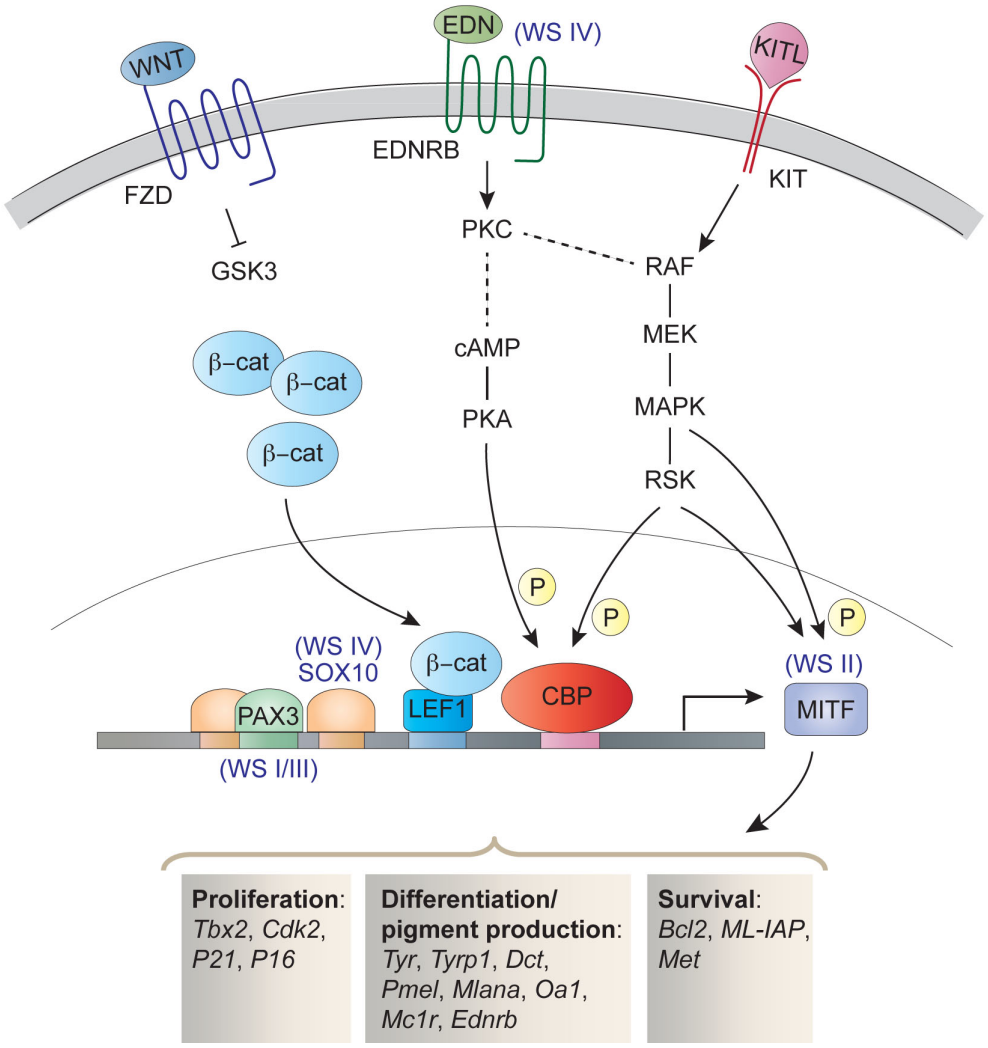

Figure 1-5. Molecular basis involved in melanocyte development. MITF is a master transcription factor of melanocyte development. It promotes melanocyte proliferation, differentiation and survival by modulating the expression of its target genes. Mutations in *Mitf* are associated with Waardenburg syndrome (WS) type II. The expression of *Mitf* is regulated by transcription factors SOX10 and PAX3, mutations in which cause WS type IV and I/III respectively. The promoter of *Mitf* also contains TCF/LEF1 binding sites, which are bound by LEF1/β-catenin complex when Wnt signaling is activated. In addition, Edn and Kit signaling can modulate the expression of *Mitf* by inducing the phosphorylation of transcription factor CREB-binding protein (CBP), which binds to CRE binding elements. The binding of endothelins (EDN) to endothelin receptor type B (EDNRB) activates protein kinase C (PKC), which activates CBP through cAMP-PKA pathway. Mutations in Edn ligands and receptors are associated with WS type IV. The binding of Kit ligands (KITL) to its receptor KIT induces MAPK pathway, which can not only modulate *Mitf* level transcriptionally through phosphorylating CBP but also regulate MITF protein function by directly phosphorylating MITF.

further studies had proposed its other functions in controlling melanocyte viability and cell-cycle progression. Other hints came from that fact that *Mitf* is an oncogene amplified in 10-20% cases of human melanoma (Garraway et al., 2005). Indeed, those MITF targets found to be regulating proliferation and survival of melanocytes are also regulating that of melanoma cells, which include genes encoding several cell-cycle regulators such as TBX2 (Carreira et al., 2000; Vance et al., 2005), CDK2 (Du et al., 2004), P21 (Carreira et al., 2005) and P16 (Loercher et al., 2005) and also survival regulators such as MET/HGFR (McGill et al., 2006), anti-apoptotic proteins ML-IAP (Dynek et al., 2008) and BCL2 (McGill et al., 2002). BCL2 is particularly interesting since *Bcl2*-null mice are born with normal hair color. Remarkably, one month later or during first hair molting, hair-graying phenotype appears due to progressive loss of melanocytes in hair follicles (Kamada et al., 1995; Mak et al., 2006; Nishimura, 2005). Thus, *Bcl2* is critical for the survival of postnatal melanocytes in the follicles especially the establishment of adult melanocyte stem cells, by which melanocytes are prevented from being depleted with age; nevertheless, the existence of other or redundant anti-apoptosis mechanisms during embryonic development are still unclear.

In human, *MITF* mutation causes Waardenburg syndrome (WS), specifically WS type IIA (Online Mendelian Inheritance in Man (OMIM) #193510). WS was described in 1951 by ophthalmologist Petrus Johannes Waardenburg when he noticed the coincidence of deafness and hypopigmentation abnormalities in many of his patients (Waardenburg, 1951). Thus far, four related syndromes displaying the core phenotypes including deafness and hypopigmentation of skin, hair and iris, have been classified and named WS type I-IV, and three of four subtypes cause the same defects as WS type II but also

accompanied with additional abnormalities in other tissues (Price and Fisher, 2001). Notably, similar defects are also seen in mice bearing mutations at *mi* locus (Hertwig, 1942; Moore, 1995). Thus, it had long been suggested that at least some forms of variants in human patients occur in the homologue of mouse *mi* (Asher and Friedman, 1990). Indeed, shortly after mouse *Mitf* gene was mapped in *mi* locus in 1993 (Hodgkinson et al., 1993; Hughes et al., 1993), mutations in human *Mitf* homologue was also found to be the cause in 20% of Waardenburg syndrome type II patients while genetic heterogeneity of the disorder has also been noticed (Tassabehji et al., 1994).

The identification of genetic variants in other subtypes of WS and the epistatic relationship between genes involved and *Mitf* have revealed a clear view of the regulatory network for melanocyte development and function. Mutations in *Pax3*, encoding a paired-homeobox-containing transcription factor, result in WS type I and III (Baldwin et al., 1994; Tassabehji et al., 1992; 1993); WS type IV is associated with mutation in SRY-box containing transcription factor *Sox10* (Pingault et al., 1998), endothelin receptor type B (*Ednrb*) (Attié et al., 1995; Puffenberger et al., 1994) or its ligand endothelin 3 (*Edn3*) (Edery et al., 1996).

Surprisingly, these genes all converge on *Mitf* (Fig. 1-5). *Pax3* and *Sox10*, which are also expressed in migratory neural-crest derivatives, bind directly to *Mitf* promoter and act in concert to activate *Mitf* expression in melanocytes (Bondurand et al., 2000; Lee et al., 2000; Potterf et al., 2000; Verastegui et al., 2000; Watanabe et al., 1998). Endothelin signals, which will be discussed in more detail in the following sections, can stabilize MITF protein through inducing its phosphorylation as well as control its level of transcription (Sato-Jin et al., 2008). Therefore, these connections could possibly account

for the phenotypic overlap seen in all subtypes of WS. Similarly, the dependence of *Mitf* activity on these genes are also observed in mouse genetics: mutations in any of these genes cause melanocyte development defects (Baynash et al., 1994; Epstein et al., 1991; Hosoda et al., 1994; Southard-Smith et al., 1998). Therefore, lying at the heart of regulatory network, *Mitf* is a center mediator that integrates extracellular signals into changes of gene expression required for melanocyte development and also their activity postnatally (Fig. 1-5).

Wnt signaling

During melanocyte development, canonical Wnt signaling plays an instructive role to direct neural crest cells to adopt a melanocyte cell fate. Triggered by receipt of Wnt ligands by transmembrane receptor Frizzleds, the activation of Wnt signaling inhibits its negative regulator GSK3 and stabilizes cytoplasmic β-catenin, which translocates into the nucleus to form a complex with LEF/TCF DNA-binding proteins leading to upregulation of Wnt target genes; whereas without Wnt stimulation, transcription factor TCF alone acts as a repressor inhibiting those targets (Logan and Nusse, 2004) (Fig. 1-5). Loss of β-catenin or two ligands Wnt1 and Wnt3a have a broad effect in reducing the number of neural crest derivatives in multiple lineages, suggesting that Wnt signaling is required for expansion of the neural crest cell population before a final fate specification occurs (Hari et al., 2002; Ikeya et al., 1997).

Apart from its function at the early stage of neural crest development, Wnt signaling, interestingly, in the following stages governs the choice of whether to become melanocytes or other neural crest cell derivatives. In zebrafish, manipulation of Wnt

activity in individual neural crest cells can switch their fates: carrying ectopic positive regulator β-catenin, neural crest cells with higher Wnt activity tend to become melanocytes; whereas Wnt-low cells with additional negative regulator TCF tend to become neurons or glia (Dorsky et al., 1998).

However, the story in the mouse system is more complicated and its preference regarding fate specification depends on timing. Before migration occurs, elevated Wnt/β-catenin signals in neural crest cells promotes the formation of neurons at the expense of other derivatives; during migration, in contrast, Wnt/β-catenin signaling later has opposite effect, inducing migratory neural crest cells to become melanocytes (Hari et al., 2012; Lee et al., 2004). Interestingly, the mechanism behind Wnt-promoted melanocyte cell fate converges on *Mitf,* whose promoter contains LEF/TCF binding sites essential for *Mitf* expression and its level depends on Wnt activity (Dorsky et al., 2000; Takeda et al., 2000) (Fig. 1-5). Therefore, Wnt signaling promotes melanocyte development at least partly through upregulating *Mitf* level, while its effect upon the fate decision of neural crest cells depends on timing and possibly other factors or cellular content.

Kit signaling

Once fate specification is determined, the survival and differentiation of melanocyte precursors or (melanoblasts) in the later stage of development requires Kit signaling. Activated by cytokine kit ligand (KITL), KIT is a transmembrane tyrosine kinase receptor, which transduces extracellular signals into the nucleus through inducing a phosphorylation cascade and ultimately altering the activity of transcription factors and

gene expression (Fig. 1-5). Mice carrying spontaneous mutations in *Kitl* (steel locus, *sl*) (Copeland et al., 1990) or its receptor *Kit* (white spotting locus, *w*) (Chabot et al., 1988; Geissler et al., 1988) have a white hair coat phenotype due to lack of melanocytes (Russell, 1979). Mutations in human *Kit* showed similar pigmentation defects, causing Piebaldism characterized by patches of white skin and hairs (Giebel and Spritz, 1991).

Digging into the mechanism of melanocyte loss upon Kit-signal deficiency, studies have found that it is essential for melanoblast survival but not required for lineage commitment, while the dependence oscillates in accordance with their proliferative activity. In *Kitl* or *Kit* mutants, the specification of melanocyte fate is unperturbed as migratory neural crest cells can become Dct^+ melanoblasts when leaving neural crest around E10.5; however, the number of Dct^+ melanoblasts greatly decreases in a very short time since their appearance (Cable et al., 1995; Mackenzie et al., 1997; Steel et al., 1992; Wehrle-Haller and Weston, 1995). By injecting KIT blocking antibodies to inhibit Kit signaling at different embryonic stages, Yoshida *et al*. found that KIT functions as a survival signal for proliferating melanoblasts, whereas dormant melanoblasts do not rely on Kit signals for survival (Yoshida et al., 1996). Thus, Kit signals are required for the melanoblast expansion that occurs before they enter the dermis and upon their arrival in the epidermis, while melanoblasts can be maintained in the environment without Kit signals once they migrate into the hair follicles or turn less proliferative.

Because early disappearance of melanoblasts in *Kit* mutant embryos makes it difficult to address its function in detail, gain-of-function and *in vitro* culture studies have provided more insights on Kit's role in melanocyte development. K14-driven overexpression of *Kitl* in epidermis induces hyperpigmentation in concert with largely

increased melanocyte number, more profoundly after E16.5 in the epidermis and also hair follicle (Kunisada et al., 1998a; 1998b). It suggests that Kit signals are sufficient to drive melanocyte proliferation and differentiation, and possibly also migration as ectopic melanocytes extend their territory into other areas such as mouth and paw skin. Consistently, addition of KITL into culture increases melanoblast number and facilitates their differentiation (Reid et al., 1995). Postnatally, Kit signaling also has similar functions in controlling melanocyte behavior to support them going through cyclical activation and inactivation during each hair cycle (Botchkareva et al., 2001; Nishikawa et al., 1991).

Behind the scene, Kit signals have been linked to MITF to induce its phosphorylation, which can have both positive and negative effects on MITF function depending on the duration of stimulation. KIT-mediated phosphorylation via MAPK pathway enhances a short-lived MITF transactivation as well as a net degradation of MITF protein mediated by proteasomes (Hemesath et al., 1998; Price et al., 1998a; Wu et al., 2000; Xu et al., 2000), while mRNA level of MITF has also been showed to increase upon KIT stimulus (Sato-Jin et al., 2008). Upon KITL binding, KIT receptors dimerize and can activate multiple downstream signal transduction cascades such as MAPK and PI3K. But melanocytes seem to favor the MAPK pathway, supported by the notion that blocking of Kit-mediated PI3K activation causes no effect on mouse pigmentation but on spermatogenesis (Blume-Jensen et al., 2000; Kissel et al., 2000). Since most of the studies were done in cultured melanocytes, it remains to be learned when and where MITF phosphorylations occur *in vivo* and whether they are mediated by the Kit-MAPK pathway.

Although the signaling connection is obscure, the genetic interactions between Kit signaling and MITF are evident (Hou et al., 2000). Given that in the condition without Kit signals MITF is not sufficient to drive the expression of tyrosinase, and double heterozygous mutants show much greater pigmentation defects than in either heterozygous alone, MITF and Kit signals are individually indispensible for melanocyte development and Kit signals act through MITF at least during a certain period of development.

Edn signaling

Endothelins (EDNs) are 21 amino-acid secreted peptides with three different isoforms including EDN1, EDN2 (containing two amino acids different from EDN1 sequence) and EDN3 (containing six amino acids different from EDN1 sequence) (reviewed in Sakurai et al., 1992). They are produced as ~200 amino acid long precursors called prepro-endothelins and are further processed to become mature forms by two proteases: first furin-like proteases and then endothelin-converting enzymes (ECEs). Two subtypes of endothelin receptors belonging to G-protein coupled receptor family have been identified including EDNRA, which prefers to bind EDN1 and EDN2, and EDNRB, which has equal affinity for all three EDNs.

After the isolation of the first endothelin or EDN1 from vascular endothelial cells as a vasopressor, endothelins later were found to exert a wide range of effects in many cell types including human melanocytes, in which endothelins especially EDN1 and EDN2 act as mitogens to stimulate their proliferation and pigment-producing activity (Yada et al., 1991). Physiologically, upon sun or UV exposure, epidermal keratinocytes

are the major source of secreted endothelins, which act on receptor EDNRB in neighboring melanocytes to induce skin hyperpigmentation (Imokawa et al., 1995; 1992). Genetically, Edn signals are required for melanocyte development. Mice carrying mutations in *Edn3* (*lethal spotting* locus) or its receptor *Ednrb* (*piebald lethal* locus) results in melanocyte loss associated with megacolon caused by the absence of the enteric ganglia (Baynash et al., 1994; Hosoda et al., 1994), the phenotypes that are also seen in WS type 4 patients with mutations in *EDNRB* human homologs (Attié et al., 1995; Edery et al., 1996; Hofstra et al., 1996; Puffenberger et al., 1994).

Similar to Kit pathway, Edn signaling is not required for melanocyte fate specification but for melanoblast proliferation, survival and differentiation. In *Ednrb* mutants, some if not all of DCT^{+} melanoblasts appear at the right time (between E10-E11.5); however, their number becomes reduced greatly, and soon after, none of melanocytes can be detected in the epidermis or hair follicles of white patches after E14.5, suggesting that Edn signal-negative melanoblasts cannot be maintained during development (Lee et al., 2003; Pavan and Tilghman, 1994). Carefully manipulating Edn signals in the melanocyte lineage reveals that proper pigmentation requires the input of Edn signals between E10-12.5, the period when melanoblasts are proliferating and migrating into epidermis (Shin et al., 1999).

In cultured melanocytes, Edn signals, mostly via protein kinase C (PKC), can regulate MITF both transcriptionally and post-translationally (Sato-Jin et al., 2008) (Fig. 1-5). Not only does EDN-mediated PKC activation trigger a quick reaction inducing MITF transactivation through MAPK-dependent protein phosphorylation, but it also exerts long-term increases of MITF amount by enhancing its transcription. The *Mitf*

promoter contains CRE binding elements bound by active transcription factor CBP, whose phosphorylation depends on biphasic induction of MAPK-RSK and cAMP-PKA pathways, in which MAPK takes action first followed by PKA activation. Again, though the signaling mechanisms underlying the connection between Edn pathway and MITF are evident *in vitro*, it still awaits to be uncovered whether similar relationship occurs *in vivo*.

As the phenotypes caused by loss of Edn pathway are similar to *Kit* mutants, the reminiscence of Kit function from Edn studies implies the potential interaction between them in melanocyte lineage. Indeed, studies in culture show that Edn and Kit pathways act synergistically to regulate melanoblast proliferation and differentiation (Aoki et al., 2005; Reid et al., 1996a). Simultaneous addition of EDN3 and KITL into culture dramatically increases melanoblast number to the extent greater than the addition of individual factors (Reid et al., 1996a), though individual factors also has significant effect in promoting melanoblast proliferation (Lahav et al., 1996; Opdecamp et al., 1998; Reid et al., 1995). In addition, melanoblasts can fully differentiate into pigmented cells in the presence of both factors, whereas adding either one of the factors is not sufficient to induce pigment production (Reid et al., 1996a). Molecularly, Edn and KIT can act in concert to rapidly induce MAPK-mediated signal transduction (Imokawa et al., 2000).

Notably, all isoforms of endothelins have a similar capability of facilitating melanoblast proliferation and differentiation *in vitro* by acting on receptor Ednrb (Opdecamp et al., 1998; Reid et al., 1996a). However, the requirement of *Edn1* and *2 in vivo* is unclear as no significant melanocyte-defects have been observed in individual mutants in contract to *Edn3*-null embryos (Chang et al., 2013; Kurihara et al., 1994; Reid et al., 1996b). It could be due to the presence of possible redundancy among endothelins

or non-essential roles of *Edn1* and *Edn2* in melanocyte development that is dominated by *Edn3*. In addition, because endothelin-deficient mutants die immediately (*Edn1*-null) or within one month (*Edn3*-null and *Edn2*-null) after birth, it's also unclear whether they play roles in controlling melanocyte behavior postnatally or in the adult.

Surprisingly, the functional similarity between Edn and KIT signals seen in a simplified *in vitro* system is not completely translated *in vivo*. Although both *Edn3* and *Kitl* upregulation in epidermis are sufficient to induce hyperpigmentation (Garcia et al., 2008), the areas with accumulated pigments in *Edn3* transgenice mice are different from what are seen in *Kitl* upregulated mice, which contain ectopic pigments in hair follicles and epidermis (Kunisada et al., 1998a; 1998b). Instead, in *K5-Edn3* transgenic mice, hyperpigmentation occurs mainly in the dermis surrounding hair follicles, while melanocyte numbers are increased in both epidermal and dermal compartments (Garcia et al., 2008). Notably, early embryonic induction of *Edn3* is required for initiating dermal pigmentation, as *Edn3* upregulation in late embryonic stage or after E10.5 is surprisingly not sufficient to cause the phenotype. But it is still unknown whether *Edn1* and *2* have similar potential to induce dermal hyperpigmentation, either during embryonic or adult stage. In addition, given that ectopic pigments are restrictedly present in the areas that normally contain melanocytes but not in regularly melanocyte-free skin such as oral cavity and paw pad, EDN3, unlike KITL, induces *in situ* hyperpigmentation but it does not act as an attractive signal inducing melanocyte migration. Thus, *in vivo*, melanocytes in different compartments respond to extracellular signals differently in such a way that dermal melanocytes are more responsive to Edn stimulus and epidermal-hair follicle melanocytes are more sensitive to Kit signals (Aoki et al., 2009).

Melanocyte stem cells in hair follicles

Coupled with hair growth and cycle in adults, melanogenesis in hair follicles also relies on cyclic activation and inactivation of stem cells called melanocyte stem cells (McSCs) (Nishimura et al., 2002). When epidermal melanoblasts migrate into the hair follicles during morphogenesis, some of them close to the dermal papilla (DP) undergo differentiation and become mature melanocytes, which upregulate MITF and the components of enzymatic machinery for melanosomes including TYR and TYRP1 to support melanin production and hair pigmentation; whereas, some of them colonizing next to the hair follicle stem cells (HFSCs) in the upper part of hair follicles, maintain an undifferentiated state and function as McCSs to support hair pigmentation long-term (Fig. 1-3a).

Thus, the hair follicle is home to two distinct stem cell populations: epithelial HFSCs, which contribute to hair growth, and McSCs, which contribute to hair pigmentation. Interestingly, they behave in concert such that both of them survive the destructive catagen phase, when differentiated melanocytes and hair cells undergo apoptosis; and both of them stay in quiescence during telogen (Fig. 1-3b). When anagen ensues, these two stem cell populations are coordinately activated to become proliferative, supplying new cells in the lower differentiating region of hair follicles, in which differentiated melanocytes produce and transfer pigments to adjacent HFSC progeny in the matrix as they stop proliferating and begin to differentiate into hair (Fig. 1-3b). Although no McCS-specific markers have been identified so far, they can be distinguished from mature melanocytes as being negative for differentiated markers including MITF, TYR and TYRP1 and positive for markers that are expressed in all

melanocytes such as KIT and DCT (Fig. 1-3b).

Understanding the molecular basis of McSC behavior and maintenance is important as loss of McSCs has been considered as the cause of hair greying (Commo et al., 2004; Nishimura, 2005). Either with age or under stress conditions, McSCs in hair follicles progressively lose their ability to self-renewal and undergo ectopic differentiation, which results in the depletion of melanocytes/pigments in the follicles (Inomata et al., 2009; Nishimura, 2005). Discussed in the following contents will be how intrinsic mechanisms and extrinsic signals from the niche modulate McSC activity.

Activation of melanocyte stem cells

Interestingly, several signaling pathways that are known to control melanocyte development have also been found to play critical roles in regulating adult McSC activity. For instance, Wnt signaling is required and sufficient to drive McSC proliferation and differentiation (Rabbani et al., 2011). At the start of a new hair cycle, McSCs next to the DP show signs of nuclear β-catenin, an indicator of activated canonical Wnt signaling; during follicle growth, Wnt-positive melanocytes move downward along with the matrix and become mature melanocytes. Manipulating Wnt signaling specifically in melanocytes by increasing or decreasing nuclear β-catenin level shows that Wnt-negative McSCs fail to proliferate and differentiate into mature melanocytes upon anagen initiation, whereas forced activation of Wnt signaling drives McSC differentiation ectopically within their residence (upper ORS), leading to hair greying due to progressive depletion of McSCs with time. In addition, Kit signals are also required for melanogenesis. Inhibition of the Kit pathway by injecting anti-KIT antibodies intradermally results in blockage of McSC

activation and differentiation, resulting in white hair coat phenotype (Botchkareva et al., 2001). Notably, in conditions lacking either signaling input, McSCs are still maintained with relatively normal number within hair follicles, suggesting that McSC survival and maintenance is independent on Wnt and Kit pathways.

While *in vitro* the MAPK cascade is thought to mediate Kit signal-induced melanocyte differentiation, *in vivo* they seem to have additional functions in regulating McSC self-renewal independent upon Kit. Melanocytes including both McSCs and mature melanocytes are normally formed during development in mice lacking Raf kinases (RAF), which are upstream activators of MAPK (Fig. 1-5); however, in agreement with the well-known implication of RAF-MAPK pathway in cell-cycle regulation, S-phase entry of *Raf*-deficient McSCs upon anagen start in adult mice is impaired, accompanied with a progressive decrease of McSC number and hair greying (Valluet et al., 2012). Owing to the fact that loss of RAFs does not have significant effects on McSC differentiation, in contrast to Kit deficiency, it is tempting to speculate that *in vivo* Kit-induce melanocyte differentiation is independent of MAPK cascade. Therefore, there are still several questions left to be answered: what are the environmental cues that activate the MAPK pathway within McSCs and drive McSC self-renewal? Where are they from? What are, on the other hand, downstream mediators of Kit signals to control McSC differentiation?

In addition to programmed inputs, McSCs also respond to accidental stimuli originating from the environment. For instance, upon wounding or UV irradiation, McSCs in hair follicles are activated, migrate upward and repopulate a new location: the epidermis (Chou et al., 2013; Walker et al., 2009; Zaidi et al., 2011). Therefore, the hair

follicle acts as a reservoir of McSCs not only supporting regular hair pigmentation but also supplying new melanocytes into epidermal surface. Understanding the mechanisms driving McSC repopulation is particularly important as it provides a protective design for skin against damage, and clinically it provides potential therapeutic methods for treating hypopigmentation diseases such as vitiligo by inducing recovery of the epidermal melanocyte population from the hair follicle reservoir (Cui et al., 1991; Falabella, 2009; Ortonne et al., 1979).

Quiescence of melanocyte stem cells

After a short window of proliferative time during early anagen, active McSCs return to quiescence, which is a non-cycling state that starts from the middle of anagen, specifically at anagen stage V, through catagen and telogen. Thus, they stay in dormancy most of the time except at the beginning of each hair cycle, when they respond to stimuli by entering the cell-cycle again (Nishimura et al., 2010). Interestingly, Nishimura *et al*. showed that transforming growth factor-β (TGF-β) signaling plays an important role in facilitating their active-state to quiescence transition. Acting on type I and type II receptors, TGF-β induces phosphorylation of regulatory R-SMADs including SMAD2 and 3, which form a complex with a mediator co-SMAD named SMAD4 and further translocate into the nucleus where they act as a bipartite transcription factor to modulate the transcription of TGF-β target genes (Siegel and Massagué, 2003). At the right timing when active McSCs are about to enter quiescence from mid anagen, TGF-β ligands are upregulated in the nearby bulge HFSCs, which provide the cues to activate TGF-β signaling within McSCs to induce cell cycle arrest and maintain McSCs in

undifferentiated form within their residence (upper ORS). When lacking TGFβRII receptor, McSCs fail to enter quiescence and instead undergo differentiation ectopically, causing accelerated hair graying due to progressive McSC loss.

Notably, in concordance with its function in regulating McSC activation negatively in follicles, TGF-β signaling has also been shown to inhibit the proliferation and differentiation of epidermal melanocytes against tanning response (Rodeck et al., 1994; Yang et al., 2008). Thus, in the absence of stimuli, epidermal keratinocytes secrete TGF-β that suppresses melanocyte activity, whereas upon UV exposure a reduced amount of TGF-β in the skin results in the increases of melanocyte proliferation and pigment production. Taken together, the TGF-β pathway has a global effect in maintaining the quiescence of McSCs and epidermal melanocyte precursors, though the molecular basis behind the scene is unclear, and whether TGF-β modulates the activity of undifferentiated melanocytes within the two different compartments in similar or different ways.

Interestingly, TGF-β seems to have an otherwise positive effect on HFSCs. At the onset of anagen, TGF-β secreted from the DP right under HFSCs can promote HFSC activation and hair cycle progression (Oshimori and Fuchs, 2012). Given that the known TGF-βs that modulate HFSC and McSC activity come from different sources and at different times, it remains unclear whether and how quiescent McSCs can respond to DP-secreted, in addition to HFSC-released, TGF-βs during the growing phase. Along the line, it is also unknown if other quiescent signals known to act on HFSCs, such as BMP and FGF18, also play similar functional roles in maintaining McSC quiescence (Hsu et al., 2011a; Kobielak et al., 2007; Zhang et al., 2006).

Besides through releasing signaling molecules, it is tempting to speculate that HFSCs, which sit right next to McSCs, might also provide a physical support for McSC maintenance. Collagen XVII (*Col17a1*) is a structural component of hemidesmosomes that function in stable attachment between HFSCs and the dermis. Indeed, in mice lacking *Col17a1*, not only do HFSCs lose stemness leading to hair loss, but nearby McSCs also undergo ectopic differentiation and progressive depletion (Tanimura et al., 2011). Interestingly, mice carrying mutations in other genes required for HFSC maintenance, such as *Lhx2*, *Sox9* and *Foxc1*, also frequently display a hair-graying phenotype after the time when HFSCs show abnormal behavior (personal communication with Alicia R Folgueras, Meelis Kadaja, and Kenneth Lay). Thus, mutations affecting one population (HFSCs) typically can affect the other (McSCs) as well. Ionizing irradiation-induced hair greying studies also supports the notion. The primary victim of radiation, which induces hair greying in mouse, was thought to be McSCs (Inomata et al., 2009), but HFSCs have also been aware to be comprised upon genotoxic stress (Aoki et al., 2013). Thus, careful characterization to distinguish between direct and secondary effects that are caused by HFSC abnormalities is especially essential in McSC studies.

Survival of melanocyte stem cells

Extrinsically, Notch signaling plays a critical role in maintaining the survival of melanoblasts and McSCs (Moriyama et al., 2006). Upon the binding of Delta ligand on the membrane of one cell to Notch receptor of the other cell, proteolytic cleavage of the Notch receptor occurs and triggers the release of the Notch intracellular domain (NICD), which enters the nucleus and forms a complex with the DNA-binding protein RBP-J to

control gene expression (Bray, 2006; Kopan and Weintraub, 1993). While mice carrying melanocyte-specific targeting of *Rbp-j* or *Notch* receptors still exhibit pigmented hairs extruding out of skin surface at 1-2 weeks after birth, melanoblasts or McSCs progressively diminish in number, which is evident from embryonic E16.5 followed by a complete disappearance of McSCs in adult mice and re-growth of a white hair coat after the first molting (Moriyama et al., 2006; Schouwey et al., 2006). Digging into the mechanism, Moriyama *et al*. found that Notch-negative melanoblasts undergo unexpected apoptosis, implying the importance of the Notch pathway in maintaining survival of melanoblasts or McSCs. Although multiple roles of Notch signaling in regulating melanoblast behavior have further been proposed (Aubin-Houzelstein et al., 2008), whether they can be applied to adult McSCs is unclear. The use of temporally controlled Cre recombinase tools for loss-of-function studies could bypass the defects resulting from a developmental abnormality, which will be helpful for future studies of adult McSCs.

Intrinsically, the anti-apoptotic gene *Bcl2* provides a way out for McSCs against death signals. Similar to the phenotype seen in Notch-deficient mice, *Bcl2*-null mice progressively lose hair color from first hair molting, and grey hairs appear in conjunction with loss of McSCs in the follicles (Kamada et al., 1995; Mak et al., 2006; Nishimura, 2005; Yamamura et al., 1996). It suggests that *Bcl2* is critical for the survival of postnatal melanocytes in hair follicles, providing a mechanism to prevent them from being depleted with age. In contrast, mice with ablation of *Pten*, which is a tumor suppressor gene that inactivates several pathways involved in anti-apoptosis and cell proliferation, are resistant to hair greying induced by multiple rounds of hair depilation (Inoue-Narita et

al., 2008). Besides increased activation of AKT and MAPK pathways, *Pten*-deficient melanocytes contain upregulated *Bcl-2*, the alteration that might prevent McSCs from depletion after several rounds of regeneration.

The coupling of epithelial-melanocyte stem cell behaviors

During the hair cycle, McSCs and HFSCs work in harmony to generate pigmented hairs (Fig. 1-3b). Synchrony is achieved such that upon initiation of a new hair cycle, stem cells of each type activate lineage commitment (Nishimura et al., 2002; Tumbar et al., 2004). They remain quiescent within hair follicles for weeks in telogen. With each new hair cycle, these two stem cell populations are coordinately activated. HFSCs divide and fuel new cells into the differentiating region or matrix, the structure of which is enlarged and accompanied by the appearance of pigments and mature melanocytes (Fig. 1-6). Thus, during anagen, differentiated melanocytes at the base of the mature hair follicle (hair bulb) produce and transfer pigments to neighboring committed HFSC progeny as they differentiate into hair cells.

Coupling of these two stem cell populations must be maintained during the hair cycle. Given that the pigments are only produced from mature melanocytes in the hair bulb but not from McSCs next to HFSCs, the coupling of stem cell behavior can result in pigments are produced at the right place (hair bulb) and transferred to the right cells, in this case differentiating hair cells. Speaking of the mechanism, recipient hair cells in the hair bulb express the transcription factor FOXN1, which controls the secretion of FGF2. Thus, through sending out FGF2 signals, hair cells can direct donor melanocytes to the correct location for depositing melanins (Weiner et al., 2007).

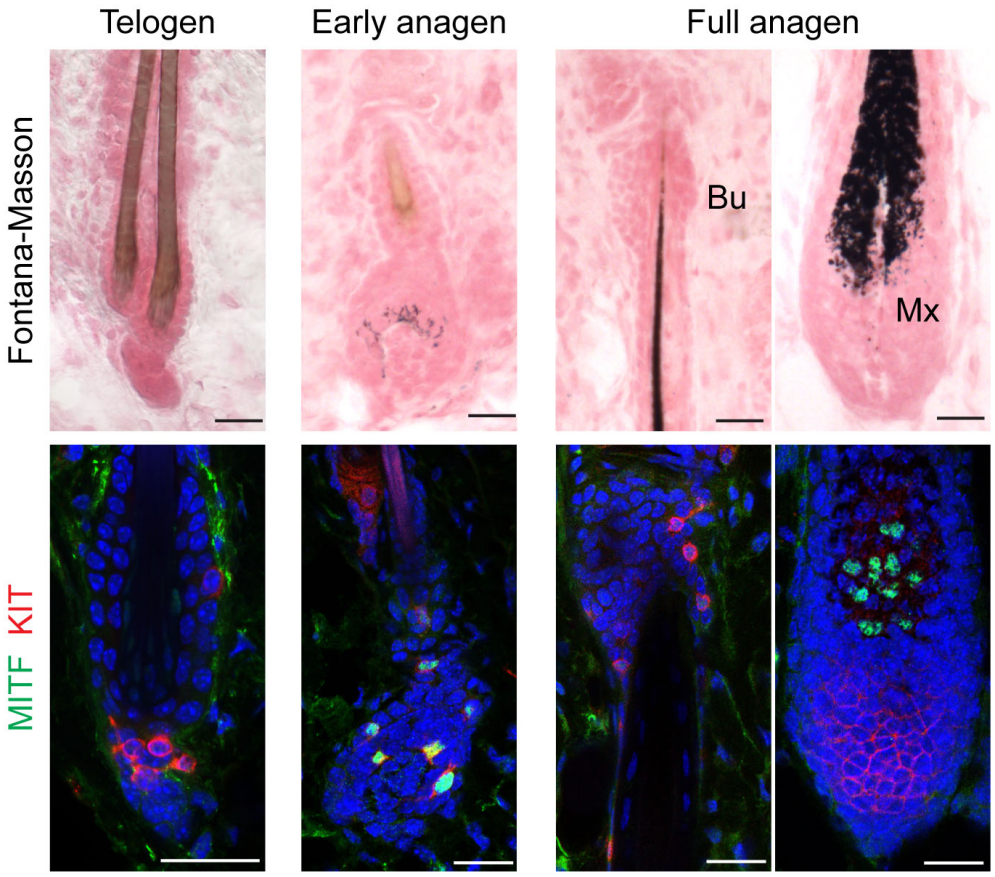

Figure 1-6. Pigmentation in hair follicles. Top row images: *Fontana-Masson* silver staining was conducted to detect melanins in hair follicles of mouse dorsal skin, followed by Nuclear Fast Red. Bottom row images: immunofluorescence with indicated antibodies. Telogen hair follicles with $KIT^{+}MITF^{-}$ melanocyte stem cells (McSCs) are pigment-free. When hair follicles enter anagen, pigments appear in the enlarged region of hair follicles close to the DP, and KIT^{+} melanocytes upregulate MITF. In full anagen, melanocytes staying close to HFSCs in the upper ORS of hair follicles are $KIT^{+}MITF^{-}$ McSCs, which don't synthesize melanins. Conversely, melanocytes migrating into the hair bulb become differentiated melanocytes ($KIT^{+}MITF^{+}$), which generate and transfer melanins to nearby differentiating hair cells. Bu: bulge. Mx: matrix. Scale bars: 10μm.

Uncoupling McSC and epithelial stem cell behaviors feature prominently not only under transient conditions, i.e. in response to ultraviolet radiation, but also in a variety of disease states. Given the global impact of Wnts and other signals on HFSCs and McSCs and their lineages (Nishimura et al., 2010; Rabbani et al., 2011), it remains a mystery as to how uncoupling is achieved and conversely, whether and/or how intercellular communication between HFSCs and McSCs might contribute to the coordination of stem cell activity.

Chapter 2:

Characterization of nuclear factor I/B's function during skin development

Introduction

Normal homeostasis of tissues and their regeneration during wound repair require stem cells. Hair follicles provide a good model system to analyze this process, since it undergoes cyclical bouts of regeneration, degeneration and rest as part of its natural homeostasis. Hair follicle stem cells (HFSCs) are responsible for driving hair growth. While slow cycling, interestingly, they apply a cascade amplification strategy by which their descendants (transit-amplifying cells) enter cell cycle more quickly to supply a sufficient pool of uncommitted cells for generating multiple lineages. In hair follicles, the most quiescent stem cells reside in the upper region of the ORS, specifically called the bulge (Fig. 1-3b) (Cotsarelis et al., 1990; Tumbar et al., 2004). When they are activated in anagen, they proliferate briefly to generate progeny traveling along the ORS trail. The lower region the cells reach, the higher their proliferation frequency becomes (Hsu et al., 2011a). When reaching the matrix, they become transit-amplifying (TA) cells, which have a fast-cycling nature but exit cell cycle suddenly to differentiate into IRS and hair shaft when reaching the top of the matrix.

Interestingly, the specification of HFSCs begins as early as when epidermis invaginates to form a follicular structure during morphogenesis (Nowak et al., 2008) (Fig. 1-3a). By E17.5, the cells within the upper region of the hair germ become SOX9-positive. SOX9 is required for the specification of HFSC precursors in the ORS, which proceed to become HFSCs by P21. During hair follicle morphogenesis, hair follicles without SOX9 face growth retardation and they degenerate prematurely with the concomitant lack of HFSC precursor population (Nowak et al., 2008; Vidal et al., 2005). Epidermal wound repair, meanwhile, is also compromised due to SOX9 loss. Thus, the

establishment of HFSC precursors is important for forming proper hair follicle structure and also maintaining skin reconstitution ability upon wound healing.

To identify candidate genes that modulate HFSC features, gene expression profiles of cells residing in the bulge/upper ORS were compared to epithelial basal cells outside the bulge region (Morris et al., 2004; Rendl et al., 2005; Tumbar et al., 2004). Seven out of 33 genes encoding nuclear or transcription factors were found enriched in HFSC population in more than one study. Interestingly, nuclear factor I/B (*Nfib*) was the only one factor that repeatedly surfaced on all three independent microarray analyses accompanying with three different strategies of HFSC isolation (Table 2-1). Meanwhile, *Nfib* is also enriched in $SOX9^+$ HFSC precursors of developing hair follicles (unpublished).

Table 2-1. *Nfib* enrichment in the hair follicle from microarray analyses

Comparison	Mouse lines	Mouse age	Cell surface markers	Enrichment	Reference
Adult bulge vs. epidermis/ORS	*TRE*-H2BGFP/ *K5*-tetVP16	8-week old with 4-week chasing	**Bulge**: GFP^{high}, $\beta4^+$ **Epidermis/ORS**: GFP^{low}, $\beta4^+$	4x enriched in the bulge	Tumbar et al., 2004
Adult bulge vs. epidermis/ORS	*K15*-EGFP	P50-P60	**Bulge**: GFP^+, $\alpha6^+$ **Epidermis/ORS**: GFP^-, $\alpha6^+$	3 x enriched in the bulge	Morris et al., 2004
ORS vs. matrix	*K14*-H2BGFP/ *Lef1*-RFP	P4	**ORS**: GFP^{high}, RFP^- **Matrix**: GFP^{low}, RFP^-	3.9 x enriched in the bulge	Rendl et al., 2005
HFSC precursors vs. ORS	*K14*-H2BGFP/ *Sox9*-RFP	P4	**HFSC precursors**: RFP^{high}, GFP^+, $\alpha6^+$ **ORS**: RFP^{low}, GFP^+, $\alpha6^+$	5.5x enriched in early HFSCs	(unpublished, done by Lisa Fish)

Nfib belongs to nuclear factor I (*Nfi*) gene family, which encodes site specific DNA-binding proteins (Gronostajski et al., 1985; Hennighausen et al., 1985; Leegwater et al., 1985; Nowock et al., 1985; Roulet et al., 2000). Originally, NFI was isolated as a host protein required for adenovirus DNA replication (Nagata et al., 1982), and was later found to function in gene regulation, playing a duel role as transcriptional activator and repressor (Jones et al., 1987) (reviewed in (Gronostajski, 2000)). In vertebrates, the *Nfi* gene family consists of four members including *Nfia*, *Nfib*, *Nfic* and *Nfix*, all of which contain a highly conserved N-terminal DNA-binding and dimerization domain, and a C-terminal transcription modulation domain with high variability due to extensive alternative splicing (Meisterernst et al., 1989; Mermod et al., 1989). Forming a homo- or hetero-dimer, NFI proteins recognize the palindromic consensus binding sequence 5'-TGGCA-(N_{3-5})-TGCCA-3', while they could also bind individual half sites with otherwise a lower affinity (Kruse and Sippel, 1994; Meisterernst et al., 1988).

Nfi genes are widely expressed in mouse tissues. Gene ablation studies revealed that each member of NFI family has essential roles in different organ development, while they also converge on the same tissues, particularly on brain. *Nfia*-knockout mice die perinatally and show evident defects in brain formation (Neves et al., 1999); due to abnormal tooth formation. *Nfic*-null mice show eating difficulty, which further causes growth retardation and premature lethality (Steele-Perkins et al., 2003). Loss of *Nfix* results in complex phenotypes including brain malformation, impaired bone ossification and developmental defects in skeletal muscle. *Nfix* mutants die within one month after birth possibly due to nutrient deprivation (Campbell et al., 2008; Driller et al., 2007; Messina et al., 2010). Loss of *Nfib*, which is the only member exhibiting preferential

expression in HFSCs, causes perinatal lethality owing to its essential role in lung and brain development (Gründer et al., 2002; Steele-Perkins et al., 2005). Interestingly, *Nfib* is often amplified and/or found at oncogenic chromosomal breakpoints in epithelial and gland cancers and thought to act as an oncogene (Dooley et al., 2011; Geurts et al., 1998; Ho et al., 2013). While the function of NFI proteins in stem cell is still unknown, the potential role in regulating developmental process makes it a candidate to study HFSC behavior.

In this study, I assessed the functional significance of NFIB in skin development. Expressed in embryonic hair progenitors upon induction of hair morphogenesis, NFIB becomes enriched in the ORS including stem cell compartment as hair follicle development progressed. In *Nfib*-null embryos, epidermal differentiation is delayed and hair follicle number is reduced during embryonic development. During morphogenesis, SOX9 expression is reduced in HFSC precursors upon NFIB loss, accompanied with diminished population of transit-amplifying cells in matrix and precocious termination of hair follicle morphogenesis. NFIB-deficient hair follicle cells also fail to support skin regeneration in a wound response. By analyzing its expression in genetic mutant embryos defective in aspects of hair follicle formation, NFIB is positioned downstream of NOG/BMP signaling necessary for follicle induction.

Results

NFIB is enriched in the bulge and the ORS of hair follicles

To validate microarray data and documented its expression pattern at different stages of skin development, I performed immunostaining with an anti-NFIB antibody.

NFIB first appeared in the epidermis at E14.5, concomitant with the beginning of stratification (Fig. 2-1a). As epidermal stratification progressed, NFIB was maintained in the basal epidermal progenitors but was down regulated in the differentiating suprabasal cells by E17.5 (Fig. 2-1b and c). At the onset of epidermal invagination from E15.5, the hair placode (Pc) upregulates P-cadherin (PCAD), but NFIB still persisted throughout the epidermal basal layer (Fig. 2-1b). Interestingly as the hair follicle elongated, NFIB became highly enriched in the hair germ (HG) specifically in the upper PCAD-low region of HG where HFSC precursors locate (lower panel of Fig. 2-1c, Nowak et al., 2008), whereas it was less expressed in the PCAD-high leading edge cells, which are the early progenitors of the transit-amplifying (TA) matrix cells of mature hair follicles (lower panel of Fig. 2-1c).

As the hair follicle become mature poatnatally, NFIB signals concentrated in the HFSC precursors within the upper ORS and also extended in a trail down along the ORS (Fig. 2-1d). During hair differentiation, NFIB signals are gradually diminished in the matrix, and eventually absent in differentiated progeny within the IRS and HS (Fig. 2-1d). In telogen (P21), NFIB was enriched in the bulge and the hair germ (HG) (Fig. 2-1e). As the hair follicle is activated to enter a new hair cycle, NFIB signals remained strong in the $CD34^{+}$ bulge throughout most of the hair cycle, while it is down regulated in the emerging TA population of committed progenitors (Fig. 2-1f and data not shown).

Within the bulge where HFSCs reside, NFIB is also co-expressed with HFSC transcription factors such as NFATc1 (Horsley et al., 2008) and LHX2 (Folgueras et al., 2013; Rhee et al., 2006), which are required for maintaining HFSC quiescence (Fig. 2-2a); conversely its expression waned in proliferative differentiating cells marked by Ki67

in the matrix (Fig. 2-2b). Thus, HFSCs in the bulge/ORS upregulate the expression of NFIB and down-regulate it when they are undergoing differentiation program, the pattern that suggests an intrinsic regulatory role of NFIB in HFSCs.

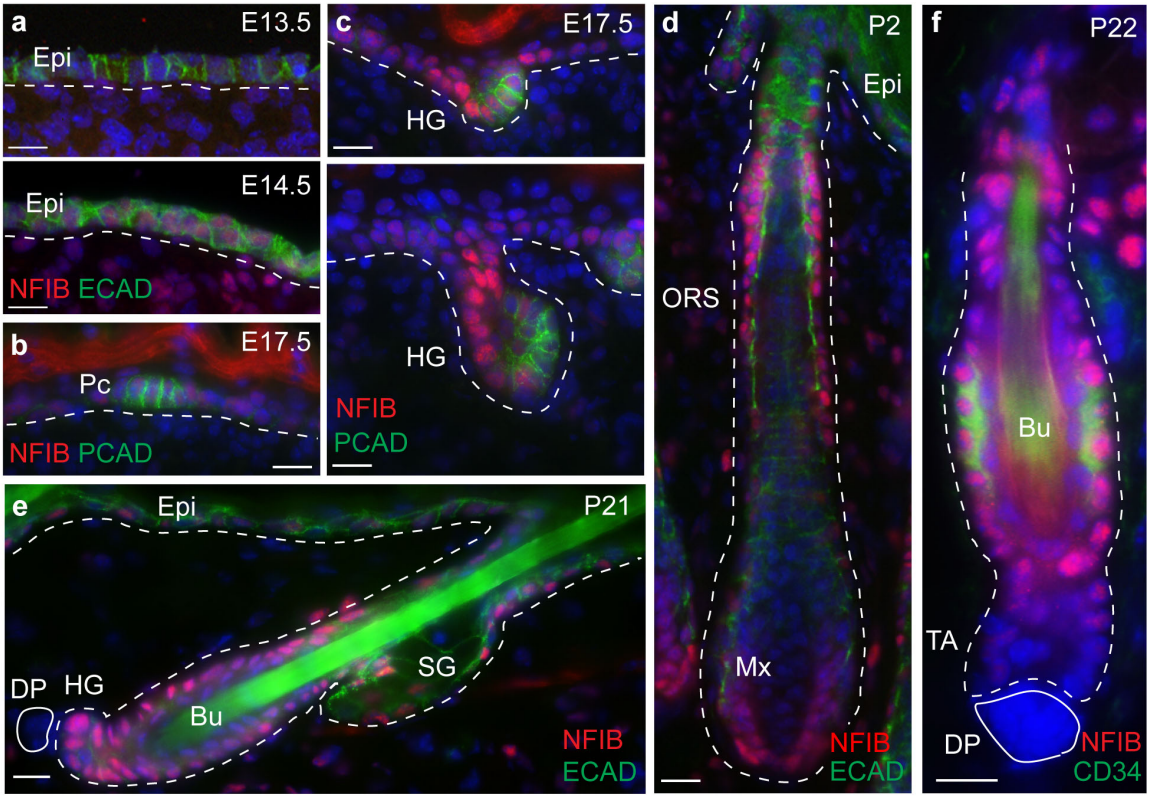

Figure 2-1. NFIB is enriched in the ORS and the bulge of hair follicles. a-f, Immunofluorescence with indicated antibodies. **a,** Nuclear NFIB appears in the basal layer of epidermis (Epi) as early as E14.5. **b,** Before or at the onset of epidermal invagination, NFIB is equally expressed in epidermal basal cells. PCAD marks placode (Pc) structure. **c,** As morphogenesis proceeds, NFIB is upregulated in the hair germ (HG), specifically in the area above PCAD^{+} leading edge where early HFSC precursors reside. **d,** Enrichment of NFIB in the ORS of developing HFs. Matrix (Mx). **e,** During telogen, NFIB is enriched in the bulge (Bu) and secondary hair germ (HG), expressed at lower level in sebaceous glands (SG) and epidermis (Epi), and absent in the dermal papilla (DP). **f,** At the onset of anagen, NFIB level remains high in CD34^{+} HFSCs but is down-regulated in the emerging transit-amplifying population (TA) of committed progenitors close to the DP. ECAD: E-cadherin. PCAD: P-cadherin. Scale bars: 10μm.

Loss of NFIB delays epidermal development

To address the physiological significance of NFIB in skin, I performed loss of function study in *Nfib*-null mice. When WT epidermal basal progenitors migrated upwards to differentiate into K10-positive cells in spinous layer and further into Loricrin (LOR)-labeled granular layer at E15.5, epidermis of *Nfib* KO mice still stayed in undifferentiated stage, in which *Nfib* KO epidermis was negative for differentiating layers until E16.5 (Figure 2-3a and b). The phenotype of epidermal stratification was manifested functionally in the delayed acquisition of the epidermal barrier, which cannot exclude X-gal dye from penetrating into skin at E17.5 but one day later (E18.5) (Fig. 2-3c). Consistently, transcriptional profiling by quantitative RT-PCR in purified basal cells through fluorescence activated cell sorting (FACS) also revealed that the expression of differentiation markers including *K1*, *K10* and epithelium secreted peptide complex

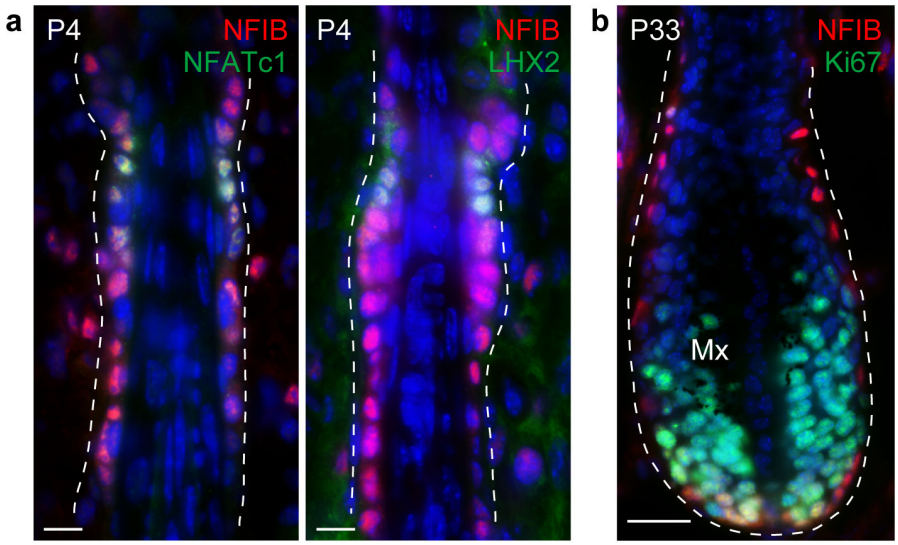

Figure 2-2. Co-localization of NFIB with HFSC markers. Immunofluorescence with indicated antibodies. **a,** NFIB is expressed in NFATC1 and LHX2 positive HFSCs in the upper ORS. **b,** NFIB level is decreased in $Ki67^{+}$ proliferative cells in the matrix (Mx). Scale bars: 10μm (a); 25μm (b).

(called SSC, including *Dmkn*, *Krtdap*, *Sbsn*) were reduced upon loss of NFIB at E15.5 while progenitor marker *K5* displayed normal level (Ezhkova et al., 2009); however, later at E17.5, their mRNA levels in KO cells reached the levels in WT cells (Fig. 2-3c).

The delayed differentiation process upon NFIB loss *in vivo* was also recapitulated *in vitro*. In culture, when undifferentiated keratinocytes isolated from the newborn skin were exposed to higher levels of calcium, they stopped proliferating and underwent terminal differentiation. Upregulated genes upon elevated calcium treatment were differentiation markers including *K1*, *K10, Lor and Filaggrin* (*Flg*) in both WT and KO cells, albeit KO cells showed the changes in a delayed fashion (Fig 2-3e). Notably, the differences in SSC expression in response to NFIB deficiency were not significant *in vitro*, suggesting that the *in vivo* changes might be due to secondary effects. Taken together, these data implied that disruption of NFIB resulted in delayed epidermal stratification.

Loss of NFIB impedes hair follicle induction and morphogenesis

Hair follicle induction is initiated around E15.5 and the hair follicle numbers are gradually increased along with the expansion of skin area. To monitor hair follicle formation, I used PCAD to label hair placodes to quantify their numbers. Starting from E15.5, *Nfib*-null embryos displayed an ~40-60% reduction in the overall density of PCAD-positive hair follicles (Fig 2-4a). In mouse skin, there are four types of hairs formed in a sequential fashion during embryonic stage, in which hair follicles of guard hairs were induced at E14.5, awl/auchene hairs from E16.5 and zigzag hairs from E18.5.

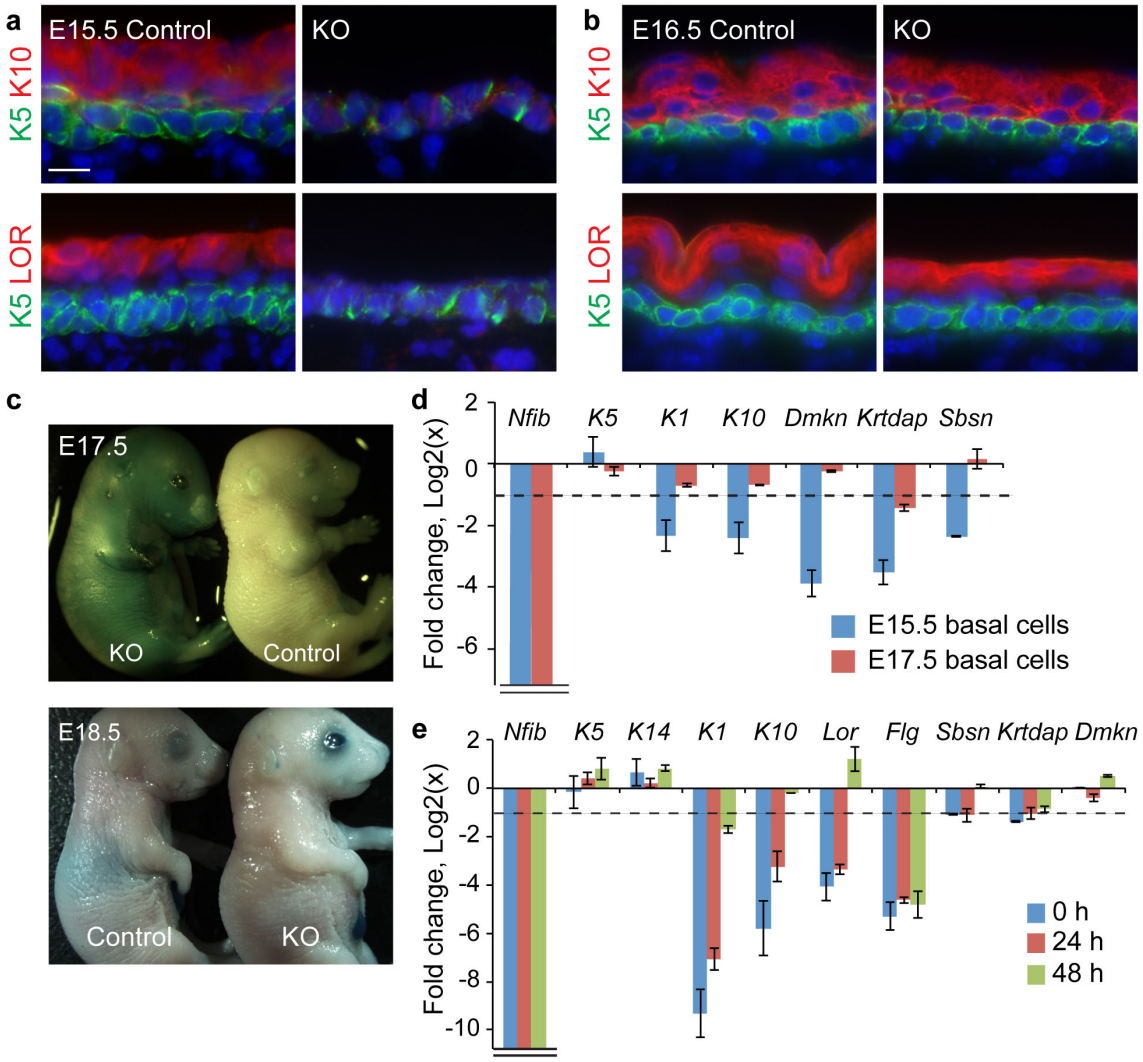

Figure 2-3. Epidermal stratification is delayed upon NFIB loss. a,b, Immunostaining shows that $K10^+$ spinous layer and LOR-labeled granular layer were formed in WT embryos in E15.5 but were formed one day later (E16.5) in *Nfib* KO embryos. K5 labels basal layer. **c,** Dye exclusion assay to measure skin barrier showed that *Nfib* KO skin acquired protective barrier later than WT skin. Failure of forming a differentiated layer (cornified barrier) resulted in the diffusion of dye into the skin and skin color darkened when embryos were immersed in X-gal reaction mix. **d,** Quantitative PCR of FACS-purified basal cells ($\alpha^+\beta^+$) from control and KO skin. **e,** Quantitative PCR of control and KO cultured keratinocytes before (0h) and after calcium elevation (24h, 48h). Scale bars: 10μm. Error bars indicate s.e.m.

To understand whether *Nfib* is generally required for hair formation or its function is hair-type specific, I quantitatively assessed the progression of the early steps of hair follicle morphogenesis in *Nfib*-null skin at E18.5, when first wave of hair follicle growth reached PEG stage while others had smaller structures. However, the percentage of hair follicles in each stage of morphogenesis showed no significant difference between WT and *Nfib*- KO mice. Thus, it implies that disruption of *Nfib* caused overall reduction of hair follicle density but the induction of individual hair types seems fine (Fig. 2-4b). Given that *Nfib*-null mice cannot survive after birth due to a severe lung structural defect, it is difficult to follow postnatal hair growth and cycle upon NFIB loss. To overcome this limitation, I grafted the skins from E18.5 KO and control embryos onto recipient *nude* mice, which provided a platform to extend the analysis of *Nfib*-KO skin development. Notably, when WT skin became hairy after 12-day grafting (D12), *Nfib*-KO grafts still lacked hairs until ~D20 (Fig. 2-5a). Morphologically, *Nfib*-KO hair

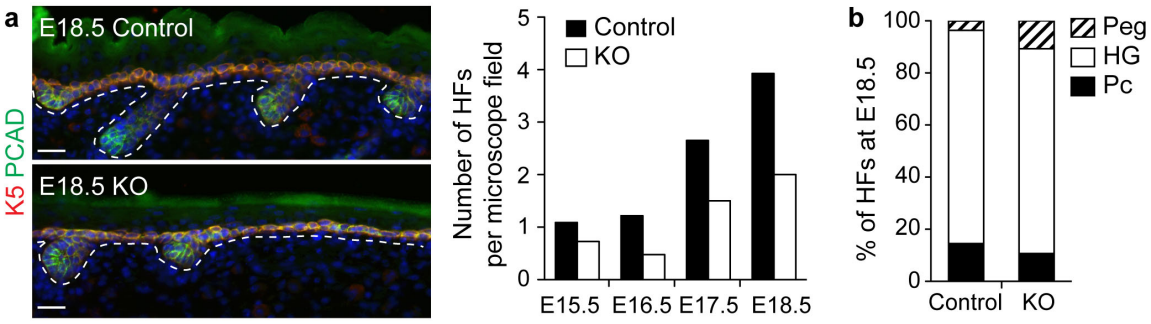

Figure 2-4. Disruption of *Nfib* reduces hair follicle density during embryonic stage. a, Immunofluorescence with indicated antibodies. Quantifications of hair follicle number per microscope field reveal that loss of NFIB results in decreased hair follicle density starting from E15.5. **b,** The progression of hair follicle growth from placode (Pc) to Peg stage is normal in KO skin. HFs: hair follicles. PCAD: P-cadherin. Scale bars: 20μm.

follicles showed growth retardation. At D8, WT hair follicles were reaching full length and forming hair shaft, while *Nfib*-KO hair were still in the early stage of morphogenesis with shorter appearance (Fig. 2-5b).

Later, surprisingly, the growth of *Nfib*-KO hair follicles became asynchronous. By D12 when most of WT hair follicles are still in growing phase, some of *Nfib*-null hair follicles showed signs of degeneration, which was visualized by histological analysis (Fig. 2-5c). Also, KO hair follicles showed positive immunostaining with active-caspase3^{+}, indicating the presence of apoptotic cells (Fig. 2-5d). Meanwhile, some of KO hair follicles were still maintained, while their matrix marked by Ki67 was smaller than of control (Fig. 2-5e). One month later, both WT and KO hair follicle entered telogen by D45 with proper formation of bulge HFSC populations indicated by CD34 staining (Fig. 2-5f and g). Taken together, these results suggested that NFIB loss impedes hair follicle induction and morphogenesis accompanied with immature formation of transit-amplifying population in the matrix, while the establishment of bulge HFSCs seems not affected.

To determine if NFIB regulates epidermal cell function in a cell-autonomous or non-autonomous manner, I generated mice with conditional knockout of *Nfib* specifically in epidermal cells by crossing *Nfib (fl/fl)* mice (Hsu et al., 2011b) to mice carrying cre recombinase (*Cre*) driven by *K14* promoter (Vasioukhin et al., 1999). In *K14Cre/Nfib (fl/fl)* (cKO) mice, ablation of *Nfib* was targeted in the basal layer of skin as early as E13.5, right before the timing of NFIB appearance. Heterozygous deletion of *Nfib* (*K14Cre/Nfib (fl/+)*) or expression of *Cre* only in skin had no obvious effect on development, and animals survived and showed normal coat formation. In contrast, most

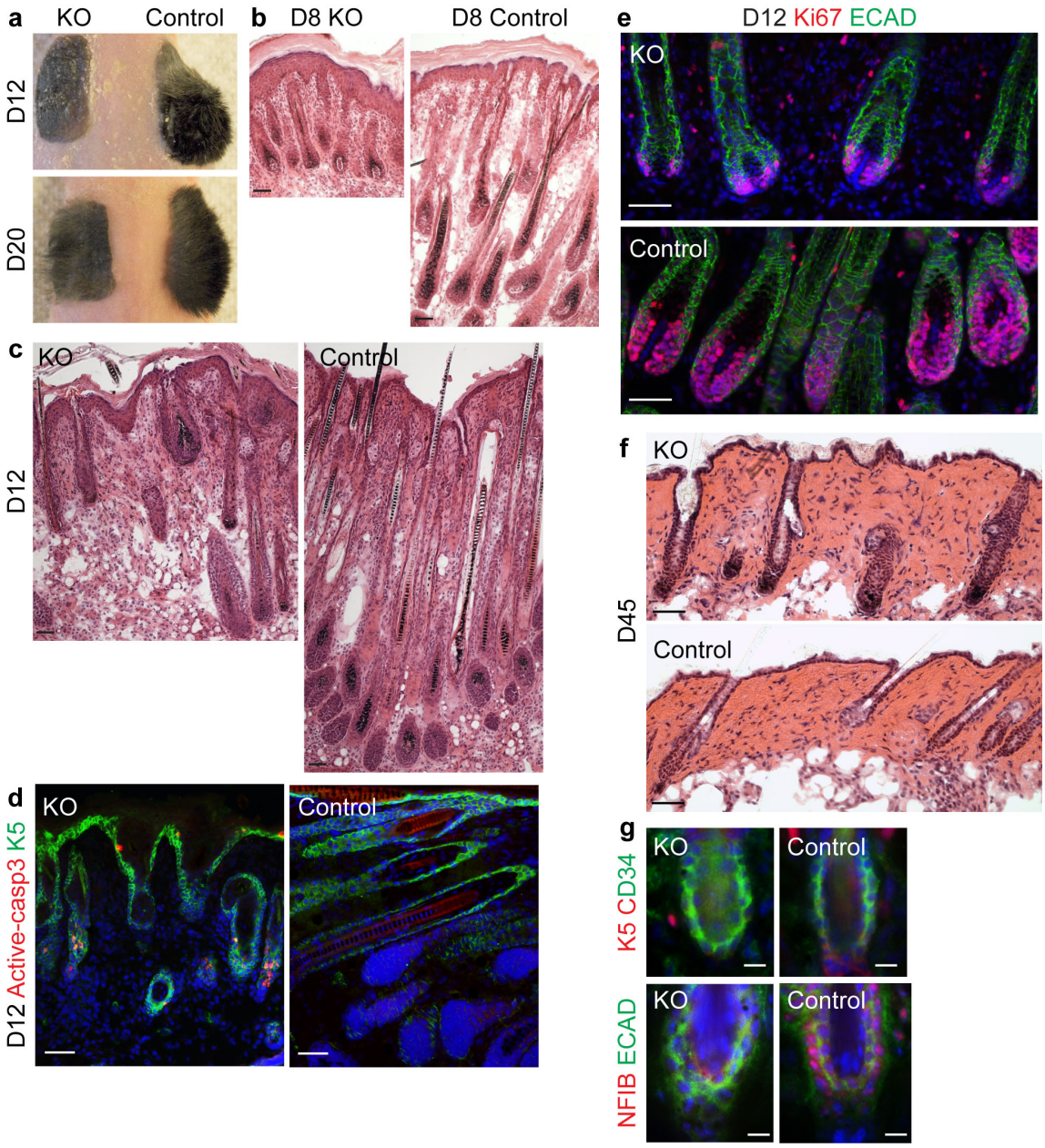

Figure 2-5. Loss of NFIB impedes hair follicle morphogenesis. a, Skin grafting on *nude* mice reveals delayed hair shaft formation upon NFIB loss. **b,** H&E staining of 8-day grafts show that the length of KO hair follicles is shorter than WT hair follicles. **c,** H&E staining of 12-day grafts reveal precocious degeneration of KO hair follicles. **d,** Apoptotic cells (active-casp3^{+}) are present in degenerating hair follicles of KO grafts. **e,** Immunofluorescence shows that the matrix, marked by Ki67, of KO hair follicles is smaller than WT hair follicles. **f,** H&E staining shows that both WT and KO hair follicles enter telogen after 45-day grafting. **g,** The bulge of KO (lacking NFIB signals) hair follicles express CD34 normally. ECAD: E-cadherin. Scale bars: 50μm (b-f); 10μm (g).

of *Nfib* cKO mice died within 1-2 days after birth. Occasionally, some cKO mice survived for ~1-2 weeks with mosaic *Nfib* targeting. They displayed sparse hairs at P15 when WT mice developed full hair coat (Fig. 2-6a). In addition, the whiskers of cKO mice were in disarray (Fig. 2-6b). In sum, epidermal *Nfib* is required for hair follicle development and proper establishment of hair structure.

Next, I performed histological analysis to investigate the possible defect in hair follicle morphology upon *Nfib* ablation. At P0, no significant abnormalities in follicle structure and length were found in cKO mice (Fig. 2-7a). However, differences in HF length became evident by P3 when cKO follicles only had 40% the length of WT follicles and remained shortened by P6 (Fig. 2-7a and b). Despite defects in HF length, overall features of HF differentiation were relatively normal: IRS, hair shaft and sebaceous gland

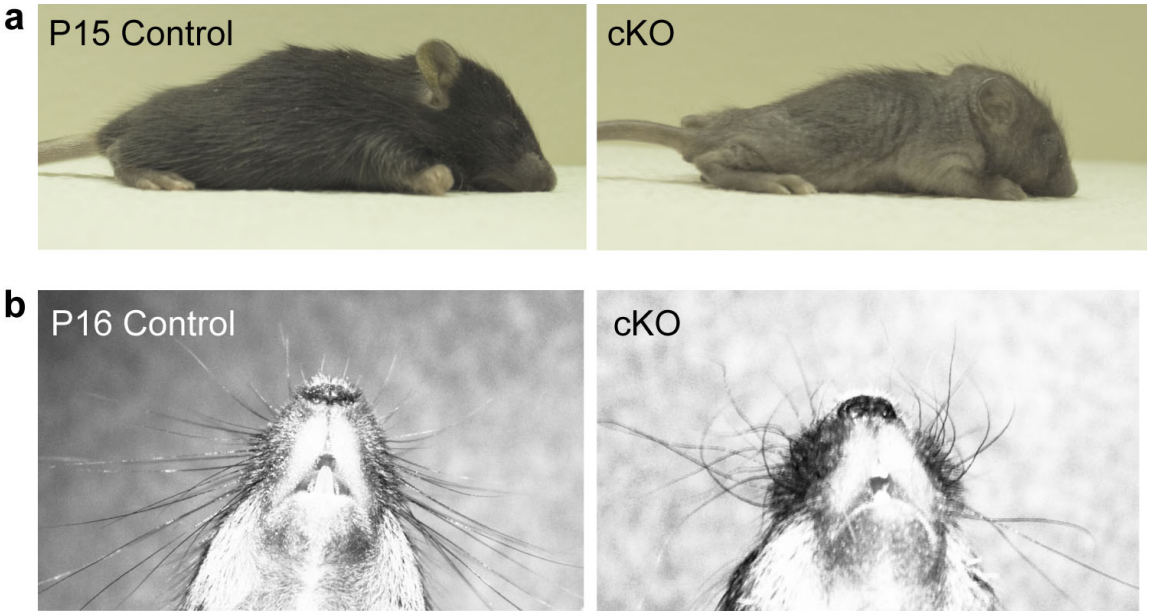

Figure 2-6. NFIB loss specifically in epidermal cells results in delayed hair coat formation. a, *K14-Cre/Nfib(fl/fl)*-cKO mice have spare hairs at P15 while WT mice have full hair coat. **b,** Whiskers of cKO mice are malformed.

were all present and properly organized (data not shown). Interesting and unexpectedly, by P13 cKO follicles were not only shorter than WT follicles, but they displayed signs of exiting the previous hair cycle precociously and going into next hair cycle. At P13, the upper region of follicles exhibited the previous (club) hair in its center, with a new hair follicle growing downward (Fig. 2-7a). In contrast, the WT follicles were still in the process of completing the first round of hair growth, which normally completes after P15. The phenotype of precocious exit from previous hair cycle in *Nfib*-cKO mice was

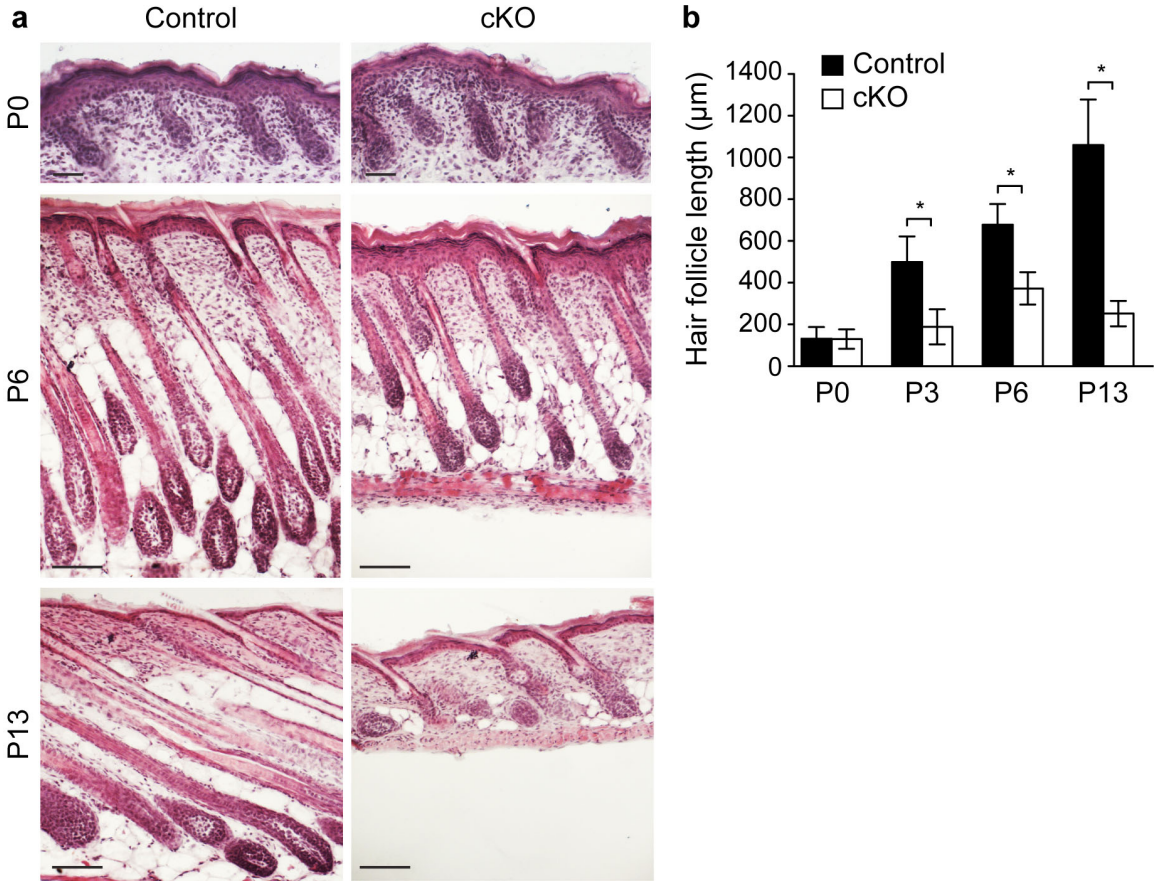

Figure 2-7. Hair follicle morphogenesis is retarded upon NFIB loss. a, H&E-stained backskins. At P0, *K14-Cre/Nfib(fl/fl)* (cKO) hair follicles have normal morphology. By P6, cKO follicles are shorter than WT follicles. By P13, cKO preciously enter anagen of first hair cycle as WT follicle is still in morphogenesis stage. **b,** Quantification of hair follicle length at different stages. Scale bars: 50μm. *$P < 0.001$. Error bars indicate s.e.m.

consistent with straight KO results (Fig. 2-5c, b), though the outcome of grafting experiments was more complicated in that hair follicles of KO grafts behaved less synchronously than of cKO skin.

Closer inspection revealed that the matrix size of *Nfib* cKO follicles was restricted (Fig. 2-8), which was also observed in engrafted straight KO skins (Fig. 2-5e). The matrix structure of these cKO follicles were smaller than of WT follicles accompanied with smaller population of $Ki67^{+}$ transit-amplifying cells, which had not reached $AE13^{+}$ differentiated layers (Fig. 2-8). Taken together, I found that hair follicle morphogenesis is retarded and shortened in NFIB-deficient skin, while the determination of differentiated HF lineages is not affected.

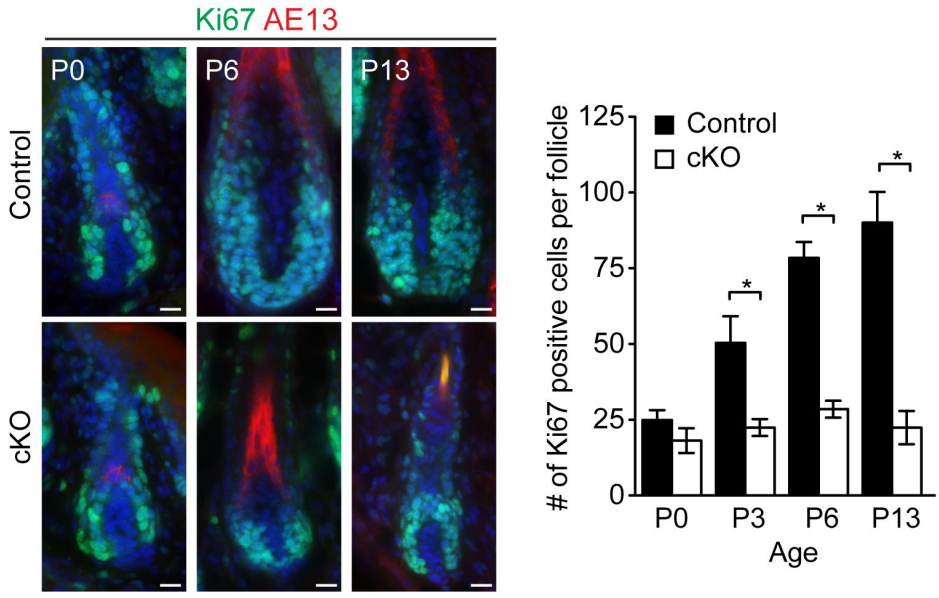

Figure 2-8. NFIB loss results in reduced transient-amplifying matrix population. Immunofluorescent tracking of Ki67-positive matrix cells over time. Quantification of the number of Ki67-positive and AE13-negative matrix cells per hair follicle cross section. Scale bars: 10μm. *$P < 0.001$. Error bars indicate s.e.m.

Hair follicle stem cell precursors cannot maintain SOX9 expression upon NFIB loss

HFSC precursors, specified in the upper ORS during morphogenesis, are required for hair follicle formation. Because *Nfib* is expressed in HFSC precursors, I speculated that impeded formation of hair follicles in *Nfib* cKO skin might be due to the defects in HFSC precursors. To examine this hypothesis, I first performed immunostaining with antibodies against SOX9, which is a marker of HFSC precursors and required for their establishment (Nowak et al., 2008). At P0, SOX9 was expressed in the upper ORS of cKO follicles (Fig. 2-9a). However, by P6, SOX9 signals were dramatically decreased in the upper ORS of cKO follicles compared to WT follicles, and only scattered cells in cKO follicles were SOX9 positive (2-9b). Quantitatively, the number of SOX9-positive cells in the upper ORS was significantly decreased in the absence of *Nfib* (Fig. 2-9c).

However, other two markers LHX2 (Folgueras et al., 2013; Rhee et al., 2006) and NFATc1 (Horsley et al., 2008), required for maintaining HFSCs in quiescence, were still expressed in the upper ORS (Fig. 2-9d). Taken together, in light of the findings that cKO follicles cannot grow normally accompanied with undersized matrix and the expression of HFSC precursor marker SOX9 is declined in the ORS, it is possible that *Nfib* might be required for forming HFSC precursors. As a consequence, there may not be sufficient HFSC precursors established and/or with sufficient function to be able to provide a sufficient input of cells toward the matrix, whose residents have low capacity for self-renewal and rely on constant influx of cells from upstream stem cells for expanding its population over time.

If NFIB is required for establishing proper HFSC precursors, *Nfib* deficiency might impair their ability of regenerating tissue in wounds. To further gain insight into

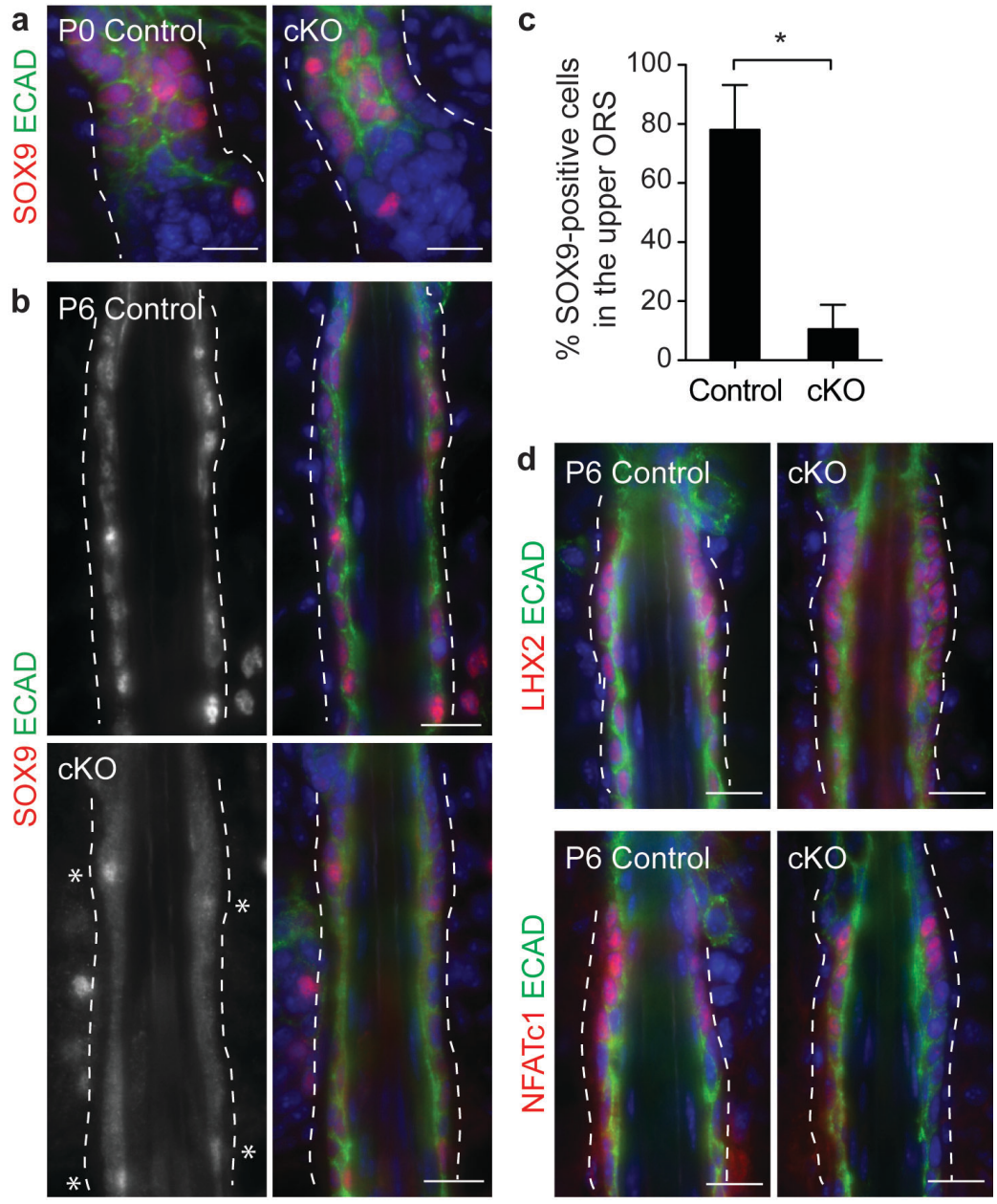

Figure 2-9. Expression of HFSC markers in *Nfib* cKO hair follicles. a, Immunofluorescence shows SOX9 is normally expressed in the ORS of cKO follicles at P0. **b,** By P6, the number of $SOX9^{+}$ cells is dramatically decreased in the upper ORS of cKO follicles. **c,** Quantifications of percentage of $SOX9^{+}$ cells in the top 30 ORS cells below sebaceous gland. **d,** Immunofluorescence shows LHX2 and NFATc1 are expressed in cKO follicles. ECAD: E-cadherin. Scale bars: 10μm. $*P < 0.001$. Error bars indicate s.e.m.

their functionality *in vivo*, I conducted engraftment experiments on *Nude* mice recipient with split dermis tissue (Nowak et al., 2008). After removing the epidermal layer, split dermis from donor mice, which contained hair follicles with HFSC precursors, were grafted above a wound on *Nude* mice recipient. To trace the behaviors of targeted cells, I crossed cKO and control mice to *Rosa26*$^{floxed/stop/floxed/YFP}$ (*Rosa*^{YFP}) Cre-reporter mice, in which Cre-targeted cells and its progeny can be followed by YFP signals. Surprisingly, when control grafts were fully covered by hairs 2 weeks after grafting, cKO grafts still lacked hairs (Fig.2-10a). Examining YFP signals, I observed that YFP^{+} hair follicle cells from control split graft emigrated upwards to regenerate epidermal tissue; meanwhile, they were also able to split their effort to support hair follicle growth downward (Fig.2-10b and c). However, in NFIB-deficient grafts, though epidermal wounds seemed to be repaired, most of them were YFP negative, suggesting that they were not generated from NFIB-targeted cells but WT cells possibly due to mosaic activity of *K14*-Cre in the grafts and the invasion of surrounding recipient epidermal cells (Fig.2-10b). More dramatically, most hair follicles were degenerated and disappeared quickly within one week in NFIB-deficient grafts left with few sporadic untargeted WT hair follicles. It suggests that NFIB loss impairs hair follicle-mediated re-epithelization (Fig.2-10c).

NFIB acts downstream of NOG/BMP signaling

Multiple signaling pathways converge to regulate hair follicle morphogenesis. To elucidate their relations with NFIB, I examined NFIB's expression in various genetic backgrounds carrying mutations in key signaling pathways responsible for hair follicle induction and growth. In Wnt signaling-deficient embryos with *Lef1*, *Tcf3/4*, or *β-catenin*

(*βcat*) knocked out, NFIB was still present in skin (Fig. 2-11a). NFIB was also expressed normally in the absence of sonic hedgehog (*Shh*), which is required for follicle down-growth (Fig. 2-11b). Only upon the ablation of *Noggin* (*Nog*) was NFIB level decreased in the hair germ accompanied with reduced formation of hair follicles, the phenotype that was also observed in *Nfib*-KO embryos (Fig. 2-11c). Given that NOG is an antagonist of BMP ligands and acts by sequestering BMPs from their receptors, I tested if NOG modulates NFIB expression through inhibiting BMP pathway *in vitro*. After 24-hour addition of BMP4 into the culture, mRNA level of *Nfib* in WT keratinocytes was

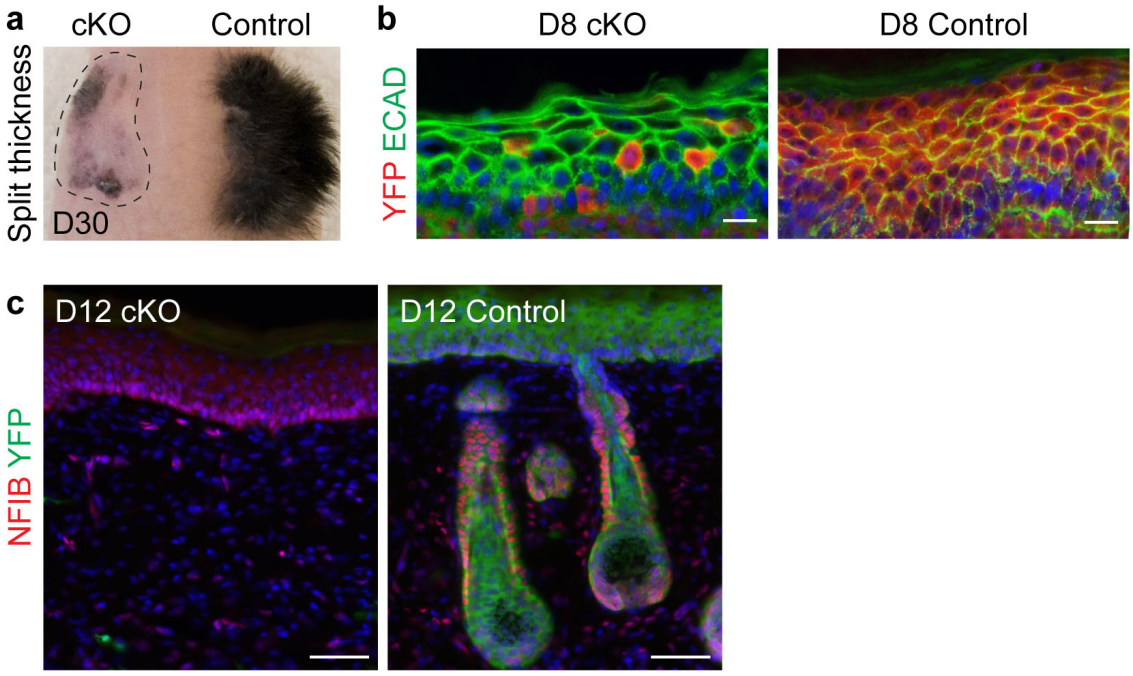

Figure 2-10. NFIB is required for hair follicle-mediated re-epithelization upon wounding. a, Split thickness (dermis with HFs) skins from E18.5 WT and cKO embryos were grafted onto *Nude* recipients. Hairs grew on WT grafts 30 days after grafting while cKO grafts were hairless. **b,** Control and cKO mice were crossed to *Rosa26*$^{floxed/stop/floxed/YFP}$ (*Rosa*^{YFP}) reporter mice to follow the behavior of targeted (YFP^{+}) cells in split-thickness grafting experiments. New epidermis formed on top of control split thickness grafts are YFP^{+}, but cKO grafts have very few YFP^{+} cells in the epidermis. **c,** Degeneration of cKO hair follicles in split thickness grafts. Scale bars: 10μm (b); 50μm (c).

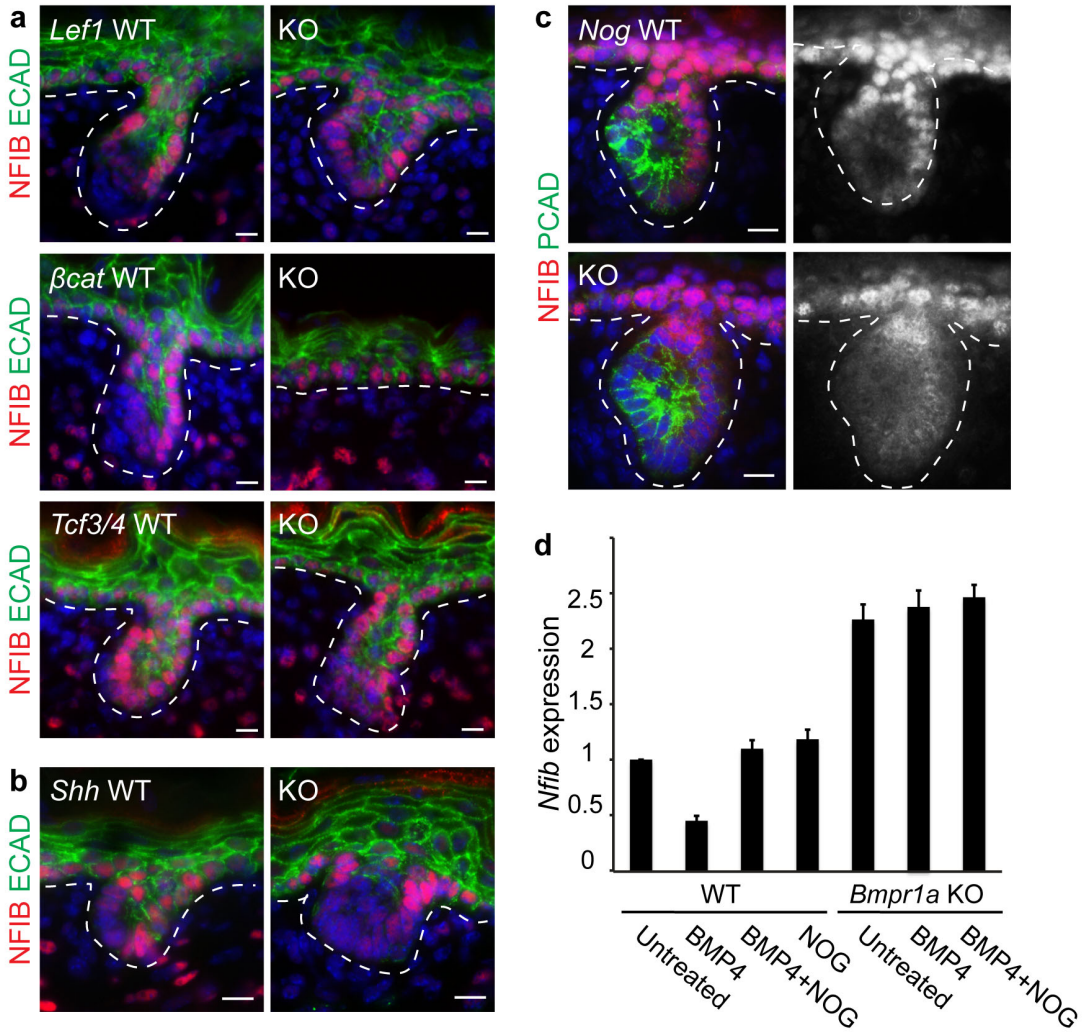

Figure 2-11. NFIB level is regulated by NOG/BMP signaling. a-c, Immunofluorescence with indicated antibodies. **a,** NFIB levels in hair follicles are unchanged in Wnt-deficient embryos. **b,** NFIB is expressed in *Shh* KO embryos. **c,** Nuclear NFIB signals are decreased in *Nog*-mutant hair follicles. **d,** Quantitative PCR indicates that *Nfib* mRNA level is decreased after 24h BMP4 addition in keratinocyte culture. The inhibition is reversed by the addition of BMP inhibitor noggin (NOG) and is not seen in BMP receptor (*Bmpr1a*)-KO keratinocytes. ECAD: E-cadherin. PCAD: P-cadherin. Scale bars: 5μm (a); 10μm (b,c). Error bars indicate s.e.m.

decreased by 2-fold and the inhibition was blocked by the presence of antagonist NOG (Fig. 2-11d). Conversely, BMP receptor *Bmpr1a* KO keratinocytes showed 2-fold increases in *Nfib* mRNA level, which is not responsive to exogenous BMP or NOG treatment (Fig. 2-11d). Taken together, these findings suggested that NFIB acts downstream of BMP/NOG pathway. Noggin, secreted from mesenchymal cells nearby placode forming region during morphogenesis, might upregulate *Nfib* expression in the follicle possibly through inhibiting BMP signals.

Discussion

Through analysis of transcriptional profiles, a novel transcriptional factor NFIB in HFSCs was identified. It is upregulated at first in the undifferentiated epidermal stem cells and further become enriched in HFSCs when the follicles appear. Conversely, NFIB is down regulated in both epidermal and hair cells when they undergo differentiation program. Although further loss-of-function studies indicated that NFIB is not required for differentiation of epidermal stem cells to form stratified epithelium, the timing is disrupted. During development, the establishment of skin barrier was delayed in *Nfib*-null mice, accompanied with delayed upregulation of differentiation markers. However, the molecular basis behind the scene is still not clear and merits further investigation. Are the defects caused by unbalanced control of epidermal stem cell proliferation and differentiation or due to ectopic apoptosis in skin? Do NFIB-deficient epidermal stem cells enter the cell cycle properly? Could NFIB-deficient epidermal stem cells perform asymmetric cell division, in which their mitotic spindle orients perpendicularly to the basement membrane to drive the generation of committed suprabasal cells? Waiting to be

addressed are also questions concerning the long-term effect of NFIB loss, such as if delayed stratification process of epidermis still remains unsolved in adult, the defect that further slows down regular skin turnover as well as regeneration process in wound healing.

Furthermore, I also found that hair follicle numbers were reduced in *Nfib*-null embyros. The induction process of follicles relies on reciprocal interactions between epidermal and underlying mesenchymal cells, in which extracellular signal exchanges take place to mediate the crosstalk. By examining if NFIB acts as an intracellular responder upon extracellular signal stimulation required for placode formation, I found that NFIB levels are regulated by NOG/BMP pathway. In *Nog*-KO embryos, hair follicle induction is retarded (Botchkarev et al., 1999), the phenotype reminiscent of *Nfib* mutants and concomitant with reduced level of NFIB in hair follicles. I also showed that NOG modulates NFIB expression by its canonical role of inhibiting BMP pathways. Digging into the mechanism, studies have indicated LEF1/Wnt signals are also diminished in *Nog*-KO hair follicles. Notably, however, forced expression of *Lef1* in *Nog* mutant cannot fully rescue hair follicle defect (Jamora et al., 2003), raising the possibility that other LEF1/Wnt-independent mechanisms might act downstream of NOG/BMP pathway to regulate hair follicle morphogenesis. Thus, knowing whether NFIB is the missing factor needs further study. Meanwhile, it also has not been examined if NFIB acts rather upstream of other well known signaling pathways. Testing the sensitivity of *Nfib*-KO keratinocytes in response to extracellular stimuli will be helpful to solve this issue. Interestingly, protein sequence analysis to search for conserved secondary structure revealed that DNA binding region of NFI family contains a N-terminal Mad Homology 1

(MH1) domain (NCBI: NP_001106680.1), which is shared by most of SMAD proteins involved in TGF-β/BMP signaling (Shi et al., 1998). However, the similarity seems not assist them to target the same genomic sites as SMAD and NFI proteins recognize specific but different DNA-binding elements (Shi et al., 1998). However, MH1 domain of SMAD proteins can negatively regulate the modulation domain (MH2) by interacting with MH2, which creates a close structure to prevent the association of several SMAD proteins becoming a functional unit in the absence of inputs (Hata et al., 1997). Thus, it is tempting to examine if MH1 domain of NFI proteins also have inhibitory effect to itself and/or to other factors such as SMADs, and what stimuli can open the structure.

As whole embryo targeting of *Nfib* results in perinatal lethality due to lung development defects, I generated conditional *Nfib*-knockout (cKO) mice with *K14-Cre*, in which *Nfib* was targeted in the epidermis and hair follicles of skin. During hair follicle morphogenesis, the growth of cKO hair follicles was retarded concomitant with a diminished population of transit-amplifying matrix cells. Premature transition from morphogenesis to next anagen in *Nfib*-cKO hair follicles reflects the possibility that diminished hair bulb, which precociously exhausts its supply of transit-amplifying matrix cells, might fail to last long. But the overall features of differentiated layers in hair follicles and sebaceous glands were relatively normal, suggesting that NFIB is not required for lineage commitment and differentiation. While the possible causes of a reduced matrix population might be due to a defect in the matrix itself with decreased proliferation, or increased differentiation or apoptosis, retarded hair follicle growth and matrix production could also be due to impaired establishment of functioning HFSC precursors, which are needed to proliferate to support the elongation of follicular

structure and fuel the production of matrix cells.

Examining the characteristics of HFSC precursors, I found that SOX9 expression was gradually decreased after birth upon NFIB loss. It suggested that HFSC precursors might be specified during embryonic stage but they either fail to mature or their characters are not maintained during hair follicle morphogenesis. Meanwhile, in a wound response created by the split-thickness grafting assay, NFIB-deficient hair follicles completely degenerate with reduced epithelial reconstitution efficiency, implying that the regenerative capacity of hair follicle cells including HFSC precursors is limited in the absence of NFIB.

Making HFSCs versus utilizing them could be two distinct processes. Since the hair follcile forms from the epidermis, defects in the epidermis and/or hair follicle specification could be at the root of the hair follicle defects that I see. In addition, establishing proper HFSCs could be dependent upon proper communication of HFSC precursors with developing niche components, which must occur in synchrony with the HFSC precursors during morphogenesis. Since *K14*-Cre targets the skin epithelium from early development, and encompasses both epidermal and hair follicle cells, it is not possible to know whether once developed the HFSCs and their niche would be able to function properly. Inducible targeting methods to knockout *Nfib* postnatally will be helpful for further studies to address this issue, and to detail the defects and the underlying mechanisms.

In sum, these results revealed that NFIB is involved in multiple processes of skin development. During embryonic stage, loss of NFIB delays the formation of skin barrier and inhibits hair follicle induction. In addition, during morphogenesis, NFIB is required

for hair follicle growth and establishing functional HFSC precursors. However, whether NFIB functions in adult HFSCs is unknown. Further exploration of this issue and characterization of NFIB's target genes and its affect on their action will shed light into the mechanisms by which this important somatic stem cell niche is established and regulated during development. Beyond morphogenesis stage, whether NFIB plays a role in regulating the homeostasis of hair follicles and in regulating adult HFSC behavior will be discussed in the following chapter (Chapter 3).

Materials and Methods

Mice, barrier assay and engraftment experiments.

Nfib(fl/fl) and *Nfib*(-/-) mice have been described (Hsu et al., 2011b; Steele-Perkins et al., 2005), as have transgenic *K14-Cre* (Vasioukhin et al., 1999) and *ROSA26*$^{flox/STOP/flox/YFP}$ (*Rosa*^{YFP}) (Srinivas et al., 2001) mice. Dye exclusion assays were performed as described (Hardman et al., 1998). Full thickness grafts from E18.5 embryos were performed as described (Rhee et al., 2006) and split thickness grafts were performed as described (Nowak et al., 2008).

All animals were maintained in an AAALAC-approved Comparative Bioscience Center (CBC) at The Rockefeller University and procedures were performed using IACUC-approved protocols that adhere to the standards of the National Institutes of Health.

Histology and immunofluorescence.

Embryos (<E16.5) or backskins were embedded in OCT (Tissue Tek), frozen on

dry ice and stored at -80°C. Only in the case of *Rosa*^{YFP} reporter mice, tissues were prefixed in 4% paraformaldehyde (PFA) for 30 min at room temperature (r.t.) before embedding in OCT in order to preserve the fluorescence signals. Un-prefixed frozen sections (10-20 μm) were fixed in 4% PFA for 10 min at (r.t.). For histological analysis, sections were stained with hematoxylin and eosin. For immunofluorescence, sections were permeabilized in 0.3% Triton X-100 in PBS for 20 min and blocked for 1 hr at r.t. in blocking buffer including 2.5% normal donkey serum, 2.5% normal goat serum (or 5% normal donkey serum alone when goat primary antibodies were used), 0.5% BSA and 0.1% Triton X-100 in PBS. MOM Basic kit (Vector Laboratories) was used for blocking when primary antibodies were generated from mouse. Primary antibodies were diluted in blocking buffer and sections were incubated overnight at 4°C. After washing with PBS for 30 min at r.t., sections were incubated for 1–2 hr at r.t. with secondary antibodies conjugated to Alexa-488, Alexa-546, Alexa-647 (Molecular Probes), or RRX (Jackson Laboratories). Nuclei were stained using 4'6'-diamidino-2-phenylindole (DAPI). Imaging was performed on a Zeiss Axioplan 2, Zeiss Apotome, Zeiss Inverted LSM 510 laser scanning confocal microscope, or Zeiss Inverted LSM 780 laser scanning confocal microscope.

The following antibodies and dilutions were used: NFIB (rabbit, 1:1,000, Active Motif; mouse, 1:500, Abcam); P-cadherin (goat, 1:100, R&D); E-cadherin (rat, 1:500, Fuchs lab); K5 (guinea pig, 1:500, Fuchs lab); CD34 (rat, 1:100, BD Pharmingen); Ki67 (rabbit, 1:300, Novocastra); cleaved-Caspases3 (rabbit, 1:300, R&D); GFP (chicken, 1:2,000, Abcam); LHX2 (rabbit, 1:500, Fuchs lab); NFATc1 (mouse, 1:100, Santa Cruz); SOX9 (rabbit, 1:1000, Fuchs lab); K10 (rabbit, 1:500, Covance); LOR (rabbit, 1:400,

Fuchs lab); AE13 (mouse, 1:500, Abcam).

Isolation of epidermal basal cells and FACS.

Back skins from one litter of E15.5 and E17.5 embryos were dissected using the shoulders and hips as landmarks, and incubated in 4ml 0.25% Collagenase (Sigma) in HBSS (GIBCO) at 37°C for 15 min to digest the dermis. 11ml cold PBS was added and dermal tissues were separated from the epidermis by repetitive pipetting. Additional 25 ml cold PBS was added before centrifugation (300g, 15min). 25ml cold PBS was added to resuspend cells, and centrifugation with 40g for 6 min was conducted to enrich epidermal cells leaving dermal cells in supernatant. The epidermal fraction was treated with 2ml 25% trypsin (GIBCO) at 37°C for 20 min. Single cells were washed once and resuspended in 10ml staining buffer (PBS with 5% fetal bovine serum treated with BioRad Chelex to remove calcium) to inactivate Trypsin, and cells were collected by centrifugation for 5 min at 300g. Cell suspensions were incubated with the appropriate antibodies diluted in staining buffer for 30 min at 4°C. The following antibodies were used: α6-PE (1:500, eBioscience); β1-FITC (1:500, eBioscience). DAPI (100 ng/ ml) was used for death cell exclusion. Cell isolations were performed on BD FACSAria II sorters equipped with BD FACSDiva software. For RNA extraction, cells were sorted directly into TRIzol LS Reagent (Life Technologies).

RNA extraction and quantitative PCR (qPCR).

RNA was extracted using Direct-zol RNA MiniPrep (Zymo Research) with DNase treatment to remove residual genomic DNA. cDNA was synthesized from isolated

RNA using SuperScript III First-Strand Synthesis System with oligo-dT primers (Invitrogen). cDNAs were mixed with indicated primers and Power SYBR Green PCR Master Mix (Applied Biosystems), and quantitative PCR (qPCR) was performed on a Applied Biosystems 7900HT Fast Real-Time PCR system for 40 cycles. Specificity was confirmed by subsequent melting curve analysis or gel electrophoresis. Levels of PCR product were expressed as a function of peptidylprolyl isomerase B (Ppib). Primers were designed through Primer 3 and amplified products encompassed exon/intron boundaries.

The following primer sequences were used:

Nfib forward 5'-ATGACCCATCCAGTCCTCAA-3',

reverse 5'-TTGAAGGAAAGGCTCTCCAA-3';

K5 forward 5'-GGCTCTCAAAGATGCCAGAA-3',

reverse 5'-TGACTGGTCCAACTCCTTCC-3';

K14 forward 5'-CGCCGCCCCTGGTGTGG-3',

reverse 5'-ATCTGGCGGTTGGTGGAGGTCA-3';

K1 forward 5'-GACACCACAACCCGGACCCAAAACTTAG-3',

reverse 5'-ATACTGGGCCTTGACTTCCGAGATGATG-3';

K10 forward 5'-GGAGGGTAAAATCAAGGAGTGGTA-3',

reverse 5'-TCAATCTGCAGCAGCACGTT-3';

Lor forward 5'-TCACTCATCTTCCCTGGTGCTT-3',

reverse 5'- GTCTTTCCACAACCCACAGGA-3';

Flg forward 5'-GGAGGCATGGTGGAACTGA-3',

reverse 5'-TGTTTATCTTTTCCCTCACTTCTACATC-3';

Dmkn forward 5'-AGACCACTGCCAAGGCGGGA-3',

reverse 5'-CCCCAGGCGAGATGACAGGC-3';

Krtdap forward 5'-GCAGCCCAAACCGGACACCA-3',

reverse 5'-AGGCCCTCTGTTGCGGTAGGG-3';

Sbsn forward 5'-GCCAGGCCGAGAAGGAAGCG-3',

reverse 5'-CCTCCGTGCTGGCCTCCGTA-3';

Cell Culture.

Enzymatic separation of epidermis from skins and primary keratinocyte culturing were conducted as described (Blanpain et al., 2004). Primary *Nfib*-null (KO) keratinocytes were isolated from epidermis of E18.5 *Nfib* knockout embryos (*Nfib*-/-) and control keratinocytes were from heterozygous *Nfib* (+/-) embryos. Keratinocytes were maintained in E-media supplemented with 15% serum and a final concentration of 0.05 mM Ca_2. Experiments were performed using primary cells with less than 15 passages. To induce keratinocyte differentiation, calcium concentration was raised from 0.05 to 1.5 mM. BMP4 (300ng/ml, R&D Systems) and noggin (300ng/ml, R&D Systems) recombinant proteins were reconstituted according to manufacture's manual.

Statistics.

To determine significance between two groups indicated in figures, comparisons were performed in Prism 5 software with unpaired two-tailed student's t-test.

Chapter 3:

The role of nuclear factor I/B in coordinating epithelial-melanocyte stem cell behavior in the hair follicle

Introduction

Adult stem cells reside in specialized niches where they receive environmental cues to maintain tissue homeostasis. In mammals, the hair follicle is home to two distinct stem cell populations including epithelial hair follicle stem cells (HFSCs) and melanocyte stem cells (McSCs), which behave cooperatively to sustain cyclical bouts of hair regeneration and pigmentation (Cotsarelis et al., 1990; Morris et al., 2004; Nishimura et al., 2002; Tumbar et al., 2004). When hair follicles are in the dormant phase (telogen), HFSCs and McSCs reside in the bulge and HG, and remain quiescent for many weeks (Fig. 1-3b). When follicle regeneration (anagen) initiates, these two stem cell populations are coordinately activated at the hair-follicle base (hair germ; HG) in response to activating cues that are secreted from specialized underlying mesenchymal cells, the dermal papilla (DP) (Blanpain and Fuchs, 2006; Greco et al., 2009; Nishimura et al., 2002; Rendl et al., 2005). Thus, at the onset of anagen, a subset of stem cells of each type enter the cell cycle and produce progeny. In the mature hair follicle, transit-amplifying HFSC progeny (matrix cells) in the hair bulb have enveloped the dermal papilla. They divide rapidly, but only briefly, progressing to differentiate to form the new hair. Just before they do so, differentiated melanocytes produce and transfer pigment to adjacent HFSC progeny in the upper matrix as they stop proliferating and begin to differentiate to form a hair shaft (Tobin et al., 1999).

For both melanocyte and hair lineages, stem cells remain in the bulge and the upper ORS of mature hair follicles. When differentiated melanocytes and matrix cells simultaneously undergo apoptosis during the destructive phase (catagen), HFSCs and McSCs in the upper hair follicles survive and stay in quiescence during telogen until the

beginning of next hair cycle (Sharov et al., 2005).

The molecular mechanisms of how HFSCs and McSCs coordinate their behaviors during hair cycle are still unclear. Given the global impact of environmental signals from the DP cells or other adjacent cell types on HFSCs and McSCs (discussed in Chapter 1), it remains a mystery as to whether and/or how intercellular communication between HFSCs and McSCs might contribute to the coordination of stem cell activity.

To study the function of *Nfib* in adult HFSC maintenance, I generated inducible *Nfib* conditional knockout mice, in which Cre recombinase activities were induced after hair follicle morphogenesis was completed. Surprisingly I found that ablation of *Nfib* in adult HFSCs did not perturb HFSC maintenance, as hair follicle growth and hair cycle proceeded relatively normally. Instead, and even more unexpected, NFIB loss in the HFSCs promoted proliferation and precocious differentiation of nearby McSCs. My findings provide new insights into how McSC and HFSC behaviors maintain reliance upon cooperative factors within hair follicles and how this might be uncoupled in injury, stress and disease states.

Results

NFIB is expressed in hair follicle stem cells but not in melanocytes

The venture into this study was inspired by the finding that relative to their progeny, HFSCs display elevated expression of transcription factor NFIB (see Chapter 2). To know within the hair follicle if NFIB is specifically expressed in HFSCs or present in both stem cell populations, I conducted co-immunostaining with antibodies recognizing NFIB and of tyrosine kinase receptor KIT, which is a marker of melanocytes.

I found that NFIB was not detected in KIT$^+$ McSCs, which were mostly located in the hair germ (HG) of telogen follicles and intermingled with NFIB$^+$ HFSCs (Fig. 3-1a).

Although in telogen KIT is only expressed in the cells of melanocyte lineage, during hair growth KIT becomes upregulated in transit-amplifying matrix cells derived from HFSCs and is not a suitable markers to label differentiated melanocytes in the hair bulb (Botchkareva et al., 2001). To circumvent this problem and identify melanocytes specifically, I used *Dct*-EGFP BAC transgenic mice, in which EGFP expression is under the control of the promoter of melanocyte-specific gene dopachrome tautomerase (*Dct*) (Fig. 3-1b). The co-localization of KIT and EGFP signals confirmed the reliability of using *Dct*-EGFP mice as a tool for labeling melanocytes (Fig. 3-1c). To examine the differential expression of *Nfib* at the RNA-level, I isolated EGFP$^+$ melanocytes as well as $\alpha6^+CD34^+$ bulge HFSCs by fluorescence-activated cell sorting (FACS) for quantitative PCR (qPCR) analysis (Fig. 3-1d). The results of qPCR showed that *Nfib* accompanied with *Sox9* were enriched in bulge HFSCs; conversely, melanocyte-specific genes such as endothelin receptor type B (*Ednrb*) and *Dct* were predominantly expressed in EGFP$^+$ melanocytes (Fig. 3-1e). At protein level, within the bulge and along the upper ORS, NFIB was not detected in EGFP$^+$ McSCs (Fig. 3-1f). NFIB was also not found in EGFP$^+$ differentiated melanocytes, which were confined to the hair bulb where they transfer pigment to differentiating hair cells. Thus, both inside and outside their residence, HFSCs and McSCs displayed synchronized behaviors but distinct expression patterns.

Postnatal ablation of *Nfib* does not perturb hair cycle or follicle architecture

In *K14-Cre Nfib* cKO mice, perturbed hair follicle morphogenesis implied that

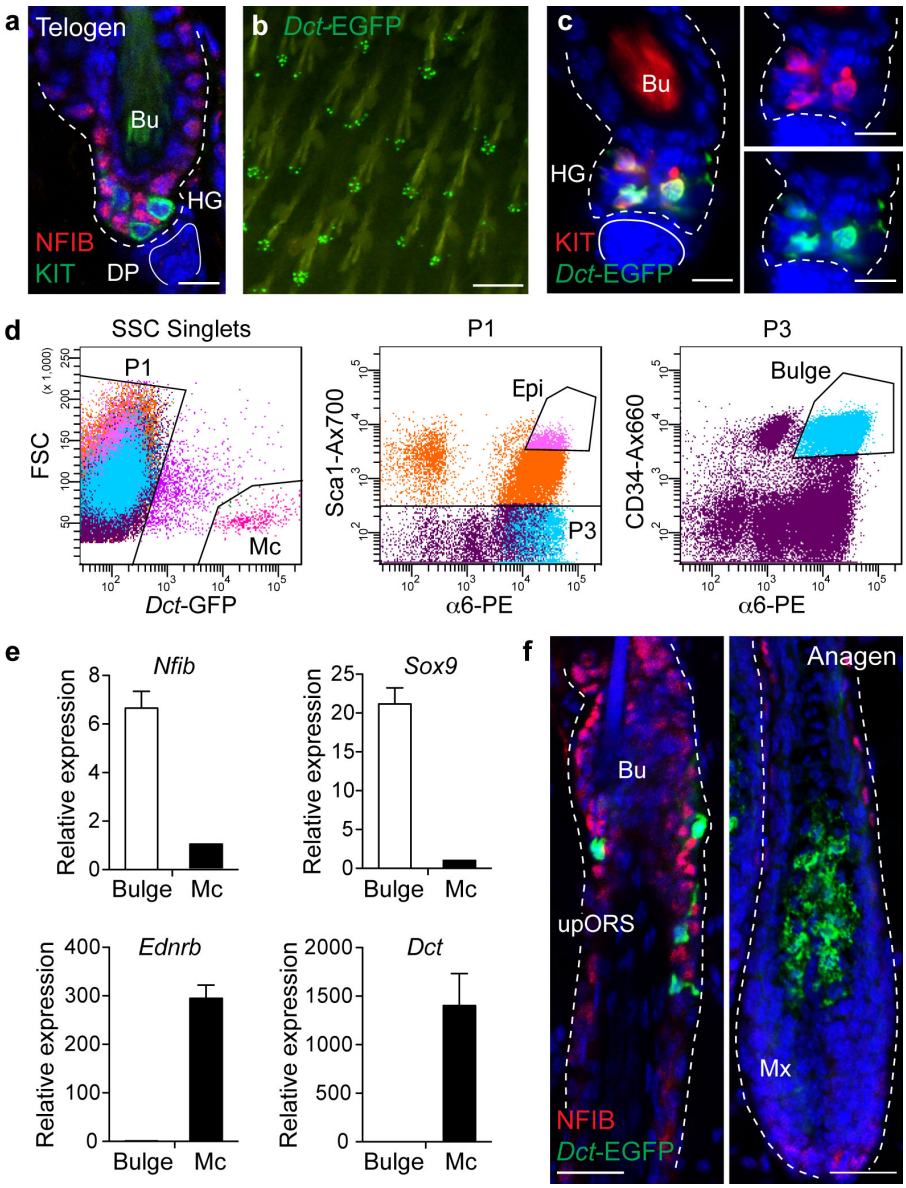

Figure 3-1. NFIB is not expressed in melanocytes. a, Immunofluorescence reveals the absence of NFIB in KIT^{+} McSCs of telogen (P59) hair follicles. **b,** Whole-mount green fluorescent imaging of dorsal skin from P53 *Dct-EGFP* BAC transgenic mouse. **c.** Immunofluorescence shows co-staining of KIT and EGFP in telogen (P100) hair follicles of *Dct-EGFP* mice. **d,** FACS isolation. Melanocytes (Mc) were EGFP^{high}; bulge HFSCs (Bulge) were isolated with markers EGFP^{neg} Sca1^{neg} α6^{high} CD34^{+}. **e,** Quantitative PCR on FACS-isolated populations confirm the enrichment of *Nfib* and *Sox9* in bulge cells and of melanocyte markers including *Ednrb* and *Dct* in Mc population. **f,** NFIB signals in anagen HFs of P32 *Dct-EGFP* transgenic mice. Note NFIB is not seen in EGFP^{+} McSCs in the ORS and also not seen in EGFP^{+} differentiated melanocytes close to the matrix (Mx). upORS: upper ORS. Bu: Bulge. HG: Hair germ. DP: Dermal papilla. Scale bars: 10 μm (a, c); 100 μm (b); 25 μm (f).

Nfib might play a role in HFSC establishment (see Chapter 2). However, *Nfib* disruption during the embryonic stage by *K14*-Cre also caused premature lethality of mice, which impeded studies to address *Nfib*'s function in mature hair follicles and adult HFSC maintenance.

To overcome these issues, I generated two inducible *Nfib* conditional knockout mice (cKO mice), one carrying *Sox9-CreER* (Soeda et al., 2010) and the other with *K15-CrePGR* (Morris et al., 2004) (Fig. 3-2a). The activities of both types of Cre recombinases can be temporally controlled and are dependent on chemical application, while two lines exhibit different advantages for gene targeting. The *Sox9* promoter displays higher efficiency than *K15* to drive Cre expression; however, Cre is not restricted solely to HFSCs, but extends upward to the so-called junctional zone of resting-phase hair follicles. On the other hand, the *K15* promoter can be used to conduct gene ablation prominently in HFSCs of bulge and HG but with relatively lower efficiency, which causes mosaic-targeting pattern (Fig. 3-2a). Notably, postnatally, the Cre activities from both lines are restricted to keratinocytes and not in melanocytes. As shown previously by transcriptional profiling analysis (Rendl et al., 2005), *K15 (*or called *Krt1-15)* and *Sox9* mRNAs were enriched in ORS/bulge, down in matrix and absent in melanocytes and DP (Fig. 3-2b); furthermore, $Rosa26^{floxed/stop/floxed/YFP}$ ($Rosa^{YFP}$) Cre-reporters marked only HFSCs and not KIT^{+} melanocytes or dermal cell types (Fig 3-2c and d). As will be shown below, both gave similar results.

To target *Nfib* in adult follicles, I treated *Sox9-CreER* cKO, *K15-CrePGR* cKO and their control mice with inducing chemicals (tamoxifen for CreER and RU486 for CrePGR) from first telogen and followed hair growth and cycle in response to NFIB loss

(Fig. 3-3a). Anti-NFIB immunofluorescence showed that *Nfib* was efficiently ablated in HFSCs of both lines (Fig. 3-3a and b). Despite efficient targeting in telogen phase HFSCs, the hair coat of *Nfib*-cKO mice appeared unaffected, and no significant abnormalities were detected in HF morphology or cycling (Fig. 3-3c). Since *Sox9-CreER* displays higher gene targeting efficiency than *K15-CrePGR* (Fig. 3-3a and b) and both lines gave similar results, *Sox9-CreER* cKO mice were used for most of the phenotype

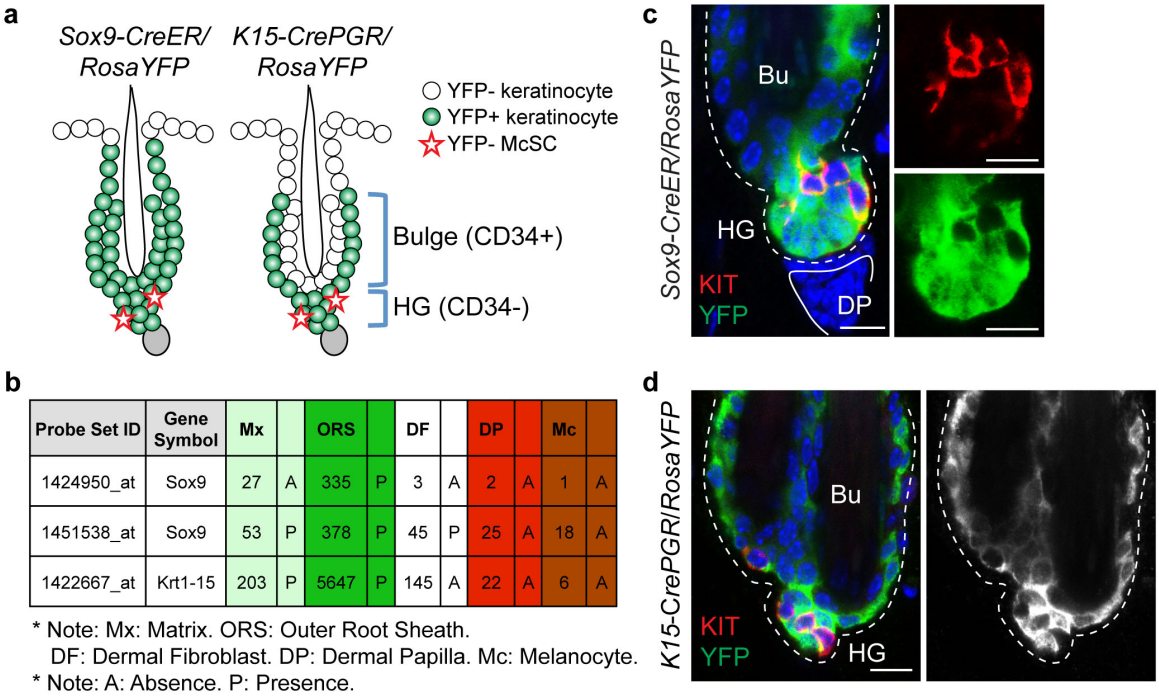

b

Probe Set ID	Gene Symbol	Mx		ORS		DF		DP		Mc	
1424950_at	Sox9	27	A	335	P	3	A	2	A	1	A
1451538_at	Sox9	53	P	378	P	45	P	25	A	18	A
1422667_at	Krt1-15	203	P	5647	P	145	A	22	A	6	A

* Note: Mx: Matrix. ORS: Outer Root Sheath.
DF: Dermal Fibroblast. DP: Dermal Papilla. Mc: Melanocyte.
* Note: A: Absence. P: Presence.

Figure 3-2. Two inducible-Cre lines used in this study to ablate *Nfib* in hair follicles. **a,** Schematic. *Rosa*^{YFP}*/Cre* reporters show *Sox9*-CreER is active in most of regions in hair follicle and *K15*-CrePGR activity is more specific to the bulge and HG HFSCs after induction. Both are not active in McSCs. **b,** Transcriptional profiling of multiple populations in P4 skin by microarray shows *Sox9* and *K15* (*Krt1-15*) are expressed in ORS but absent in Mc, DP and DF. Array data are from Rendl *et al.*, 2005. **c, d,** Immunofluorescence of *Sox9-CreER/Rosa*^{YFP} and *K15-CrePGR/Rosa*^{YFP} reporters with anti-YFP and KIT antibodies. Note YFP signals are absence in KIT^{+} melanocytes. Bu: Bulge. HG: Hair germ. DP: Dermal papilla. Scale bars: 10 μm (c-d).

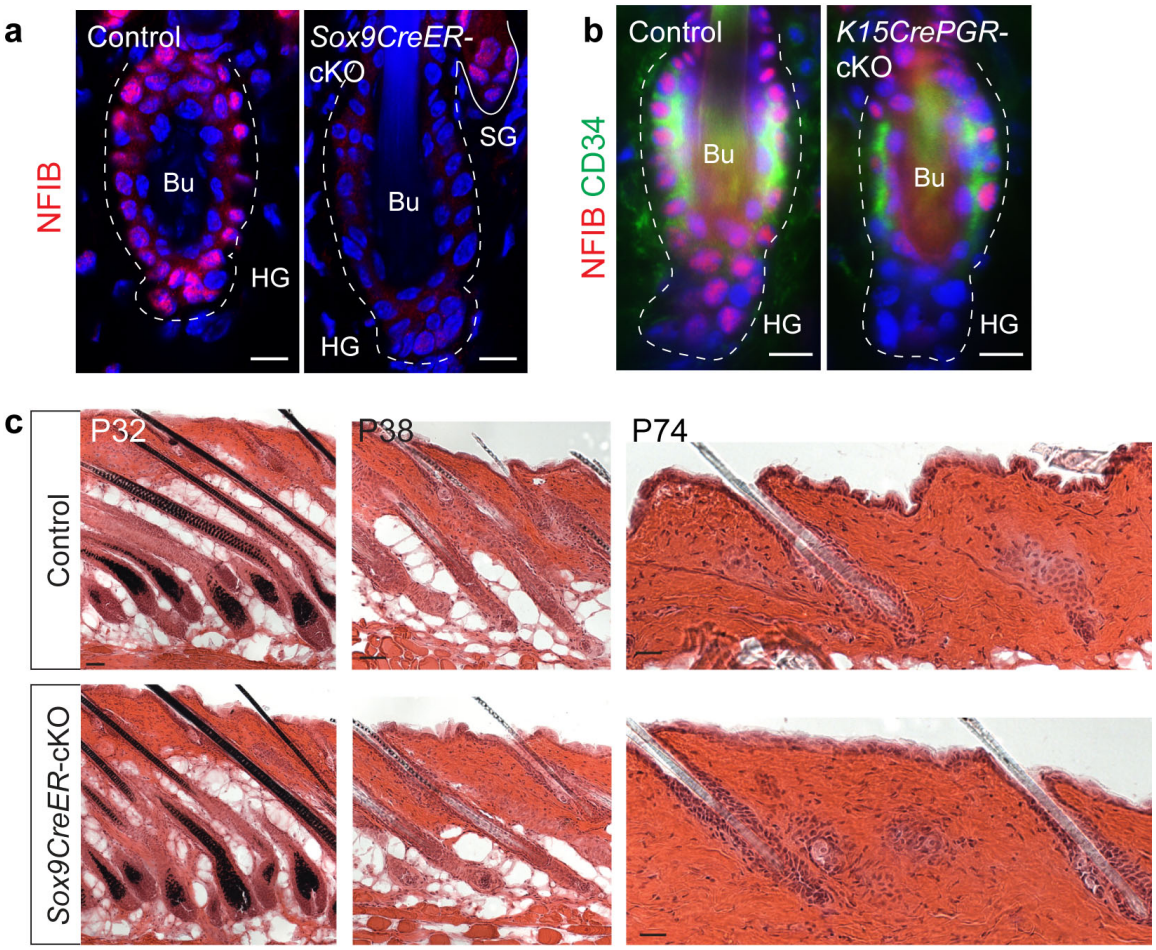

Figure 3-3. Conditional *Nfib* targeting in HFSCs does not perturb hair growth and cycle. a, Immunofluorescence showed *Nfib* targeting in the bulge and HG cells and not in sebaceous gland (SG) by *Sox9-CreER* 4 days after tamoxifen treatment. **b,** Immunofluorescence showed NFIB loss in the $CD34^{+}$ bulge HFSCs and HF cells in *K15-CrePGR* cKO mice 5 days after RU486 treatment. **c,** H&E-stained dorsal skin sections reveal normal hair cycle and follicle architecture upon NFIB loss. Bu: Bulge. HG: Hair germ. Scale bars: 10μm (b); 50 μm (P32, P38 in c); 25 μm (P74 in c).

characterization in the following context while some key results were shown from both lines.

NFIB loss disrupts the stem cell synchrony within the hair follicle

Equally surprising to the absence of HFSC-lineage defects was the presence of melanocyte-lineage abnormalities. Fontana-Masson staining gave the first indication, unveiling atypical pigmentation at the base of both *Sox9-CreER* cKO and *K15-CrePGR* cKO hair follicles but not in control telogen hair follicles (Fig. 3-4a and b). Additional abnormalities in the *Nfib*-null stem cell-residing region were exposed by immunostaining and quantifications, which revealed an increase in KIT^+ and DCT^+ melanocytes throughout both HG and bulge (Fig. 3-4c and d), and that some of the KIT^+ melanocytes, mostly within the HG, were differentiated melanocytes carrying pigment-producing proteins including MITF, TYRP1, and TYR (Fig. 3-4e-g). To further test for melanocyte activity, I mated *Sox9-CreER* cKO and control to *Dct-EGFP* mice and isolated $EGFP^+$ cells from telogen-phase follicles. Melanocyte differentiation markers, e.g. *Mitf, Tyrp1, Tyr*, *Sox10* and *Kit,* were all upregulated in $EGFP^+$ cells from cKO follicles, while genes expressed by both McSCs and differentiated melanocytes showed no change upon NFIB loss (Fig. 3-4h).

A priori, ectopic differentiated melanocytes in *Nfib*-ablated HGs could have arisen from precocious differentiation of nearby McSCs. Alternatively, differentiated melanocytes could have somehow escaped apoptosis during catagen-phase, and therefore derive from the hair bulb. To distinguish between these possibilities, I analyzed melanocyte behavior at each hair cycle stage (Fig 3-5 and 6).

Figure 3-4. NFIB loss enhances McSC self-renewal and perturbs McSC activity. Analyses shown were from second telogen hair follicles. **a, b,** Ectopic pigmentation in telogen cKO HG of *Sox9-CreER* and *K15-CrePGR* lines as detected by *Fontana-Masson* melanin staining. Quantifications show the percentage of melanin$^+$ hair follicles in skin cross-sections (>40 hair follicles per mouse sample, n=3 mice per experiment). **c-g,** Immunofluorescence and quantifications (*Sox9-CreER* cKO and control mice). Quantifications were conducted on skin cross sections (>30 hair follicles per mouse sample, 2-3 mice per experiment). **c, d,** Increased melanocyte numbers in telogen cKO hair follicles. KIT and DCT mark both McSCs and differentiated melanocytes. **e-g,** Ectopic presence of differentiated melanocytes in telogen cKO HFs. MITF, TYRP1 and TYR are differentiated melanocyte markers. Quantifications of the percentage of double positive melanocytes (KIT$^+$ together with MITF$^+$, TYRP1$^+$ or TYR$^+$) among KIT-only cells in the bulge and HG per hair follicle cross section. **h,** Quantitative PCR on FACS-isolated melanocytes. *Dct-EGFP*/*Sox9-CreER* cKO and *Dct-EGFP* control mice were used to fluorescently tag melanocytes for purification. Bu: Bulge. HG: Hair germ. DP: Dermal papilla. Ctrl: control. Scale bars: 10μm. Error bars indicate s.e.m.

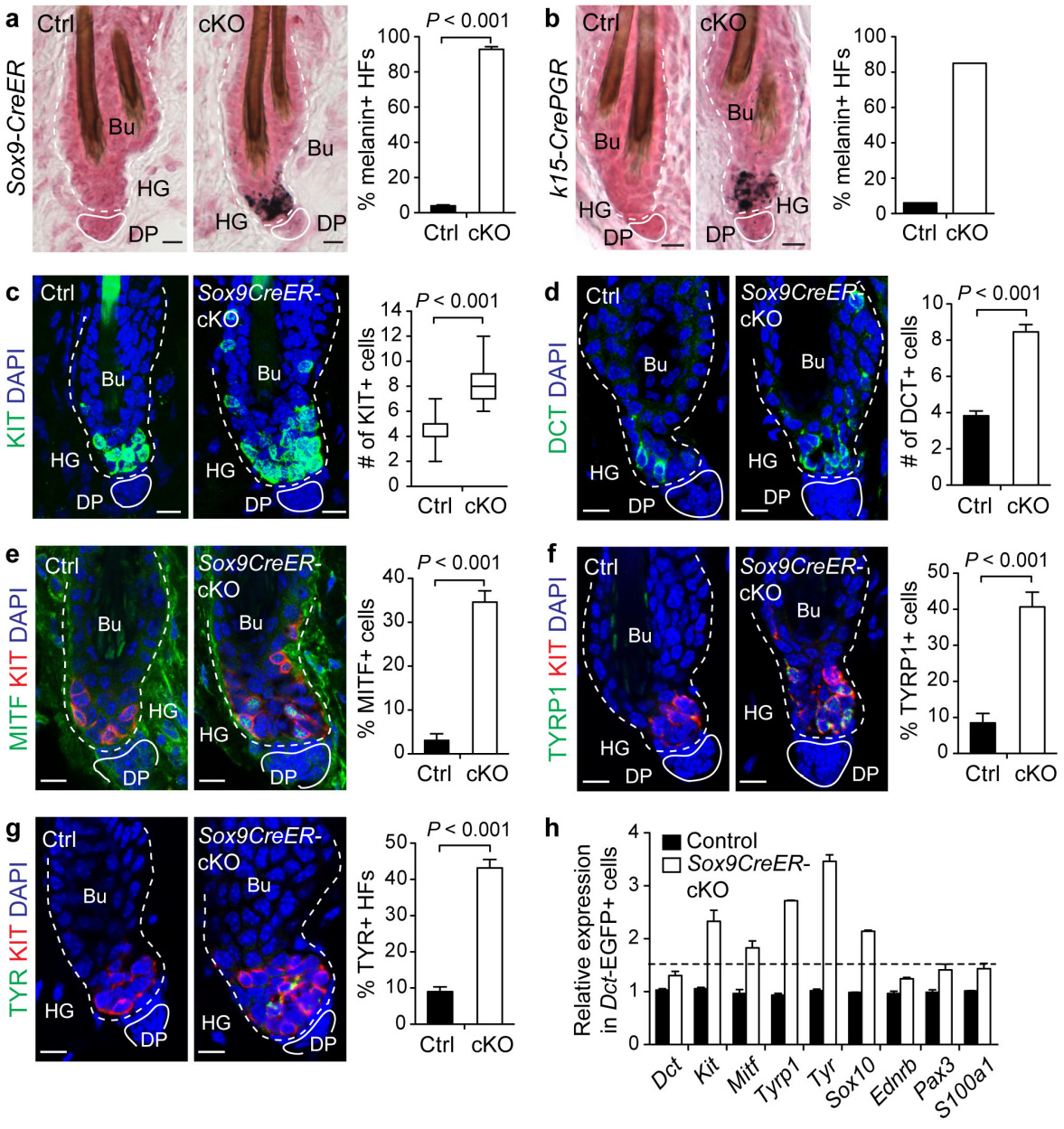
a
Sox9-CreER
Ctrl
cKO
Bu
HG
DP
% melanin+ HFs
P < 0.001
Ctrl cKO
b
k15-CrePGR
c
KIT DAPI
Sox9CreER-cKO
# of KIT+ cells
d
DCT DAPI
# of DCT+ cells
e
MITF KIT DAPI
% MITF+ cells
f
TYRP1 KIT DAPI
% TYRP1+ cells
g
TYR KIT DAPI
% TYR+ HFs
h
Relative expression in Dct-EGFP+ cells
Control
Sox9CreER-cKO
Dct
Kit
Mitf
Tyrp1
Tyr
Sox10
Ednrb
Pax3
S100a1

During anagen, TYRP1^{+} EGFP^{+} melanocyte numbers were as wild-type levels in the *Sox9-CreER* cKO bulge/upper ORS, and were restricted to their customary location in HF bulb (more specifically upper matrix), where pigment transfer to the differentiating recipient hair cells occurred normally (Fig. 3-5a and f-g). In contrast to differentiated melanocytes, TYRP1^{-} EGFP^{+} McSCs sustained their higher levels, where they remained largely in the *Sox9-CreER* cKO bulge/upper ORS but also spread to lower ORS ectopically (Fig. 3-5a and g). At catagen, TYRP1^{+} or TYR^{+} melanocytes (EGFP^{+} and KIT^{+}) underwent apoptosis and were eliminated by mid-catagen in both control and *Sox9-CreER* cKO hair bulbs (Fig. 3-5b-c and g). However, as the DP returned and were close to stem cell-residing region during late catagen to telogen, TYRP1^{+} or TYR^{+} melanocyte numbers again soared, persisting until the next anagen (Fig. 3-5d-e and f-g). On the other hand, it is the time at which McSCs dropped transiently in the *Sox9-CreER* cKO bulge/HG, when McSCs near DP precociously differentiated (Fig. 3-5g).

Taken together, these results pinpointed McSC increase and differentiation defects in the *Nfib*-ablated hair follicles; furthermore, the DP proximity seemed to affect primarily the uncoupling and premature differentiation of McSCs rather than self-renewal (Fig. 3-6). In addition, McSCs in anagen stem-cell-residing region were still negative for TYRP1 even in one-year-old *Sox9-CreER* cKO hair follicles (Fig. 3-5f), indicating that ectopic differentiated melanocytes from telogen do not accumulate within the stem cell residing region over hair cycles.

Figure 3-5. Ectopic differentiation of McSCs induced by NFIB loss occurs from late catagen. a-e, Immunofluorescence with indicated antibodies (*Sox9-CreER* cKO and control mice). **a,** In both cKO and control HFs, lineage committed melanocytes (TYRP1$^+$ *Dct*-EGFP$^+$) are only present in the upper matrix (Mx) of hair bulb (HB) but not in the stem cell-residing resgion including the bulge (Bu) and upper ORS (upORS). Note the number of McSCs is increased in cKO HFs and undifferentiated melanocytes also propagate to lower ORS in anagen. **b-c,** Differentiated melanocytes (TYRP1$^+$/ or TYR$^+$/KIT$^+$) disappear from both cKO and control HFs during mid catagen when the hair bulb, which encases the DP, is degenerated. The DP is spared and draws upward to the stem cell-residing region at the end of catagen. **d-e,** During late catagen, melanocytes close to DP precociously express differentiating markers including TYRP1 and TYR in *Nfib* cKO hair follicles. **f,** Percentage of differentiated melanocytes (TYRP1$^+$ with *Dct*-EGFP$^+$ in anagen hair follicles and with KIT$^+$ in catagen/telogen hair follicles) among total melanocytes (EGFP$^+$ of anagen hair follicles and KIT$^+$ of catagen/telogen hair follicles) in the stem cell (SC)-residing region at different hair follicle stages (anagen/catagen: upper ORS; telogen: bulge and HG) in skin cross sections. **g,** Quantifications of the number of melanocytes (MCs) in hair follicles at different hair follicle stages in skin cross sections. Co-staining of TYRP1 with *Dct*-EGFP$^+$ in anagen hair follicles and with KIT$^+$ in catagen/telogen hair follicles. The regions examined in telogen hair follicles included the bulge and HG. Ana: anagen. Cata: catagen. Telo: telogen. Bulb: hair bulb. Ctrl: control. Scale bars: 25 μm (a-b); 10 μm (c-e). *P<0.001. Error bars indicate s.e.m.

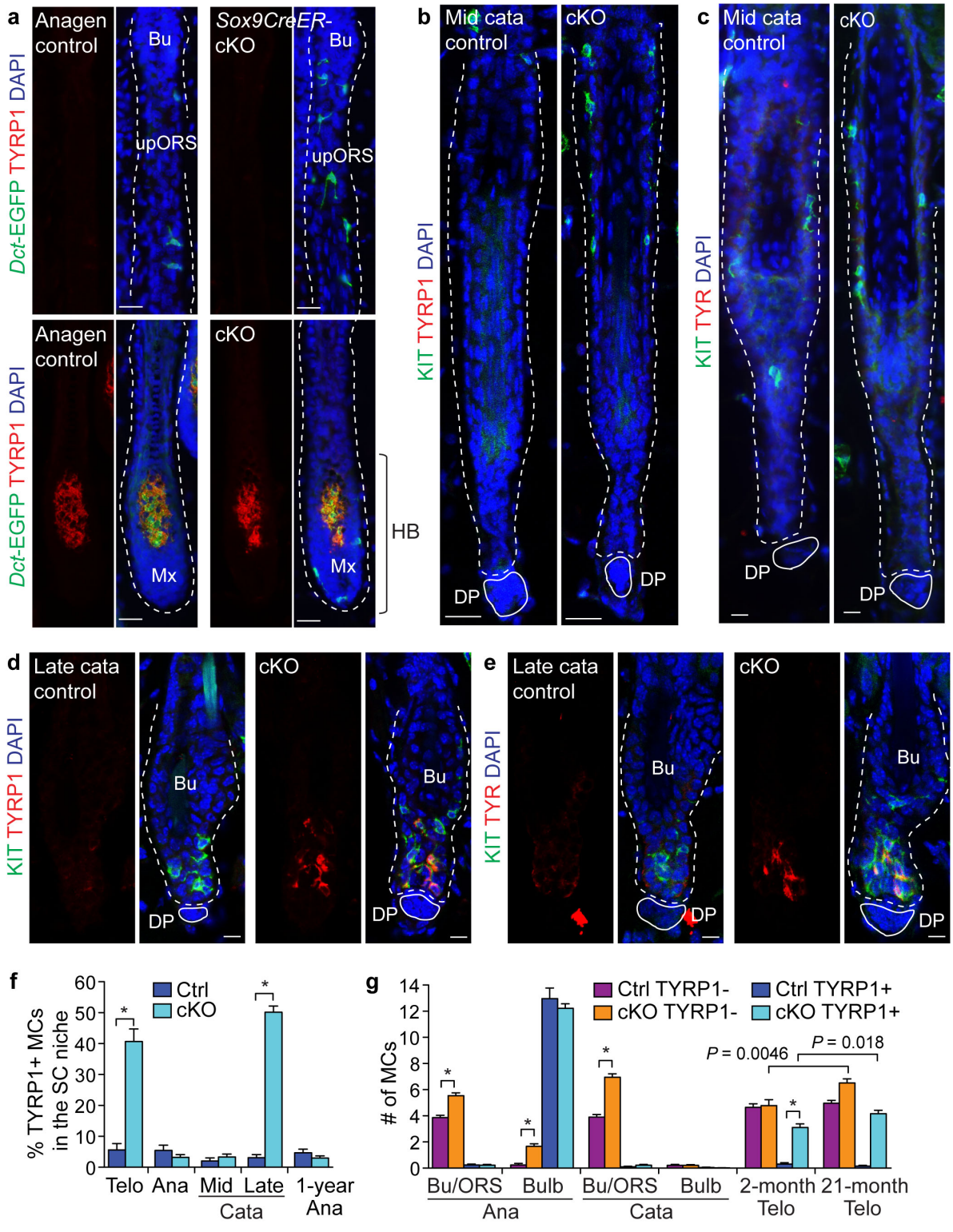
a
Anagen control
Bu
upORS
Sox9CreER-cKO
Bu
upORS
Dct-EGFP TYRP1 DAPI
Anagen control
Mx
cKO
Mx
HB
b
Mid cata control
cKO
KIT TYRP1 DAPI
DP
DP
c
Mid cata control
cKO
KIT TYR DAPI
DP
DP
d
Late cata control
Bu
DP
cKO
Bu
DP
KIT TYRP1 DAPI
e
Late cata control
Bu
DP
cKO
Bu
DP
KIT TYR DAPI
f
% TYRP1+ MCs in the SC niche
Ctrl
cKO
Telo
Ana
Mid
Late
Cata
1-year Ana
g
# of MCs
Ctrl TYRP1-
cKO TYRP1-
Ctrl TYRP1+
cKO TYRP1+
P = 0.0046
P = 0.018
Bu/ORS
Bulb
Ana
Bu/ORS
Bulb
Cata
2-month Telo
21-month Telo

Finally, if McSCs more distant from DP were still fully functional in cKO animals, then the hair coat should escape graying, customarily featured in McSC differentiation mutants (Inomata et al., 2009; Nishimura et al., 2010; Rabbani et al., 2011; Tanimura et al., 2011). Indeed, hair coats of aged *Sox9-CreER* cKO mice were fully pigmented and McSC levels were sustained (Fig. 3-5g and 3-7a). Interestingly in older *Sox9-CreER* cKO mice, black-pigmented dermal cells swarmed HFs and were even visible from the skin surface (Fig. 3-7a and b). Although dermal melanoblasts exist in certain skin regions such as ear, and have been reported to differentiate in backskin under certain aberrant conditions (Aoki et al., 2009), very few $TYRP1^{+}$ melanocytes were found in the dermis of *Sox9-CreER* cKO mice (Fig. 3-7c). Rather, a number of cells encompassing this pigment were Mac1-positive with features of macrophages (Fig. 3-7d). Irrespective of whether the pigment-laden vacuoles within the dermal cells reflected

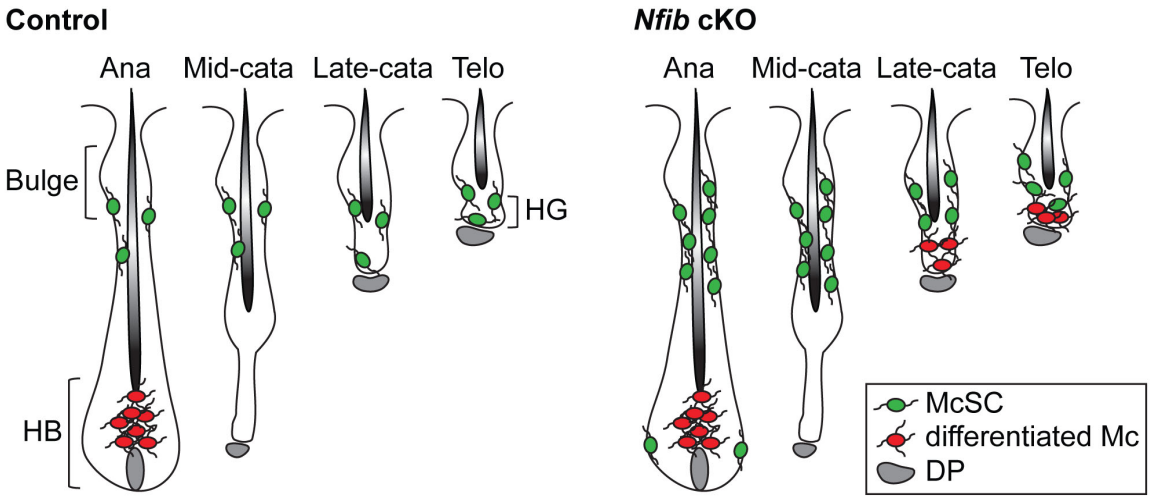

Figure 3-6. Schematic summary of melanocyte behavior upon NFIB loss. In anagen, *Nfib* ablation in HFSCs increases McSC numbers, whereas hair pigmentation is unaffected concomitant with normal differentiated melanocyte (Mc) numbers in cKO hair bulb. Upon follicle degeneration, however, the proximity of DP to the stem cells at the end of catagen induces precocious McSC differentiation in *Nfib*-ablated hair follicles.

indirect uptake of dying, pigmented cells, or direct uptake of pigment from McSCs, these defects made the normalcy of the hair coat of aged *Sox9-CreER* cKO mice all the more remarkable. Taken together, these data provided compelling evidence that NFIB loss in HFSCs affects the timing of melanocyte differentiation without compromising McSC biology and/or function. In this regard, the *Nfib*-cKO mutant phenotype differed from most melanocyte-differentiation mutants, which exhibit hair graying reflective of global McSC malfunction (Inomata et al., 2009; Nishimura et al., 2010; Rabbani et al., 2011; Tanimura et al., 2011).

Premature transfer of pigment promotes apoptotic cell death of hair follicle stem cells in the NFIB-deficient hair follicles

Ultrastructural analysis unveiled new defects of the stem cells in hair follicles. In the NFIB-deficient hair follilces, melanocytes (pseudocolored-red) closest to the DP (pseudocolored-blue) indeed displayed features of differentiated melanocytes, including pigment granules and immature melanosomes (Fig. 3-8a and b). Surprisingly however, adjacent HFSCs (pseudocolored-green) in the HG also displayed pigment granules (Fig. 3-8a). Their epithelial identity was evidenced by keratin filament bundles, desmosomes and hemidesmosomes. Although poorly understood, hair cell uptake of pigment from differentiated melanocytes is thought to be dependent upon Foxn1 (Weiner et al., 2007), expressed by differentiating matrix cells but not by HFSCs (Lien et al., 2011).

Inappropriate accumulation of pigment seemed calamitous for quiescent telogen-phase HFSCs in the HG: it elicited their apoptotic death, as reflected by condensed

chromatin, mitochondrial destruction, and cleaved Caspase-3-immunolabeling (Fig. 3-8a, 3-9a and d). In addition, unaffected neighboring K5-positive HG cells proliferated, as judged by Ki67 and incorporation of nucleotide analogue EdU (Figs. 3-9b-d). Although HG proliferation is a normal sign of telogen to anagen transition (Greco et al., 2009), precocious hair cycle entry did not accompany telogen-phase HG proliferation in *Nfib*-ablated HFs.

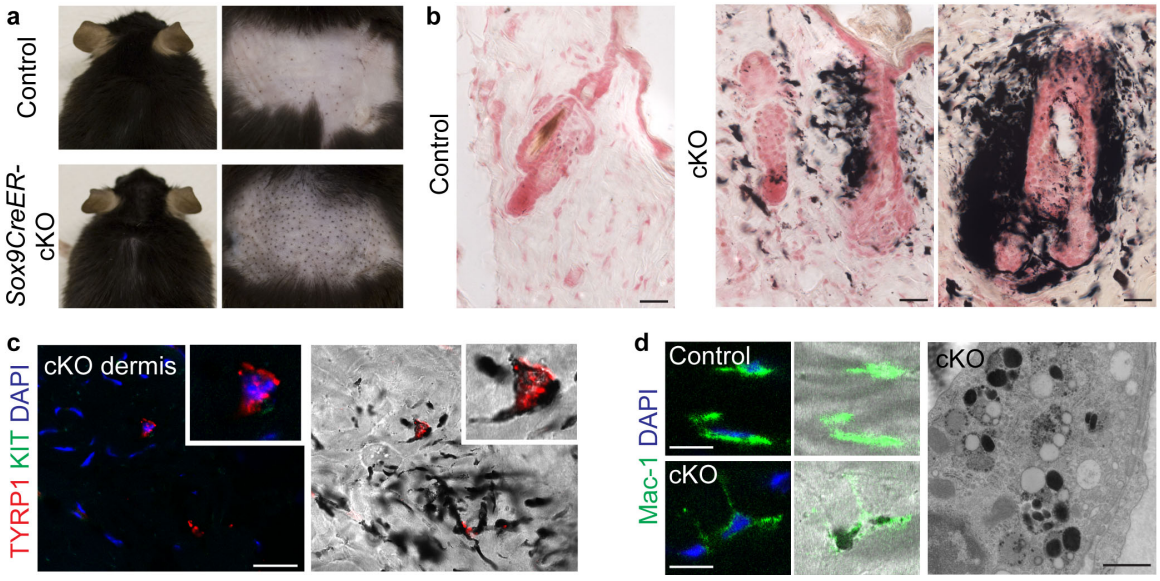

Figure 3-7. Hyperpigmentation in the dermis of aged *Sox9-CreER/Nfib* cKO skin. a, Black pigmented spots on the skin surface of control and cKO mice. **b,** Melanin is detected by *Fontana-Masson* staining. Note hyperpigmentation in the dermis of *Nfib*-cKO animals become more severe with age. **c,** $TYRP1^{+}KIT^{-}$ dermal melanocytes in *Nfib* cKO skin. Given that $TYRP1^{+}KIT^{-}$ dermal melanocytes are not frequently seen in the pigmented area, they could not account for the majority of pigmented cells in the dermis. **d,** Pigmented macrophages marked by Mac-1 and identified by ultrastructural analysis were prevalent in the dermis of old *Nfib*-cKO skin. EM image is courtesy of H. Amalia Pasolli. Scale bars: 25 μm (b); 10 μm (c,d).

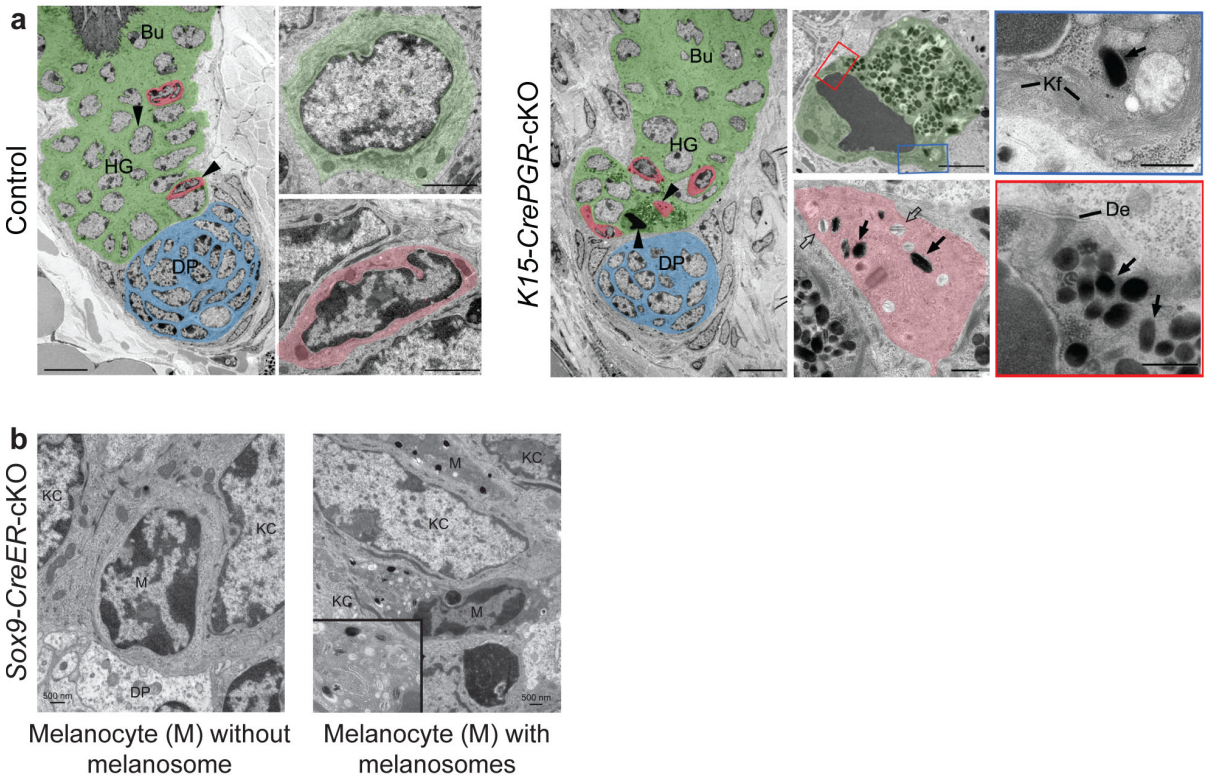

Figure 3-8. Ultrastructure of *Nfib* cKO hair follicles. a, *K15-CrePGR* cKO and control hair follicles. Pseudo-coloring highlights distinct cell types in the hair follicles: green-HFSC; red-melanocyte; blue-DP. Arrowheads mark cells shown at higher magnification. Note the presence of differentiated melanocytes in cKO hair follicles, judged by that their cytoplasm contains immature (open arrow) and mature (solid arrow) melanosomes, the structure used for synthesizing pigments and absent in McSCs. Note pigment-laden apoptotic HFSC whose boxed regions at higher magnification reveal condensed chromatin, degenerating mitochondrion, keratin filaments (Kf), desmosomes (De) and melanosomes. **b,** Undifferentiated (without melanosomes) and differentiated (containing melanosomes) melanocytes (M) were observed in *Sox9-CreER* cKO hair follicles. Kc: keratinocyte. DP: dermal papilla. Scale bars: 10 μm (low magnifications in a); 2 μm (apoptotic HFSC in a); 0.5 μm (cytoplasmic segments and melanocyte in a and b). Courtesy of H. Amalia Pasolli.

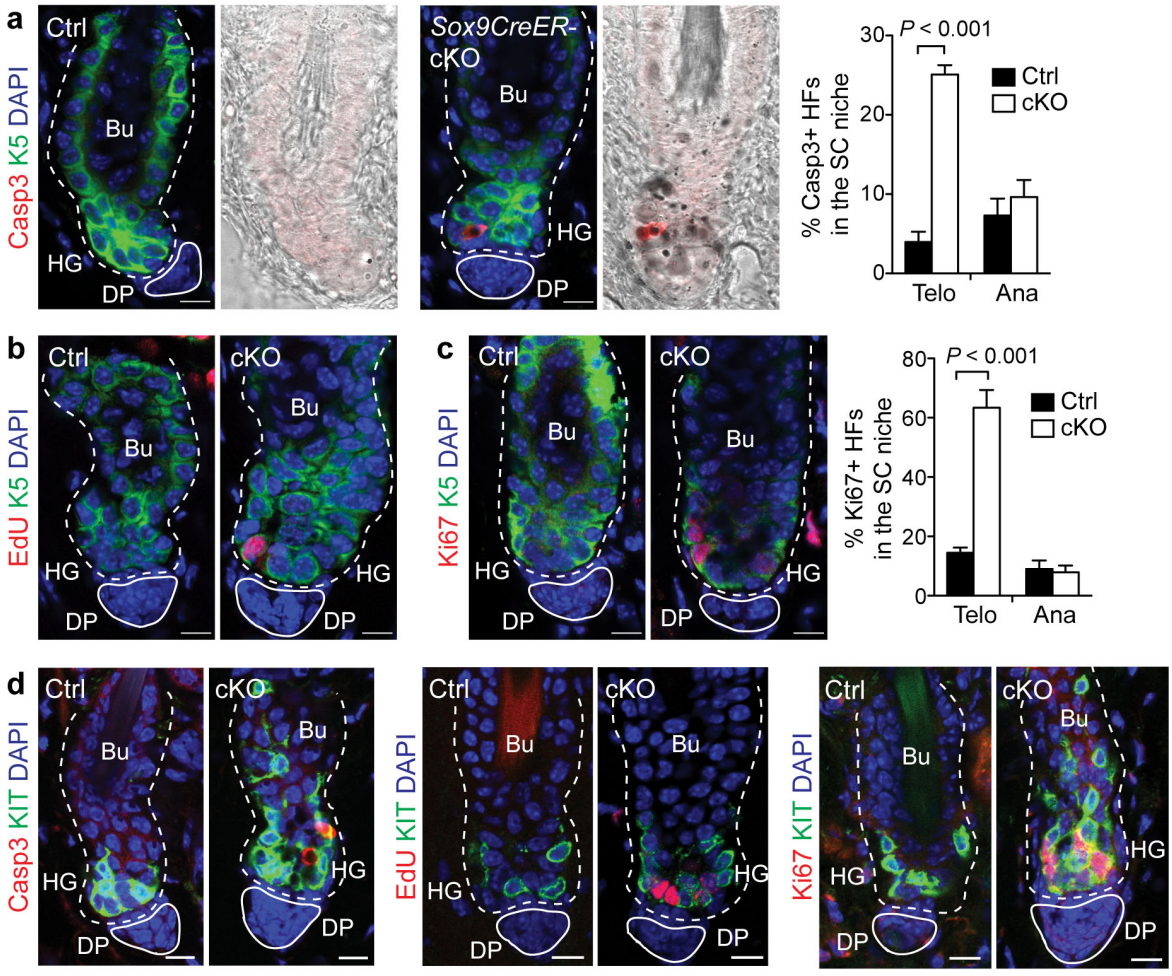

Figure 3-9. Apoptosis and proliferation of *Nfib* cKO HFSCs. Immunofluorescence with indicated antibodies (*Sox9-CreER* cKO and control mice). **a,** Activated caspase3 (Casp3) antibody marks $K5^+$ apoptotic cKO HFSCs, seen in telogen but not anagen. Quantifications of the percentage of hair follicles with $Casp3^+$ $K5^+$ cells in the bulge and HG in skin cross sections. **b-c,** Increased HFSC proliferation in telogen but not anagen *Nfib*-cKO HFs. Assessment was by EdU incorporation (administered twice, 24h before analysis) and Ki67 immunostaining. Quantifications of the percentage of hair follicles with $Ki67^+$ $K5^+$ cells in the bulge and HG in skin cross sections. **d,** Apoptotic ($Casp3^+$) and proliferative (EdU^+ or $Ki67^+$) cells in cKO HFs are not KIT^+ melanocytes. Bu: Bulge. HG: Hair germ. DP: Dermal papilla. Ctrl: control. Telo: telogen. Ana: anagen. Scale bars: 10μm. Error bars indicate s.e.m.

Apoptotic and proliferative defects of HFSCs disappeared in anagen (Fig. 3-9a and c), concomitant with the movement of differentiated melanocytes from the bulge/upper ORS to the hair bulb (Fig. 3-5a and 3-6). These results imply that apoptosis and hyperproliferation of *Nfib*-null HFSCs depend upon precocious differentiation of neighboring McSCs. They also suggest that when precociously differentiated melanocytes inappropriately bequeath pigment to HFSCs rather than their customary differentiated progeny (hair cells), pigment-laden HFSCs are unable to cope, while healthy HFSC neighbors proliferate to restock the stem cell population.

RNA-seq and ChIP-seq analyses identify endothelin 2 (*Edn2*) as a direct NFIB-regulated gene

To identify factors mediating the molecular miscommunication between HFSCs and McSCs in hair follicles, I used high throughput RNA-seq to transcriptionally profile bulge and HG HFSCs. Fluorescence activated cell sorting (FACS) of skins of *K15-CrePGR/Rosa*^{YFP}/*Nfib*$^{fl/fl}$ (cKO) and *Nfib*$^{fl/+}$ (control) mice were used for purifying HFSCs. Restricted YFP expression pattern in *K15-CrePGR/Rosa*^{YFP} mice provided an advantage to enrich bulge (YFP^{+}Sca1^{-}α6^{high}CD200^{+}CD34^{+}) and HG (YFP^{+}Sca1^{-}CD200^{+}CD34^{-}) HFSCs during FACS (Fig. 3-2a and 3-10a). RNA-seq results confirmed the ablation of *Nfib* exon 2, encoding the DNA-binding domain, in *K15-CrePGR* cKO cells (Fig. 3-10b).

Of 800-1000 mRNAs that were changed by ≥2X in NFIB-deficient HFSCs relative to control, 145 were upregulated and 99 were downregulated in both bulge and HG (Fig. 3-10c and Table 1). I selected ten of these genes and validated their differences by qPCR in independently purified samples (Fig. 3-10d). Notably absent among the 244

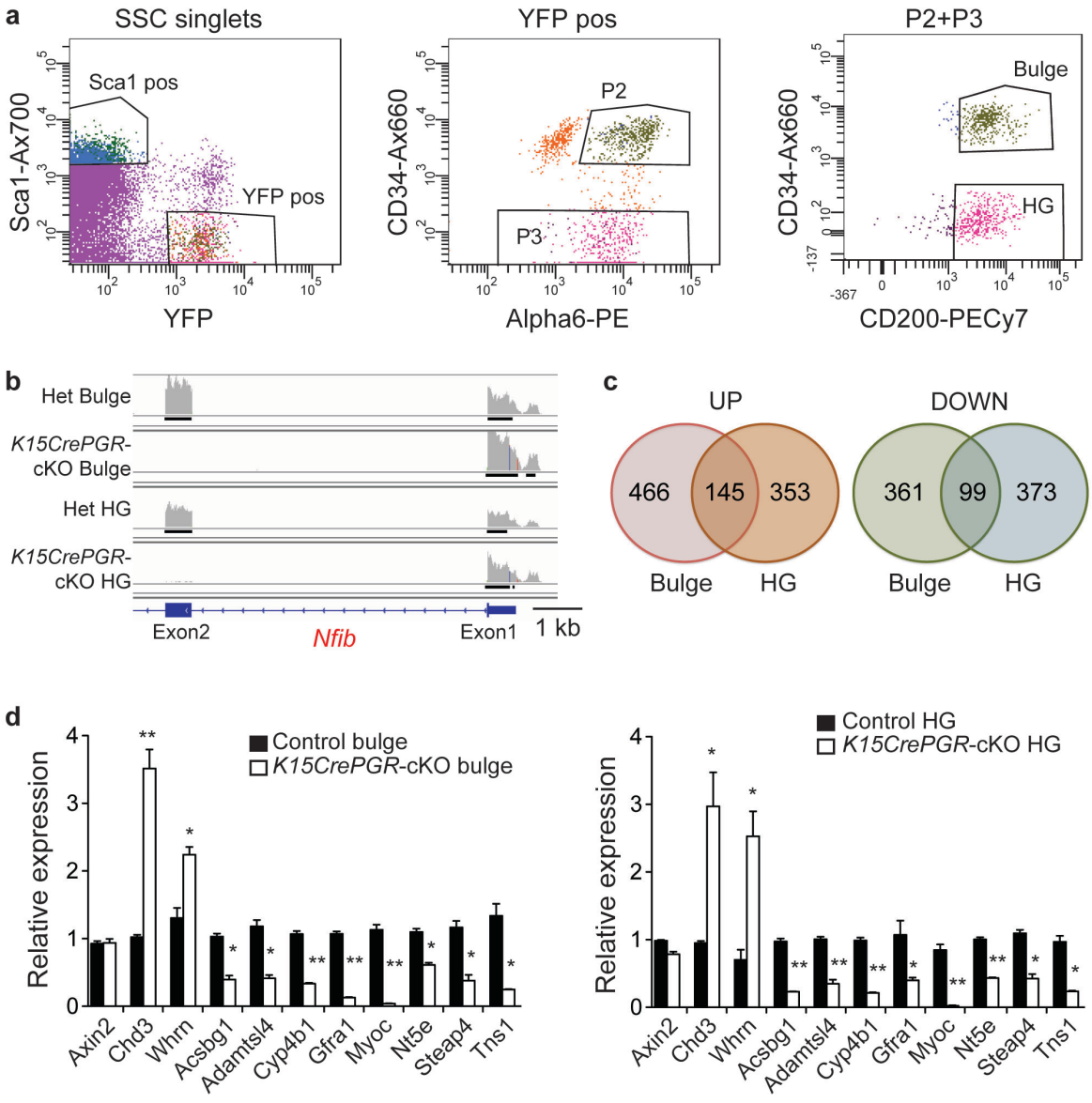

Figure 3-10. Isolation of bulge and HG HFSCs from *K15-CrePGR/Nfib* cKO skins for RNA-seq analysis. a, FACS isolation. Bulge HFSCs were isolated with markers YFP^{+} Sca1^{-} α6^{high} CD34^{+} CD200^{+}; HG HFSCs with the markers YFP^{+} Sca1^{-} CD34^{-} CD200^{+}. **b,** Visualization of RNA-seq profiles in *Nfib*. Note the ablation of *Nfib* exon 2 in cKO cells. **c,** Venn diagrams representing gene expression changes in cKO bulge/HG cells compared to control by RNA-seq analysis (≥ 2-fold). **d,** Quantitative PCR confirms the results from RNA-seq analysis. *$P < 0.05$. **$P < 0.001$. Error bars indicate s.e.m.

changes were *Foxn1, Fgf2, Nog, Egfr, F2rl1* and derivatives of *Pomc1*, all of which were previously implicated in melanocyte differentiation and/or pigment-transfer in skin (D'Orazio et al., 2006; Fitch et al., 2003; Weiner et al., 2007). Also absent were genes involved in TGFβ/BMP signaling, known to function in maintaining quiescence of HFSCs. Similarly, NFIB loss did not seem to affect canonical Wnt signaling, a key stimulus for both SC activity and fate commitment: the Wnt-sensitive target gene *Axin2* was unchanged in NFIB-deficient HFSCs, and upregulated Wnt pathway genes included negative and positive Wnt regulators (indicated by arrows in Fig. 3-11).

These results were in good agreement with the normal hair cycle displayed by *Nfib*-cKO skin (Fig. 3-3c), and with the prediction that had there been major perturbations in any of these signaling pathways, both stem cell populations—not just McSCs—should have been affected. Conversely, hair follicles from mice genetically defective for Wnt, BMP and TGFβ signaling still displayed NFIB protein in the bulge HFSCs, and *Nfib* mRNA levels did not appear to be dramatically changed in these mutants (Fig. 3-12a and b). Thus at least within HFSCs, these signaling pathways appeared to be refractory to loss of NFIB, and NFIB appeared to be refractory to these signaling pathways.

To identify direct NFIB target genes in HFSCs that might act to stimulate McSCs, I performed chromatin immunoprecipitation with deep sequencing (ChIP-seq) analysis. I collaborated with Olivier Elemento and his postdoc Jenny Giannopoulou at at Weill Cornell Medical College for bioinformatics analyses. At first, I tested the performance of NFIB antibody for immunoprecipitation (IP) in enriched hair follicle cells from newborn skins (Fig. 3-13). NFIB antibody raisedfrom rabbits were used for IP followed by

Figure 3-11. Pathway analysis of RNA-seq results. The heatmap shows the enriched biological processes (Gene Ontology) for the up- or down-regulated genes in *K15-CrePGR* cKO bulge and HG HFSCs relative to control in RNA-seq results, compared to the rest of the known genes in RefSeq annotation database. The categories indicate genes over/under expressed in cKO bulge (Bulge Up/Bulge Down), and over/under expressed in HG HFSCs (HG Up/HG Down). Note: for this analysis, we excluded the small subset of pigment mRNAs, which might appear to arise from ectopic melanosome uptake by HFSCs nearest the DP. Courtesy of Eugenia Giannopoulou.


Enrichment
p=1e-04
p=1e-02
p=1
p=1e-02
p=1e-04
Depletion
Rest RefSeq genes
Bulge Up genes
HG Up genes
Bulge Down genes
HG Down genes
0
1
2
3
4
Chromatin modification, GO:0016568
Fat-soluble vitamin metabolic process, GO:0006775
Negative regulation of alpha-beta T cell activation, GO:0046636
Regulation of organ growth, GO:0046620
Homeostasis of number of cells within a tissue, GO:0048873
Positive regulation of B cell proliferation, GO:0030890
Positive regulation of B cell activation, GO:0050871
Positive regulation of organ growth, GO:0046622
Regulation of inhibitory postsynaptic membrane potential, GO:0060080
Membrane hyperpolarization, GO:0060081
Eating behavior, GO:0042755
Wnt receptor signaling pathway, GO:0016055
Negative regulation of Wnt receptor signaling pathway through beta-ca
Cochlea development, GO:0090102
Outer ear morphogenesis, GO:0042473
Positive regulation of developmental process, GO:0051094
Wnt receptor signaling pathway, calcium modulating pathway, GO:000722
Positive regulation of pigment cell differentiation, GO:0050942
Positive regulation of melanocyte differentiation, GO:0045636
Mammary duct terminal end bud growth, GO:0060763
Positive regulation of developmental pigmentation, GO:0048087
Regulation of peptidyl-serine phosphorylation, GO:0033135
Regulation of pigment cell differentiation, GO:0050932
Regulation of melanocyte differentiation, GO:0045634
Mammary gland duct morphogenesis, GO:0060603
Wnt receptor signaling pathway, planar cell polarity pathway, GO:0060
Cochlea morphogenesis, GO:0090103
Nucleobase, nucleoside and nucleotide catabolic process, GO:0034656
Nucleobase, nucleoside, nucleotide and nucleic acid catabolic process
Cellular nitrogen compound catabolic process, GO:0044270
Digestion, GO:0007586
Nucleoside metabolic process, GO:0009116
Positive regulation of synaptic transmission, GABAergic, GO:0032230
Regulation of synaptic transmission, GO:0050804
Regulation of transmission of nerve impulse, GO:0051969
Regulation of neurological system process, GO:0031644
Ribonucleoside metabolic process, GO:0009119
Negative regulation of defense response, GO:0031348
Regulation of cell-substrate adhesion, GO:0010810
Positive regulation of cell-substrate adhesion, GO:0010811
Positive regulation of transcription factor import into nucleus, GO:0
Positive regulation of NF-kappaB import into nucleus, GO:0042346
Cell cycle phase, GO:0022403
Cell cycle, GO:0007049
Regulation of cell cycle, GO:0051726
Cell cycle process, GO:0022402
Mitosis, GO:0007067
Nuclear division, GO:0000280
M phase of mitotic cell cycle, GO:0000087
Organelle fission, GO:0048285
Chromosome segregation, GO:0007059
Mitotic cell cycle, GO:0000278
Regulation of microtubule-based process, GO:0032886
Leukocyte chemotaxis, GO:0030595
Cell chemotaxis, GO:0060326
Regulation of interleukin-12 production, GO:0032655
Icosanoid metabolic process, GO:0006690
Unsaturated fatty acid metabolic process, GO:0033559
Regulation of establishment of blood-brain barrier, GO:0090210
Hair follicle morphogenesis, GO:0031069
Epidermis morphogenesis, GO:0048730
Extracellular structure organization, GO:0043062
Regulation of cartilage development, GO:0061035
Activation of Ras GTPase activity, GO:0032856
Activation of Rho GTPase activity, GO:0032862
Arginine transport, GO:0015809
Regulation of germinal center formation, GO:0002634
Regulation of synaptic transmission, GABAergic, GO:0032228
Positive regulation of neuron differentiation, GO:0045666
Establishment of apical/basal cell polarity, GO:0035089
Prostanoid metabolic process, GO:0006692
Prostaglandin metabolic process, GO:0006693
Pyrimidine ribonucleoside metabolic process, GO:0046131
Purine nucleoside monophosphate catabolic process, GO:0009128
Purine ribonucleoside monophosphate catabolic process, GO:0009169
Activation of phospholipase C activity by muscarinic acetylcholine re
Adenosine biosynthetic process, GO:0046086
Positive regulation of Rac GTPase activity, GO:0032855
AMP catabolic process, GO:0006196
Vitamin E metabolic process, GO:0042360
Ribonucleoside monophosphate catabolic process, GO:0009158
Pyrimidine base catabolic process, GO:0006208
Gastric acid secretion, GO:0001696
Lysine transport, GO:0015819
Negative regulation of establishment of blood-brain barrier, GO:00902
Nucleobase catabolic process, GO:0046113
Uridine metabolic process, GO:0046108
Activation of Rac GTPase activity, GO:0032863
Ornithine transport, GO:0015822
Regulation of neuron differentiation, GO:0045664
Oxygen transport, GO:0015671
Midgut development, GO:0007494
Leukocyte migration, GO:0050900
M phase, GO:0000279
Gas transport, GO:0015669

Western blotting with the same antibody as well as the antibody raised from different species (mouse), which can avoid antibody heavy-chain and light-chain background on the blot. NFIB proteins were immuneprecipitated by NFIB antibody accompanied with decreased NFIB proteins in the fraction after binding (flow through) (Fig. 3-13).

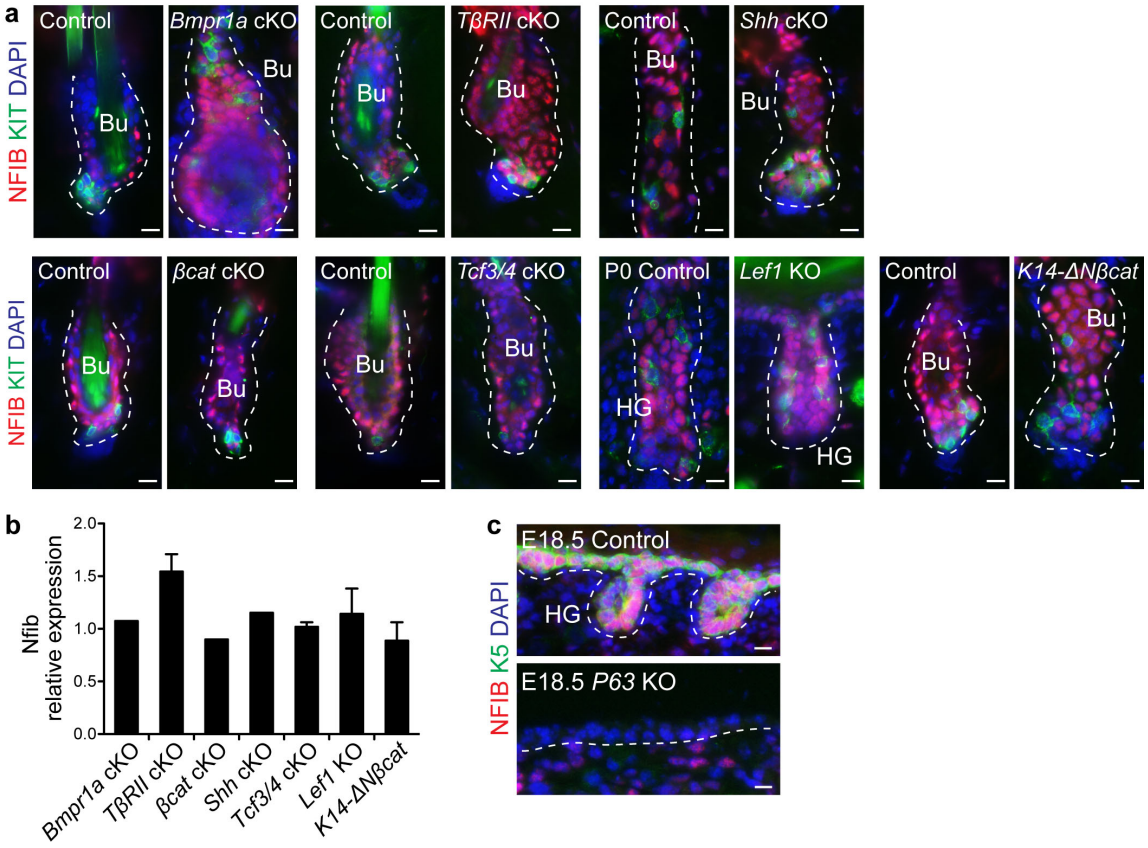

Figure 3-12. NFIB expression in mutants lacking major signaling pathways. a,c, Immunofluorescence with indicated antibodies. Frozen skin sections were from the following genetic backgrounds and where relevant, induced for Cre expression: *K15-CrePGR X Bmpr1a* fl/fl, *K14-Cre X TGFβRII (TβRII)* fl/fl, *K15-CrePGR X Sonic Hedgehog (Shh)* fl/fl, *K15-CrePGR X β-catenin* (*βcat*) fl/fl, *K15-CrePGR X Tcf3(fl/fl) X Tcf4-null, Lef1*-null, *K14-ΔNβcat, P63-null*. **b,** Relative *Nfib* RNA levels in HFSCs FACS-purified from these different backgrounds ($CD34^+\alpha6^+$) followed by transcriptional profiling analyses (full array databases to be reported elsewhere). The HFs ($Pcad^+\alpha6^+$) were isolated from E17.5 *Lef1* KO and control embryos. Bu: bulge. HG: Hair germ. Scale bars: 10 μm. Error bars indicate s.e.m.

Two independent NFIB ChIP-seq experiments were conducted. For each experiment, 10-15 X 10^6 WT bulge HFSCs ($\alpha6^+\beta1^+CD34^+$) from 15-20 mice were isolated by FACS (Fig. 3-14a). Applying immunoprecipitation-grade NFIB antibody to chromatin, I identified 1,449 genes that were directly and reproducibly bound by NFIB (Table 2). NFIB-bound genes included *Krt5 (K5)* (Fig. 3-14b). Intriguingly, like K5 and its regulators of the transcription factor-AP2 (TCFAP2) family, NFIB was lost in most areas of *p63*-null skin (Fig 3-12c). Additionally, *Nfib* is bound by p63 (McDade et al., 2012) and harbors binding motifs for TCFAP2 (data not shown), suggesting a possible link to early epithelial stem cell markers. NFIB peaks were particularly enriched in ±2kb (12%) and upstream 2-50kb (29%) sequences proximal to gene transcription initiation sites compared to genomic representation of each compartment (Fig. 3-14c and d). A *de novo* motif search identified five sequences within these peaks (Fig. 3-14e). Most

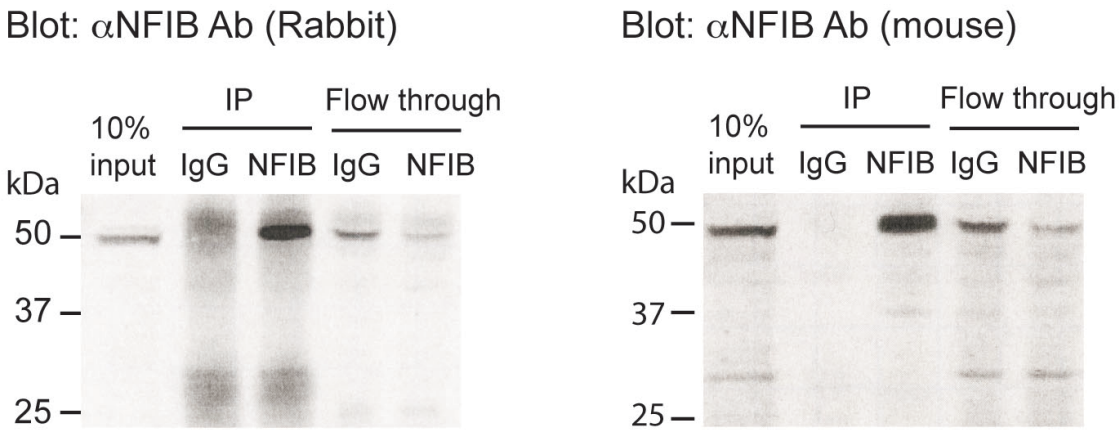

Figure 3-13. Immunoprecipitation with NFIB antibody. Hair follicle cells from newborn skins were used for immunoprecipitation (IP) with NFIB antibody (raised from rabbits) and control IgG produced from rabbits. NFIB proteins were detected by Western blot (Blot) with the same rabbit anti-NFIB antibody and also mouse NFIB antibody to avoid background from antibody heavy chain and light chain. Flow through: the lysate after IP.

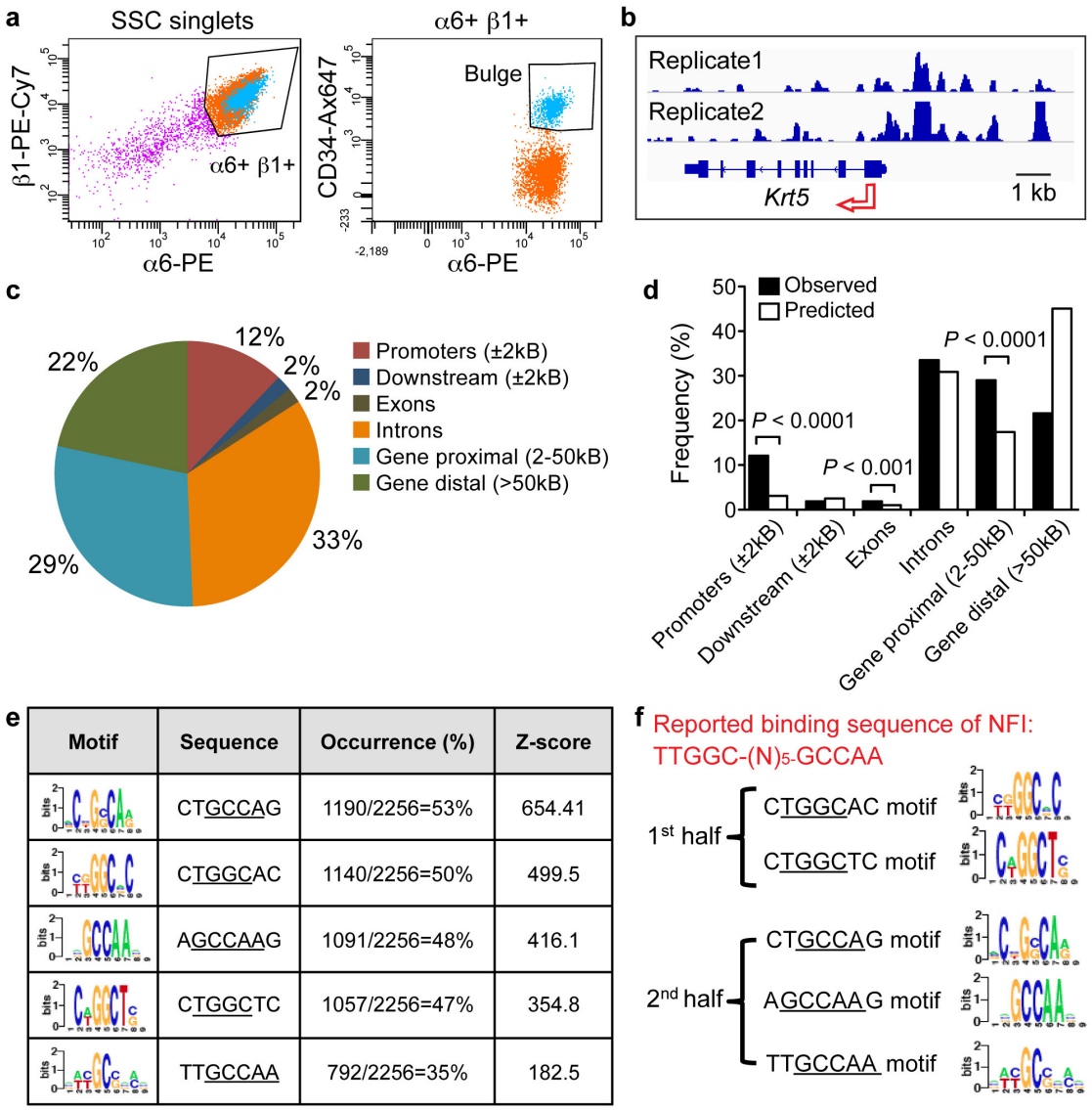

Motif	Sequence	Occurrence (%)	Z-score
	CTGCCAG	1190/2256=53%	654.41
	CTGGCAC	1140/2256=50%	499.5
	AGCCAAG	1091/2256=48%	416.1
	CTGGCTC	1057/2256=47%	354.8
	TTGCCAA	792/2256=35%	182.5

Figure 3-14. Genomic distributions of NFIB ChIP-seq peaks and motif analysis. a, FACS strategy for isolating bulge HFSCs ($\beta1^+\alpha6^+$ $CD34^+$) for NFIB ChIP-seq. **b,** Visualization of NFIB ChIP-seq profiles of *Krt5* promoter. **c,** Genomic distribution of NFIB ChIP-seq peaks relative to RefSeq transcripts. Promoter: within ±2kB of transcription start site. Downstream: within ±2kB of transcription end site. Gene proximal: within upstream 2-50kB of transcription start site. Gene distal: beyond upstream 50kB of transcription start site. **d,** Comparison of the observed NFIB bound peak distribution to the predicted distribution based on the genomic representation of each compartment, using the Binomial test. **e,** The motifs discovered from *de novo* motifs analysis using FIRE program are shown. The percentage of NFIB bound peaks occurrences and the corresponding z-scores are indicated for each motif. **f,** The discovered motifs are grouped based on their similarity to reported first and second halves of the NFIB palindromic motif. **c-e,** courtesy of Eugenia Giannopoulou.

common were TGGC$^{A/T}$ and $^{A/T}$GCCA, which when combined, comprised a palindromic motif (Fig. 3-14f). Notably, NFIB protein self-dimerizes, and its preferred binding motif is a TTGGCANNNTGCCAA palindrome (Roulet et al., 2000).

I next examined how NFIB target genes in HFSCs change in response to NFIB loss. 201 (~14%) NFIB target genes were differentially expressed in *K15-CrePGR* cKO versus control HFSCs (Fig. 3-15). Of these, 44% were upregulated while 56% were downregulated in NFIB-deficient HFSCs. By these criteria, there did not seem to be a strong bias for whether NFIB functions in activation or repression. In contrast, based upon studies from cultured fibroblasts, NFIC has been regarded as an activator (Pjanic et al., 2011).

Searching for possible genes whose altered expression might enhance McSC proliferation and differentiation, I focused on the 33 NFIB-binding genes whose expression was ≥2-fold up- or down-regulated in HFSCs of both bulge and HG upon *Nfib*-ablation (Fig. 3-15). Among them the most attractive of these candidates was the gene *Edn2* encoding endothelin-2. Within the *Edn2* promoter was an NFI-binding palindrome sequence containing an optimal spacer, and in both ChIP-seq replicates, NFIB bound to this site (Fig. 3-16a).

Endothelins are secreted factors with the ability to mediate intercellular crosstalk. All three endothelins stimulate the proliferation and differentiation of cultured melanocytes (Opdecamp et al., 1998; Reid et al., 1996a). Additionally, endothelin-3 is required for neural crest migration and melanocyte specification during embryogenesis (Pla and Larue, 2003), and *Edn1* was recently implicated in Wnt-mediated melanocyte proliferation (Rabbani et al., 2011). Neither *Edn3* nor *Edn1* surfaced on the list of HFSC

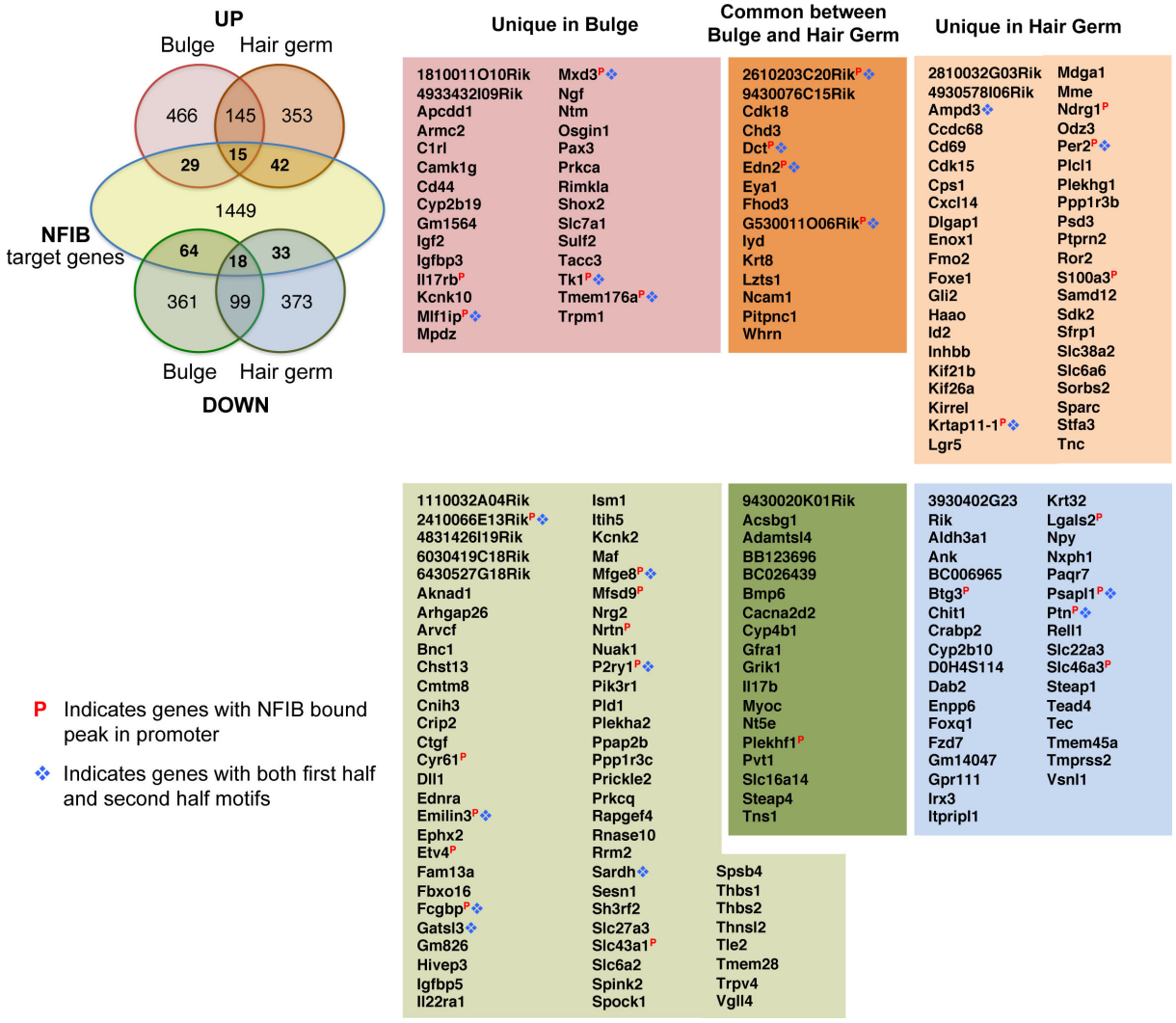

Figure 3-15. Identification of direct NFIB target genes in HFSCs. The Venn diagram on the left shows the comparison between 1449 NFIB direct target genes from ChIP-seq analysis and genes up or down-regulated in *K15-CrePGR* cKO bulge/HG HFSCs from RNA-seq. Genes that are bound by *and* regulated by NFIB are listed. Unique in Bulge or HG means their expression levels are only changed in each population. Common between Bulge and HG indicates genes that are changed in both populations. Genes with NFIB bound peak in their promoter (± 2kb from TSS), and with both halves of NFIB palindromic motif are explicitly marked. Courtesy of Eugenia Giannopoulou.

genes bound by NFIB. Moreover, by RNA-seq and qPCR, *Edn3* was not expressed in HFSCs, and *Edn1* showed very low expression and little change upon NFIB loss (Fig. 3-16b; Table 1). Interestingly, in wild-type follicles, *Edn2* is the only family member that is repressed in telogen HFSCs, but transiently activated in early anagen HFSCs (Lien et al., 2011), and *Edn2* was upregulated >2X-fold in purified *Nfib*-ablated HFSCs relative to controls (Fig. 3-16b; Table 1). Pan anti-endothelin immunolabeling was markedly stronger in *Nfib*-null HFSCs relative to control HFs (Fig. 3-16c). Immunolabeling showed no endothelin expression in McSCs or DP. Finally, since HFSCs express

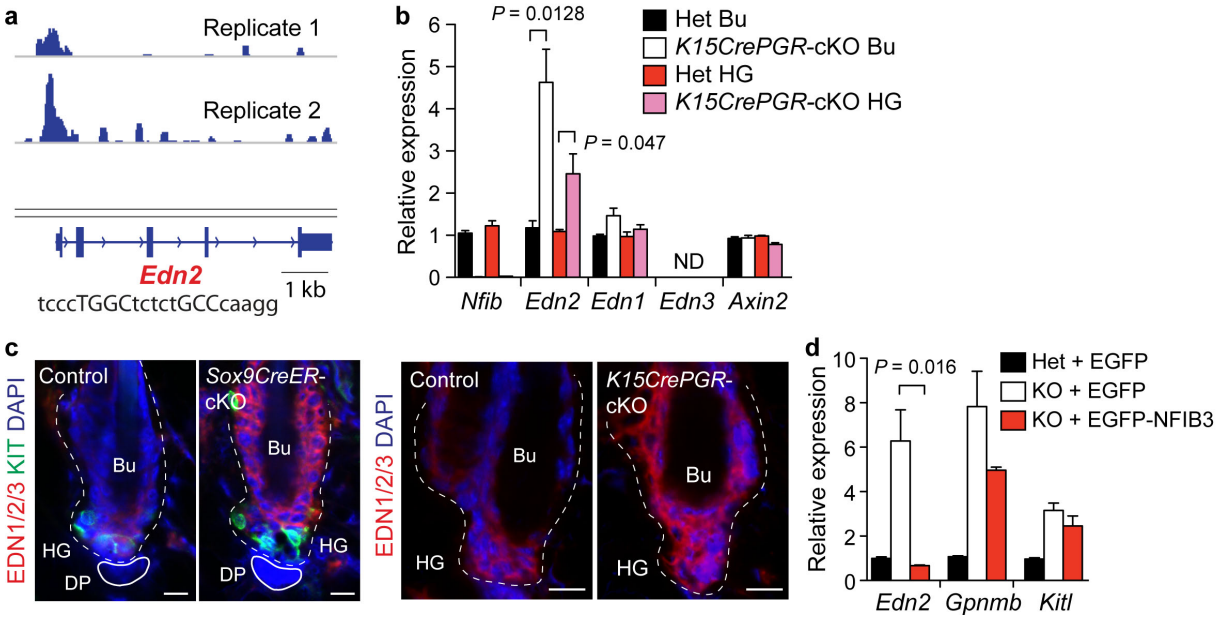

Figure 3-16. RNA-seq and ChIP-seq analyses identify *Edn2* as a direct NFIB-regulated gene. a, NFIB ChIP-seq profiles of *Edn2* promoter. NFIB palindromic-binding-sequence exists within the peak. **b,** Quantitative PCR on FACS-isolated populations confirm RNA-seq results (normalizations to Het). **c,** Immunofluorescence shows ectopic endothelins in *Sox9-CreER* cKO and *K15-CrePGR* cKO hair follicles. **d,** Regulation of *Edn2* expression by NFIB *in vitro*. Quantitative PCR from *Nfib* het or KO keratinocyte cultures transfected with *EGFP* or *EGFP-NFIB3* transgenes. Bu: Bulge. HG: Hair germ. DP: Dermal papilla. ND: not determined. Scale bars: 10μm. Error bars indicate s.e.m.

endothelial converting enzyme (ECE1) necessary to process/activate endothelin-2, these data increasingly supported *Edn2* as the prime NFIB target gene for explaining the *Nfib*-cKO phenotype (Lien et al., 2011).

The changes I observed in *Edn2* expression were cell-autonomous, since *Edn2* mRNA was also upregulated in cultured *Nfib*-null keratinocytes (Fig. 3-16d). Moreover, this difference was dependent upon NFIB, as it was rescued by transfecting an expression vector encoding the main keratinocyte isoform, NFIB3 (red bars). In contrast, even though *Kit-ligand* (Kitl) mRNA appeared to be modestly induced in *Nfib*-null HFSCs (Table 1), the levels were not influenced by NFIB3-rescued *Nfib*-null keratinocytes (Fig. 3-16d), nor did I observe NFIB binding to the *Kitl* promoter/enhancer in ChIP-seq analyses. Interestingly however, while KITL was not detected in HFSCs, it was seen in the DP (Botchkareva et al., 2001) (Fig. 3-17a).

Together, these results suggest a model whereby endothelin-2 induction by *Nfib*-null HFSCs enhances proliferation of neighboring McSCs and sensitizes them to precociously differentiate when they encounter KITL and possibly additional signals from DP. If true, then blocking KIT signaling should ameliorate precocious McSC differentiation in *Nfib*-cKO follicles, while elevating endothelin-2 levels in wild-type HFSCs should recapitulate the phenotypic features of *Nfib*-cKO HFs. I first tested this hypothesis by injecting a KIT-receptor blocking antibody into skins of *Sox9-CreER* cKO mice beginning in late catagen (assessed by transition of skin color from dark to pink). By telogen, marked reductions were seen in TYRP1^{+} melanocytes and in activated-Casp3^{+} HFSCs (Fig. 3-17b). Importantly and in agreement with previous findings (Botchkareva et al., 2001; Nishikawa et al., 1991), KIT-inhibition in anagen-phase hair

follicles only affected lineage-committed proliferation and differentiation; thus, undifferentiated McSCs remained elevated in the *Nfib*-cKO hair follicles (Fig. 3-17c).

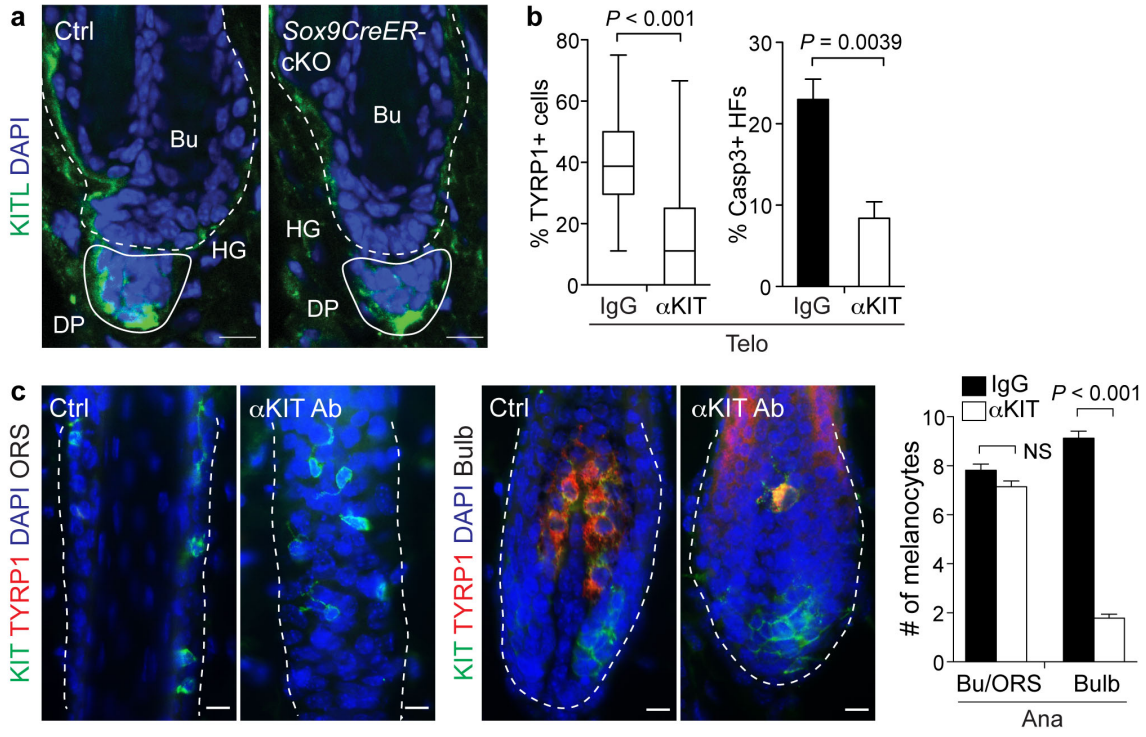

Figure 3-17. Inhibition of Kit signaling reduces ectopic McSC differentiation upon NFIB loss. a, Immunofluorescence reveals KITL in DP of *Sox9-CreER* cKO and control skins. **b,** Reductions in TYRP1$^+$ melanocytes and apoptosis (judged by activated Casp3 staining) in *Sox9-CreER* cKO hair follicles after injecting anti-KIT blocking antibody (αKIT) during catagen/telogen transition. IgG: control IgG. Quantifications indicated the percentage of TYPR1$^+$ KIT$^+$ cells among KIT$^+$-only cells per hair follicle cross section, and the percentage of hair follicle with Casp3+ signals in the bulge and HG in skin cross sections. **c,** Immunofluorescence of anagen hair follicles with indicated antibodies after anti-KIT blocking antibody or control IgG treatment in *Sox9-CreER* cKO skin. Note the disappearance of TYRP1$^+$KIT$^+$ mature melanocytes in the hair bulb after αKIT antibodies treatment during anagen. McSCs (TYRP1$^-$KIT$^+$) in the bulge/ORS were not affected. Quantifications of the number of TYRP1$^-$KIT$^+$ melanocytes in the bulge (Bu)/ORS and TYRP1$^+$KIT$^+$ differentiated melanocytes in the hair bulb (bulb) per hair follicle cross section. Bu: Bulge. HG: Hair germ. DP: Dermal papilla. NS: not significant. Scale bars: 10 μm. Error bars indicate s.e.m.

Upregulation of *Edn2* in skin induces hyperpigmentation

I next induced *Edn2* in wild-type adult skin by co-transducing E9.5 mouse embryos *in utero* with high-titer lentiviruses harboring: a) tetracycline-regulatable transactivator (*rtTA*) coupled in a bicistronic transcript to *EGFP* and b) *H2BmRFP1* and a tetracycline-inducible promoter driving either *Edn2* (*TRE-Edn2*) or empty control (*TRE*-only) (Fig. 3-18a). This lentiviral-delivery method confers efficient and sustained epithelial-specific expression to adult skin (Beronja et al., 2010), which I confirmed by immunofluorescence (Fig. 3-18b). Notably, KIT^+ melanocytes were not be targeted by lentiviruses since the timing when injection was conducted is earlier than their arrival time at epidermis from neural crest.

Transduced mice were fed with doxycycline-containing chow beginning at P21 to induce *Edn2* expression. Quantitative PCR from FACS-isolated cells confirmed that *Edn2* was only upregulated in double infected cells (Fig. 3-18c). Interestingly, mice with ectopic *Edn2* showed apparent hyperpigmentation in the epidermis of ear skin where melanocytes are normally distributed (Fig. 3-18d). In hair follicles, *Edn2*-transduced hair follicles displayed increased numbers of KIT^+ McSCs (Fig. 3-18e). Quantification of Fontana-Masson-stained sections showed that melanin production had been induced in HGs of *rtTA/TRE-Edn2*-transduced skin but not *rtTA/TRE*-only skin (Fig. 3-18f). Notably, *de novo* melanogenesis was not detected in doubly-transduced epidermis of hairy backskin, suggesting that the effects of endothelin-2 were confined to locations where preexisting McSCs reside.

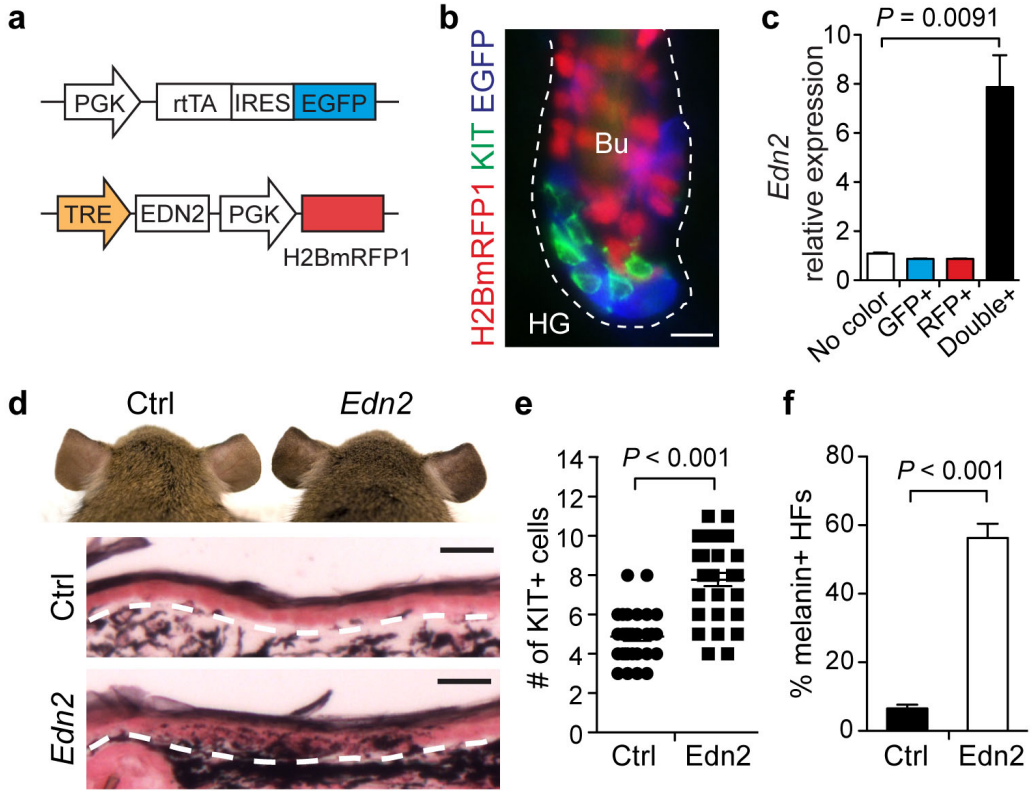

Figure 3-18. Up-regulation of *Edn2* induces hyperpigmentation in skin. a, Schematic of lentiviral constructs used to upregulate *Edn2* expression in skin. **b,** Immunofluorescence with KIT and GFP antibodies. As judged by H2BmRFP1/GFP expression, transduction is confined to skin epithelial cells and not seen in KIT$^+$ McSCs. **c,** Upregulation of *Edn2* in doubly transduced cells examined by qPCR on FACS-isolated populations after 10 or 30 days of feeding on Doxcycline-containing chow. Values are normalized to no-color control. **d,** *Edn2* upregulation in epithelial cells induce hyperpigmentation in mouse ear epidermis and dermis. *Fontana-Masson* melanin staining was conduced on ear sections. Edn2: mice infected with lentiviruses carrying *rtTA*/*TRE* driven *Edn2* constructs. Ctrl: mice infected with lentiviruses carrying *rtTA*/*TRE*-empty constructs. **e,** Quantifications reveal increased KIT$^+$ melanocyte number upon EDN2 induction. Edn2: doubly transduced hair follicles. Control (Ctrl): singly-transduced and uninfected hair follicles. Quantifications indicated the number of cells per hair follicle cross section. **f,** Quantifications of percentage of melanin$^+$ hair follicles in Edn2 (infected with lentiviruses carrying *rtTA*/*TRE* driven *Edn2*) skin and Ctrl (infected with lentiviruses carrying *rtTA*/*TRE*-empty constructs) skin cross section. Bu: Bulge. HG: Hair germ. Scale bars: 10μm (b); 25μm (d). Error bars indicate s.e.m.

To determine whether premature McSC differentiation in the *Nfib*-cKO hair follicles appears to depend upon EDN2, I performed a rescue assay. Chemical BQ788, which inhibits endothelin-receptor type B (EDNRB), was injected intradermally into *Sox9-creER* cKO skin at mid-catagen (assessed by transition of skin color from dark to pink). After 5-days application, hair follicles showed marked reductions in the number of TYRP1+ melanocytes and in activated-Casp3+ HFSCs (Fig. 3-19a and b).

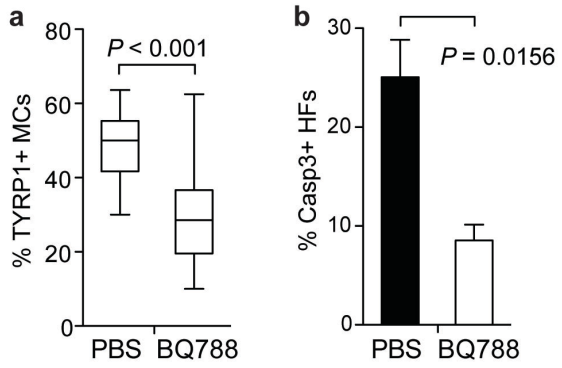

Figure 3-19. Inhibition of Edn signaling reduces precocious melanocyte differentiation in *Nfib* cKO hair follicles. a, Quantification of percentage of $TYRP1^+$ KIT^+ melanocytes in *Sox9-CreER* cKO hair follicles after injection of endothelin receptor (EDNRB) inhibitor BQ788 during catagen/telogen transition. **b,** Quantification of percentage of activated $Casp3^+$ hair follicles in cKO skin upon BQ788 treatment. Error bars indicate s.e.m.

Discussion

In summary, my findings expose an unexpected gatekeeper, NFIB, which governs the coordination of stem cell behavior in the hair follicle. While NFIB-deficiency resulted in many changes in HFSC gene expression, upregulation of NFIB target, *Edn2,* was sufficient to disrupt the intricate synchronization of McSC and HFSC proliferation and differentiation that normally accompanies hair growth and maintenance. In contrast

to all known genetic pathways perturbing McSC function within hair follicles, precocious melanocyte differentiation and ensuing chaos was cyclical and did not compromise stem cell pools, hair pigmentation or growth, even in aged animals. The mechanism underlying this unprecedented phenotype lends new insights to the importance of the two-tiered structure of the HFSC-residing region coupled with the existence of DP/Kit-ligand-independent and dependent steps in unleashing *Edn2*'s effect. Thus, through *Nfib* ablation, upregulated *Edn2* promoted self-renewal of McSCs, whose numbers remained elevated throughout aging but were still checked by the quiescent microenvironment. *Edn2* also primed McSCs to trigger differentiation, but since the second differentiation signal comes from DP and is cyclic, only McSCs in the HG and not bulge were affected. Similarly, even though aberrant pigment uptake by quiescent HFSCs resulted in their death, only some HG cells were affected, and all bulge HFSCs were spared.

The ability of *Edn2* to uncouple the normal timing of melanogenesis was at first surprising given that *Edn2* has not been implicated hitherto in normal cutaneous melanocyte physiology, and that *Edn3* showed only non-cutaneous effects on melanogenesis in neonatal transgenic mice expressing *Edn3* under the control of the *keratin 14* promoter (Aoki et al., 2009; Garcia et al., 2008). Based upon this and seemingly normal melanogenesis in *Edn1* and *Edn2* knockout mice (Chang et al., 2013; Kurihara et al., 1994; Reid et al., 1996a), researchers have posited that endothelins function primarily in embryogenesis and not postnatally (Garcia et al., 2008). Like *Edn3,* elevating *Edn2* in epidermis did not promote melanogenesis; however, by unearthing *Edn2*'s impact on adult McSCs, this findings show that when provided with the proper microenvironment, endothelins can influence adult McSCs and their differentiation.

Recently NFIB was linked oncogenically to lung cancer, and it has an established role in lung development (Dooley et al., 2011; Gründer et al., 2002; Steele-Perkins et al., 2005). In this regard, NFIB's high level in HFSCs is intriguing, since long-term stemness is required of both normal and cancerous tissues. While beyond the scope of the present study, testing this possible function merits future investigation with methods that challenge regenerative capacity and remove possible NFI redundancy.

Overall, this work reveals how McSC and HFSC behaviors maintain reliance upon cooperative factors within the hair follicles and how this might be uncoupled in injury and disease states. Notably, *Edn2* is upregulated upon UV irradiation and a variety of other stress conditions that are associated with increased pigmentation (Adur et al., 2007; Klipper et al., 2010). In the future, it will be interesting to see the extent to which *Nfib* downregulation will function in tipping the balance from a coupled to uncoupled state; my studies here emphasize the importance of endothelins as important messengers to achieve McSC-HFSC asynchrony.

Materials and Methods

Mice.

P52-60 CD1 mice from Charles River laboratories were used for NFIB ChIP-seq experiments. *Nfib*(fl/fl) and *Nfib*(-/-) mice have been described (Hsu et al., 2011b; Steele-Perkins et al., 2005), as have transgenic *K15-CrePGR* (Morris et al., 2004), knock-in *Sox9-CreERT2* (Soeda et al., 2010) and $ROSA26^{flox/STOP/flox/YFP}$ ($Rosa^{YFP}$) (Srinivas et al., 2001) mice. *DCT-EGFP* animals were generated by GENSAT project (Heintz, 2004). CreER was activated by intraperitoneal (IP) injection of P20-21 mice with 20 mg/ml

Tamoxifen (Sigma) in corn oil (Sigma) (1mg/10g body weight per day). Cre-PGR was induced by RU486 treatment: 5-day IP injection of 10 mg/ml RU486 (VWR) in sesame oil (sigma) (0.75mg/10g body weight per day), together with 2-week topical application with 4% RU486 in Ethanol.

All animals were maintained in an AAALAC-approved Comparative Bioscience Center (CBC) at The Rockefeller University and procedures were performed using IACUC-approved protocols that adhere to the standards of the National Institutes of Health.

Histology and immunofluorescence.

Embryos (<E16.5) or backskins were embedded in OCT (Tissue Tek), frozen on dry ice and stored at -80°C. Only in the case of *Rosa*^{YFP} reporter or lentiviral transduced mice, tissues were prefixed in 4% paraformaldehyde (PFA) for 30 min at room temperature (r.t.) before embedding in OCT in order to preserve the fluorescence signals. Un-prefixed frozen sections (10-20 μm) were fixed in 4% PFA for 10 min at (r.t.). For histological analysis, sections were stained with hematoxylin and eosin. Melanin staining was performed using a *Fontana-Masson* Stain Kit (MarketLab Inc.) according to the manufacturer's directions. For immunofluorescence, sections were permeabilized in 0.3% Triton X-100 in PBS for 20 min and blocked for 1 hr at r.t. in blocking buffer including 2.5% normal donkey serum, 2.5% normal goat serum (or 5% normal donkey serum alone when goat primary antibodies were used), 0.5% BSA and 0.1% Triton X-100 in PBS. For melanocyte markers, including DCT, TYRP1, and TYR, sections were permeabilized with 0.3% H_2O_2 in cold methanol for 30 min at-20°C (Govender et al., 2006). MOM

Basic kit (Vector Laboratories) was used for blocking when primary antibodies were generated from mouse. Primary antibodies were diluted in blocking buffer and sections were incubated overnight at 4°C. After washing with PBS for 30 min at r.t., sections were incubated for 1–2 hr at r.t. with secondary antibodies conjugated to Alexa-488, Alexa-546, Alexa-647 (Molecular Probes), or RRX (Jackson Laboratories). EdU staining was performed using Click-iT EdU Alexa Fluor 594 Imaging Kit (Life Technologies) and following manufacturer's directions. Nuclei were stained using 4'6'-diamidino-2-phenylindole (DAPI). Imaging was performed on a Zeiss Axioplan 2, Zeiss Apotome, Zeiss Inverted LSM 510 laser scanning confocal microscope, or Zeiss Inverted LSM 780 laser scanning confocal microscope.

For quantifications, the images from individual hair follicles with clear bulge and HG structures on sections were acquired by microscopes first and then counted on computer.

The following antibodies and dilutions were used: NFIB (rabbit, 1:1,000, Active Motif); KIT (rat, 1:1,000, BD Pharmingen); P-cadherin (goat, 1:100, R&D); E-cadherin (rat, 1:500, Fuchs lab); K5 (guinea pig, 1:500, Fuchs lab); CD34 (rat, 1:100, BD Pharmingen); Ki67 (rabbit, 1:300, Novocastra); cleaved-Caspases3 (rabbit, 1:300, R&D); GFP (chicken, 1:2,000, Abcam); EDN 1/2/3 (rabbit, 1:100, Santa Cruz); KITL (rat, 1:300, R&D); Mac-1 (rat, 1:100, eBioscience) MITF (mouse,1:100, Abcam); DCT (rabbit, 1:500, gift of Dr. V.J. Hearing, National Cancer Institute, National Institutes of Health, Bethesda, MD); TYRP1 (rabbit, 1:1,000, gift of Dr. V.J. Hearing); TYR (rabbit, 1:1,000, gift of Dr. V.J. Hearing).

Electron Microscopy.

Electron Microscopy (EM) was conducted by H. Amalia Pasolli. Backskins were fixed in 2% glutaraldehyde, 4% PFA, and 2 mM CaCl2 in 0.05 M sodium cacodylate buffer, pH 7.2, at r.t. for > 1 hr, postfixed in 1% osmium tetroxide, and processed for Epon embedding. Ultrathin sections (60–70 nm) were counterstained with uranyl acetate and lead citrate. Images were taken with a transmission electron microscope (Tecnai G2-12; FEI) equipped with a digital camera (model XR60; Advanced Microscopy Techniques, Corp.).

Isolation of HFSCs and FACS.

Subcutaneous fat was removed from skins with a scalpel. To isolate bulge HFSCs for NFIB ChIP-seq experiment, skins were placed on 0.25% Trypsin (GIBCO) at 37°C for 30 min with dermis side down. For isolation of bulge and HG HFSCs, skins were first incubated in 0.25% Collagenase (Sigma) in HBSS (GIBCO) at 37°C for 1 h to remove dermis. After gentle PBS washing, skins were treated with Trypsin as described above. Single cell suspensions were obtained by scrapping the skin gently and filtering through 70 μm strainers, followed by 40 μm strainers. Staining buffer (PBS with 5% FBS treated with BioRad Chelex to remove calcium) was added to inactivate Trypsin, and cells were collected by centrifugation for 5 min at 300g. Cell suspensions were incubated with the appropriate antibodies diluted in staining buffer for 30 min at 4°C. The following antibodies were used: CD34-Alexa 660 (1:200, eBioscience); α6-PE (1:500, eBioscience); β1 -PE-Cy7 (1:500, eBioscience); Sca1-Alexa 700 (1:200, eBioscience); CD200-biotin (1:200, AbD Serotec); Streptavidin-PE-Cy7 (1:200, eBioscience). DAPI

(100 ng/ ml) was used for death cell exclusion. Cell isolations were performed on BD FACSAria II sorters equipped with BD FACSDiva software. For RNA extraction, cells were sorted directly into TRIzol LS Reagent (Life Technologies).

RNA extraction and RNA-seq analysis.

Cells were isolated from *Nfib*(fl/+)/*K15-CrePGR*/*Rosa*^{YFP} (het) and *Nfib*$^{fl/fl}$/*K15-CrePGR*/*Rosa*^{YFP} (cKO) mice. *Nfib* ablation was induced from second telogen (P50-60) with RU486 treatment, and mice were taken during third telogen (P120-130). The protocol of cell sorting was described above with antibodies: CD34-Alexa 660, CD200-biotin, α6-PE, Sca1-Alexa 700 and Streptavidin-PE-Cy7. Cells were lysed with TRIzol LS Reagent (Life Technologies) and RNA was extracted using Direct-zol RNA MiniPrep (Zymo Research) with DNase treatment to remove residual genomic DNA. Isolated RNA samples were provided to the Genomics Resources Core Facility at Weill Cornell Medical College for quality control, library preparation, clustering and sequencing. RNA-seq reads were aligned to the mouse genome (mm9, NCBI Build 37) using TopHat (Trapnell et al., 2009) (http://tophat.cbcb.umd.edu/). Cufflinks (Trapnell et al., 2010) (http://cufflinks.cbcb.umd.edu/) was subsequently used to assemble the aligned reads into transcripts and then estimate the transcript abundances. Pathway analysis was performed using iPAGE algorithm (Goodarzi et al., 2009), included in the ChIPseeqer framework (Giannopoulou and Elemento, 2011).

Quantitative PCR (qPCR).

RNA isolation was described above. cDNA was synthesized from isolated RNA using SuperScript III First-Strand Synthesis System with oligo-dT primers (Invitrogen). cDNAs were mixed with indicated primers and Power SYBR Green PCR Master Mix (Applied Biosystems), and quantitative PCR (qPCR) was performed on a Applied Biosystems 7900HT Fast Real-Time PCR system for 40 cycles. Specificity was confirmed by subsequent melting curve analysis or gel electrophoresis. Levels of PCR product were expressed as a function of peptidylprolyl isomerase B (Ppib). Primers were designed through Primer 3 and amplified products encompassed exon/intron boundaries. The following primer sequences were used:

Nfib forward 5'-ATGACCCATCCAGTCCTCAA-3',

reverse 5'-TTGAAGGAAAGGCTCTCCAA-3'

Sox9 forward 5'-CCACGGAACAGACTCACATC-3',

reverse 5'-CCCTCTCGCTTCAGATCAAC-3'

Ednrb forward 5'-CTCTGTTGGCTTCCCCTTC-3',

reverse 5'-CGATTGGATTGATGCAGGA-3'

Dct forward 5'-AGAGAAACAACCCTTCCACAGA-3',

reverse 5'-CCAATGACCACTGAGAGAGTTG-3'

Kit forward 5'-GGGCTAGCCAGAGACATCAG -3',

reverse 5'-AGGAGAAGAGCTCCCAGAGG -3'

Mitf forward 5'-TTGAAAACCGACAGAAGAAGC -3',

reverse 5'-TGGATGGGATAAGGGAAAGTC -3'

Tyrp1 forward 5'-GCCTCCAGTTACCAACACAGA -3',

reverse 5’-AACGGATCAGACAAGAAGCAA-3’

Tyr forward 5’-CCAGAAGCCAATGCACCTAT-3’,

reverse 5’-ATAACAGCTCCCACCAGTGC -3’

Sox10 forward 5’-GACCAGTACCCTCACCTCCA-3’,

reverse 5’-AGCCTCTCAGCCTCCTCAAT -3’

Pax3 forward 5’-GCGAGAAAAAGGCTAAACACA-3’,

reverse 5’-CGGAGCCTTCATCTGACTG-3’

S100a1 forward 5’-CAAGGAAGGGGACAAATATAAGC-3’,

reverse 5’-CGTTTTCATCCAGTTCCTTCA-3’

Edn1 forward 5’-TACTTCTGCCACCTGGACATC-3’,

reverse 5’-CCCTGAGTTCTTTTCCTGCTT-3’

Edn2 forward 5’-TTCTGCCATCGAAGACACTG-3’,

reverse 5’-TGGCCTTTCTTGTCACCTCT-3’

Edn3 forward 5’-TGGGAAACAAGAGGACAAGG-3’,

reverse 5’-CTGGGAGCTTTCTGGAACTG-3’

Axin2 forward 5’-ACTGACCGACGATTCCATGT-3’,

reverse 5’-CTGCGATGCATCTCTCTCTG-3’

Gpnmb forward 5’-TGCCTGCTGTCTGTGAGAAG-3’,

reverse 5’-GGCAGTTTCCTATTGGCTTG-3’

Kitl forward 5’-CAAGTCTTACAAGGGCAGTTGA-3’,

reverse 5’-ACAAGGTCACGGGTAGCAAG-3’

Chd3 forward 5’-ACTTTGATGAGCGTCCTGAAG-3’,

reverse 5’-GGCTTGTCCTTCTCATTTCG-3’

Whrn forward 5'-TGGCTTATAGACCTGATGGAGAA-3',

reverse 5'-CTTCTGAGGGGGATTTGACAT-3'

Acsbg1 forward 5'-AAGTTCCTGTCCATGCTGCT-3',

reverse 5'-TGGAGAAGTCACGTTGGAGA-3'

Adamtsl4 forward 5'-GGCAACCAGACTCTCAGCTC-3',

reverse 5'-CGGCAGCAGGTAGTTGTGTA-3'

Cyp4b1 forward 5'-GCCTGATCTCTCTGCACATCTA-3',

reverse 5'-CACCTTCATCTCGTTCATAGCA-3'

Gfra1 forward 5'-TGCTGGCCCTCTAGATCCATAAC-3',

reverse 5'-ACAGCGCTTCTGGCAGTTGATA-3'

Myoc forward 5'-TCGGCTTTAGAGGAAGAGAAGA-3',

reverse 5'-CATACTTGCCAGCGATTGTTT-3'

Nt5e forward 5'-ATGAACATCCTGGGCTACGA-3',

reverse 5'-GTCCTTCCACACCGTTATCAA-3'

Steap4 forward 5'-TGATTCCTATCCGTTACTATGTTCG-3',

reverse 5'-ATGGGCTGTCTTTATTAGTTAGGG-3'

Tns1 forward 5'-TCTTACCATTGCCCTCAATCC-3',

reverse 5'-CCACGGACTCCACATAGCTC-3'

Ppib forward 5'-GTGAGCGCTTCCCAGATGAGA-3',

reverse 5'-TGCCGGAGTCGACAATGATG-3'.

NFIB ChIP-seq analysis.

At first, the quality of NFIB antibody for immunoprecipitation was examined in hair follicle cells of newborn skins. Back skins from nine CD-1 newborns were dissected using the shoulders and hips as landmarks and treated with dispase (Gibco, 0.4mg/mL) at 4°C overnight. Separated from the epidermis, the dermis were incubated in 8ml 0.25% collagenase solution, which was made by adding 0.1ml 20% collagenase (Sigma, solved in PBS) into 7.9ml Hanks' balanced salt solution (Gibco), for 45 minutes at 37°C. PBS was added to bring the volume up to 40 ml, followed by repetitive pipetting to dissociate dermal cells from hair follicles and centrifugation at 300g for 10 minutes at 4°C. The pellet was resuspended in 30ml PBS, followed by low-speed centrifugation (40g, 6 minutes, 4°C) to enrich hair follicles. Hair follicles were treated with 10ml 0.25% trypsin with EDTA (Gibco, 0.25%) for 10 minutes at 37°C. Trypsin was inactivated by the addition of 20ml PBS with 5% fetal bovine serum (5% FBS), followed by centrifugation at 300g for 10 minutes at 4°C. Single cells were washed once by 20ml PBS. 0.55ml RIPA buffer (Cell signaling) with protease inhibitors (Roche) was added to lyse cells with 10-minute incubation on ice. After centrifugation at 13k rpm for 10 minutes at 4°C, 20μl supernatant were collected as input control (5ul were loaded in Western blot), and 250ul cell lysate were incubated with 6μg NFIB antibody (Active Motif, rabbit) conjugated with Dynabeads (Life technologies) accompanied with 250ul cell lysate with IgG control at 4°C overnight. RIPA buffer was used to wash beads and proteins (IP) were reconstituted in 50ul SDS-PAGE sample buffer, 20% of which were used for Western blot. For Western blotting, anti-NFIB antibodies (Active Motif, rabbit, 1:1000; Abcam, mouse, 1:100) were used.

All materials and methods for ChIP-seq experiments have been described (Lien et al., 2011). For each independent NFIB ChIP experiment, 10-15 X 10^6 bulge HFSCs were isolated by FACS from 15-20 CD-1 mice, and then used to isolate chromatin and incubate with 5μg anti-NFIB antibody (Active Motif) for ChIP-seq analysis. ChIP-Seq reads were aligned to the mouse genome (mm9, build 37) with the Bowtie program (Langmead et al., 2009) and the Illumina Analyzer Pipeline. ChIP-seq peak calling, genomic annotation of NFIB peaks, and comparison between NFIB targets and gene expression signature genes were performed using ChIPseeqer (Giannopoulou and Elemento, 2011). Motif analysis was performed using FIRE algorithm (Elemento et al., 2007), included in the ChIPseeqer framework.

Plasmid DNA Constructions.

Plasmids encoding full-length *Nfib1* cDNA were obtained from ATCC (clone: **MGC-13959**). Since NFIB3 is the major isoform present in epidermal keratinocytes, *Nfib3* cDNA was used in this study. *Nfib3* DNA fragment was amplified from *Nfib1* cDNA clone by PCR with primers: forward 5'-GTTGCGAGCTCTCATGATGTATTCTC-3'; reverse 5'-GTCAACCCGGGCTAGCCCAGGTACCAGGACTGGCTCGTTTGAGGA-3'. For expression of EGFP-NFIB3, *Nfib3* DNA fragment was then inserted into *pEGFP-C1* between SacI and XmaI.

All lentiviral vectors (LV) were present in the *pLKO* lentiviral backbone (*pLKO-no-stuffer-PGK-MCS*, Addgene 10879). For construction of *LV-rtTA-IRES-EGFP*, DNA fragment of *rtTA-IRES-EGFP* was excised from *pMSCV-rtTA2S-M2-IRES-EGFP* with

BglII and SalI restriction enzymes (RE) and cloned between BamHI and SalI sites of *pLKO* backbone. *rtTA2S-M2* (Tet-On Advanced) was cloned from *pUHD-rtTA2S-M2*. This was excised by digesting with BamHI and SacII, and blunting with Klenow. The blunted fragment was subcloned into *pMSCV-IRES-EGFP* digested with HpaI, and dephosphorylated with SAP. For construction of *LV-TRE-PGK-H2BmRFP1*, TRE promoter was first inserted into ClaI and AgeI sites of pLKO vector to replace U6 promoter (*pLKO-TRE-PGK*). The TRE promoter from Clontech's pTRE2 was amplified by PCR using primers flanked with ClaI and AgeI sites: forward 5'-CGTATATCGATGCCCTTTCGTCTCGA-3', reverse 5'-GAATTACCGGTCGCGGAGGCTGGAT-3'. *H2BmRFP1* DNA fragment was obtained from *pCR-H2BmRFP1* by BglII and NsiI RE digestion (Beronja et al., 2010), which was then inserted between BamHI and NsiI sites of *pLKO-TRE-PGK*. *Edn2* cDNA were amplified from keratinocyte cDNA library with primers flanked with EcoRI site: forward 5'-CGCCAGAATTCATGGTCTCCGCCTGGT-3'; reverse 5'-CGCCAGAATTCGGTGTTATCTCTTCCTCCATC -3'. Afterwards, DNA fragment was inserted into EcoRI site of *LV-H2BmRFP1-TRE* vector. All insertions were verified by DNA sequencing.

Cell Culture and *in vitro Nfib* overexpression.

Primary *Nfib*-null (KO) keratinocytes were isolated from epidermis of E18.5 *Nfib* knockout embryos (*Nfib*-/-) and control keratinocytes were from heterozygous *Nfib* (+/-) embryos. Keratinocytes were maintained in E-media supplemented with 15% serum and a final concentration of 0.05 mM Ca_2. Experiments were performed using primary cells

with less than 15 passages. Plasmids expressing EGFP or EGFP-NFIB3 were introduced into control and KO keratinocytes with Fugene 6 Transfection Reagent (Roche). After 24 h transfection, GFP-positive cells were isolated by FACS for qPCR analysis.

Intradermal injection of EDNRB receptor inhibitor BQ788 and anti-KIT blocking antibody.

To inhibit EDNRB receptor from late catagen, 100μl BQ788 dissolved in PBS (1mg/ml, Tocris Bioscience) or PBS alone was injected intradermally into backskin of mice on first catagen when skin color turned from black to pink[6]. To inhibit KIT signaling, 100μl anti-KIT antibody (BD Pharmingen, 1.0 mg/ml, clone: ACK45 NA/LE) or control Rat IgG was used (Botchkareva et al., 2001). Injections were conducted every other day for 3 days (day 0, 2, 4), and mice were taken and analyzed on day 5. For inhibition of KIT signaling during anagen, 100μl anti-KIT antibody or control IgG was injected intradermally into backskin one day after depilation. Injections were conducted every other day for 5 days (day 0, 2, 4, 6, 8) and mice were taken and analyzed on day10.

Statistics.

To determine significance between two groups indicated in figures, comparisons were performed in Prism 5 software with unpaired two-tailed student's t-test.

Chapter4:

Summary and future directions

In the hair follicle "miniorgan", hair follicle stem cells (HFSCs) support their long-term repetitive regeneration. To investigate the molecular basis in modulating follicle formation, HFSCs and basal epidermal keratinocytes were selectively isolated from adult mouse skin using genetic methods and cell surface markers. Comparing the gene expression profiles of these isolated cell populations revealed several uncharacterized transcription factors with a HFSC-specific expression pattern, among which was NFIB.

With cell-type-restricted expression patterns, lineage-specifying transcription factors have been recognized as key components in orchestrating tissue development. Surprisingly, these factors are not only required for the specification of cell fates during development, but, in many cases, they are also sufficient to direct the formation of specific cell types from other differentiated cell types. As early as 1987, the phenomenon was observed from the studies of transcription factor MyoD, which, when ectopically introduced into fibroblasts, can convert them to become myoblasts (Davis et al., 1987). Other examples include MITF, which can reprograms fibroblasts to become melanocyte-like cells (Tachibana et al., 1996); C/EBPβ, which can trans-differentiate pancreatic cells into hepatocytes (Shen et al., 2000); and PAX6, which can induce ectopic eye formation on the fly body outside its head (Halder et al., 1995). Recently, an additional example of cellular reprogramming was the finding that several coordinated transcription factors (Oct4, Sox2, Klf4, and c-Myc) are able to convert somatic cells to pluripotent stem cells (Takahashi and Yamanaka, 2006). Therefore, because of their fascinating ability to direct cell fate determination, transcription factors have attracted a lot of attention from researchers when they are looking for the secret ingredients of organogenesis.

The importance of stem cells in tissue regeneration

To understand the functional significance of NFIB in HFSCs, I followed the morphogenesis and cycling of hair follicles in the absence of NFIB. At first, I generated *Nfib* cKO mice with *K14-Cre*, in which *Nfib* was targeted during the embryonic stage. Upon NFIB loss, the morphogenesis of hair follicles was slowed and hair follicles degenerated precociously. Further, I found that in the absence of NFIB, the expression of SOX9, which is required for the specification of HFSC identity, was gradually diminished in hair follicles. However, there were differences between the phenotypes in loss of SOX9 and NFIB mutants. *Sox9*-ablated hair follicles lost HFSC markers including LHX2 and NFATc1 due to the failure of forming HFSC precursors; conversely, these markers were still present in *Nfib*-deficient hair follicles. It implies that HFSC precursors might be specified but they fail to maintain a high level of SOX9 expression upon NFIB loss and do not appear to be functional in their ability to fuel tissue growth, either in hair follicle formation or wound-repair. To identify the role of NFIB in hair follicle morphogenesis, more studies are required to further quantify the number and qualify the functionality of HFSC precursors in *Nfib*-deficient hair follicles. Meanwhile, it would be interesting to examine the relationship between NFIB and SOX9 (i.e. is the level of NFIB decreased upon SOX9 loss? Is *Sox9* a direct target of NFIB during morphogenesis?).

Preliminary results imply the importance of NFIB in hair follicle-mediated wound repair; however, more functional studies are required to confirm this notion. First, lineage tracing of NFIB-deficient hair follicle cells can provide insights into the questions of how they are lost during epithelial reconstitution and whether they show defects in proliferation or migration during this process. Meanwhile, it would be interesting to

identify if, after hair follicle maturation, NFIB also regulates the adult HFSC's capacity for wound healing. It could be examined by following HFSC behavior after scratching the skin surface of adult mice, which remove the epidermal layer. Do NFIB-deficient HFSCs migrate out of the bulge upon wounding? Do they give rise to new epithelial cells? Do they contribute to re-epithelization at the expense of the HFSC population? Elucidating the molecular details by which NFIB acquires and maintains stem cell character will also further our understanding into the specification and development of HFSCs. Identifying genes directly regulated by *Nfib* will be important in this regard.

Although retarded hair follicle morphogenesis upon NFIB loss is evident, NFIB seems not to be required for hair growth after HFSCs are established. Surprisingly, quantitative ablation of *Nfib* in adult hair follicle stem cells by using inducible Cre recombinases including *Sox9*-CreER and *K15*-CrePGR didn't cause significant hair growth or hair cycle defects. Genome-wide RNA-seq analysis also confirmed this notion. NFIB-deficient HFSCs expressed comparable levels of most HFSC genes (such as *CD34*, *Sox9*, *Lhx2*, *Nfatc1*, *Tcf3/4*) when compared to control HFSCs. Most importantly, they not only expressed these genes but also appeared to be fully functional in performing their duties in driving the hair cycle. This suggests that NFIB is not essential for HFSC maintenance and its function in HFSCs can be replaced by other factors.

It is possible that in adult hair follicles, the established interaction between HFSCs and other surrounding cell types compensates for NFIB's function in HFSCs. In the mature stem cell niche of hair follicles, involved in maintaining HFSCs are multiple cell types surrounding them including the inner layer of the bulge (Hsu et al., 2011a), the DP (Greco et al., 2009), the dermis and adipocytes in the subcutis (Festa et al., 2011;

Plikus et al., 2008). Nerve endings, arrector pili muscles and melanocytes are also close to HFSCs. Thus, it will be interesting to examine if the cross talk between developing hair follicles and nearby cells is disrupted upon NFIB loss.

Intrinsically, factors expressed in mature HFSCs might take over the role of NFIB. The potential redundancy from other members of the NFI family, particularly if this changes developmentally, needs to be taken into consideration. *Nfic* has been shown to regulate hair cycling (Plasari et al., 2010). In *Nfic*-null skin, the overall morphology of hair follicles is intact, but the transition of hair follicles from resting telogen to the growth phase anagen is delayed both during hair cycle and in response to hair growth-stimuli after depilation. However, the underlying mechanism of *Nfic*-regulated hair growth induction is unclear. Since *Nfic* mutants used in the study are straight knockout mice, it is unclear whether the defects are caused by loss of *Nfic* in HFSCs or whether *Nfic* modulates hair cycle in a indirect way, for instance, through regulating the function of dermal papilla or other cells that surround HFSCs. From transcriptional profiling analysis, *Nfic* RNA is detected in adult HFSCs (Fig. 4-1a), implying that the hair cycle defects in *Nfic* KO mice might be due to impaired HFSCs.

But, notably, *Nfic* levels in HFSCs are much lower than *Nfib* and the other family member *Nfix* (Fig. 4-1a). Immunostaining with an anti-NFIX antibody revealed that NFIX displays similar a expression patter to NFIB. The antibody is specific for NFIX judged by the disappearance of immunofluorescent signals in *Nfix* KO skin (Fig. 4-1b). In mature hair follicles of P10 skin, both NFIB and NFIX are enriched in the ORS of hair follicles, and their levels are diminished in the matrix when hair cells are differentiating and absent in the differentiated follicular layers (Fig. 4-1c). The differences are in the

epidermis. NFIB's level is lower in the epidermis compared to in hair follicles whereas NFIX displays comparable level in both compartments. Meanwhile, in hair follicles of adult mice, NFIX is only present in CD34^{+} bulge HFSCs but not KIT^{+} McSCS similar to the expression pattern seen for NFIB (Fig. 4-1d). While *Nfix* is involved in maintaining the quiescence of neural stem cells (Martynoga et al., 2013), it will be interesting in the future to examine if *Nfix* is involved in the biology of skin, and if *Nfix* also plays a role in stem cells of the skin, modulating hair follicle regeneration or wound repair.

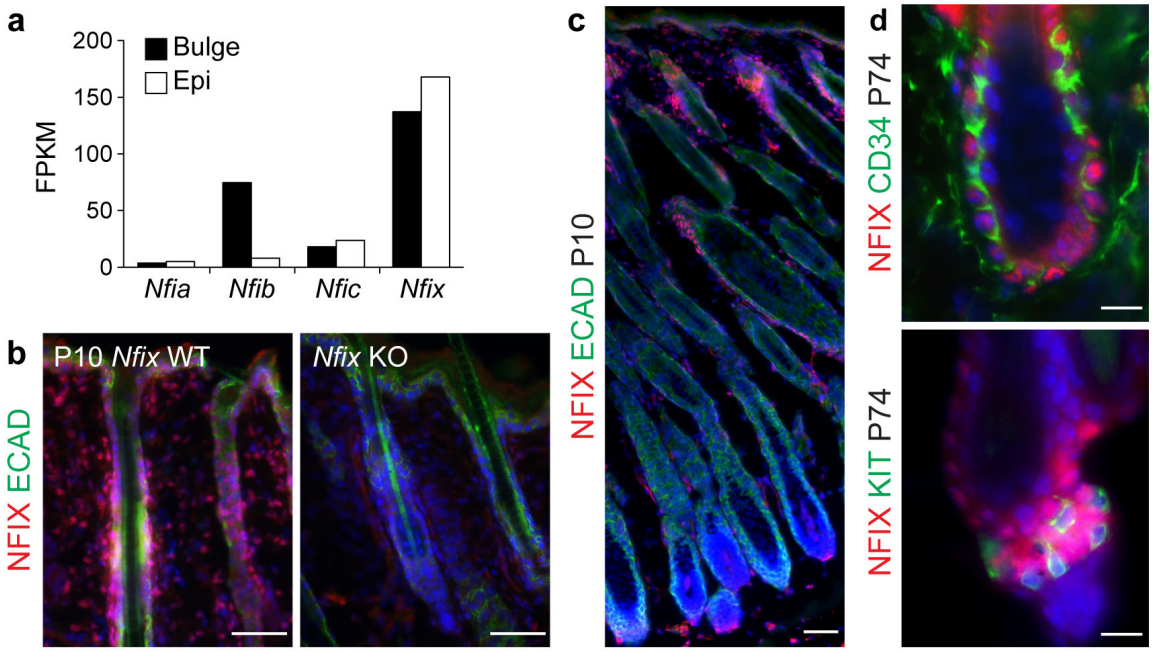

Figure 4-1. NFIX expression pattern in hair follicles. a, Expression levels of all *Nfi* family members from RNA-seq analysis of bulge HFSCs (Bulge) and epidermal cells (Epi), conducted by Brice Keyes. Cells were isolated from telogen (P50-60) hair follicles by FACS with antibodies conjugated with fluorochromes (bulge: Sca1^{-} CD34^{+} α6^{+}; Epi: Sca1^{+} CD34^{-} α6^{+}). FPKM: Fragments Per Kilobase of transcript per Million mapped reads. **b-d,** immunofluorescence with indicated antibodies. Note NFIX is expressed in the ORS and the bulge of hair follicles but not in KIT^{+} melanocytes. *Nfix* KO tissues were from Dr. Gronostajski. Scale bars: 50μm (b,c); 10μm (d).

Stem cell quiescence

Quiescence is a state of cessation. Cells in quiescence are not proliferative but able to respond to extracellular stimuli that originate from their niche environment by activating and entering the cell cycle. For tissue stem cells, the ability to stay in quiescence is crucial so that they can withstand metabolic stress and preserve genomic integrity over an organism's lifetime. Thus, balancing between quiescence and activation allows tissue stem cells to properly maintain the architecture of the tissue during homoeostasis, and meanwhile fulfill the immediate demands for tissue regeneration following damage without compromising long-term stem cell maintenance. Dysregulation and loss of quiescence in tissue stem cells often results in their short-term expansion but ultimately leads to stem cell depletion due to their limitation in proliferative capacity (Orford and Scadden, 2008).

The hair follicle is special as it is home to two distinct stem cell populations, McSCs and HFSCs. Synchrony is achieved such that they stay in quiescence together during telogen, a break period in the hair cycle that can last for weeks. Several mechanisms have been found to regulate the quiescence of individual types of stem cells independently. For instance, the absence of transcription factors such as LHX2 (Folgueras et al., 2013; Rhee et al., 2006), NFATc1 (Horsley et al., 2008), and FOXP1 (Leishman et al., 2013) specifically in HFSC lineage leads to the shortening of telogen due to HFSC activation precociously. Extrinsically, BMP signals coming from the microenvironment maintain HFSC quiescence during telogen (Kobielak et al., 2007). While the intrinsic mechanism is still not identified, maintaining the quiescence of McSCs requires TGF-β signaling (Nishimura et al., 2010). Given the closeness of HFSCs

and McSCs in space and their synchronized behaviors in time, it was tempting to speculate the involvement of direct communication between them for achieving this coupling.

Unexpectedly, I came upon a factor NFIB, which is responsible for mediating this crosstalk. In the absence of the HFSC-specific transcription factor NFIB, the quiescence of McSCs is perturbed: their population is expanded and some undergo ectopic differentiation in telogen when HFSCs are still dormant. Thus, the uncoupling happens when HFSCs lack NFIB. They can no longer repress the expression of *Edn2*, which encodes a secreted ligand acting on EDNRB receptor present on the surface of McSCs, whereby McSCs precociously undergo differentiation. It reveals an interesting notion that factors within HFSCs not only can regulate the quiescence of themselves, but they also play an important role in modulating their neighbor's activity through signal exchanges.

Given that in the NFIB-deficient hair follicles, only McSCs close to the dermal papilla (DP) are affected but McSCs away from the DP are relatively unperturbed, it led the study one step further showing that the DP signal KITL is required for EDN2-induced melanocyte differentiation in the absence of NFIB. The DP is a specialized mesenchymal structure lying under the stem cell niche and thought to act as a major signal center by secreting regulatory factors to modulate stem cell activity and the hair cycle. Thus, the DP releases inhibitory cues during telogen to maintain stem cells in quiescence; conversely, it upregulates the secretion of activating signals to counterbalance the inhibitory environment present during the transition from telogen to anagen.

Surprisingly, noticeable levels of activating signals such as KITL can be detected in telogen DP, while its presence in telogen is not sufficient to drive McSC activation

until anagen ensues. It could result from that the environmental inhibitory signals are so strong to override its activating effect, and it is also possible that there are not enough activating stimuli in the telogen niche to push McSCs to take action in response to KITL. *In vitro* melanocyte culture experiments provide some hints. While the addition of KITL alone into melanoblast culture is not sufficient to induce pigment production, in the presence of both factors EDN and KITL melanoblasts can fully differentiate into pigmented cells (Reid et al., 1996a). Meanwhile, simultaneous addition of EDN and KITL into culture dramatically increases melanoblast number to an extent greater than the addition of each individual factor (Reid et al., 1996a), although each factor has significant effect in promoting melanoblast proliferation (Lahav et al., 1996; Opdecamp et al., 1998; Reid et al., 1995). Thus, EDN and KITL act synergistically to promote the proliferation and differentiation of melanocytes, a finding that can explain at least partly why Kit signals are not able to induce McSC activation in telogen but in anagen when EDN is present. Thus, through repressing the level of EDN2, NFIB in HFSCs acts as a gatekeeper to maintain McSCs in quiescence. It makes the bulge/HG favorable for McSCs without being agitated by the stimuli in the environment.

How are HFSCs involved in McSC activation in the normal hair cycle? To explore the dynamics of HFSC gene expression changes during the hair cycle, transcriptional profiling and chromatin mapping have been conducted in HFSCs when they are quiescent, being activated, and when their progeny are differentiating (Lien et al., 2011). Interestingly, *Edn2* has been shown to be upregulated naturally in activated HFSCs. Thus, it is tempting to speculate that EDN2 released from neighboring HFSCs during hair growth might act as an important factor to promote the self-renewal of

McSCs within the hair follicles. Later, as melanocytes reach the follicle base, EDN factors from differentiated hair cells (Rabbani et al., 2011) could not only promote their proliferation but also differentiation with the help from the DP signals including Kit (Botchkareva et al., 2001). While *Edn2*-null mice exhibit normal coat color, the premature lethality of the mutants makes it hard to study the potential function of *Edn2* in adult McSC maintenance. Conditional ablation of *Edn2* in adult HFSCs would be helpful to address this question and to investigate the long-term influence of *Edn2* loss in hair pigmentation. Meanwhile, also awaiting further investigation is what are the upstream positive regulators of *Edn2* in activated HFSCs and how they outcompete the repressive regulator NFIB to activate *Edn2* expression.

Beyond the NFIB-EDN2 axis, it would be also interesting to identify other possible mechanisms in mediating the crosstalk between HFSCs and McSCs within hair follicles. At first, transcriptional profiling of the melanocyte lineage might reveal some clues about the mechanisms modulating McSC activation. By crossing *Lef1*-RFP transgenic mice (Rendl et al., 2005) to *Dct*-EGFP mice, it should be possible to separate McSCs ($EGFP^+$ only) from differentiated melanocytes ($EGFP^+$ RFP^+) in the follicles during FACS isolation for RNA-seq analyses. Further, through combining the profiles from HFSCs and McSCs, we might be able to identify signal exchanges between them, either the signals from HFSCs to McSC or *vice versa*. Predicted components and relationships in this network could then be tested quickly by *in utero* lentiviral-mediated overexpression or loss of function experiments with hair coat color changes as one rapidly scored phenotypic readout. Furthermore, recent studies have shown that both HFSCs and McSCs react to tissue damage, migrating out of their residence to the

wounded region for skin regeneration (Chou et al., 2013; Ito et al., 2005; Tumbar et al., 2004), implying that not only do they coordinate their behaviors during hair cycle but also during wound healing process. Thus, dissecting the crosstalk between HFSCs and McSCs would provide new insights in stem cell-mediated tissue regeneration, revealing the potential for developing therapies for skin disorders or injury impairing.

Surprisingly, besides within hair follicles, adult targeting of *Nfib* also induces hyperpigmentation in dermis, specifically the dermal region nearby hair follicles, and the phenotype becomes more severe with age. However, it is unclear where dermal pigments are from. In dorsal skin of WT mice, dermal melanocytes are rarely seen. Thus, it is possible that NFIB loss in hair follicles induces proliferation and differentiation of *in situ* dermal melanocytes. It is also possible that melanocytes within mutant hair follicles invade the dermis, although I didn't observe signs of abnormal melanocyte migration even inside hair follicles upon NFIB loss.

The phenotype is reminiscent of other factors such as HGF and EDN3, which, when upregulated in epidermal cells by *K14* promoter from embryonic stage, results in dermal pigmentation concomitant with increased dermal melanocytes (Garcia et al., 2008; Kunisada et al., 2000). Thus, it has been proposed that in transgenic HGF or EDN3 mice, melanoblasts are not able to invade the epidermis and accumulate in the dermis when migrating toward skin during development. But this cannot explain the induced appearance of dermal pigments in adult *K15-CrePGR* X *Nfib*-conditional knockout mice since this targeting happens postnatally, that is to say, after most of melanocytes enter the epidermis/hair follicles.

Another possibility is trans-differentiation of Schwann cells into pigmented cells. Besides retaining heat, hair follicles also work like a sensory organ with nerve fibers attached to the region above the bulge (Li et al., 2011). This network of neurons in skin allows animals to sense the touch or stimuli in the surroundings. Interestingly, these sensory nerves and associated glial Schwann cells are derived from the same origin (neural crest) with melanocytes, and Adameko *et al*., reported that Schwann cells are competent to differentiate into pigmented cells when in a challenged microenvironment, such as when losing contact with nerves (Adameyko et al., 2009). Thus, it would be interesting to examine if pigmented cells that are ectopically present in the dermis nearby NFIB-deficient hair follicles, are derived from Schwann cells, and what signals induce the trans-differentiation. Meanwhile, it is also unknown if a perturbation of Schwann cell homeostasis would comprise neuron function and animal sensation.

Implications beyond the hair follicle

During development, NFIB is also required for lung formation. Like in skin, NFIB is expressed in the mesenchymal and epithelial cells in lung (Gründer et al., 2002; Hsu et al., 2011b; Steele-Perkins et al., 2005). Loss of NFIB causes a delay in lung development accompanied with reduced formation of multiple differentiated cell types and branching structure; as a consequence, mutant mice have breathing difficulty and die shortly after birth. The importance of *Nfib* in lung tissue has been emphasized recently. Hinsz *et al*. proposed that NFIB might be one of the master transcription factors that control lung development (Hnisz et al., 2013). In lung, *Nfib* is strongly associated with

super-enhancers, which are large clusters of transcriptional enhancers that drive expression of genes that define cell identity.

Interestingly, by using tissue specific *K14* promoter to drive *Nfib* ablation in the epithelium, I found that the mutants, although they exhibit a functional skin barrier, were still not able to survive after labor, implying the possible cause of lethality from the epithelial defect is in the respiratory system (see Chapter 2). It supports this notion that besides in skin, *K14* promoter is also active in the airway epithelium, specifically in their basal cells that are thought to be multipotent stem cells capable of regenerating the epithelium upon injury (Hong et al., 2004a; 2004b; Rock et al., 2009). Thus, it would be interesting to further investigate if mice with *K14*-Cre driven *Nfib* loss suffer from respiratory failure during development and whether they exhibit abnormal airway structure. Given that transcription factor P63 is required for the formation of basal cells in the airway (Daniely et al., 2004) and P63 is an upstream regulator of *Nfib* in skin epithelium (McDade et al., 2012), it also would be interesting to test if *Nfib* is involved in P63-dependent basal cell development in lung. Beyond the embryonic stage, it is also unknown if *Nfib* plays a role in regulating the function and maintenance of adult $K14^{+}$ basal stem cells in lung during homeostasis and in the wound response. The idea can be examined by using an inducible *K14-CreER* line to temporarily control *Nfib* targeting in adult mice. The results from lineage tracing of *Nfib*-deficient basal cells during lung regeneration might provide new insights into pathological airway remodeling.

Meanwhile, the identification of *Nfib* targets in skin might provide some hints in the understanding of lung development. Interestingly, knockout mice of *Edn2*, one of *Nfib* targets I identified in this study, also display abnormalities in lung structure

including enlarged air space and reduced alveologenesis, suggesting its importance in lung maintenance (Chang et al., 2013). Thus, the implication of our findings in the link between *Nfib* and *Edn2* or other potential targets might be extended into the studies outside the skin and also provide insights into why mutations in *Nfib* are frequently seen in lung cancer cells (Dooley et al., 2011) as well as salivary gland cancer cells (Geurts et al., 1998; Ho et al., 2013).

In sum, future studies on the molecular basis regulating tissue stem cells, regardless of within hair follicles or other tissues, will provide new insights in the biology of organ development, homeostasis and aging. Given the importance of transcription factors in regulating lineage specification, perhaps further understandings of the molecular basis behind their regulation will reveal the mechanisms of tissue construction and hopefully lead to the development of therapies to advance medical care.

Table 3-1. Gene list from RNA-seq analysis of bulge/HG HFSCs from *K15-CrePGR/Nfib* cKO and heterozygous (WT) skins. Fold change is estimated as log2 ratio between cKO and WT.

Bulge Up							
GENE	**Description**	**WT Bulge**	**KO Bulge**	**WT HG**	**KO HG**	**Log2 KO Bulge/WT Bulge**	**Log2 KO HG/WT HG**
Mir23b		0	101.69	0	0	6.682151888	0
Snord47		0	98.06	0	184.98	6.630230716	7.539003674
Snord100		0	92.27	86.05	80.26	6.543341212	-0.099298933
Mir24-1		0	90.59	0	0	6.517118185	0
Mir5117		0	73.77	42.16	67.79	6.224387628	0.672503991
Snord2		0	63.97	0	0	6.0217018	0
Slc15a2	solute carrier family 15 member 2 isoform 2	0	53.71	0	65.66	5.773732651	6.058749412
Mir3058		0	53.23	0	0	5.761019265	0
Mir5133		0	44.93	0	0	5.521364878	0
Snora75		0	39.71	15.14	0	5.347311316	-4.012568674
Snora3		0	35.51	28.45	53.48	5.190219764	0.887459069
Snord22		0	35.37	26.81	59.57	5.184677021	1.122999667
Snora68		0	33.21	37.66	51.34	5.096346199	0.437072287
Mir675		0	32.93	0	32.47	5.084489525	5.064796646
Snora30		0	29.96	0	0	4.952333566	0
Snora7a		0	29.45	0	0	4.928370323	0
Snora44		0	25.97	16.53	28.7	4.753283616	0.760636935
H19		1.26	41.51	1.04	68.06	4.233407581	5.081209277
Ccl20	C-C motif chemokine 20 isoform 2	0	12.8	18.46	39.31	3.786596362	1.050626073
Snora24		0	12.48	16.41	0	3.752748591	-4.121844298
Ugt1a10	UDP glycosyltransferase 1 family, polypeptide	0.12	13.69	0	0	3.713263758	0
Rmrp		0	11.42	0	0	3.634593268	0
Insl3	insulin-like 3 precursor	0.23	13.65	0.16	5.31	3.574170444	2.4435152
Mir678		2.56	41.05	0	0	3.562156654	0
Prr9	proline-rich protein 9	0	10.27	1.42	12.3	3.49441561	2.458347293
Itga8	integrin alpha-8 precursor	2.28	34.84	1.03	9.41	3.449802917	2.358418436
Hist2h2bb	histone H2B type 2-B	0	9.84	2.49	8.22	3.438292852	1.401539714
Atp12a	potassium-transporting ATPase alpha chain 2	3.34	45.42	32.8	60.65	3.418979575	0.867077648
Gap43	neuromodulin	0	9.49	0	0	3.390942773	0
Kcnn3	small conductance calcium-activated potassium	3.86	45.31	0.36	2.22	3.252295538	1.243454037
Kcnip2	Kv channel-interacting protein 2 isoform b	0	8.51	9.79	38.71	3.249445341	1.879807496
Slc18a3	vesicular acetylcholine transporter	2.67	33.85	0	3.76	3.247306688	2.250961574
C2cd4b	family with sequence similarity 148, member B	4.21	46.26	7.52	22.76	3.181264352	1.479609501
Hba-a2	hemoglobin alpha, adult chain 2	1.98	25.27	2.98	4.62	3.140031965	0.4978017
Car2	carbonic anhydrase 2	0	7.52	1.38	8.39	3.09085343	1.980163584
Sphkap	A-kinase anchor protein SPHKAP	19.75	174.31	0.36	6.42	3.078725051	2.447812535
Fam71a	hypothetical protein LOC619288	4.05	40.2	2.22	14.87	3.028289044	2.301169535
Crygn	gamma-crystallin N	0	7.05	4.47	2.79	3.008988783	-0.529342985
Rpph1		0	7	0	0	3	0
Hmga2	high mobility group protein HMGI-C	2.88	28.84	0.39	3.66	2.943118978	1.745245072
Mpp4	MAGUK p55 subfamily member 4 isoform 1	0.28	8.41	0.22	0.26	2.878050913	0.046542586
Ptgds	prostaglandin-H2 D-isomerase	1.5	16.67	9.06	11.58	2.82130204	0.322501617
Chst9	carbohydrate sulfotransferase 9	0	5.56	0	0	2.713695815	0
C2	complement C2 precursor	15.85	104.06	5.32	16.24	2.640392993	1.447763311
Nts	neurotensin/neuromedin N	0	5.22	0	1.49	2.63691458	1.316145742
Nppc	C-type natriuretic peptide preproprotein	180.97	1130.03	71.35	315.96	2.635864668	2.131235863
Pcp4	Purkinje cell protein 4	2.06	17.68	2.62	11.06	2.609890897	1.736168305
Glrb	glycine receptor subunit beta precursor	25.67	155.33	9.57	34.39	2.551304931	1.743366385
Hbb-b2	hemoglobin subunit beta-2	1.68	14.68	8.31	11.46	2.548620654	0.420450995
Plekha6	pleckstrin homology domain-containing family A	3.08	22.26	13.46	20.29	2.51121004	0.558108398
Sync	syncoilin	0.9	9.68	0.71	1.32	2.490840323	0.44012848
Sprr1b	cornifin-B	0	4.45	2.62	5.74	2.44625623	0.896758894
Nuf2	kinetochore protein Nuf2	2.65	18.77	35.81	22.58	2.437344502	-0.642534031
Wnt16	protein Wnt-16 precursor	2.86	19.78	18.63	30.86	2.428522902	0.698686094
Gpihbp1	glycosylphosphatidylinositol-anchored high	0	4.34	0	0	2.416839742	0
Klk14	kallikrein-14 preproprotein	0	4.3	0	0	2.40599236	0
Cpa6	carboxypeptidase A6 precursor	0	4.26	0	3.36	2.3950628	2.124328135
As3mt	arsenite methyltransferase	0.82	8.53	2.55	3.79	2.388537764	0.432206631
Asphd2	aspartate beta-hydroxylase domain-containing	0	4.22	0	2.13	2.384049807	1.646162657
Pcdh20	protocadherin-20 precursor	20.9	113.02	7.95	29.84	2.380284132	1.784843178
Lst1	leukocyte-specific transcript 1 protein	0	4.19	0	0	2.375734539	0
Nxf7	nuclear RNA export factor 7 isoform 2	0	4.17	0.91	13.78	2.370164281	2.952001726
1700125H03Rik		0	4.16	5.12	12.61	2.367371066	1.153063509
Tas1r2	taste receptor type 1 member 2 precursor	0	4.13	0	0	2.358958826	0
Serpinb6e	serine (or cysteine) peptidase inhibitor, clade	4.01	24.57	3.66	19.05	2.351569652	2.105200377
Birc5	baculoviral IAP repeat-containing protein 5	5.78	33.07	69.33	46.56	2.329144769	-0.564391502
Ifitm5	interferon-induced transmembrane protein 5	0	4.02	3.71	0	2.327687364	-2.23572706
Fhod3	FH1/FH2 domain-containing protein 3	1.23	10.09	7.66	30.59	2.31414375	1.867029007
Hmmr	hyaluronan mediated motility receptor	2.32	15.29	33.6	20.41	2.294731457	-0.692487242
Kcnq3	potassium voltage-gated channel subfamily KQT	0.77	7.67	0	0	2.292282633	0
Ccnb2	G2/mitotic-specific cyclin-B2	4.59	26.36	57.53	41.29	2.291148042	-0.468859718
Kirrel3	kin of IRRE-like protein 3 isoform D precursor	0	3.88	3.15	2.98	2.286881148	-0.060342906
Cdk1	cyclin-dependent kinase 1	6.08	33.47	69.51	42.86	2.283520033	-0.684922069
Shcbp1	SHC SH2 domain-binding protein 1	1.65	11.9	36.07	19.55	2.283306801	-0.851113721
Ntm	neurotrimin precursor	2.7	16.57	0	0	2.247517015	0
Ephb1	ephrin type-B receptor 1 isoform 1	4.53	25.25	3.38	4.72	2.246966037	0.385084277
Icam2	intercellular adhesion molecule 2 precursor	0	3.73	0	1.9	2.241840184	1.5360529
Pthlh	parathyroid hormone-related protein	74.71	355.93	679.17	418.8	2.237085392	-0.696193208
Klrd1	natural killer cells antigen CD94	0	3.71	0	0	2.23572706	0
Nlgn1	neuroligin-1 isoform 2	2.25	14.28	0.82	2.33	2.23313292	0.871583727
Anxa9	annexin A9	5.33	28.6	23.26	12.86	2.225319771	-0.807652293
Iqgap3	IQ motif containing GTPase activating protein 3	2.97	17.56	36.56	20.87	2.224985798	-0.780243843
Mki67	antigen KI-67	8.13	41.51	114.46	72.14	2.219115494	-0.658660599
Tpx2	TPX2, microtubule-associated protein homolog	3.69	20.6	42.7	29.93	2.203371485	-0.498626446
Pdgfc	platelet-derived growth factor C	18.44	88.47	29.41	49.65	2.202375797	0.736016453
Fmod	fibromodulin precursor	43.76	204.85	5	26.21	2.201311507	2.181102551
C1qtnf5	complement C1q tumor necrosis factor-related	0.17	4.37	0.02	0.03	2.198413558	0.014075185

Adamtsl1	ADAMTS-like protein 1	1.22	9.17	3.42	10.49	2.195688098	1.378260523
Lmo3	LIM domain only protein 3	0	3.55	0	0.88	2.185866545	0.910732662
1500015A07Rik		7.16	36.08	13.82	40.7	2.184000187	1.492501936
Cenpf	centromere protein F	1.76	11.54	26.72	16.58	2.183797176	-0.656992187
Mlana	melanoma antigen recognized by T-cells 1	0	3.53	0	6	2.17951105	2.807354922
Top2a	DNA topoisomerase 2-alpha	17.01	79.85	215.36	130.29	2.166449592	-0.720676768
Pbk	lymphokine-activated killer T-cell-originated	7.16	35.49	63.7	49.15	2.160860094	-0.367516011
Pitpnm3	membrane-associated phosphatidylinositol	1.05	8.15	3.84	13.43	2.158147834	1.575992347
A330040F15Rik		0	3.46	0	0	2.15704371	0
Kif22	kinesin-like protein KIF22	3.78	20.29	47.06	27.98	2.155093426	-0.729779054
D4Bwg0951e	hypothetical protein LOC52829	4.23	22.29	68.71	120.22	2.154827788	0.798190215
Lce6a	late cornified envelope 6A	0	3.44	6.2	12.73	2.150559677	0.931262814
Nme3	nucleoside diphosphate kinase 3	26.43	119.59	60.33	63.47	2.136283749	0.072035033
1190002F15Rik		5.72	28.44	45.91	29.85	2.131244533	-0.604625011
B930003M22Rik		0	3.37	1.42	1.68	2.12763328	0.147225953
Timp3	metalloproteinase inhibitor 3 precursor	63.68	279.68	460.54	686.08	2.117534684	0.574022402
Bub1	mitotic checkpoint serine/threonine-protein	1.37	9.27	20.34	15.2	2.115477217	-0.397566363
Nek2	serine/threonine-protein kinase Nek2	2.41	13.75	27.3	17.88	2.11287131	-0.583943288
Gpnmb	transmembrane glycoprotein NMB precursor	55.7	243.45	16.13	44.41	2.108118765	1.406484885
Rpl39l	ribosomal protein L39-like protein	0	3.31	0	0	2.107687869	0
Loxl2	lysyl oxidase homolog 2 precursor	9.21	42.79	2.27	21.7	2.100618584	2.795329757
Lmcd1	LIM and cysteine-rich domains protein 1	47.45	206.43	46.98	74.42	2.098055991	0.652513993
Ifi27l2a	interferon, alpha-inducible protein 27 like 2A	22.79	100.78	24.15	47.38	2.09702692	0.943852369
Gm14005		0	3.25	3.2	0	2.087462841	-2.070389328
St3gal5	lactosylceramide alpha-2,3-sialyltransferase	1.76	10.68	1.63	5.21	2.081300102	1.239530469
Wfdc2	WAP four-disulfide core domain protein 2	0	3.23	0	0	2.080657663	0
Ube2c	ubiquitin-conjugating enzyme E2 C	9.52	43.49	93.58	62.16	2.080346394	-0.582523971
Ttr	transthyretin	0	3.19	0	0	2.066950244	0
Ltc4s	leukotriene C4 synthase	0	3.17	0	0	2.060047384	0
Fxyd4	FXYD domain-containing ion transport regulator 4	0	3.15	0	3.89	2.053111336	2.289834465
E130306D19Rik	vav-like protein C9orf100 homolog	1.61	9.8	11.94	9.49	2.0489096	-0.302822939
Prc1	protein regulator of cytokinesis 1	12.11	53.04	93.92	62.41	2.043359989	-0.582001724
Fam64a	family with sequence similarity 64, member A	2.47	13.29	29.25	19.58	2.041998349	-0.55569216
Tmem95	transmembrane protein 95	0	3.11	0	3.25	2.039138394	2.087462841
Slc16a1	monocarboxylate transporter 1	21.3	90.05	119.29	172.13	2.029615307	0.525339024
Eya1	eyes absent homolog 1	2.76	14.25	2.6	9.74	2.020004676	1.576925182
Slc20a1	sodium-dependent phosphate transporter 1 isoform	33.31	136.72	59.44	144.45	2.005037055	1.266947731
Adcy7	adenylate cyclase type 7	6.46	28.87	37.86	68.23	2.001449702	0.833111447
Neil3	endonuclease 8-like 3	1.56	9.24	24.07	12.48	2	-0.8951415
Kif20a	kinesin-like protein KIF20A	5.41	24.42	49.6	45.69	1.987567768	-0.116023796
Depdc1a	DEP domain-containing protein 1A isoform 2	0.86	6.36	14.1	9.31	1.984403145	-0.550504217
Itga1	integrin alpha-1 precursor	9.54	40.69	4.71	23.77	1.983826505	2.117031218
Ccna2	cyclin-A2	10.15	42.68	101.36	60.21	1.969929146	-0.741812779
Col4a4	collagen alpha-4(IV) chain precursor	3.44	16.36	22.19	15.67	1.967135366	-0.476248716
Kif23	kinesin family member 23	5.18	23.12	52.37	34.21	1.964551164	-0.600043784
Vit	vitrin isoform 2	54.79	215.96	5.92	6.7	1.959350627	0.154086408
Bst1	ADP-ribosyl cyclase 2	5.75	25.16	6.53	12.41	1.954403134	0.832587467
Spc24	kinetochore protein Spc24	3.55	16.62	41.66	27.45	1.953275474	-0.584455313
Fam84a	family with sequence similarity 84, member A	141.94	552.53	681.87	936.24	1.953251816	0.456807573
Fgf21	fibroblast growth factor 21 precursor	0	2.87	0	3.58	1.952333566	2.195347598
Anln	actin-binding protein anillin	21.37	85.35	130.24	75.94	1.948630921	-0.770401764
Ckap2	cytoskeleton-associated protein 2	7.47	31.51	59.59	32.08	1.940449681	-0.873120471
Aurkb	serine/threonine-protein kinase 12	4.06	18.37	35.63	21.72	1.936614664	-0.689062866
Kcnmb4	calcium-activated potassium channel subunit	2.45	12.2	3.27	4.69	1.935869663	0.414192583
Nusap1	nucleolar and spindle-associated protein 1	6.44	27.42	66.17	39.19	1.933532028	-0.740980452
Pglyrp1	peptidoglycan recognition protein 1 precursor	2.62	12.81	0	0	1.931651717	0
Wnt6	protein Wnt-6 precursor	4.81	21.15	48.38	88.69	1.93069663	0.861020304
Tyrp1	5,6-dihydroxyindole-2-carboxylic acid oxidase	5.47	23.58	11.16	35.15	1.925647298	1.571852418
Il17rb	interleukin-17 receptor B precursor	17.45	69.03	16.74	32.25	1.924352271	0.906348331
Amtn	amelotin precursor	0	2.79	0	24.97	1.922197848	4.698774109
Cdca5	sororin	2.44	12.02	24.87	13.4	1.920248978	-0.845211242
C1s	complement C1s-A subcomponent	106.07	402.95	9.14	84.23	1.915622423	3.07130368
S100a9	protein S100-A9	0	2.74	0	4.59	1.90303827	2.482848283
9430076C15Rik		3.77	16.76	1.69	6.28	1.89657041	1.436332278
Dlgap5	disks large-associated protein 5 isoform 1	2.29	11.19	26.44	16.24	1.889538637	-0.670520707
BC002163		5.16	21.8	12.72	7.35	1.888031568	-0.716432379
2810417H13Rik	PCNA-associated factor	4.08	17.75	71.63	32.1	1.883990193	-1.133734363
Spag5	sperm-associated antigen 5	1.93	9.8	23.1	16.41	1.882058743	-0.469116943
AI662270		0	2.68	0.91	0	1.879705766	-0.933572638
Melk	maternal embryonic leucine zipper kinase	2.65	12.38	33.35	19.92	1.874109747	-0.715427247
Rbpjl	recombining binding protein suppressor of	1.07	6.58	0	2.03	1.872567081	1.599317794
Wif1	wnt inhibitory factor 1 precursor	136.91	502.54	154.15	384.03	1.868379315	1.311307162
Xlr3b	X-linked lymphocyte-regulated protein 3B	1.07	6.54	0.53	6.05	1.864933756	2.204091605
Batf3	basic leucine zipper transcriptional factor	0	2.64	0	0	1.86393845	0
2810408I11Rik		0	2.63	5.6	2.95	1.859969548	-0.740613371
Kifc1	kinesin-like protein KIFC1	3.79	16.25	34.09	21.31	1.848498801	-0.653369434
Gja1	gap junction alpha-1 protein	731.73	2620.21	564.38	2167.39	1.838879351	1.939331504
Cdc25c	M-phase inducer phosphatase 3	2.04	9.85	22.18	12.08	1.835551814	-0.825518026
Racgap1	rac GTPase-activating protein 1	7.16	27.97	63.84	46.42	1.827918627	-0.451388428
Tubb6	tubulin beta-6 chain	17.12	63.24	34.14	73.24	1.825888937	1.079082519
Spc25	kinetochore protein Spc25 isoform 1	6.8	26.64	45.54	31.4	1.825211587	-0.522477398
Thy1	thy-1 membrane glycoprotein preproprotein	84.33	301.04	27.86	74.08	1.823614669	1.37935735
Kif11	kinesin-like protein KIF11	5.76	22.83	60.69	37.37	1.8176838	-0.685057881
Cep55	centrosomal protein of 55 kDa isoform 1	2.61	11.68	27.67	17.26	1.812484003	-0.650855139
Scrg1	scrapie-responsive protein 1 precursor	103.44	363.68	2.13	50.76	1.803956718	4.047603055
Ccnb1	G2/mitotic-specific cyclin-B1	4.43	17.71	45.95	24.89	1.784785455	-0.858730193
Edn2	endothelin-2 precursor	11.99	43.53	35.72	81.25	1.777376181	1.16344962
Foxm1	forkhead box protein M1	4.26	17.02	32.94	24.26	1.776464307	-0.426131926
F630043A04Rik	spindle and kinetochore-associated protein 3	1.42	7.29	16.51	12.13	1.776365054	-0.415312168
Agrp	agouti-related protein precursor	0	2.42	0	0	1.773996325	0
Casc5	protein CASC5	1.47	7.42	17.47	11.64	1.769309191	-0.547187403
Crct1	cysteine-rich C-terminal 1	27.56	96.31	104.44	117.85	1.768592091	0.172719628

Gm5506	hypothetical protein LOC433182	12.4	44.28	24.53	54.2	1.756640957	1.112474729
Gm4532		0	2.36	2.07	1.75	1.748461233	-0.158807037
Bhlhe40	class E basic helix-loop-helix protein 40	110.53	372.58	1033.25	1092.58	1.743985394	0.080473806
Cnksr2	connector enhancer of kinase suppressor of ras	3.05	12.51	0.45	2.62	1.738033862	1.319936797
Cks2	cyclin-dependent kinases regulatory subunit 2	8.98	32.21	73.71	51.89	1.734506002	-0.498306387
Cdca3	cell division cycle-associated protein 3	11.14	39.26	92.43	55.19	1.729578751	-0.733572468
Hist3h2ba	histone H2B type 3-A	0	2.3	4.15	6.18	1.722466024	0.479411412
Diap3	protein diaphanous homolog 3	3.9	15.11	43.54	21.57	1.71710284	-0.98069514
Cdc20	cell division cycle protein 20 homolog	10.2	35.76	78.29	45.53	1.714638034	-0.768977739
Akr1cl	aldo-keto reductase family 1, member C-like	0	2.27	1.89	5.09	1.709290636	1.075372735
Gm16386		0	2.27	4.65	2.83	1.709290636	-0.560906475
Kntc1	kinetochore-associated protein 1	1.32	6.56	17.19	12.84	1.704261429	-0.3943016
Abcc8	ATP-binding cassette, sub-family C (CFTR/MRP),	0	2.23	0	0.3	1.691534165	0.378511623
Calml4	calmodulin-like protein 4 isoform b	0	2.23	0	0	1.691534165	0
Tspan12	tetraspanin-12	0	2.23	0	0	1.691534165	0
Tnfsf13	tumor necrosis factor ligand superfamily member	3.09	12.19	6.63	5.41	1.689271816	-0.2513587
Kif4	chromosome-associated kinesin KIF4	1.87	8.2	21.58	12.86	1.680583124	-0.704118229
Mis18bp1	mis18-binding protein 1	1.98	8.53	19.02	11.32	1.677163883	-0.700439718
Ccnb1ip1	E3 ubiquitin-protein ligase CCNB1IP1	0	2.18	0	5.1	1.669026766	2.608809243
D630032N06Rik		0	2.18	0	0	1.669026766	0
Klk6	kallikrein related-peptidase 6 precursor	0	2.17	16.83	6.2	1.66448284	-1.308237891
Asf1b	histone chaperone ASF1B	5.78	20.49	43.72	26.83	1.664308304	-0.68427928
Gpr64	G-protein coupled receptor 64 isoform 2	4.07	15.04	5.49	8.27	1.661616489	0.514350861
Gm12166		0.53	3.83	5.36	7.98	1.658491536	0.497688679
Airn		17.56	57.51	3.71	21.18	1.656486508	2.235460401
Gm13124	hypothetical protein LOC627085	0	2.15	0	0	1.655351829	0
Vpreb2	immunoglobulin omega chain precursor	0	2.15	0	0	1.655351829	0
Pkp2	plakophilin-2	1.44	6.6	7.3	5.34	1.639118271	-0.388628496
Cdca8	borealin	9.68	32.14	68.58	43.31	1.633661956	-0.651040352
Serpinb11	serpin B11	452.94	1405.65	587.66	541.76	1.631689879	-0.117120197
Aspm	abnormal spindle-like microcephaly-associated	1.66	7.23	21.33	12.1	1.629466185	-0.769416439
Tgif2	homeobox protein TGIF2	5.84	20.16	12.98	32.98	1.629271397	1.281321492
Bub1b	mitotic checkpoint serine/threonine-protein	5.84	20.15	51	34.77	1.628589433	-0.539761505
Ngb	neuroglobin	0	2.09	0	0	1.627606838	0
Hs6st2	heparan-sulfate 6-O-sulfotransferase 2 isoform	1.18	5.73	4.27	11	1.62627837	1.187159539
Mest	mesoderm-specific transcript protein	18.81	60.13	12.51	18.18	1.625651687	0.505575046
Cdca2	cell division cycle-associated protein 2	1.27	5.99	15.25	10.51	1.622600158	-0.497551885
Rpl26	60S ribosomal protein L26	7.39	24.81	39.84	21.8	1.621187426	-0.840949042
Rbp7	retinoid-binding protein 7	0	2.07	0	0	1.618238656	0
4833422C13Rik		0.01	2.1	2.08	3.58	1.617912923	0.572417247
4930474M22Rik		0	2.06	9.43	8.81	1.613531653	-0.088414116
Adamts20	A disintegrin and metalloproteinase with	0	2.06	0.23	1.87	1.613531653	1.222392421
Cenpe	centromere-associated protein E	1.51	6.68	17.68	10.94	1.613418947	-0.645691618
Esco2	N-acetyltransferase ESCO2	3.31	12.18	35.63	19.2	1.612590596	-0.858670408
Cd36	platelet glycoprotein 4	7.82	25.97	17.44	26.24	1.612504961	0.562888048
Gm14403		8.52	28.07	4.6	22.21	1.610497593	2.05124779
1700086O06Rik		10.52	34.08	6.46	30.39	1.606508031	2.073057493
Gfra3	GDNF family receptor alpha-3 preproprotein	2.84	10.68	4.25	3.32	1.604862058	-0.28128611
Gm889	hypothetical protein LOC380755	0	2.04	0	1.23	1.604071324	1.15704371
Kif2c	kinesin-like protein KIF2C	1.75	7.36	23.65	14.86	1.604071324	-0.636194876
Synpo2	synaptopodin-2	16.25	51.41	25.2	119.15	1.603245747	2.197197932
Gm106	RPE-spondin precursor	6.2	20.86	4.22	12.55	1.602224589	1.37617114
Sprr2d	small proline-rich protein 2D	0	2.02	0	0	1.59454855	0
Kif15	kinesin-like protein KIF15	2.63	9.87	25.38	16.22	1.582310487	-0.615359422
Kif20b	kinesin-like protein KIF20B	3.23	11.66	20.06	12.63	1.581547836	-0.627719874
Gm13363		2.22	8.62	29.53	14.22	1.578976206	-1.004259231
Gm5077	complement C1s-B subcomponent precursor	21.24	65.43	2.53	15.12	1.578678126	2.191111655
Snhg11	small nucleolar RNA host gene 11 (non-protein	2.14	8.37	0.86	2.25	1.577284489	0.805137097
Matn4	matrilin-4 precursor	0	1.98	0	0	1.575312331	0
Lonrf3	LON peptidase N-terminal domain and RING finger	1.23	5.62	3.87	3.94	1.569787507	0.02058927
Arhgap11a	rho GTPase-activating protein 11A	3.84	13.3	25.78	15.5	1.562936194	-0.698689936
Iyd	iodotyrosine dehalogenase 1 precursor	1.02	4.94	0	4.22	1.556107638	2.384049807
Ly6g5b	lymphocyte antigen 6 complex locus protein G5b	0	1.94	1.83	0	1.555816155	-1.500802053
Nhedc2	mitochondrial sodium/hydrogen exchanger NHA2	2.28	8.62	3.58	7.69	1.552341079	0.924008579
Fabp4	fatty acid-binding protein, adipocyte	45.4	134.71	24.43	43.67	1.548330321	0.812774793
Gm1564	hypothetical protein LOC268491	0.59	3.64	0	0.48	1.54509804	0.565597176
Fanca	Fanconi anemia group A protein homolog	0.73	4.04	7.25	7.12	1.542651696	-0.022914392
Lzts1	leucine zipper putative tumor suppressor 1	1.58	6.48	4.72	12.83	1.535667204	1.273714104
Col4a3	collagen alpha-3(IV) chain precursor	2.9	10.29	21.07	16.71	1.533499457	-0.317522418
Ly6k	lymphocyte antigen 6K precursor	0	1.89	5.37	10.88	1.531069493	0.899169559
Lrrc23	leucine-rich repeat-containing protein 23	0	1.88	0	0	1.526068812	0
Cxcl3	C-X-C motif chemokine 3 precursor	0	1.86	0	0	1.516015147	0
Slc1a3	excitatory amino acid transporter 1	1.3	5.57	16.82	10.1	1.514259509	-0.68293766
Gpx2-ps1		11.47	34.6	27.41	36.51	1.513415776	0.400876431
Hoxc12	homeobox protein Hox-C12	0	1.85	0	2.68	1.510961919	1.879705766
Mir17hg		18.26	53.84	24.85	44.07	1.509620868	0.80200317
Bgn	biglycan precursor	175.19	499.83	87.56	254.79	1.507188939	1.530232737
Plk1	serine/threonine-protein kinase PLK1	3.53	11.87	29.07	18.32	1.506429098	-0.638229774
Mxd3	max dimerization protein 3	7.59	23.38	37.06	23.29	1.504968089	-0.647913072
Galnt14	polypeptide N-acetylgalactosaminyltransferase	22.72	66.18	15.33	49.23	1.501927786	1.621024484
Tnni2	troponin I, fast skeletal muscle	0	1.83	0	0	1.500802053	0
Dact1	dapper homolog 1 isoform 1	11.15	33.34	3.57	7.76	1.498933726	0.938736705
Sgol1	shugoshin-like 1	1.34	5.61	14.73	7.62	1.498141742	-0.867758896
Cry1	cryptochrome-1	23.44	67.9	35.45	59.45	1.495259698	0.729823525
Ect2	protein ECT2 isoform 2	10.46	31.28	53.66	35.29	1.494033535	-0.590913403
Gm5577		0	1.81	3.25	1.24	1.49057013	-0.923964109
Car9	carbonic anhydrase 9 precursor	0.76	3.93	1.75	2.27	1.486012218	0.249859017
Frat2	GSK-3-binding protein FRAT2	6.6	20.26	16.87	31.47	1.484070273	0.86156775
Eid3	EP300-interacting inhibitor of differentiation	2.32	8.24	5.22	11.01	1.47670961	0.949249666
Clspn	claspin	0.96	4.45	16.64	6.95	1.475402576	-1.149823795
Dct	L-dopachrome tautomerase precursor	20.76	59.2	37.62	85.03	1.46808493	1.155491673
Tacc3	transforming acidic coiled-coil-containing	8.17	24.35	56.22	37.56	1.466992108	-0.569414446

Klhl34	kelch-like protein 34	1.08	4.75	0	1.74	1.466978428	1.454175893
5730405O15Rik		0	1.76	0	0	1.464668267	0
Ebi3	interleukin-27 subunit beta precursor	0	1.76	0	0	1.464668267	0
Rem1	GTP-binding protein REM 1	0	1.76	0	0	1.464668267	0
Cdk18	cyclin-dependent kinase 18	4.68	14.67	3.85	13.6	1.464042345	1.589911717
Stmn1	stathmin	61.59	171.61	457.59	408.28	1.463511967	-0.164116727
Tsc22d1	TSC22 domain family protein 1 isoform 3	177.46	489.86	394.68	1417.4	1.459710862	1.841858391
Zfp618	zinc finger protein 618	0	1.75	0	2.97	1.459431619	1.989139007
Pitpnc1	cytoplasmic phosphatidylinositol transfer	4.06	12.87	3.77	10.31	1.454758498	1.245537758
Dnajb13	dnaJ homolog subfamily B member 13	0	1.74	1.18	3.43	1.454175893	1.022978564
Ear2	eosinophil cationic protein 2 precursor	0	1.73	27.83	3.09	1.448900951	-2.817398089
Xlr3c	X-linked lymphocyte-regulated protein 3C	0.79	3.88	0.3	3.36	1.44692156	1.745816512
Tmem88b	transmembrane protein 88B	1.87	6.82	1.61	5.21	1.446117871	1.250543462
Reep1	receptor expression-enhancing protein 1	4.73	14.56	8.46	11.95	1.441235016	0.453040009
Cenpi	centromere protein I	2.23	7.73	15.31	10.43	1.434447489	-0.512931378
Tmem37	voltage-dependent calcium channel gamma-like	0	1.7	0	0	1.432959407	0
Kif18b	kinesin-like protein KIF18B	1.51	5.76	19.21	12.05	1.429335882	-0.631019515
Bves	blood vessel epicardial substance	5.42	16.23	0	1.33	1.424277499	1.220329955
C1rl	complement C1r subcomponent-like protein	3.21	10.29	0	0.68	1.423153348	0.748461233
Fgf13	fibroblast growth factor 13	4.39	13.42	6.18	6.04	1.419713986	-0.028408415
Hlf	hepatic leukemia factor	8.01	23.09	7.99	19.14	1.418835382	1.163670662
Wnt11	protein Wnt-11 precursor	8.81	25.21	14.99	10.58	1.417792312	-0.465534685
Beta-s	hemoglobin subunit beta-1-like	21.23	58.25	16.81	25.97	1.414307206	0.598668005
Malat1		279.88	746.53	496.29	681.06	1.412177578	0.455811237
Troap	tastin	1.21	4.87	13.38	7.11	1.409314134	-0.826289856
Kif14	kinesin-like protein KIF14	0.7	3.51	8.21	6	1.407592687	-0.395846234
Rgag1	retrotransposon gag domain-containing protein 1	0	1.65	0	0	1.40599236	0
Zglp1	GATA-type zinc finger protein 1	0	1.65	1.37	0	1.40599236	-1.244887059
D630041G03Rik		2.11	7.22	9.7	9.54	1.402223814	-0.02173593
Ptprcap	protein tyrosine phosphatase receptor type	1.37	5.26	2.59	0	1.401275598	-1.843983844
Tmem176a	transmembrane protein 176A	29.26	78.72	53.86	57.3	1.397529723	0.087741261
Gngt2	guanine nucleotide-binding protein	2.28	7.64	4.32	0	1.397335498	-2.411426246
Prex2	phosphatidylinositol	1.87	6.56	1.49	9.61	1.397335498	2.091207009
Pmel	melanocyte protein PMEL precursor	11.29	31.31	14.02	41.97	1.394495835	1.516444964
Ncapg	non-SMC condensin I complex, subunit G	4.77	14.15	37.05	16.14	1.39267457	-1.150529344
Gpx2	glutathione peroxidase 2	41.43	110.09	93.38	116.08	1.388572372	0.310941574
Ncam1	neural cell adhesion molecule 1 isoform 2	1.22	4.79	2.48	13.66	1.383003672	2.074725892
Krt8	keratin, type II cytoskeletal 8	6.53	18.61	8.31	20.19	1.380867766	1.186530515
Slc17a9	solute carrier family 17 member 9	2.43	7.93	1.86	2.33	1.380451599	0.21950703
Ska1	spindle and kinetochore-associated protein 1	0.93	4.01	10.75	7.18	1.376209756	-0.522488009
Uhrf1	E3 ubiquitin-protein ligase UHRF1 isoform B	12.95	35.19	77.51	56.11	1.375325986	-0.459133041
Thsd4	thrombospondin type-1 domain-containing protein	3.08	9.58	22.71	32.38	1.37469857	0.493488292
Gzmm	granzyme M	1.79	6.23	3	3.83	1.373730525	0.272023189
AI593442	hypothetical protein LOC330941 isoform 2	0	1.59	0.78	2.7	1.372952098	1.05564803
Tnmd	tenomodulin	4.81	14.04	1.58	3.21	1.372194498	0.706449168
Tk1	thymidine kinase, cytosolic	10.02	27.51	62.8	44.27	1.371343815	-0.495001117
Morn3	MORN repeat-containing protein 3	0	1.58	0	0	1.367371066	0
Ndc80	kinetochore protein NDC80 homolog	2.68	8.49	25.6	12.95	1.366702321	-0.931161124
Gpx3	glutathione peroxidase 3 isoform 2	21.51	57	8.7	35.7	1.365486843	1.919723411
Gnal	guanine nucleotide-binding protein G(olf)	4.85	14.04	6.53	10.38	1.362296037	0.595778788
Pi15	peptidase inhibitor 15	336.21	864.61	137.78	86.22	1.360069846	-0.670068776
E330013P04Rik		0	1.56	0	0	1.35614381	0
Htr2b	5-hydroxytryptamine receptor 2B	0	1.56	1.14	1.47	1.35614381	0.206900245
Ecscr	endothelial cell-specific chemotaxis regulator	10.82	29.24	1.83	4.5	1.355228104	0.958629566
Dtl	denticleless protein homolog	2.76	8.61	30.95	18.46	1.353803769	-0.715304221
Olr1	oxidized low-density lipoprotein receptor 1	0.62	3.14	4.45	4.33	1.353636955	-0.032120697
Gm6994		0.46	2.73	0	0.67	1.353207261	0.739848103
1700001K19Rik	hypothetical protein LOC66323	0	1.55	1.96	1.63	1.350497247	-0.170534376
Kpna2	importin subunit alpha-2	6.85	19.01	30.36	25.02	1.349956608	-0.269304597
Apcdd1	protein APCDD1 precursor	40.88	105.48	457.74	518.03	1.346249129	0.17814122
Chi3l1	chitinase-3-like protein 1	0	1.54	16.23	15.45	1.344828497	-0.066835118
Gch1	GTP cyclohydrolase 1 precursor	5.05	14.31	28.26	19.86	1.339467235	-0.488190612
Gpr27	probable G-protein coupled receptor 27	0	1.53	2.49	1.63	1.339137385	-0.408164237
Ltb	lymphotoxin-beta	0	1.53	0	0	1.339137385	0
Sgol2	shugoshin-like 2 isoform 2	3	9.12	20.74	11.56	1.339137385	-0.791515476
Mpdz	multiple PDZ domain protein	35.67	91.76	34.78	58.15	1.338902554	0.725224781
2010015L04Rik	hypothetical protein LOC544678 isoform 2	0	1.51	0	0.56	1.327687364	0.641546029
Shox2	short stature homeobox protein 2	0	1.51	0	0	1.327687364	0
Zdhhc12	probable palmitoyltransferase ZDHHC12 isoform b	13.56	35.39	30.89	11.81	1.321531696	-1.315833622
Tgm3	protein-glutamine gamma-glutamyltransferase E	4	11.49	1.1	3.42	1.320773477	1.073657042
Fstl1	follistatin-related protein 1 precursor	155.66	390.03	65.22	127.49	1.319642433	0.956317167
Col12a1	collagen alpha-1(XII) chain	111.27	279.2	8.04	54.72	1.319484483	2.62380058
Slc12a1	solute carrier family 12 member 1 isoform F	0.58	2.94	0.68	1.61	1.318271071	0.635588574
Btnl9	butyrophilin-like protein 9	0	1.49	0	0	1.316145742	0
Cpa2	carboxypeptidase A2 precursor	0	1.49	0	0	1.316145742	0
Lrrc46	leucine-rich repeat-containing protein 46	0	1.49	1.16	1.67	1.316145742	0.30580843
Ripply3	protein ripply3	0	1.49	9.09	8.02	1.316145742	-0.161726836
Camk1g	calcium/calmodulin-dependent protein kinase type	0.45	2.61	1.28	0.86	1.315945937	-0.293731203
Aox1	aldehyde oxidase	3.47	10.12	4.67	7.03	1.314810052	0.502051253
Tmem173	transmembrane protein 173	11.06	28.96	11.52	46.93	1.312807717	1.936694378
Ankle1	ankyrin repeat and LEM domain containing 1	0.54	2.82	6.88	5.21	1.310642287	-0.343602361
1700040L02Rik	hypothetical protein LOC73287	0	1.48	1.33	1.54	1.310340121	0.124498542
Fam178b	hypothetical protein LOC381337 isoform A	0	1.48	2.51	4.41	1.310340121	0.624157564
Krt35	keratin, type I cuticular Ha5	0	1.48	13.98	20.64	1.310340121	0.530662875
Orm3	alpha-1-acid glycoprotein 3 precursor	0	1.48	1.05	0	1.310340121	-1.03562391
Tmem180	transmembrane protein 180	8.92	23.58	11.58	11.31	1.30907289	-0.03130116
Nnat	neuronatin isoform beta	4.1	11.63	6.9	9.12	1.308285487	0.357284732
Stil	SCL-interrupting locus protein homolog	1.09	4.17	9.41	7.66	1.306661338	-0.265531139
Syt4	synaptotagmin-4	0.59	2.93	1.37	3.36	1.305502547	0.879441076
Ngf	beta-nerve growth factor isoform A	4.28	12.05	1.95	2.1	1.305439972	0.071553261
Hsd17b2	estradiol 17-beta-dehydrogenase 2	0	1.47	4.62	3.47	1.304511042	-0.330295299
Chst15	carbohydrate sulfotransferase 15	7.62	20.26	42.03	29.94	1.302381822	-0.475869643

Apitd1	centromere protein S	6	16.23	24.98	18.83	1.299495874	-0.389716753
0610005C13Rik		0	1.46	0	0	1.298658316	0
Rep15	rab15 effector protein	0	1.46	1.86	0	1.298658316	-1.516015147
Gmnn	geminin	5.15	14.08	40.49	26.11	1.293978113	-0.613938544
AI428936	nesprin-4	0	1.45	0	1.24	1.292781749	1.163498732
Cldn11	claudin-11	0	1.45	0	0	1.292781749	0
Gm10451		0	1.45	0	2.55	1.292781749	1.827819025
E2f8	transcription factor E2F8	1.72	5.65	14.16	8.54	1.289747689	-0.668208582
C8g	complement component C8 gamma chain precursor	0	1.44	1.39	2.05	1.286881148	0.351798624
Trpm1	transient receptor potential cation channel	0	1.44	0.57	1.51	1.286881148	0.676922805
Slfn10-ps	schlafen 10	4.04	11.28	5.73	8.16	1.284814922	0.444741093
Acsm3	acyl-coenzyme A synthetase ACSM3, mitochondrial	1.37	4.74	3.37	9.65	1.276163678	1.285148246
Gm436	hypothetical protein LOC230890	0	1.42	20.06	31.77	1.275007047	0.637870237
Hsf3	heat shock factor protein 3	0	1.42	0.79	0	1.275007047	-0.839959587
Cnih2	protein cornichon homolog 2	4.92	13.3	7.52	12.89	1.272346066	0.705121264
Ccdc3	coiled-coil domain-containing protein 3	690.23	1663.94	160.91	329.3	1.268232449	1.028584876
Wnt5a	protein Wnt-5a precursor	4.4	11.97	3.69	13.4	1.264147167	1.618408984
Osgin1	oxidative stress-induced growth inhibitor 1	9.01	23.04	39.55	47.53	1.263994922	0.259174946
Nrp	neural regeneration protein	0.75	3.2	2.41	4.72	1.263034406	0.746243408
Slc25a2	mutant ornithine transporter 2	0	1.4	0.89	2.06	1.263034406	0.695145418
Atp8b5	probable phospholipid-transporting ATPase FetA	0.55	2.71	0	0.45	1.259150971	0.5360529
Nsl1	kinetochore-associated protein NSL1 homolog	2.03	6.25	13.22	8	1.258663201	-0.659924558
Sit1	signaling threshold-regulating transmembrane	0	1.39	0	0	1.257010618	0
Tsc22d2	TSC22 domain family protein 2	64.87	156.42	60.66	99.11	1.25692539	0.699179298
Pdpn	podoplanin precursor	6.1	15.95	4.65	12.12	1.255394344	1.215444947
Cdkn3	cyclin-dependent kinase inhibitor 3	2.6	7.59	29.72	15.9	1.254661225	-0.86215497
Brca1	breast cancer type 1 susceptibility protein	1.92	5.96	14.43	8.7	1.253118937	-0.669681409
Lag3	lymphocyte activation gene 3 protein precursor	5.79	15.18	9.04	13.42	1.252728128	0.522311895
Tm4sf1	transmembrane 4 L6 family member 1	24.16	58.93	449.12	206.75	1.252146452	-1.115461192
4930547N16Rik	PARP1-binding protein	1.44	4.81	11.46	5.98	1.251657016	-0.836005127
Rpp25	ribonuclease P protein subunit p25	0	1.38	10.91	4.49	1.250961574	-1.117295359
Mcm10	protein MCM10 homolog	0.77	3.21	9	6.47	1.250070873	-0.420819852
Spon1	spondin-1 precursor	2.51	7.33	2.14	5.27	1.246845465	0.997700884
D2Ertd750e	putative TRAF4-associated factor 1	5.33	14	27.54	20.25	1.244685096	-0.425522494
Smc2	structural maintenance of chromosomes protein 2	14.68	36.11	62.69	41.67	1.242882442	-0.577844761
Gimap4	GTPase IMAP family member 4 isoform b	1.21	4.22	0	0.99	1.240003437	0.992768431
2700099C18Rik		2.15	6.4	13.86	8.67	1.232173442	-0.619846321
Kifc5b	kinesin family member C5B	3.73	10.11	19.98	12.52	1.231946728	-0.633919526
Trh	prothyroliberin	4.56	12.02	1.13	6.19	1.22757266	1.75513834
Fam47e	hypothetical protein LOC384198 isoform 3	0	1.34	0	0	1.22650853	0
Gm438	hypothetical protein LOC329993	0	1.34	0	1.8	1.22650853	1.485426827
Mir27a		245.88	576.44	117.62	226.8	1.225861081	0.94142047
Prelp	prolargin precursor	18.16	43.8	6	8.5	1.225401171	0.440572591
Slfn9	schlafen 9	3.79	10.2	28.53	16.76	1.225401171	-0.733549775
Igfbp3	insulin-like growth factor-binding protein 3	841.05	1965.65	100.49	99.17	1.223762421	-0.018887084
2610021K21Rik	EF-hand calcium-binding domain-containing	0.63	2.8	4.1	3.46	1.221127454	-0.193453537
Gm885	allergin-1 precursor	0	1.33	0	0	1.220329955	0
Cldn19	claudin-19 isoform 1	0.5	2.49	0.36	0.52	1.218264536	0.160464672
Epha4	ephrin type-A receptor 4 precursor	219.15	511.16	127.81	203.46	1.218107738	0.666574026
Rprm	protein reprimo	0	1.32	0	0	1.214124805	0
Tac4	tachykinin-4 precursor	0	1.32	0	1.09	1.214124805	1.063502942
Rrad	GTP-binding protein RAD	4.75	12.32	5.73	35.39	1.211960221	2.434863641
Fam70a	family with sequence similarity 70, member A	5.08	13.08	2.34	13.32	1.211504105	2.100111485
Slc7a1	high affinity cationic amino acid transporter 1	9.13	22.45	22.48	40.31	1.210953749	0.815058652
Lgals3	galectin-3	1504.4	3479.72	1161.48	1568.52	1.209238887	0.433117517
Slc25a18	mitochondrial glutamate carrier 2	0	1.31	0.9	1.91	1.207892852	0.615019735
Dusp18	dual specificity protein phosphatase 18	8.43	20.76	11.89	13.25	1.206348881	0.144709656
Dgat2l6	diacylglycerol O-acyltransferase 2-like protein	1.22	4.12	0	1.3	1.205584134	1.201633861
Cyp2b19	cytochrome P450 2B19	5.6	14.21	38.01	51.02	1.204482223	0.415222401
Prkca	protein kinase C alpha type	13.03	31.25	7.79	13.28	1.200784152	0.700060909
Chd3	chromodomain helicase DNA binding protein 3	52.75	122.2	53.86	159.55	1.196665596	1.549196138
4933433C11Rik	hypothetical protein LOC74472	0	1.29	0	0	1.195347598	0
G530011O06Rik		1.15	3.92	1.68	4.62	1.194321656	1.06833713
Ces4a	carboxylesterase 4A	2.13	6.15	1.28	3	1.191780585	0.810966176
Gsdma3	gasdermin-A3	9.59	23.17	172.3	88.35	1.190514884	-0.95573202
Ncf4	neutrophil cytosol factor 4	0	1.28	1.06	0	1.189033824	-1.042644337
F730043M19Rik		0	1.27	5.83	5.61	1.182692298	-0.047235307
Kir3dl1	killer cell immunoglobulin-like receptor 3DL1	0	1.27	0	0	1.182692298	0
2010317E24Rik	protein C9orf140 homolog	1.2	3.99	10.63	5.97	1.181536292	-0.738620536
Peg10	retrotransposon-derived protein PEG10 isoform 2	1.25	4.1	0.27	0.88	1.180572246	0.565904165
Lrr1	peptidylprolyl isomerase-like 5	0.95	3.42	7.21	3.83	1.180572246	-0.765359033
1810011O10Rik	thyroid cancer-1	40.43	92.9	390.27	531.37	1.180449338	0.444264777
Fam113b	hypothetical protein LOC239647	1.91	5.58	4.37	4.46	1.177068431	0.023978863
4930512B01Rik		0	1.26	0.59	0.37	1.176322773	-0.214850872
Krt85	keratin, type II cuticular Hb5	0	1.26	0	5.52	1.176322773	2.704871964
Ybx2	Y-box-binding protein 2	3.12	8.31	4.45	5.08	1.17613683	0.157815094
Cnn1	calponin-1	6.78	16.57	4.59	4.98	1.175272131	0.097297201
Rad51ap1	RAD51-associated protein 1	2.58	7.07	19.31	11.41	1.172609086	-0.710687124
Gpr18	N-arachidonyl glycine receptor	0	1.25	0	0	1.169925001	0
Cenpn	centromere protein N	3.35	8.77	22.08	17.51	1.167343161	-0.318338329
Mtap1b	microtubule-associated protein 1B	12.39	29.04	25.53	55.87	1.165728852	1.100043129
Lck	proto-oncogene tyrosine-protein kinase LCK	1.06	3.62	2.25	3.28	1.165248514	0.397171078
Sqle	squalene monooxygenase	51.54	116.82	145.08	153.44	1.165096353	0.080287789
Apobec2	probable C->U-editing enzyme APOBEC-2	0	1.24	0	0	1.163498732	0
Mettl7b	methyltransferase-like protein 7B precursor	0	1.24	10.77	23.4	1.163498732	1.051766827
Mylk	myosin light chain kinase, smooth muscle	20.72	47.6	5.27	13.2	1.161932211	1.179353582
Grk5	G protein-coupled receptor kinase 5	12.64	29.48	9.16	9.65	1.160019258	0.067953028
Ehf	ETS homologous factor	1.11	3.71	55.51	65.6	1.158484061	0.237015988
Dpysl2	dihydropyrimidinase-related protein 2	2.67	7.18	2.45	3.04	1.15632078	0.227758931
Ppifos		6.75	16.24	28.26	28.28	1.153491559	0.000985784
Mlf1ip	centromere protein U	1.18	3.84	8.95	7.23	1.150678912	-0.273804095
Prdm11	PR domain containing 11	6.63	15.92	3.79	5.08	1.148974606	0.344045668

Mthfd2	bifunctional methylenetetrahydrofolate	2.76	7.32	12.75	11.63	1.145850866	-0.12257698
2610203C20Rik		13.77	31.63	10.73	30.67	1.143529161	1.432913854
Pax3	paired box protein Pax-3 isoform a	0.93	3.26	1	2.78	1.142252583	0.918386234
Dio2	type II iodothyronine deiodinase	8.35	19.63	3.69	8.09	1.141705551	0.954692372
1190002H23Rik	response gene to complement 32 protein	16.49	37.58	177.07	165.08	1.141322854	-0.100566133
Meis2	homeobox protein Meis2 isoform 6	3.24	8.35	3.5	15.71	1.1409021	1.892714827
Tnfsf12	tumor necrosis factor ligand superfamily member	1.74	5.04	2.13	2.11	1.140372656	-0.009248077
Nr1h5	nuclear receptor subfamily 1, group H, member 5	0	1.2	0	4.13	1.137503524	2.358958826
Gucy2g	guanylate cyclase 2G precursor	1.39	4.25	4.91	4.72	1.135306805	-0.047142983
Pisd-ps1		82.57	182.47	13.64	66.33	1.13448714	2.201333911
Vegfa	vascular endothelial growth factor A isoform 6	20.25	45.63	53.24	62.88	1.133795588	0.236007134
Rsph4a	radial spoke head protein 4 homolog A	25.07	56.16	3.53	9.94	1.132615334	1.272029783
Plk3	serine/threonine-protein kinase PLK3	53.51	118.45	114.53	138.5	1.131814028	0.271997593
Asb2	ankyrin repeat and SOCS box protein 2	0	1.19	0	0	1.13093087	0
Pla2g2c	group IIC secretory phospholipase A2 precursor	0	1.19	0.71	0	1.13093087	-0.773996325
Sap25	histone deacetylase complex subunit SAP25	4.42	10.86	5.84	7.32	1.129739253	0.282587203
Sulf2	extracellular sulfatase Sulf-2 precursor	60.75	134.12	33.03	36.98	1.129730191	0.158432754
Olfm1	noelin isoform c	152.27	334.13	83.1	148.62	1.128645497	0.83112533
Sdk1	protein sidekick-1 precursor	14.37	32.6	3.91	10.68	1.128344068	1.250245345
AI450353		1.34	4.11	3.32	4.24	1.126814761	0.278535499
Snai1	zinc finger protein SNAI1	2.58	6.8	3.44	4.51	1.123514536	0.311492642
Gm9790	HIG1 domain family, member 1A-like	19.55	43.75	52.28	57.13	1.122749288	0.125688826
Ccrn4l	nocturnin	55.55	122.02	140.84	189.74	1.121293952	0.427342981
Ccl2	C-C motif chemokine 2	41.5	91.44	168.31	237.32	1.121054419	0.493232843
Chsy3	chondroitin sulfate synthase 3	28.32	62.73	10.59	18.6	1.120087557	0.757973088
Irf1	interferon regulatory factor 1 isoform a	74.9	163.6	201.33	238.12	1.116792545	0.241024554
Tgfb1i1	transforming growth factor beta-1-induced	34.72	76.36	25.02	29	1.114855714	0.205341539
Depdc1b	DEP domain-containing protein 1B	1.07	3.48	8.24	3.58	1.113867965	-1.012545253
Emr4	EGF-like module-containing mucin-like hormone	0.59	2.44	0.66	0.76	1.113381799	0.084392187
Afap1l1	actin filament-associated protein 1-like 1	4.57	11.05	24.03	27.65	1.113283914	0.194876848
Ckap2l	cytoskeleton-associated protein 2-like	12.41	27.97	67.09	42.39	1.111250447	-0.650080347
Zbtb10	zinc finger and BTB domain containing 10	20.91	46.29	27.75	25.86	1.109945657	-0.098102651
Tmc4	transmembrane channel-like protein 4	6.37	14.9	10.32	10.99	1.109290241	0.082957701
Whrn	whirlin isoform 6	20.33	44.98	8.91	26.25	1.1081225	1.459299267
Mlf1	myeloid leukemia factor 1 isoform a	3.77	9.28	9.25	18.33	1.107779093	0.915217728
Pappa	pappalysin-1 precursor	26.03	57.21	16.61	14.78	1.106705506	-0.158297704
Ccdc30	coiled-coil domain-containing protein 30	0.86	3	0.78	1.3	1.104697379	0.36975662
Ndp	norrin precursor	0	1.15	3.16	3.19	1.10433666	0.010366716
Pnma5	paraneoplastic antigen-like protein 5	0	1.15	0	0	1.10433666	0
Hs3st6	heparan sulfate glucosamine 3-O-sulfotransferase	93.69	202.52	106.9	198.67	1.103886597	0.887922722
Prrt2	proline-rich transmembrane protein 2	14.56	32.38	6.08	13.04	1.101141894	0.98772167
Cyp2g1	cytochrome P450, family 2, subfamily g,	38.18	83	30.35	187.36	1.10027193	2.58695528
Ccne1	G1/S-specific cyclin-E1	1.6	4.57	6.5	7.11	1.099165704	0.112811319
Fbn2	fibrillin-2 precursor	1.21	3.73	2.82	8.93	1.097793814	1.378221079
A630001G21Rik	hypothetical protein LOC319997	0	1.14	1.16	5	1.097610797	1.473931188
Gm5887	MANSC domain-containing protein ENSP00000370673	0	1.14	0	0	1.097610797	0
Ntn5	netrin-5	0	1.14	0	0	1.097610797	0
A430110N23Rik	soluble scavenger receptor cysteine-rich	4.38	10.51	0.68	2.37	1.097209756	1.004287358
Glt1d1	glycosyltransferase 1 domain-containing protein	4.1	9.9	5.1	7.81	1.095758983	0.530332776
Hbegf	proheparin-binding EGF-like growth factor	164.1	351.75	229.06	430.08	1.095305963	0.905945463
D130020L05Rik		4.64	11.05	5.94	5.25	1.095266079	-0.151079473
Creb5	cyclic AMP-responsive element-binding protein 5	100.41	215.57	34.01	96.51	1.094633487	1.477783118
Krt17	keratin, type I cytoskeletal 17	3364.52	7182.85	12026.7	12564.9	1.093927797	0.063153215
S100a7a	protein S100-A15A	14.68	32.44	7.13	9.5	1.092649288	0.36906207
Rgs16	regulator of G-protein signaling 16	6.39	14.76	6.41	15.07	1.092621265	1.116824481
Ncaph	condensin complex subunit 2	7.34	16.78	53.52	26.02	1.092136035	-1.012757887
Gkn1	gastrokine-1	0	1.13	0	0	1.09085343	0
Lepr	leptin receptor isoform 2	3.26	8.06	2.3	3.84	1.08865762	0.552541023
Plekho1	pleckstrin homology domain-containing family O	4.22	10.1	6.12	7.43	1.088437965	0.24365539
Nrg1	pro-neuregulin-1, membrane-bound isoform	2.2	5.8	0	2.02	1.087462841	1.59454855
F2rl3	proteinase-activated receptor 4 precursor	0	1.12	0	0	1.084064265	0
Rimkla	N-acetylaspartyl-glutamate synthetase A	0	1.12	0	0.58	1.084064265	0.659924558
Nr2f2	COUP transcription factor 2 isoform 1	1.14	3.53	2.03	1.85	1.081900254	-0.088355874
Fibin	fin bud initiation factor homolog precursor	1.67	4.65	3.07	1.53	1.081411126	-0.68589141
Homer1	homer protein homolog 1 isoform S	36.49	78.22	55.24	69.96	1.079358876	0.335409415
Rsph1	radial spoke head 1 homolog	0	1.11	3.77	2.56	1.077242999	-0.422112025
Wdr86	WD repeat domain 86	0	1.11	0	1.81	1.077242999	1.49057013
6330403K07Rik	hypothetical protein LOC103712	3.21	7.88	5.86	19.09	1.076739443	1.550197083
Akr1c19	aldo-keto reductase family 1, member C19	0.94	3.09	26.02	33.59	1.076044191	0.356327339
Psors1c2	psoriasis susceptibility 1 candidate gene 2	1.42	4.1	2.87	4.07	1.0754902	0.389652181
Igf2	insulin-like growth factor II isoform 2	0.96	3.13	0.49	1.84	1.075288127	0.930578599
E2f1	transcription factor E2F1	7.91	17.77	39.12	24.99	1.074931313	-0.626364972
Bard1	BRCA1-associated RING domain protein 1	2.28	5.9	10.79	8.31	1.072900547	-0.340710645
Egfl6	epidermal growth factor-like protein 6	329.68	694.3	96.8	166.47	1.072199798	0.775996309
Nkain2	sodium/potassium-transporting ATPase subunit	0	1.1	0	0.64	1.070389328	0.713695815
Tmem200a	transmembrane protein 200A	1.08	3.36	0	2.25	1.067744607	1.700439718
Pcdhb11	protocadherin beta 11	2.47	6.27	1.37	4.55	1.067019701	1.227600712
Rasd2	GTP-binding protein Rhes precursor	2	5.28	1.84	7.43	1.065802058	1.569641701
Thpo	thrombopoietin precursor	0	1.09	0.45	9.61	1.063502942	2.871299851
H2-T24	histocompatibility 2, T region locus 24	2.96	7.25	8.84	10.21	1.058893689	0.188056057
Cnrip1	CB1 cannabinoid receptor-interacting protein 1	1.19	3.56	1.35	1.67	1.058102955	0.184178985
Zwilch	protein zwilch homolog	5.58	12.69	25.3	19.42	1.056962958	-0.365079933
Ctsl	cathepsin L1 preproprotein	404.4	842.31	252.81	752.53	1.056716973	1.569916039
Rad51	DNA repair protein RAD51 homolog 1	9.8	21.44	43.21	28.28	1.055041364	-0.594457181
Rerg	ras-related and estrogen-regulated growth	18.41	39.29	30.46	102.1	1.053621687	1.712453757
Ttk	dual specificity protein kinase TTK isoform 1	6.57	14.71	28.31	17.56	1.053317975	-0.659196258
Gm13308	C-C motif chemokine 27-like	2.58	6.42	1.84	0.99	1.051459599	-0.513122499
Fam54a	DUF729 domain containing 1	0.84	2.81	8.11	3.56	1.050085231	-0.99841723
2310046A06Rik	hypothetical protein LOC69642	0	1.07	0	0	1.049630768	0
Cd40	tumor necrosis factor receptor superfamily	0	1.07	0	0	1.049630768	0
G6b		0	1.07	2.8	3.45	1.049630768	0.227805918
Slc47a2	multidrug and toxin extrusion protein 2	0	1.07	0.6	0	1.049630768	-0.678071905

Ifit2	interferon-induced protein with	2.01	5.23	1.73	2.37	1.049468676	0.30384764
A3galt2	alpha-1,3-galactosyltransferase 2 precursor	2.16	5.54	1.75	2.72	1.049366077	0.435871003
Pif1	ATP-dependent DNA helicase PIF1	0.59	2.29	5.99	4.27	1.049060818	-0.407489494
Chek1	serine/threonine-protein kinase Chk1	3.56	8.43	20.24	14.81	1.048223947	-0.425946398
9530077C05Rik	hypothetical protein LOC68283	4.51	10.39	1.64	3.43	1.047643523	0.746768769
Trps1	zinc finger transcription factor Trps1	34.69	72.75	26.57	58.28	1.047123148	1.10444618
Slc16a4	monocarboxylate transporter 5	1.01	3.15	2.11	2.95	1.045915835	0.344938073
Gm129	hypothetical protein LOC229599	1.03	3.19	2.48	3.05	1.045470517	0.218834602
Adamts1	A disintegrin and metalloproteinase with	211.81	437.88	702.48	734.9	1.044260582	0.065000327
Pdgfd	platelet-derived growth factor D	3.82	8.94	0	1.01	1.044212705	1.007195501
Gas5		115.77	239.71	178.96	284.23	1.043626407	0.664449458
Apln	apelin precursor	3.11	7.47	17.79	17.38	1.043223576	-0.0318283
2510049J12Rik	hypothetical protein LOC70291	0	1.06	0.82	0.58	1.042644337	-0.204013892
Galnt12	polypeptide N-acetylgalactosaminyltransferase	0	1.06	0	0	1.042644337	0
Hsd17b13	17-beta-hydroxysteroid dehydrogenase 13 isoform	0	1.06	61.86	21.22	1.042644337	-1.500283455
Tagln	transgelin	24.79	52.12	18.77	63.36	1.042443374	1.702851455
Tmem117	transmembrane protein 117	1.19	3.51	0	0.85	1.042196564	0.887525271
Gm13177	arylacetamide deacetylase-like 4	8.37	18.29	6.92	8.68	1.04173219	0.289506617
Incenp	inner centromere protein	15.2	32.35	54.19	40.62	1.041692948	-0.40712992
Rasa4	ras GTPase-activating protein 4 isoform 1	2.61	6.43	1.73	2.93	1.041363374	0.525628361
Grrp1	glycine/arginine-rich protein 1	2.99	7.2	2.92	2.26	1.039235163	-0.26598169
Bcl3	B-cell lymphoma 3 protein homolog	7.72	16.92	25.08	38.41	1.039170597	0.59561788
Hbb-b1	hemoglobin subunit beta-1	11.9	25.49	4.33	6.51	1.038076778	0.494677375
Cd44	CD44 antigen isoform f precursor	410.92	844.48	666.41	873.38	1.037406453	0.389687099
Snora28		81.89	169.13	83.39	112.85	1.037367594	0.431990333
Degs2	sphingolipid delta(4)-desaturase/C4-hydroxylase	1.88	4.91	7.4	6.09	1.037089319	-0.2446037
Procr	endothelial protein C receptor	9.55	20.64	6.2	17.05	1.0364575	1.325930025
Sema3b	semaphorin-3B	9.5	20.53	2.08	7.26	1.035958992	1.423211431
Gimap1	GTPase IMAP family member 1	0	1.05	0	0	1.03562391	0
ORF63	TAK1-like protein	0	1.05	0	0	1.03562391	0
Slc5a3	sodium/myo-inositol cotransporter	9.48	20.47	12.79	19.49	1.034683474	0.571297527
Igfbp7	insulin-like growth factor-binding protein 7	913.81	1871.86	139.17	255.99	1.033699018	0.874534614
Ogn	mimecan precursor	9.49	20.43	3.15	5.63	1.030617172	0.675897534
Cd72	B-cell differentiation antigen CD72 isoform 4	16.28	34.26	22.16	3.44	1.028929257	-2.383003672
Fgf17	fibroblast growth factor 17 precursor	0	1.04	0	0	1.028569152	0
Hes1	transcription factor HES-1	125.53	257.06	209.55	215.84	1.028227052	0.042468037
Ager	advanced glycosylation end product-specific	1.28	3.65	0.83	2.94	1.028196892	1.106351981
Kcnk10	potassium channel subfamily K member 10	18.68	39.12	1.4	2.06	1.027591385	0.350497247
Car3	carbonic anhydrase 3	0	1.03	0	0	1.021479727	0
Foxj1	forkhead box protein J1	0	1.03	0	1.1	1.021479727	1.070389328
Gm5151	hypothetical protein LOC381582	0	1.03	0	0	1.021479727	0
Cd3g	T-cell surface glycoprotein CD3 gamma chain	9.45	20.2	7.85	5.37	1.020561322	-0.474384083
Dusp10	dual specificity protein phosphatase 10	19.85	41.29	50.91	59.11	1.020269177	0.211592532
Mybl2	myb-related protein B	1.54	4.15	8.29	6.49	1.019743935	-0.310712878
Dbf4	protein DBF4 homolog A isoform 1	6.51	14.2	29.3	23.71	1.017186511	-0.294222783
Gm4925	ribosomal protein S12-like	0	1.02	0	0	1.014355293	0
Pvr	poliovirus receptor	37.91	77.56	16.28	29.17	1.013653949	0.804011479
Cit	citron Rho-interacting kinase	0.61	2.25	5.68	3.97	1.01337903	-0.426602251
Kif26b	kinesin-like protein KIF26B	1.7	4.45	7.48	22.95	1.013296823	1.497889486
Armc2	armadillo repeat-containing protein 2	1.52	4.08	0.89	1.16	1.011404763	0.192645078
Slfn8	schlafen 8 isoform 2	1.92	4.88	2.27	3.02	1.009847786	0.297904866
Mir24-2		161.61	326.39	108.93	154.05	1.009594275	0.496148373
Ednrb	endothelin B receptor isoform 1	1.61	4.25	1.85	2.56	1.008267616	0.320915322
4933432I09Rik		0	1.01	0	0	1.007195501	0
Ppm1n	probable protein phosphatase 1N	0	1.01	0	0	1.007195501	0
Soat2	sterol O-acyltransferase 2	0	1.01	0	0	1.007195501	0
Arl5c	ADP-ribosylation factor-like protein 5C	2.93	6.89	1.57	1.26	1.005495988	-0.185445587
Cd97	CD97 antigen isoform 4	15.09	31.29	46.99	35.57	1.004923115	-0.392073186
Lrrk2	leucine-rich repeat serine/threonine-protein	2.75	6.52	2.92	6.61	1.003842066	0.957042799
Gm11428	activated macrophage/microglia WAP domain	3.22	7.46	0	0	1.003414664	0
Kcnj13	inward rectifier potassium channel 13	2.08	5.17	3.21	3.07	1.002340138	-0.048791439
Robo4	roundabout homolog 4	0.81	2.62	0.61	0.62	1	0.008933125
Tgtp1	T-cell specific GTPase	0.6	2.2	1.2	0.75	1	-0.330148602
BB283400		0	1	0	0	1	0

HG Up

GENE	Description	WT Bulge	KO Bulge	WT HG	KO HG	Log2 KO Bulge/WT Bulge	Log2 KO HG/WT HG
Snord69		0	0	0	232.99	0	7.870303065
Snord47		0	98.06	0	184.98	6.630230716	7.539003674
Mir3109		0	0	0	83.95	0	6.408542042
Mir705		69	71.9	0	81.65	0.058563892	6.368942914
Mir5114		70.08	0	0	79.43	-6.151371776	6.329661815
Mir5121		0	0	0	78.95	0	6.321026129
Slc15a2	solute carrier family 15 member 2 isoform 2	0	53.71	0	65.66	5.773732651	6.058749412
Snord16a		0	0	0	63.42	0	6.009436756
Mirlet7d		31.52	34.93	0	39.43	0.143861678	5.337354298
H19		1.26	41.51	1.04	68.06	4.233407581	5.081209277
Mir675		0	32.93	0	32.47	5.084489525	5.064796646
Snord89		0	0	0	30.79	0	4.990501111
Mir5122		34.36	0	0	28.32	-5.14404637	4.873813198
Amtn	amelotin precursor	0	2.79	0	24.97	1.922197848	4.698774109
Scrg1	scrapie-responsive protein 1 precursor	103.44	363.68	2.13	50.76	1.803956718	4.047603055
Snora43		0	0	0	15.33	0	4.029452886
Bex1	protein BEX1	1.54	2.97	4.83	77.62	0.64431051	3.753328575
Krtap8-1	keratin-associated protein 8-1	0	0	0	10.32	0	3.500802053
C1s	complement C1s-A subcomponent	106.07	402.95	9.14	84.23	1.915622423	3.07130368
Nxf7	nuclear RNA export factor 7 isoform 2	0	4.17	0.91	13.78	2.370164281	2.952001726
Thpo	thrombopoietin precursor	0	1.09	0.45	9.61	1.063502942	2.871299851
Mlana	melanoma antigen recognized by T-cells 1	0	3.53	0	6	2.17951105	2.807354922
Krt73	keratin, type II cytoskeletal 73	2.32	1.08	0.79	11.44	-0.674599713	2.796954993
Loxl2	lysyl oxidase homolog 2 precursor	9.21	42.79	2.27	21.7	2.100618584	2.795329757
1700084E18Rik		0	0	0	5.67	0	2.737686761
Lrrc4	leucine-rich repeat-containing protein 4	39.86	76.33	7.89	57.39	0.920339009	2.715465987
Krt85	keratin, type II cuticular Hb5	0	1.26	0	5.52	1.176322773	2.704871964
A830018L16Rik	hypothetical protein LOC320492 isoform 1	0.22	0.9	0.71	9.95	0.639118271	2.67886264
Krtap7-1	keratin-associated protein 7-1	0	0	0	5.29	0	2.653060017
Sstr2	somatostatin receptor type 2 isoform A	0	0	0	5.17	0	2.625270489
Col12a1	collagen alpha-1(XII) chain	111.27	279.2	8.04	54.72	1.319484483	2.62380058
Krtap11-1	keratin associated protein 11-1	0	0	0	5.14	0	2.618238656
Ccnb1ip1	E3 ubiquitin-protein ligase CCNB1IP1	0	2.18	0	5.1	1.669026766	2.608809243
Cyp2g1	cytochrome P450, family 2, subfamily g,	38.18	83	30.35	187.36	1.10027193	2.58695528
Gm1673	neuropeptide-like protein C4orf48 homolog	0	0	0	4.86	0	2.550900665
Fmo2	dimethylaniline monooxygenase [N-oxide-forming]	2.01	2.04	5.61	37.63	0.014307837	2.546999501
S100a9	protein S100-A9	0	2.74	0	4.59	1.90303827	2.482848283
Pamr1	inactive serine protease PAMR1 precursor	2.83	4.4	1.14	10.86	0.495615015	2.470421308
Prr9	proline-rich protein 9	0	10.27	1.42	12.3	3.494415561	2.458347293
Sphkap	A-kinase anchor protein SPHKAP	19.75	174.31	0.36	6.42	3.078725051	2.447812535
Insl3	insulin-like 3 precursor	0.23	13.65	0.16	5.31	3.574170444	2.4435152
Ifnk	interferon kappa precursor	0	0	0	4.43	0	2.440952198
Rrad	GTP-binding protein RAD	4.75	12.32	5.73	35.39	1.211960221	2.434863641
Iyd	iodotyrosine dehalogenase 1 precursor	1.02	4.94	0	4.22	1.556107638	2.384049807
Tmem178	transmembrane protein 178 precursor	0	0	0	4.15	0	2.364572432
Nr1h5	nuclear receptor subfamily 1, group H, member 5	0	1.2	0	4.13	1.137503524	2.358958826
Itga8	integrin alpha-8 precursor	2.28	34.84	1.03	9.41	3.449802917	2.358418436
Mkx	homeobox protein Mohawk	11.15	18.13	2.18	15.01	0.65488056	2.331874637
Fam71a	hypothetical protein LOC619288	4.05	40.2	2.22	14.87	3.028289044	2.301169535
Tnc	tenascin	487.81	801.82	48.02	238.72	0.715802758	2.28990789
Fxyd4	FXYD domain-containing ion transport regulator 4	0	3.15	0	3.89	2.053111336	2.289834465
AW112010	hypothetical protein LOC107350	4.49	8.82	0	3.88	0.838916875	2.286881148
Ugt1a9	UDP-glucuronosyltransferase 1-9 precursor	0.03	0	2.59	16.4	-0.042644337	2.277031557
Relt	tumor necrosis factor receptor superfamily	0.66	1.36	0.81	7.71	0.507603618	2.266683022
Prtn3	myeloblastin precursor	2.96	3.61	0	3.81	0.21926632	2.266036894
Slc18a3	vesicular acetylcholine transporter	2.67	33.85	0	3.76	3.247306688	2.250961574
Airn		17.56	57.51	3.71	21.18	1.656486508	2.235460401
Dbn1	drebrin isoform 2	37.14	50.23	12	60.17	0.425684048	2.234312653
Stfa1	stefin-1	1.72	0	0	3.69	-1.443606651	2.229587923
Xlr3b	X-linked lymphocyte-regulated protein 3B	1.07	6.54	0.53	6.05	1.864933756	2.204091605
Pisd-ps1		82.57	182.47	13.64	66.33	1.13448714	2.201333911
Synpo2	synaptopodin-2	16.25	51.41	25.2	119.15	1.603245747	2.197197932
Fgf21	fibroblast growth factor 21 precursor	0	2.87	0	3.58	1.952333566	2.195347598
Gm5077	complement C1s-B subcomponent precursor	21.24	65.43	2.53	15.12	1.578678126	2.191111655
Fmod	fibromodulin precursor	43.76	204.85	5	26.21	2.201311507	2.181102551
Mcoln3	mucolipin-3	3.07	5.88	2.11	12.78	0.75737977	2.147589403
Gm1045	hypothetical protein LOC381651 precursor	11.63	17.21	4.14	21.76	0.527876283	2.146660293
Nppc	C-type natriuretic peptide preproprotein	180.97	1130.03	71.35	315.96	2.635864668	2.131235863
Cpa6	carboxypeptidase A6 precursor	0	4.26	0	3.36	2.3950628	2.124328135
Itga1	integrin alpha-1 precursor	9.54	40.69	4.71	23.77	1.983826505	2.117031218
Col14a1	collagen alpha-1(XIV) chain	3.38	4.12	6.78	32.62	0.22521294	2.111477664
Fam198b	protein ENED	18.59	34.68	4.53	22.84	0.864998218	2.10803285
Serpinb6e	serine (or cysteine) peptidase inhibitor, clade	4.01	24.57	3.66	19.05	2.351569652	2.105200377
Fam70a	family with sequence similarity 70, member A	5.08	13.08	2.34	13.32	1.211504105	2.100111485
Prex2	phosphatidylinositol	1.87	6.56	1.49	9.61	1.397335498	2.091207009
Cpt1b	carnitine O-palmitoyltransferase 1, muscle	0	0	0	3.25	0	2.087462841
Tmem95	transmembrane protein 95	0	3.11	0	3.25	2.039138394	2.087462841
Ncam1	neural cell adhesion molecule 1 isoform 2	1.22	4.79	2.48	13.66	1.383003672	2.074725892
1700086O06Rik		10.52	34.08	6.46	30.39	1.606508031	2.073057493
Gm14403		8.52	28.07	4.6	22.21	1.610497593	2.05124779
2810429I04Rik		0	0	0	3.11	0	2.039138394
Krtap17-1	keratin-associated protein 17-1	245.56	365.04	37.99	158.56	0.570062545	2.032922969
Islr	immunoglobulin superfamily containing	2.82	4.26	0	2.97	0.461490161	1.989139007
Zfp618	zinc finger protein 618	0	1.75	0	2.97	1.459431619	1.989139007
Car2	carbonic anhydrase 2	0	7.52	1.38	8.39	3.09085343	1.980163584
5430421N21Rik	type II hair keratin	0.53	0	0	2.9	-0.613531653	1.963474124
Cmah	cytidine monophosphate-N-acetylneuraminic acid	1.47	3.29	1	6.77	0.796466606	1.957914599

Camk2n2	calcium/calmodulin-dependent protein kinase II	3.35	2.33	0	2.88	-0.385493224	1.956056652
Krt25	keratin, type I cytoskeletal 25	32.89	48.23	10.23	42.51	0.538678103	1.953989089
Tmem151b	transmembrane protein 151B	0	0	1.11	7.16	0	1.951326153
Fam71f2	hypothetical protein LOC245884	1.26	1.52	0	2.84	0.157100961	1.941106311
Gja1	gap junction alpha-1 protein	731.73	2620.21	564.38	2167.39	1.838879351	1.939331504
Tmem173	transmembrane protein 173	11.06	28.96	11.52	46.93	1.312807717	1.936694378
Gm684	hypothetical protein LOC270157	0	0	0	2.81	0	1.929790998
Sfrp1	secreted frizzled-related protein 1 precursor	1557.95	1076.39	35.57	138.21	-0.533034078	1.928530318
Gpx3	glutathione peroxidase 3 isoform 2	21.51	57	8.7	35.7	1.365486843	1.919723411
Foxe1	forkhead box protein E1	0	0	0	2.77	0	1.914564523
Rab42-ps	RIKEN cDNA 9530096D07	3.76	4.09	0	2.74	0.096704083	1.90303827
Ica1l	islet cell autoantigen 1-like protein	0.67	0.59	2.4	11.69	-0.070821337	1.900085418
Ppp1r3b	protein phosphatase 1 regulatory subunit 3B	37.08	49.83	4.07	17.85	0.416646752	1.894506871
Meis2	homeobox protein Meis2 isoform 6	3.24	8.35	3.5	15.71	1.1409021	1.892714827
Nanos3	nanos homolog 3	0	0	0	2.71	0	1.891419187
Expi	extracellular peptidase inhibitor precursor	0	0	5.25	22.15	0	1.889084099
Ly6g6d	lymphocyte antigen 6 complex locus protein G6d	0	0	0	2.7	0	1.887525271
Scube3	signal peptide, CUB and EGF-like	0.8	1.89	9.67	38.36	0.683072586	1.883170045
Kcnip2	Kv channel-interacting protein 2 isoform b	0	8.51	9.79	38.71	3.249445341	1.879807496
Hoxc12	homeobox protein Hox-C12	0	1.85	0	2.68	1.510961919	1.879705766
4921530L18Rik		1.99	2.59	0	2.67	0.26383836	1.875780063
Fhod3	FH1/FH2 domain-containing protein 3	1.23	10.09	7.66	30.59	2.31414375	1.867029007
Nell2	protein kinase C-binding protein NELL2	0	0	0	2.63	0	1.859969548
Tsc22d1	TSC22 domain family protein 1 isoform 3	177.46	489.86	394.68	1417.4	1.459710862	1.841858391
Krt28	keratin, type I cytoskeletal 28	2.73	3.85	8.17	31.66	0.378809117	1.832531152
BC089491	selenoprotein V	2.22	1.16	0	2.55	-0.576029376	1.827819025
Gm10451		0	1.45	0	2.55	1.292781749	1.827819025
Rapgef3	rap guanine nucleotide exchange factor 3 isoform	16.75	9.52	1.33	7.17	-0.75468432	1.810006123
Plcd4	1-phosphatidylinositol-4,5-bisphosphate	5.58	1.95	1.16	6.55	-1.157372629	1.805445332
Cxcl14	C-X-C motif chemokine 14 precursor	16599.7	33042.5	1845.22	6409.26	0.99312243	1.795808395
Pcdh20	protocadherin-20 precursor	20.9	113.02	7.95	29.84	2.380284132	1.784843178
Bex4	protein BEX4	0	0	1.11	6.19	0	1.768748772
Mfap5	microfibrillar-associated protein 5 precursor	3.67	7.18	0	2.4	0.808678293	1.765534746
Trh	prothyroliberin	4.56	12.02	1.13	6.19	1.22757266	1.75513834
Xlr3c	X-linked lymphocyte-regulated protein 3C	0.79	3.88	0.3	3.36	1.44692156	1.745816512
Hmga2	high mobility group protein HMGI-C	2.88	28.84	0.39	3.66	2.943118978	1.745245072
Glrb	glycine receptor subunit beta precursor	25.67	155.33	9.57	34.39	2.551304931	1.743366385
Pcp4	Purkinje cell protein 4	2.06	17.68	2.62	11.06	2.609890897	1.736168305
Lmx1b	LIM homeobox transcription factor 1-beta	16.3	16.5	1.64	7.73	0.016582884	1.725443724
Ptprn2	receptor-type tyrosine-protein phosphatase N2	0	0.69	0.64	4.42	0.757023247	1.724597037
Gzmc	granzyme C preproprotein	2.25	4.17	0	2.3	0.669724562	1.722466024
Slc7a8	large neutral amino acids transporter small	147.69	144.26	25.08	84.52	-0.033670138	1.713317983
Rerg	ras-related and estrogen-regulated growth	18.41	39.29	30.46	102.1	1.053621687	1.712453757
Tagln	transgelin	24.79	52.12	18.77	63.36	1.042443374	1.702851455
Tmem200a	transmembrane protein 200A	1.08	3.36	0	2.25	1.067744607	1.700439718
Sorbs2	sorbin and SH3 domain-containing protein 2	30.68	55.98	1.86	8.29	0.846883286	1.69966345
4932441J04Rik		2.67	3.3	0	2.23	0.228556597	1.691534165
AI646023	leucine-rich repeat-containing protein C22orf36	6.25	4.09	1.41	6.71	-0.510315339	1.677697714
Fgg	fibrinogen gamma chain precursor	0	0	0	2.19	0	1.673556424
Pclo	protein piccolo isoform 2	1.02	1.93	2.14	8.97	0.536545372	1.666828946
Chn2	beta-chimaerin isoform 1	21.1	31.9	3.13	12.11	0.574041214	1.666453999
Enox1	ecto-NOX disulfide-thiol exchanger 1	126.75	129.34	17.63	58.13	0.028956609	1.666262603
2310043J07Rik	uroplakin-3b-like protein	0	0	0	2.16	0	1.659924558
Ace	angiotensin-converting enzyme isoform 2	6.96	13.33	3.84	14.26	0.848198274	1.65667601
Ccdc152	coiled-coil domain-containing protein 152	1.94	1.79	0	2.15	-0.075551033	1.655351829
Mdk	midkine precursor	4.13	5.17	4.82	17.3	0.266311664	1.65275259
Asphd2	aspartate beta-hydroxylase domain-containing	0	4.22	0	2.13	2.384049807	1.646162657
Dhrs9	dehydrogenase/reductase SDR family member 9	30	51.15	2.2	9	0.750399037	1.64385619
Smarca1	probable global transcription activator SNF2L1	29.63	38.96	4.21	15.24	0.383611216	1.640196355
Hoxd4	homeobox protein Hox-D4	19.15	34.33	1.8	7.66	0.81011391	1.628940198
Galnt14	polypeptide N-acetylgalactosaminyltransferase	22.72	66.18	15.33	49.23	1.501927786	1.621024484
Wnt5a	protein Wnt-5a precursor	4.4	11.97	3.69	13.4	1.264147167	1.618408984
Fez1	fasciculation and elongation protein zeta-1	7.22	5.06	0	2.07	-0.4398206	1.618238656
Cd209e	CD209 antigen-like protein E	2.03	3.58	0	2.05	0.596029805	1.608809243
Ly86	lymphocyte antigen 86 precursor	3.41	3.34	0	2.05	-0.023083613	1.608809243
Enho	adropin precursor	14.78	8.55	9.45	30.67	-0.724524567	1.599613925
Rbpjl	recombining binding protein suppressor of	1.07	6.58	0	2.03	1.872567081	1.599317794
Cpxm1	probable carboxypeptidase X1 precursor	6.26	10.21	3.75	13.38	0.626744825	1.598064257
Nrg1	pro-neuregulin-1, membrane-bound isoform	2.2	5.8	0	2.02	1.087462841	1.59454855
Timp4	metalloproteinase inhibitor 4 precursor	0	0	0	2.02	0	1.59454855
Hist2h3c2-ps	histone H3.2	6.73	11.67	2.99	11.04	0.712876205	1.593374741
Cdk18	cyclin-dependent kinase 18	4.68	14.67	3.85	13.6	1.464042345	1.589911717
Eya1	eyes absent homolog 1	2.76	14.25	2.6	9.74	2.020004676	1.576925182
Pitpnm3	membrane-associated phosphatidylinositol	1.05	8.15	3.84	13.43	2.158147834	1.575992347
Stfa3	stefin-3	45.61	33.59	22.4	68.64	-0.430284499	1.573407673
Antxr1	anthrax toxin receptor 1 precursor	143.25	124.01	13.71	42.74	-0.206527813	1.572155974
Tyrp1	5,6-dihydroxyindole-2-carboxylic acid oxidase	5.47	23.58	11.16	35.15	1.925647298	1.571852418
Ctsl	cathepsin L1 preproprotein	404.4	842.31	252.81	752.53	1.056716973	1.569916039
Rasd2	GTP-binding protein Rhes precursor	2	5.28	1.84	7.43	1.065802058	1.569641701
Batf	basic leucine zipper transcriptional factor	0	0	0	1.96	0	1.565597176
Krt83	keratin, type II cuticular Hb3	0.44	0.43	0.7	4.03	-0.010053665	1.565023654
Slc2a13	proton myo-inositol cotransporter	2.18	2.67	1.95	7.69	0.206753298	1.558641223
Vcan	versican core protein isoform 2	3.13	4.52	2.15	8.25	0.418526485	1.554101537
6330403K07Rik	hypothetical protein LOC103712	3.21	7.88	5.86	19.09	1.076739443	1.550197083
Chd3	chromodomain helicase DNA binding protein 3	52.75	122.2	53.86	159.55	1.196665596	1.549196138
Fgl1	fibrinogen-like protein 1 precursor	1.94	1.5	0	1.92	-0.23388806	1.545968369
Hoxd3	homeobox protein Hox-D3	5.78	9.48	0	1.92	0.628281538	1.545968369
Hmgcs2	hydroxymethylglutaryl-CoA synthase,	320.76	156.46	378.61	1104.9	-1.030999603	1.542631034
9430007A20Rik	arylacetamide deacetylase-like 4	0	0	2.94	10.44	0	1.537819517
Lgr5	leucine-rich repeat-containing G-protein coupled	636.34	361.81	109.28	319.06	-0.812848987	1.537171213
Icam2	intercellular adhesion molecule 2 precursor	0	3.73	0	1.9	2.241840184	1.5360529
Dlgap1	disks large-associated protein 1 isoform 3	8.26	10.06	2.65	9.56	0.256267287	1.532641466

3110021A11Rik		1.89	1.96	0	1.89	0.034527683	1.531069493
Il24	interleukin-24	0	0	0	1.89	0	1.531069493
Slc10a1	sodium/bile acid cotransporter isoform 2	1.48	3.28	0	1.89	0.787270676	1.531069493
Bgn	biglycan precursor	175.19	499.83	87.56	254.79	1.507188939	1.530232737
Hist1h3d	histone H3.2	0	0.36	0.16	2.35	0.443606651	1.53003629
Kif26a	kinesin-like protein KIF26A	4.29	3.58	0.99	4.71	-0.207920124	1.520722315
Pmel	melanocyte protein PMEL precursor	11.29	31.31	14.02	41.97	1.394495835	1.516444964
Serpine1	plasminogen activator inhibitor 1 precursor	23.77	46.93	74.12	212.86	0.952335071	1.5093977
Fndc1	fibronectin type III domain-containing protein	8.64	5.15	1.73	6.77	-0.648446736	1.509013647
Stk32c	serine/threonine-protein kinase 32C isoform 2	2.04	1.84	0	1.84	-0.098180394	1.50589093
Myl9	myosin regulatory light polypeptide 9	193.68	385.51	52.62	151.07	0.989401061	1.503892445
Gm6498		2.19	2.39	0	1.83	0.087728849	1.500802053
Icam4	intercellular adhesion molecule 4 precursor	2.64	2.04	0	1.83	-0.259867127	1.500802053
Kif26b	kinesin-like protein KIF26B	1.7	4.45	7.48	22.95	1.013296823	1.497889486
1500015A07Rik		7.16	36.08	13.82	40.7	2.184000187	1.492501936
Wdr86	WD repeat domain 86	0	1.11	0	1.81	1.077242999	1.49057013
Gm438	hypothetical protein LOC329993	0	1.34	0	1.8	1.22650853	1.485426827
Plcl1	inactive phospholipase C-like protein 1	29.42	52	3.92	12.76	0.800972207	1.483750249
Cd3d	T-cell surface glycoprotein CD3 delta chain	1.45	2.34	0	1.79	0.447066353	1.480265122
C2cd4b	family with sequence similarity 148, member B	4.21	46.26	7.52	22.76	3.181264352	1.479609501
Tnfrsf11b	tumor necrosis factor receptor superfamily	183.14	359.85	74.77	210.09	0.970596203	1.478159582
Creb5	cyclic AMP-responsive element-binding protein 5	100.41	215.57	34.01	96.51	1.094633487	1.477783118
Krt33a	keratin, type I cuticular Ha3-I	0.52	0	1.16	5.01	-0.604071324	1.476333679
A630001G21Rik	hypothetical protein LOC319997	0	1.14	1.16	5	1.097610797	1.473931188
Shisa4	protein shisa-4 precursor	2.45	3.73	0	1.77	0.455243822	1.469885976
Whrn	whirlin isoform 6	20.33	44.98	8.91	26.25	1.1081225	1.459299267
Gli2	zinc finger protein GLI2	90.87	98.42	41.62	115.91	0.113942275	1.455795839
Klhl34	kelch-like protein 34	1.08	4.75	0	1.74	1.466978428	1.454175893
Nppa	atrial natriuretic factor	1.73	0	0	1.73	-1.448900951	1.448900951
C2	complement C2 precursor	15.85	104.06	5.32	16.24	2.640392993	1.447763311
Prdm5	PR domain zinc finger protein 5	8.55	9.13	4.33	13.51	0.085061536	1.444840081
Ctf2	cardiotrophin-2 precursor	0	0	0	1.71	0	1.438292852
9430076C15Rik		3.77	16.76	1.69	6.28	1.89657041	1.436332278
2610203C20Rik		13.77	31.63	10.73	30.67	1.143529161	1.432913854
Samd12	sterile alpha motif domain-containing protein	50.34	32.52	13.62	38.46	-0.615061147	1.432447645
Robo1	roundabout homolog 1 precursor	5.52	8.05	16.53	46.13	0.473045828	1.426819685
Efnb3	ephrin-B3 precursor	6.2	7.37	4.41	13.54	0.217230716	1.42632677
Sema3b	semaphorin-3B	9.5	20.53	2.08	7.26	1.035958992	1.423211431
Gm8773		1.12	1.49	0	1.66	0.232081478	1.411426246
Cps1	carbamoyl-phosphate synthase [ammonia],	0	0.8	0.24	2.29	0.847996907	1.407747463
Gpnmb	transmembrane glycoprotein NMB precursor	55.7	243.45	16.13	44.41	2.108118765	1.406484885
Tex19.2	testis-expressed protein 19.2	0.94	1.16	0	1.65	0.15497466	1.40599236
Hist2h2bb	histone H2B type 2-B	0	9.84	2.49	8.22	3.438292852	1.401539714
Phyhd1	phytanoyl-CoA dioxygenase domain-containing	7.53	13.48	3.46	10.77	0.763443956	1.399998705
Efemp2	EGF-containing fibulin-like extracellular matrix	71.92	89.22	13.11	36.23	0.307132725	1.399747628
Grb10	growth factor receptor-bound protein 10 isoform	6.3	9.53	2.67	8.67	0.528537067	1.397735827
Susd3	sushi domain-containing protein 3	2.05	1.66	0	1.63	-0.197382997	1.3950628
Upk1b	uroplakin-1b	0	0	0	1.62	0	1.389566812
Kif21b	kinesin-like protein KIF21B	38.35	27.06	6.26	18	-0.487848627	1.387957965
Nkd1	protein naked cuticle homolog 1 isoform 1	41.66	14.66	10.61	29.32	-1.445799753	1.384901781
1700028P14Rik	hypothetical protein LOC67483	0	0	0	1.61	0	1.384049807
Thy1	thy-1 membrane glycoprotein preproprotein	84.33	301.04	27.86	74.08	1.823614669	1.37935735
Odz3	teneurin-3 isoform 1	23.88	39.14	6.51	18.53	0.690054131	1.378807136
Adamtsl1	ADAMTS-like protein 1	1.22	9.17	3.42	10.49	2.195688098	1.378260523
Fbn2	fibrillin-2 precursor	1.21	3.73	2.82	8.93	1.097793814	1.378221079
Pdlim7	PDZ and LIM domain protein 7 isoform a	95.36	97.04	39.09	103.21	0.024936091	1.378179403
Kirrel	kin of IRRE-like protein 1 precursor	79.09	105.38	34.92	92.33	0.409532917	1.377553546
C2cd4a	family with sequence similarity 148, member A	4.95	9.11	2.65	8.48	0.764821424	1.376990595
Gm106	RPE-spondin precursor	6.2	20.86	4.22	12.55	1.602224589	1.37617114
Ramp1	receptor activity-modifying protein 1 isoform 3	133.79	153.81	36.26	95.6	0.199785198	1.374395515
Rab6b	ras-related protein Rab-6B	56.11	73.85	17.88	47.87	0.390258932	1.37209034
Mfap2	microfibrillar-associated protein 2	46.63	77.49	81.44	212.14	0.720638311	1.370384959
Gpr137c	G protein-coupled receptor 137C	0	0	0	1.58	0	1.367371066
Pkd1l3	polycystic kidney disease protein 1-like 3	1.02	2.76	0.46	2.75	0.896377369	1.360922227
Ldoc1	protein LDOC1	0	0	0	1.56	0	1.35614381
Ror2	tyrosine-protein kinase transmembrane receptor	35.7	38.39	15.38	40.84	0.102049354	1.352947495
Mme	neprilysin	92.61	62.2	25.63	66.82	-0.566738097	1.348658356
Xkr6	X Kell blood group precursor related family	1.91	1.57	0	1.54	-0.179250794	1.344828497
Dlg4	disks large homolog 4 isoform 1	34.03	38.64	7.61	20.83	0.178365974	1.342226988
Asb16	ankyrin repeat and SOCS box protein 16	0	0	0	1.52	0	1.333423734
Trim9	E3 ubiquitin-protein ligase TRIM9 isoform a	0.26	0.82	0	1.52	0.530514717	1.333423734
Plaur	urokinase plasminogen activator surface receptor	8.75	13.42	4.39	12.53	0.564597041	1.327804661
Cyp2a5	cytochrome P450 2A5	0	0	0.59	2.99	0	1.327361981
Procr	endothelial protein C receptor	9.55	20.64	6.2	17.05	1.0364575	1.325930025
4930578I06Rik	hypothetical protein LOC67750	0	0	0	1.5	0	1.321928095
Haao	3-hydroxyanthranilate 3,4-dioxygenase	0	0	0	1.5	0	1.321928095
Cnksr2	connector enhancer of kinase suppressor of ras	3.05	12.51	0.45	2.62	1.738033862	1.319936797
Prune2	protein prune homolog 2	6.94	8.81	1.65	5.6	0.305114129	1.316473665
Shank1	SH3 and multiple ankyrin repeat domains 1	19.03	32.99	7.57	20.34	0.762947941	1.316193067
Nts	neurotensin/neuromedin N	0	5.22	0	1.49	2.63691458	1.316145742
Ccdc60	coiled-coil domain-containing protein 60	3.56	3.66	0.9	3.73	0.03129613	1.315840765
Fhl1	four and a half LIM domains protein 1 isoform 2	134.89	156.56	34.82	88.17	0.213462028	1.31579308
Cntfr	ciliary neurotrophic factor receptor subunit	7.86	12.27	43.78	110.4	0.582789767	1.314822799
Phactr1	phosphatase and actin regulator 1 isoform 3	2.75	3.13	1.81	5.98	0.139251186	1.312656906
Wif1	wnt inhibitory factor 1 precursor	136.91	502.54	154.15	384.03	1.868379315	1.311307162
Gcnt1	beta-1,3-galactosyl-O-glycosyl-glycoprotein	8.26	6.65	3.44	9.98	-0.275552446	1.306246473
Pid1	PTB-containing, cubilin and LRP1-interacting	30.94	34.98	3.25	9.51	0.171830874	1.306227923
Nckap5l	nck-associated protein 5-like	5.88	11.88	8.19	21.7	0.904652123	1.304555531
Magee2	melanoma antigen, family E, 2	1.39	3.32	0	1.47	0.854020694	1.304511042
Zpbp2	zona pellucida-binding protein 2 isoform 1	2.08	1.24	0	1.47	-0.459431619	1.304511042
Sparc	SPARC precursor	3462.6	1983.38	230.49	569.32	-0.803584006	1.300821753
Ano7	anoctamin-7	1.32	1.91	2.97	8.76	0.326894348	1.29774214

Ccdc68	coiled-coil domain-containing protein 68	6.94	9.11	1.69	5.6	0.348572085	1.294859852
Acot7	cytosolic acyl coenzyme A thioester hydrolase	81.58	97.44	59.66	147.58	0.253452239	1.292422528
Heyl	hairy/enhancer-of-split related with YRPW	0.61	0.63	0.62	2.96	0.017811276	1.289506617
Kcnc4	potassium voltage-gated channel subfamily C	11.82	16.27	1.77	5.77	0.429871821	1.289269858
Gda	guanine deaminase	61.01	66.08	7.02	18.6	0.113381799	1.289179513
Vegfc	vascular endothelial growth factor C precursor	2.15	2.91	0	1.44	0.311816779	1.286881148
Rasl11b	ras-like protein family member 11B	19.23	10.82	7.37	19.42	-0.775266284	1.286683338
Acsm3	acyl-coenzyme A synthetase ACSM3, mitochondrial	1.37	4.74	3.37	9.65	1.276163678	1.285148246
Tgif2	homeobox protein TGIF2	5.84	20.16	12.98	32.98	1.629271397	1.281321492
1810024B03Rik	hypothetical protein LOC329509	1.35	1.71	0	1.43	0.205632095	1.280956314
Ccdc85a	coiled-coil domain-containing protein 85A	5.59	6.96	0	1.43	0.272489966	1.280956314
Dlx4	homeobox protein DLX-4	2.23	0.81	0	1.43	-0.835544468	1.280956314
Cyp21a1	steroid 21-hydroxylase	0	0.5	0.74	3.22	0.584962501	1.278155693
Mettl7a1	methyltransferase-like protein 7A	29.28	29.95	22.38	55.62	0.031574204	1.276036819
Bdh2	3-hydroxybutyrate dehydrogenase type 2 isoform	1.75	3.1	0	1.42	0.576192291	1.275007047
Lzts1	leucine zipper putative tumor suppressor 1	1.58	6.48	4.72	12.83	1.535667204	1.273714104
Rsph4a	radial spoke head protein 4 homolog A	25.07	56.16	3.53	9.94	1.132615334	1.272029783
Fblim1	filamin-binding LIM protein 1	16.02	20.48	5.22	14.02	0.335762956	1.271898327
Lgals6	galectin-6	6.57	9.95	6.73	17.66	0.532565665	1.271408667
Slc20a1	sodium-dependent phosphate transporter 1 isoform	33.31	136.72	59.44	144.45	2.005037055	1.266947731
Zc3h12c	probable ribonuclease ZC3H12C	17.71	32.87	24.8	61.03	0.856198428	1.265595059
Ndrg1	protein NDRG1	560.51	1094.15	172.8	415.5	0.963744865	1.260888413
Ggt1	gamma-glutamyltranspeptidase 1 precursor	0	0	0	1.39	0	1.257010618
Pcdhb9	protocadherin beta 9	2.42	4.69	0.64	2.91	0.734432327	1.253472793
Tnni1	troponin I, slow skeletal muscle	0	0	0	1.38	0	1.250961574
Tmem88b	transmembrane protein 88B	1.87	6.82	1.61	5.21	1.446117871	1.250543462
Sdk1	protein sidekick-1 precursor	14.37	32.6	3.91	10.68	1.128344068	1.250245345
Psd3	PH and SEC7 domain-containing protein 3 isoform	14.56	20.39	11.21	28.03	0.459094422	1.249481372
Igfbp2	insulin-like growth factor-binding protein 2	34.8	54.85	74.9	179.27	0.641597693	1.247987537
Msi1	RNA-binding protein Musashi homolog 1	1.11	1.59	3.8	10.39	0.295709099	1.246661436
Pitpnc1	cytoplasmic phosphatidylinositol transfer	4.06	12.87	3.77	10.31	1.454758498	1.245537758
Klhl35	kelch-like protein 35	1.26	2.43	0	1.37	0.601885804	1.244887059
Mettl7a2	methyltransferase like 7A2	3.92	3.75	2.53	7.36	-0.050730802	1.243834759
Kcnn3	small conductance calcium-activated potassium	3.86	45.31	0.36	2.22	3.252295538	1.243454037
St3gal5	lactosylceramide alpha-2,3-sialyltransferase	1.76	10.68	1.63	5.21	2.081300102	1.239530469
Serpind1	heparin cofactor 2 precursor	0	0	0	1.36	0	1.23878686
Gm1987	predicted gene 1987	1.97	3.5	0.77	3.17	0.59946207	1.236298023
Hpcal4	hippocalcin-like protein 4	0	0.81	0	1.35	0.855989697	1.232660757
Gm8898	KRAB box and zinc finger C2H2 type domain	1.94	4.79	1.49	4.84	0.977747193	1.229822627
Pcdhb11	protocadherin beta 11	2.47	6.27	1.37	4.55	1.067019701	1.227600712
Hsd17b1	estradiol 17-beta-dehydrogenase 1	0	0	0	1.34	0	1.22650853
2810032G03Rik		24.46	20.34	1.99	5.98	-0.254672243	1.223081552
Adamts20	A disintegrin and metalloproteinase with	0	2.06	0.23	1.87	1.613531653	1.222392421
Bves	blood vessel epicardial substance	5.42	16.23	0	1.33	1.424277499	1.220329955
Gnao1	guanine nucleotide-binding protein G(o) subunit	5.54	7.48	2.2	6.44	0.374773629	1.217230716
Pdpn	podoplanin precursor	6.1	15.95	4.65	12.12	1.255394344	1.215444947
Clec3b	tetranectin precursor	68.71	81.32	14.42	34.78	0.239877355	1.214350622
Hhipl1	HHIP-like protein 1 precursor	0	0	1.44	4.66	0	1.213920905
Anxa3	annexin A3	2.67	4.22	1.87	5.63	0.508269744	1.207958133
Csn3	kappa-casein precursor	0	0	0	1.31	0	1.207892852
Amt	aminomethyltransferase, mitochondrial precursor	11.52	14.02	4.24	11.08	0.262650251	1.204981738
Sdk2	protein sidekick-2 precursor	86.59	47.84	15.83	37.77	-0.842702969	1.203905558
Dgat2l6	diacylglycerol O-acyltransferase 2-like protein	1.22	4.12	0	1.3	1.205584134	1.201633861
Tspan10	tetraspanin-10	0	0	0	1.3	0	1.201633861
Krt71	keratin, type II cytoskeletal 71	4.35	0.87	3.84	10.13	-1.516500621	1.20137464
Ntrk3	NT-3 growth factor receptor isoform b	0.98	1.82	0	1.29	0.510194732	1.195347598
Phxr4		0	0	0	1.29	0	1.195347598
Tbx1	T-box transcription factor TBX1	983.76	1359.55	153.15	350.89	0.466345909	1.190789627
Hs6st2	heparan-sulfate 6-O-sulfotransferase 2 isoform	1.18	5.73	4.27	11	1.62627837	1.187159539
Ddah2	N(G),N(G)-dimethylarginine	172.7	148.29	39.25	90.63	-0.218480222	1.186831236
Krt8	keratin, type II cytoskeletal 8	6.53	18.61	8.31	20.19	1.380867766	1.186530515
Mylk	myosin light chain kinase, smooth muscle	20.72	47.6	5.27	13.2	1.161932211	1.179353582
Mgst2	microsomal glutathione S-transferase 2	14.85	17.19	50.76	116.11	0.198662703	1.17795475
Efhc2	EF-hand domain-containing family member C2	0	0.64	0	1.26	0.713695815	1.176322773
Gm12216		0	0	0	1.26	0	1.176322773
Gprc5d	G-protein coupled receptor family C group 5	0	0	0	1.26	0	1.176322773
Pcdhb5	protocadherin beta 5	1.31	1.06	0	1.26	-0.165248514	1.176322773
Pmepa1	transmembrane prostate androgen-induced protein	12.45	22.59	25.44	58.56	0.810569246	1.171621577
Trerf1	transcriptional-regulating factor 1 isoform 1	14.41	27.96	7.46	17.96	0.910194741	1.164229396
Serpina3j	serine (or cysteine) peptidase inhibitor, clade	25.58	26.31	35.57	80.94	0.039088209	1.163907266
Hlf	hepatic leukemia factor	8.01	23.09	7.99	19.14	1.418835382	1.163670662
AI428936	nesprin-4	0	1.45	0	1.24	1.292781749	1.163498732
Edn2	endothelin-2 precursor	11.99	43.53	35.72	81.25	1.777376181	1.16344962
Usp11	ubiquitin carboxyl-terminal hydrolase 11	20.05	34.82	13.48	31.4	0.766945104	1.161932211
Per2	period circadian protein homolog 2	1.73	4.39	2.68	7.23	0.981384322	1.161186664
Gm14431	KRAB box and zinc finger C2H2 type domain	2.13	5	1.66	4.94	0.938799844	1.159036685
Gm889	hypothetical protein LOC380755	0	2.04	0	1.23	1.604071324	1.15704371
Sh2d4b	SH2 domain-containing protein 4B	0	0	0	1.23	0	1.15704371
Dct	L-dopachrome tautomerase precursor	20.76	59.2	37.62	85.03	1.46808493	1.155491673
Slc38a2	sodium-coupled neutral amino acid transporter 2	2984.97	4637.41	781.11	1739.44	0.635430678	1.154008644
Nupr1	nuclear protein 1	64.8	118.62	86.82	194.41	0.862299134	1.153882859
1700125H03Rik		0	4.16	5.12	12.61	2.367371066	1.153063509
Ccno	cyclin-O	7.99	15.68	6.7	16.12	0.891726268	1.152752351
Lrrn2	leucine rich repeat protein 2, neuronal	0.34	0.65	0	1.22	0.300233024	1.150559677
Rarres2	retinoic acid receptor responder protein 2	49.98	81.15	16	36.52	0.688329202	1.142125081
Klhl13	kelch-like protein 13	7.05	11.9	1.98	5.57	0.680310377	1.14058104
Ccl11	eotaxin precursor	11.5	23.51	3.43	8.76	0.971442389	1.139574449
1700019B03Rik	hypothetical protein LOC76406	0	0	0	1.2	0	1.137503524
Ttc7b	tetratricopeptide repeat domain 7B	7.21	12.85	3.91	9.79	0.754431849	1.135899935
Mex3a	RNA-binding protein MEX3A	5.14	6.01	12.85	29.43	0.191175789	1.135608358
Smoc1	SPARC-related modular calcium-binding protein 1	52.01	5.41	25.37	56.85	-3.047868279	1.133419388
Fxyd1	phospholemman isoform b precursor	12.39	25.64	7.53	17.71	0.992438122	1.133191912

Tnfsf9	tumor necrosis factor ligand superfamily member	8.46	17.47	8.29	19.36	0.965271778	1.13198706
Syn2	synapsin-2 isoform IIa	0	0	1.41	4.28	0	1.131504783
Esm1	endothelial cell-specific molecule 1 precursor	0	0	0	1.19	0	1.13093087
Vamp1	vesicle-associated membrane protein 1 isoform b	3.93	7.03	7.63	17.88	0.703812341	1.1294263
Ms4a10	membrane-spanning 4-domains subfamily A member	5.09	1.77	1.21	3.83	-1.136556252	1.127976819
Srsf12	serine/arginine-rich splicing factor 12	4.85	7.59	2.64	6.95	0.554221507	1.12701641
Atp6v1b1	V-type proton ATPase subunit B, kidney isoform	26.52	20.63	85.67	188.16	-0.347446805	1.126002437
Hexa	beta-hexosaminidase subunit alpha precursor	175.65	184.61	41.94	92.61	0.071380691	1.124340464
5730422E09Rik		0.68	0	0	1.18	-0.748461233	1.124328135
Egfem1	EGF-like and EMI domain-containing protein 1	0	0	0	1.18	0	1.124328135
Snord22		0	35.37	26.81	59.57	5.184677021	1.122999667
Ppp1r14a	protein phosphatase 1 regulatory subunit 14A	30.18	30.34	9.66	22.19	0.007384252	1.121295382
Adamts10		12.99	19.27	6.78	15.89	0.534950126	1.118327268
Emcn	endomucin isoform 1	3.21	6.05	0	1.17	0.743803024	1.117695043
Tas1r1	taste receptor type 1 member 1 precursor	1.04	0.51	0	1.17	-0.434020603	1.117695043
Rgs16	regulator of G-protein signaling 16	6.39	14.76	6.41	15.07	1.092621265	1.116824481
BC005764		28.6	27.09	19.53	43.52	-0.075540551	1.116719965
Ampd3	AMP deaminase 3	202.65	183.33	33.76	74.32	-0.143800923	1.115604918
Gm5506	hypothetical protein LOC433182	12.4	44.28	24.53	54.2	1.756640957	1.112474729
Krt33b	keratin, type I cuticular Ha3-II	0	0	0	1.16	0	1.111031312
Srpx	sushi-repeat-containing protein SRPX precursor	17.14	25.69	3.09	7.83	0.55712485	1.110312595
Ager	advanced glycosylation end product-specific	1.28	3.65	0.83	2.94	1.028196892	1.106351981
Slc6a17	sodium-dependent neutral amino acid transporter	3.48	3.24	1.24	3.82	-0.079434467	1.105534414
Trps1	zinc finger transcription factor Trps1	34.69	72.75	26.57	58.28	1.047123148	1.10444618
Mfap4	microfibril-associated glycoprotein 4 precursor	61.8	113.39	19.28	42.53	0.865124473	1.101952368
Clip3	CAP-Gly domain-containing linker protein 3	2.87	4.58	0.72	2.69	0.527931556	1.101212251
Mtap1b	microtubule-associated protein 1B	12.39	29.04	25.53	55.87	1.165728852	1.100043129
Nhs	Nance-Horan syndrome protein	4.52	6.33	7.23	16.64	0.409144931	1.099886225
Inpp5j	phosphatidylinositol 4,5-bisphosphate	8.92	8.13	1.19	3.69	-0.11972526	1.098657053
Fjx1	four-jointed box protein 1 precursor	57.23	105.25	28.26	61.62	0.867628317	1.097693739
1200009I06Rik	exocyst complex component 3-like protein 4	2.32	4.52	3.9	9.47	0.733485025	1.095407788
Fscn1	fascin	29.84	39.34	17.95	39.45	0.387408319	1.093941854
Hectd2	probable E3 ubiquitin-protein ligase HECTD2	19.35	17.37	4.35	10.41	-0.147677168	1.092687995
Arhgef15	rho guanine nucleotide exchange factor 15	1.53	1.75	0.61	2.43	0.120294234	1.091147888
Ebf4	transcription factor COE4	17.92	10.69	1.99	5.35	-0.694637159	1.086611107
Foxi3	forkhead box protein I3	15.87	4.78	22.64	49.2	-1.545318576	1.086457329
Chst11	carbohydrate sulfotransferase 11	76.13	70.16	34.8	75	-0.1162256	1.086039831
Sdc3	syndecan-3 precursor	46.06	32.05	30.1	65.01	-0.509851049	1.085770018
Kitl	kit ligand precursor	134.33	124.65	77.66	165.85	-0.107071021	1.084849595
Astn2	astrotactin-2 isoform b	0	0	0	1.12	0	1.084064265
C1qtnf2	complement C1q tumor necrosis factor-related	2.72	5.41	0	1.12	0.785021736	1.084064265
Slc7a3	cationic amino acid transporter 3	0	0.64	0	1.12	0.713695815	1.084064265
Sfxn4	sideroflexin-4	7.3	13.03	2.12	5.61	0.757331767	1.083104243
Espn	espin isoform 1	10.15	7.58	5.05	11.81	-0.377994157	1.082263428
Dleu2		51.12	64.52	17.93	39.03	0.330098273	1.080407205
Tubb6	tubulin beta-6 chain	17.12	63.24	34.14	73.24	1.825888937	1.079082519
Fam110c	family with sequence similarity 110, member C	23.76	19.74	14.86	32.49	-0.25559542	1.078337605
Lrat	lecithin retinol acyltransferase	1.22	1.5	0.53	2.23	0.171368418	1.078002512
Kera	keratocan precursor	2.49	3.24	0	1.11	0.280837228	1.077242999
Tm6sf2	transmembrane 6 superfamily member 2	0	0	0	1.11	0	1.077242999
Tmc1	transmembrane channel-like protein 1	1.22	2.35	0	1.11	0.593601419	1.077242999
Cd248	endosialin precursor	9.25	14.52	2.06	5.45	0.598504648	1.075767508
Slc39a8	zinc transporter ZIP8	197.69	189.68	82.32	174.62	-0.059365734	1.075722407
Akr1cl	aldo-keto reductase family 1, member C-like	0	2.27	1.89	5.09	1.709290636	1.075372735
Tgm3	protein-glutamine gamma-glutamyltransferase E	4	11.49	1.1	3.42	1.320773477	1.073657042
Plscr1	phospholipid scramblase 1	1.97	1.95	1.89	5.08	-0.009747977	1.073001831
Tbc1d24	TBC1 domain family member 24 isoform b	9.26	15.12	3.77	9.02	0.651821013	1.070821337
Bdkrb2	B2 bradykinin receptor	0	0	0	1.1	0	1.070389328
Foxj1	forkhead box protein J1	0	1.03	0	1.1	1.021479727	1.070389328
Hist2h3b	histone H3.2	4.21	4.3	1.7	4.67	0.024708987	1.070389328
S100a3	protein S100-A3	62.48	68.75	10.92	24.03	0.135891089	1.070274055
Ankrd6	ankyrin repeat domain-containing protein 6	14.05	12.97	7.04	15.87	-0.107431466	1.069192567
Slc6a6	sodium- and chloride-dependent taurine	1011.39	1103.17	128.17	269.88	0.125197147	1.068382838
G530011O06Rik		1.15	3.92	1.68	4.62	1.194321656	1.06833713
Tsga10	testis-specific gene 10 protein	5.47	5.82	1.48	4.2	0.076006027	1.068171503
Npr3	atrial natriuretic peptide receptor 3 isoform a	1.26	0.86	5.92	13.5	-0.281020151	1.067208957
Plekhg1	pleckstrin homology domain containing, family G	15.8	25.97	15.49	33.51	0.682894289	1.065423075
Ptprz1	receptor-type tyrosine-protein phosphatase zeta	1.22	2.96	7.1	15.95	0.834940754	1.06529146
Lonrf2	LON peptidase N-terminal domain and RING finger	0	0.44	0.3	1.72	0.526068812	1.065095028
Tac4	tachykinin-4 precursor	0	1.32	0	1.09	1.214124805	1.063502942
Lamb1	laminin subunit beta-1	41.04	68.74	53.21	112.17	0.730223695	1.061860656
Awat1	acyl-CoA wax alcohol acyltransferase 1	14.22	14.39	4.87	11.21	0.016024873	1.056630792
Slc45a2	membrane-associated transporter protein	0.85	0	0	1.08	-0.887525271	1.056583528
Ptpla	3-hydroxyacyl-CoA dehydratase 1 isoform 1	27.87	31.83	5.63	12.79	0.185443642	1.056541681
Serpinb6d	serine (or cysteine) peptidase inhibitor, clade	10.24	5.57	4.28	9.98	-0.77467676	1.05626822
AI593442	hypothetical protein LOC330941 isoform 2	0	1.59	0.78	2.7	1.372952098	1.05564803
Mettl7b	methyltransferase-like protein 7B precursor	0	1.24	10.77	23.4	1.163498732	1.051766827
Ccl20	C-C motif chemokine 20 isoform 2	0	12.8	18.46	39.31	3.786596362	1.050626073
Cyp2a4	cytochrome P450 2A4	0	0	0	1.07	0	1.049630768
Fut4	alpha-(1,3)-fucosyltransferase	0.99	1.03	0	1.07	0.028711297	1.049630768
Plekhb1	pleckstrin homology domain-containing family B	1.47	3.7	2.06	5.32	0.928149715	1.046392905
Arhgef19	rho guanine nucleotide exchange factor 19	141.71	193.56	78.73	163.56	0.447128703	1.045419125
Ddx26b	protein DDX26B	83.73	141.26	48.87	101.89	0.747585294	1.044858664
Srgap3	SLIT-ROBO Rho GTPase-activating protein 3	10.99	5.85	4.17	9.66	-0.807655766	1.043971252
Hist1h2bq	H2b histone family, member A	0.35	1.27	1.14	3.41	0.74973289	1.043167859
Hist1h2br	histone cluster 1 H2br	0.35	1.27	1.14	3.41	0.74973289	1.043167859
Apol7a	apolipoprotein L 7a	1.37	2.54	0	1.06	0.578862301	1.042644337
Tmsb15l	Tmsb15b1-Tmsb15b2 readthrough transcript	22.66	20.41	9.88	21.38	-0.144165278	1.04053148
Lce1a2	small proline rich-like 2	6.48	9.51	4.81	10.95	0.490652494	1.040400549
Sox4	transcription factor SOX-4	38.03	53.51	106.78	220.68	0.481937458	1.040389124
Nrip3	nuclear receptor-interacting protein 3	104.7	84.29	33.34	69.6	-0.309526872	1.039778144
Lrp3	low density lipoprotein receptor-related protein	1.73	2.52	1.81	4.77	0.366674478	1.038001188

Wnt9a	protein Wnt-9a precursor	3.63	6.32	2.08	5.32	0.660831455	1.036994207
Basp1	brain acid soluble protein 1	12.29	16.11	40.61	84.37	0.364498655	1.036798891
Fbln2	fibulin-2 isoform b	150.07	112.24	14.59	30.98	-0.415833539	1.036549011
Mapk15	mitogen-activated protein kinase 15	4.81	5.94	2.16	5.48	0.256397499	1.036069255
Hepacam2	HEPACAM family member 2 precursor	0.81	0.7	0	1.05	-0.090454951	1.03562391
Omd	osteomodulin precursor	1.33	2.12	0	1.05	0.421216074	1.03562391
2210404O07Rik	transmembrane protein C19orf77 homolog	9.25	18.27	7.62	16.67	0.910732662	1.035542265
Gmpr	GMP reductase 1	3.06	7.07	3.8	8.82	0.991088946	1.032688619
Gpx7	glutathione peroxidase 7 precursor	1.59	3.87	2.67	6.5	0.910969674	1.031110533
Xlr3a	X-linked lymphocyte-regulated protein 3A	1.09	2.86	0.67	2.41	0.885097905	1.029923637
Ccdc3	coiled-coil domain-containing protein 3	690.23	1663.94	160.91	329.3	1.268232449	1.028584876
Sp5	transcription factor Sp5	0	0	0	1.04	0	1.028569152
Spo11	meiotic recombination protein SPO11 isoform b	0	0	2.56	6.26	0	1.028092307
2700046A07Rik		1.36	2.62	3.81	8.79	0.617202838	1.025271966
Dnajb13	dnaJ homolog subfamily B member 13	0	1.74	1.18	3.43	1.454175893	1.022978564
Lmtk3	serine/threonine-protein kinase LMTK3 precursor	1.69	2.3	0.89	2.84	0.294859852	1.022720077
Vsig8		7.32	9.01	1.53	4.14	0.266786541	1.022630974
9930012K11Rik	hypothetical protein LOC268759 isoform 2	3.65	5.94	8.63	18.51	0.577704947	1.018606075
4930550C14Rik	hypothetical protein LOC75311	3.31	2.54	4.81	10.75	-0.283938509	1.016050688
Mdga1	MAM domain-containing	5.49	10.3	1.81	4.68	0.800032389	1.015320799
Tcp11l1	T-complex protein 11-like protein 1	7.62	10.07	2.77	6.62	0.360895448	1.015226474
Cd69	early activation antigen CD69	1.07	2.16	0	1.02	0.610293791	1.014355293
C1ra	complement C1r-A subcomponent precursor	21.62	40.71	3.72	8.53	0.882794383	1.013689355
Icam1	intercellular adhesion molecule 1 precursor	129.26	164.56	194.27	392.8	0.345960022	1.011992791
Cald1	caldesmon 1	195.2	377.77	104.65	212.05	0.948997027	1.011899284
Penk	proenkephalin-A	4.69	9.82	3.32	7.7	0.927199942	1.009984089
Id2	DNA-binding protein inhibitor ID-2	2174.28	1606.45	222.14	447.97	-0.436427252	1.008669894
Pdgfd	platelet-derived growth factor D	3.82	8.94	0	1.01	1.044212705	1.007195501
Tyr	tyrosinase precursor	0.49	1.55	1.44	3.9	0.775184916	1.005900601
Slc1a4	neutral amino acid transporter A	18.48	20.1	9.17	19.42	0.115249322	1.005663187
Ly6c1	lymphocyte antigen 6C2 precursor	40.65	67.15	12.28	25.66	0.710397161	1.005421634
Cyp2d22	cytochrome P450, family 2, subfamily d,	62.98	44.22	7.9	16.86	-0.50066	1.004854839
A430110N23Rik	soluble scavenger receptor cysteine-rich	4.38	10.51	0.68	2.37	1.097209756	1.004287358
Cd302	CD302 antigen	6.71	12.64	4.8	10.63	0.823040879	1.003726291
Plod2	procollagen-lysine,2-oxoglutarate 5-dioxygenase	3.01	3.42	3.97	8.96	0.140444133	1.002899891
Hoxd8	homeobox protein Hox-D8	117.76	118.48	17.96	36.97	0.008720144	1.001901035
Inhbb	inhibin beta B chain precursor	121.35	99.19	57.34	115.83	-0.288275582	1.001853491
Sat2	diamine acetyltransferase 2	7.33	4.62	1.89	4.78	-0.567746365	1
Arid3b	AT-rich interactive domain-containing protein	4.11	5.07	0.74	2.48	0.248373225	1
Cdk15	cyclin-dependent kinase 15	0	0	0	1	0	1
Pla1a	phospholipase A1 member A precursor	1.21	0	0	1	-1.14404637	1
Stx1b	syntaxin-1B	0	0	0	1	0	1
Wnt2	protein Wnt-2 precursor	0	0	0	1	0	1

Bulge Down

GENE	Description	WT Bulge	KO Bulge	WT HG	KO HG	Log2 KO Bulge/WT Bulge	Log2 KO HG/WT HG
Mir5114		70.08	0	0	79.43	-6.151371776	6.329661815
Skint4	selection and upkeep of intraepithelial T-cells	86.55	0.44	142.39	0	-5.925966462	-7.163800604
Mir568		43.3	0	0	0	-5.469234794	0
Krt13	keratin, type I cytoskeletal 13	89.24	1.22	30.2	0.85	-5.345135486	-4.075948853
Cck	cholecystokinin preproprotein	207.3	4.29	3.43	3.04	-5.299251307	-0.132951406
Mir1306		36.97	0	45.16	0	-5.246788094	-5.528571319
Krt27	keratin, type I cytoskeletal 27	123.6	2.32	42.75	11.95	-5.229977017	-1.756330919
Mir5122		34.36	0	0	28.32	-5.14404637	4.873813198
St6galnac5	alpha-N-acetylgalactosaminide	69.99	1.48	2.37	1.99	-4.839203788	-0.172603107
Mir671		27.61	0	25.04	0	-4.838447593	-4.702657543
Sval2	seminal vesicle antigen-like 2	21.01	0	11.13	0	-4.46008724	-3.600507645
Gdf10	bone morphogenetic protein 3B precursor	63.64	2.64	4.1	2.73	-4.150416843	-0.451321617
Myoc	myocilin precursor	586.87	35.65	33.32	3.58	-4.003612053	-2.905630049
Krt24	keratin, type I cytoskeletal 24	1264.3	83.79	5.59	4.86	-3.89944155	-0.169377801
Skint9	selection and upkeep of intraepithelial T-cells	12.04	0	46.94	0	-3.704871964	-5.583158004
Rpl34-ps1	ribosomal protein L34, pseudogene 1	14.04	0.29	13.07	23	-3.543361596	0.770412077
Slc43a1	large neutral amino acids transporter small	78.39	6.56	47.05	43.55	-3.392499157	-0.109110999
Skint3	selection and upkeep of intraepithelial T-cells	8.72	0	214.86	0	-3.280956314	-7.753952119
AA465934		8.04	0	8.1	7.15	-3.176322773	-0.159066486
Camk4	calcium/calmodulin-dependent protein kinase type	43	4.01	4.33	4.99	-3.134621015	0.16842047
Ltbp2	latent-transforming growth factor beta-binding	376.86	42.65	19.33	32.97	-3.113798245	0.740651003
Smoc1	SPARC-related modular calcium-binding protein 1	52.01	5.41	25.37	56.85	-3.047868279	1.133419388
Ccrl1	C-C chemokine receptor type 11	857.26	109.4	518.48	150.46	-2.95867459	-1.778131373
Dpysl4	dihydropyrimidinase-related protein 4	6.77	0	2.29	0	-2.957914599	-1.718087584
Lrrc18	leucine-rich repeat-containing protein 18	18.74	1.61	4.89	1.42	-2.919000278	-1.283260587
Ngef	ephexin-1 isoform 1	85.59	10.71	13.49	6.07	-2.886459347	-1.035275475
BB123696		5.95	0	1.29	0	-2.797012978	-1.195347598
Scn5a	sodium channel protein type 5 subunit alpha	5.85	0	1.27	0.16	-2.776103988	-0.968567492
6030419C18Rik	hypothetical protein LOC319477	28.39	3.36	5.7	4.66	-2.752925319	-0.243359043
Ptchd3	patched domain-containing protein 3	5.59	0	1.37	0	-2.720278465	-1.244887059
Il3ra	interleukin-3 receptor subunit alpha precursor	19.46	2.24	14.9	2.89	-2.658740427	-2.031184705
Hist1h4c	histone H4	5.25	0	2.27	0.55	-2.64385619	-1.07702242
Gfra1	GDNF family receptor alpha-1 precursor	238.92	38.03	29.12	12.89	-2.619898059	-1.116675171
Adora2a	adenosine receptor A2a	31.78	4.36	9.39	1.96	-2.612510949	-1.811526573
Abcb1b	multidrug resistance protein 1	23.35	3.01	14.33	4.89	-2.602247631	-1.380018158
Tmem196	transmembrane protein 196	4.65	0	0	0	-2.498250868	0
Serpina9	serpin A9 precursor	4.55	0	3.79	1.49	-2.472487771	-0.943879914
Krt2	keratin, type II cytoskeletal 2 epidermal	4.54	0	1.25	0.5	-2.469885976	-0.584962501
Wdfy4	WD repeat and FYVE domain containing 4	7.74	0.62	0.55	0.2	-2.431639467	-0.36923381
1110032A04Rik	small subunit of serine palmitoyltransferase B	4.17	0	5.73	6.5	-2.370164281	0.156284091
Xcl1	lymphotactin precursor	4.15	0	0	0	-2.364572432	0
1700019D03Rik	hypothetical protein LOC67080	65.33	12.34	1.52	3.4	-2.313902859	0.80407979
Aass	alpha-aminoadipic semialdehyde synthase,	8.15	0.85	1.24	0.44	-2.306246473	-0.637429921
Htr1b	5-hydroxytryptamine receptor 1B	3.84	0	0	0	-2.275007047	0
AI506816		3.78	0	3.26	5.75	-2.257010618	0.664034072
Trpc1	short transient receptor potential channel 1	19.48	3.3	2.77	1.98	-2.25180715	-0.339252193
Crp	C-reactive protein precursor	3.72	0	0	0	-2.23878686	0
Lhb	lutropin subunit beta precursor	3.71	0	0	0	-2.23572706	0
Ecm1	extracellular matrix protein 1 precursor	2342.99	500.06	379.66	164.88	-2.225911139	-1.198363026
Tll1	tolloid-like protein 1 precursor	13.34	2.07	6.03	4.59	-2.223734463	-0.330676406
Arsi	arylsulfatase I precursor	14.94	2.43	3.26	4.48	-2.216371148	0.363322463
Cybrd1	cytochrome b reductase 1	21.3	3.82	4.82	2	-2.209938659	-0.956056652
Htr1d	5-hydroxytryptamine receptor 1D	11.37	1.68	7.89	3.98	-2.206540595	-0.836037677
Tspan8	tetraspanin 8	91.55	19.31	20.1	15.08	-2.18804275	-0.391975592
Pvt1		22.44	4.26	13.41	4.51	-2.155837865	-1.386946112
Chst13	carbohydrate sulfotransferase 13	22.17	4.26	3.56	2.06	-2.13912334	-0.575502171
Spink2	serine protease inhibitor Kazal-type 2	149.27	33.34	3.71	3.61	-2.129595073	-0.030960309
Tbc1d30	TBC1 domain family member 30	8.25	1.13	2.91	3.13	-2.118599935	0.078973174
Zdhhc2	palmitoyltransferase ZDHHC2	103.93	23.31	13.9	7.26	-2.109805412	-0.851098644
Anpep	aminopeptidase N	88.48	20.29	243.89	109.22	-2.071389307	-1.151747831
BC028528	hypothetical protein LOC229600 precursor	3.17	0	0	0	-2.060047384	0
Upp1	uridine phosphorylase 1	22.11	4.65	7.69	2.85	-2.032194487	-1.174497731
Arrdc3	arrestin domain-containing protein 3	432.41	105.03	556.93	311.91	-2.031259924	-0.834336362
Unc79	protein unc-79 homolog	22.05	4.68	7.68	4.02	-2.020803916	-0.790007678
C1ql3	complement C1q-like protein 3 precursor	6.56	0.88	0.48	0.23	-2.007653573	-0.26693886
Abcc3	canalicular multispecific organic anion	30.21	6.81	9.63	5.52	-1.998613904	-0.705197727
Fam83a	hypothetical protein LOC239463	33.26	7.63	76.28	60.95	-1.989092687	-0.318990812
Odf3l1	outer dense fiber protein 3-like protein 1	11.94	2.28	2.06	1.66	-1.980069897	-0.202105407
BC100530	stefin A-like protein	2.87	0	0	0	-1.952333566	0
Slc27a3	long-chain fatty acid transport protein 3	285.11	73.18	67.77	40.79	-1.94746775	-0.718621587
Cish	cytokine-inducible SH2-containing protein	349.56	90.48	463.92	185.62	-1.938133119	-1.316878882
7420461P10Rik	hypothetical protein LOC100038657	4.2	0.36	0.3	0	-1.934904972	-0.378511623
Slc7a2	low affinity cationic amino acid transporter 2	16.59	3.66	172.68	53.29	-1.916353623	-1.677673242
1700056E22Rik	hypothetical protein LOC73363	2.76	0	4.01	3.36	-1.910732662	-0.200482468
Pik3r1	phosphatidylinositol 3-kinase regulatory subunit	430.77	114.64	239.99	179.09	-1.900622492	-0.420255209
Npnt	nephronectin isoform b	482.66	129.76	139.8	142.86	-1.887071946	0.031018175
Cntn5	contactin-5 isoform 1	2.68	0	0.47	0	-1.879705766	-0.555816155
Dmrtc1a	doublesex- and mab-3-related transcription	2.66	0	0	0	-1.871843649	0
Usp18	ubl carboxyl-terminal hydrolase 18	35.04	8.89	3.96	3.53	-1.865556585	-0.13082907
Mmp2	72 kDa type IV collagenase precursor	365.91	100.58	84.03	66.66	-1.852809846	-0.329668761
Nptx1	neuronal pentraxin-1 precursor	12.36	2.7	1.11	1.06	-1.852322832	-0.034598662
Adh7	alcohol dehydrogenase class 4 mu/sigma chain	526.18	145.22	473.24	223.87	-1.850154982	-1.076526149
Rps23	40S ribosomal protein S23	34.89	9.01	40.6	67.51	-1.842139949	0.719731057
Slc15a1	solute carrier family 15 member 1	67.44	18.2	116.55	63.9	-1.833733449	-0.856984156
Slc34a3	sodium-dependent phosphate transport protein 2C	2.56	0	0	0	-1.831877241	0
Tns1	tensin 1	448	125.41	165.48	68.25	-1.828604849	-1.265462894
Fut4-ps1		2.55	0	2.94	0	-1.827819025	-1.97819563

Fhit	bis(5'-adenosyl)-triphosphatase	52.32	14.08	20.33	30.95	-1.822040352	0.582931965
Kcnk2	potassium channel subfamily K member 2 isoform	334.81	94.09	10.47	18.04	-1.820279657	0.731168087
Gng4	guanine nucleotide-binding protein	19.89	4.94	2.93	2.88	-1.814277656	-0.01847266
Fam55d	hypothetical protein LOC244853	7.22	1.34	5.66	3.72	-1.812629864	-0.496735318
Eda2r	tumor necrosis factor receptor superfamily	2.51	0	22.69	5.16	-1.811471031	-1.943275943
Art5	ecto-ADP-ribosyltransferase 5 precursor	2.5	0	0.65	0	-1.807354922	-0.722466024
Ccl12	C-C motif chemokine 12 precursor	2.5	0	0	0	-1.807354922	0
Itih5	inter-alpha-trypsin inhibitor heavy chain H5	22.9	5.86	40.43	35.21	-1.800730137	-0.194287644
Adig	adipogenin	2.46	0	3.63	5.45	-1.790772038	0.478286967
Mesp2	mesoderm posterior protein 2	12.07	2.8	15.3	5.79	-1.782187817	-1.263388485
Spsb4	SPRY domain-containing SOCS box protein 4	2.43	0	10.23	9.22	-1.778208576	-0.135962731
Rtn4rl1	reticulon-4 receptor-like 1 precursor	41.11	11.29	17.64	18.64	-1.77667796	0.07539307
Prickle2	prickle-like protein 2 isoform b	143.12	41.27	74.35	47.58	-1.769564539	-0.633245022
Pld1	phospholipase D1	58.33	16.43	25.39	14.98	-1.767189213	-0.723723942
Smpdl3b	acid sphingomyelinase-like phosphodiesterase 3b	72.51	20.6	51.11	33.19	-1.766909209	-0.607985832
Rnf182	E3 ubiquitin-protein ligase RNF182	8.05	1.68	1.94	1.05	-1.755684792	-0.520192245
Rad54l	DNA repair and recombination protein RAD54-like	12.06	2.87	27.63	19.37	-1.754749425	-0.49108169
Mfge8	lactadherin isoform 2	564.59	166.67	69.62	113.07	-1.754132032	0.691770692
Gm5084		11.47	2.71	17.1	5.88	-1.748970373	-1.395509227
Tmem171	transmembrane protein 171	2.35	0	1.53	0	-1.744161096	-1.339137385
Emilin3	EMILIN-3	22.8	6.11	3.14	1.23	-1.743040109	-0.892587058
Mmp15	matrix metalloproteinase-15 precursor	28.98	7.99	38.92	25.78	-1.737607362	-0.57595576
Gulo	L-gulonolactone oxidase	47.21	13.53	7.75	7.29	-1.730297727	-0.077910915
Dclk1	serine/threonine-protein kinase DCLK1 isoform 7	30.3	8.45	50.88	16.33	-1.727776423	-1.581906825
Cstad	CSA-conditional, T cell activation-dependent	2.31	0	2.01	2.33	-1.726831217	0.14575869
Ppp1r3c	protein phosphatase 1 regulatory subunit 3C	34.1	9.65	1.13	1.9	-1.7206176	0.44519947
Krtap3-2	keratin-associated protein 3-2	2.26	0	2.8	0	-1.704871964	-1.925999419
Grik1	glutamate receptor, ionotropic kainate 1 isoform	24.91	6.95	2.74	0.75	-1.70448225	-1.095683348
BC048671	hypothetical protein LOC243535	2.24	0	0	0	-1.695993813	0
Slc2a3	solute carrier family 2, facilitated glucose	12.27	3.1	5.18	2.6	-1.694472556	-0.779609932
4732415M23Rik	hypothetical protein LOC320869	2.23	0	0	0	-1.691534165	0
Fads6	fatty acid desaturase 6	5.97	1.17	2.87	0	-1.683463613	-1.952333566
Apobec1	C->U-editing enzyme APOBEC-1 isoform 2	11.87	3.01	28.75	12.79	-1.682337912	-1.109267212
6430531B16Rik	hypothetical protein LOC381933	2.19	0	0.99	1.7	-1.673556424	0.440190977
Ccdc88c	protein Daple	19.95	5.57	19.54	10.25	-1.672984968	-0.86851118
Chrm3	muscarinic acetylcholine receptor M3	2.18	0	1.74	0	-1.669026766	-1.454175893
Ednra	endothelin-1 receptor precursor	105.99	32.65	26.46	20.52	-1.668797549	-0.351653548
Eng	endoglin isoform 2	30.08	8.79	17.43	17.47	-1.666605739	0.003127795
Tsc22d3	TSC22 domain family protein 3 isoform 1	505.75	158.74	537.46	207.35	-1.665548565	-1.369830077
Wnt7a	protein Wnt-7a precursor	2.15	0	7.41	9.22	-1.655351829	0.281217491
Maf	transcription factor Maf	251.41	79.78	66.41	47.1	-1.643699017	-0.486925731
Fam159b	membrane protein FAM159B	2.11	0	2.99	1.2	-1.63691458	-0.858885223
D030025P21Rik		5.46	1.09	0.3	0.64	-1.628031223	0.335184192
A330069E16Rik		2.09	0	2.22	2.21	-1.627606838	-0.004487391
Msrb2	methionine-R-sulfoxide reductase B2,	23.36	6.92	16.33	9.15	-1.620941798	-0.771791927
Chac1	cation transport regulator-like protein 1	8.84	2.2	2.59	0	-1.62058641	-1.843983844
Tspan2	tetraspanin-2	45.87	14.27	10.71	12.09	-1.617964733	0.160724021
Mettl13	methyltransferase-like protein 13	82.24	26.12	31.25	25.63	-1.617919787	-0.276246732
Zfp365	protein ZNF365	38.87	11.99	55.67	26.11	-1.617902175	-1.063760089
H60b	histocompatibility 60b	2.06	0	5.75	0	-1.613531653	-2.754887502
Steap4	metalloreductase STEAP4	615.44	201.56	371.58	142.06	-1.60561117	-1.380929886
Tmem28	transmembrane protein FAM155B	2.04	0	0	0	-1.604071324	0
Ccdc113	coiled-coil domain-containing protein 113	7.83	1.91	2.49	2.26	-1.601394285	-0.098355072
Gjd3	gap junction delta-3 protein	2.03	0	2.91	0	-1.599317794	-1.967168608
1700108M19Rik	hypothetical protein LOC71156 isoform 2	2.02	0	2.61	2.57	-1.59454855	-0.016074763
Tmprss7	transmembrane protease serine 7 isoform 2	4.66	0.88	9.43	5.84	-1.590069391	-0.608670928
Clec2d	C-type lectin domain family 2 member D	627.29	209.41	512.72	222.92	-1.578227346	-1.197998849
Crybb3	beta-crystallin B3	1.98	0	0	0	-1.575312331	0
Itm2a	integral membrane protein 2A	286.47	95.82	17.09	19.48	-1.570034407	0.179023307
Sec14l2	SEC14-like protein 2	23.54	7.27	25.07	20.01	-1.569176014	-0.311314421
Skint11	selection and upkeep of intraepithelial T-cells	5.29	1.12	4.84	0	-1.568995752	-2.545968369
Slc16a14	monocarboxylate transporter 14	19.1	5.8	49.51	21.1	-1.56358885	-1.192522672
Nlrp10	NACHT, LRR and PYD domains-containing protein	27.41	8.65	47.73	29.58	-1.557797984	-0.672221816
Rnd1	rho-related GTP-binding protein Rho6 precursor	30.6	9.74	32.79	14.04	-1.556930565	-1.167791783
Lnx1	E3 ubiquitin-protein ligase LNX isoform 1	23.97	7.49	6.7	6.16	-1.556359362	-0.104898858
Ptpru	receptor-type tyrosine-protein phosphatase U	45.53	14.86	36.8	62.27	-1.552768416	0.743135361
Slc38a5	sodium-coupled neutral amino acid transporter 5	4.56	0.9	6.21	10.33	-1.549085464	0.652076697
Fbxl7	F-box/LRR-repeat protein 7	6.21	1.47	1.54	1.19	-1.545488218	-0.213897627
Foxi3	forkhead box protein I3	15.87	4.78	22.64	49.2	-1.545318576	1.086457329
Acss1	acetyl-coenzyme A synthetase 2-like,	11.6	3.32	21.72	10.34	-1.544320516	-1.002542195
Rapgef4	rap guanine nucleotide exchange factor 4 isoform	50.81	16.78	11.37	12.14	-1.542975259	0.087119775
1810062G17Rik	hypothetical protein LOC72282	1.89	0	5.25	2.37	-1.531069493	-0.891107598
Hist1h4b	histone H4	1.89	0	1.91	0.42	-1.531069493	-1.035128223
Gdf5	growth/differentiation factor 5 precursor	1.88	0	6.24	1.12	-1.526068812	-1.771925433
Sncg	gamma-synuclein	147.54	50.62	5.65	12.08	-1.524849437	0.975936295
Cldn20	claudin-20	1.87	0	0	0	-1.521050737	0
Gm13306	chemokine (C-C motif) ligand 27b isoform 2	495.12	172.29	731.31	307.99	-1.517500714	-1.244894348
Tbc1d2	TBC1 domain family, member 2	59.72	20.21	19.16	13.93	-1.51742717	-0.433281473
Krt71	keratin, type II cytoskeletal 71	4.35	0.87	3.84	10.13	-1.516500621	1.20137464
Actr3b	actin-related protein 3B	1.86	0	1.29	1.28	-1.516015147	-0.006313774
Rbm46	probable RNA-binding protein 46	1.85	0	0	0	-1.510961919	0
1700030C10Rik		5.32	1.22	8.3	1.58	-1.509364882	-1.849859651
Aqp9	aquaporin-9	8.96	2.5	14.25	6.68	-1.50879082	-0.989631027
Il10	interleukin-10 precursor	1.84	0	0	0	-1.50589093	0
Fzd9	frizzled-9 precursor	10.31	2.99	1.72	0	-1.503138278	-1.443606651
Spock2	testican-2 precursor	29.61	9.81	26.18	17.46	-1.501636522	-0.558142903
Scg3	secretogranin-3 isoform 2 precursor	1.82	0	0	0	-1.495695163	0
Fcgbp	Fc fragment of IgG binding protein	1038.06	368.87	1130.6	611.4	-1.49018877	-0.885817894
Tox	thymocyte selection-associated high mobility	6.33	1.63	3.94	3.55	-1.478750399	-0.118644496
Ugt1a1	UDP-glucuronosyltransferase 1-1	55.22	19.23	109.82	61.32	-1.474587134	-0.830451134
Col8a2	collagen alpha-2(VIII) chain precursor	776.45	279.02	60.27	30.7	-1.473220021	-0.950698011
Cacna2d2	voltage-dependent calcium channel subunit	11.18	3.39	7.05	2.34	-1.472221288	-1.269140681

Fam13a	family with sequence similarity 13, member A1	61.5	21.53	59.7	59.61	-1.472008876	-0.002140674
Mc5r	melanocortin receptor 5	1.77	0	26.7	17.29	-1.469885976	-0.598830901
Grem1	gremlin-1 precursor	755.7	273.5	279.66	68.27	-1.462915296	-2.018520885
Cyp4b1	cytochrome P450 4B1	243.35	87.84	355.9	155.16	-1.459667807	-1.192494943
Gjb6	gap junction beta-6 protein	6.68	1.8	81.6	22.37	-1.455679484	-1.821484048
9530053A07Rik	Fc fragment of IgG binding protein-like	51.01	18	55.02	28.21	-1.452789619	-0.939479625
Frmd4a	FERM domain-containing protein 4A isoform 3	50.59	17.86	38.3	38.48	-1.45176177	0.006592677
Nppa	atrial natriuretic factor	1.73	0	0	1.73	-1.448900951	1.448900951
Sox5	transcription factor SOX-5 isoform a	1.73	0	4.66	2.4	-1.448900951	-0.735267307
Nkd1	protein naked cuticle homolog 1 isoform 1	41.66	14.66	10.61	29.32	-1.445799753	1.384901781
LOC668917		1.72	0	0	0	-1.443606651	0
Stfa1	stefin-1	1.72	0	0	3.69	-1.443606651	2.229587923
Ctgf	connective tissue growth factor precursor	9132.35	3366.87	1364.35	944.78	-1.439307669	-0.529694286
Nt5e	5'-nucleotidase precursor	883.96	326.67	352.42	133.83	-1.433368655	-1.390242149
P2ry1	P2Y purinoceptor 1	143.78	52.87	101.31	55.47	-1.426308351	-0.857390628
Zfp941	hypothetical protein LOC407812	15.74	5.25	5.44	3.67	-1.421371433	-0.463638138
Msx1	homeobox protein MSX-1	37.88	13.53	4.83	6.76	-1.419993516	0.412560769
Fgfbp1	fibroblast growth factor-binding protein 1	349.74	130.09	1887.26	622.55	-1.419844336	-1.598480273
LOC100502920		1.65	0	0	0	-1.40599236	0
B4galt1	beta-1,4-galactosyltransferase 1	277.81	104.29	163	124.83	-1.404913885	-0.382219889
Nuak1	NUAK family SNF1-like kinase 1	209.7	78.58	192.67	169.71	-1.40471251	-0.182052922
Kcnh1	potassium voltage-gated channel subfamily H	55.6	20.4	7.88	8.8	-1.403191256	0.142222073
Itpka	inositol-trisphosphate 3-kinase A	7.21	2.11	5.36	3.32	-1.400467642	-0.557995453
0610010O12Rik	hypothetical protein LOC66060	22.6	7.94	12.59	12.54	-1.400440123	-0.005317717
Fxyd6	FXYD domain-containing ion transport regulator 6	375.86	141.87	151.15	113.44	-1.399325666	-0.410902931
Apoo-ps		6.33	1.78	0.82	0.56	-1.398728315	-0.222392421
Me3	NADP-dependent malic enzyme, mitochondrial	14.61	4.94	0	0.59	-1.393935701	0.669026766
Cpeb1	cytoplasmic polyadenylation element-binding	20.14	7.05	11.84	4.89	-1.392914688	-1.124305663
Sesn1	sestrin-1 isoform 2	353.77	135.16	275.65	150.94	-1.381581076	-0.864560197
Kbtbd13	kelch repeat and BTB domain-containing protein	1.6	0	0.82	0.87	-1.378511623	0.03909982
Orm1	alpha-1-acid glycoprotein 1 precursor	24.42	8.79	65.81	17.61	-1.376583265	-1.843986003
Tmem56	transmembrane protein 56	16.33	5.68	33.72	16.23	-1.375351647	-1.010844246
Cyp1b1	cytochrome P450 1B1	88.63	33.55	338.56	66.29	-1.375295986	-2.335202494
BC026439	prostaglandin-specific organic anion	32.17	11.79	8.11	2.44	-1.374862748	-1.405042489
Camkv	caM kinase-like vesicle-associated protein	1.59	0	3.84	2.29	-1.372952098	-0.556919464
Cldn22	claudin-22	1.59	0	0	0	-1.372952098	0
E030003E18Rik		1.59	0	15.87	2.49	-1.372952098	-2.273161032
Lmod3	leiomodin-3	1.59	0	0.58	0	-1.372952098	-0.659924558
Lgr6	leucine-rich repeat-containing G-protein coupled	143.02	55.05	338.88	106.7	-1.361482894	-1.65800722
Dusp23	dual specificity protein phosphatase 23	51.34	19.4	14.21	8.58	-1.359344772	-0.666922592
Tacr1	substance-P receptor	3.24	0.66	0.54	0.38	-1.352881023	-0.158262084
Clec4b1	C-type lectin domain family 4, member b1 isoform	1.55	0	0	0	-1.350497247	0
Rufy4	RUN and FYVE domain-containing protein 4 isoform	20.5	7.47	11.25	3.51	-1.343902785	-1.441582411
Cyr61	protein CYR61 precursor	15412.8	6087	3520.57	1876.12	-1.340182313	-0.907697879
Ttpa	alpha-tocopherol transfer protein	26.45	9.85	15.03	6.06	-1.339111107	-1.183034337
Rrm2	ribonucleoside-diphosphate reductase subunit M2	171.44	67.26	81.65	67.57	-1.336982148	-0.269437297
H60c	histocompatibility 60c	102.14	39.98	64.81	39.67	-1.331612061	-0.694341831
Cnih3	protein cornichon homolog 3 isoform 2	5.29	1.51	0	0	-1.325372653	0
Atp6v0d2	V-type proton ATPase subunit d 2	18.05	6.62	1.29	0.65	-1.321928095	-0.472881574
B4galnt3	N-acetyl-beta-glucosaminyl-glycoprotein	66.35	25.96	6.44	8.81	-1.320857449	0.398950515
Dpysl5	dihydropyrimidinase-related protein 5	17.46	6.39	22.31	11.57	-1.320756283	-0.890964355
Gas7	growth arrest-specific protein 7 isoform b	134.3	53.24	337.48	115.91	-1.318732756	-1.533672253
Ntrk2	BDNF/NT-3 growth factors receptor isoform b	9.81	3.34	11.43	12.76	-1.316599575	0.146654174
Odc1	ornithine decarboxylase	202.46	80.79	108.43	102.74	-1.314748821	-0.077036029
Gm12839		34.36	13.28	56.09	24.92	-1.308122295	-1.139172344
Tmem140	transmembrane protein 140	42.68	16.66	24.24	13.76	-1.306487513	-0.774019189
Calr4	calreticulin 4	1.46	0	0	0	-1.298658316	0
Nat1	arylamine N-acetyltransferase 1	1.46	0	0	0	-1.298658316	0
Kctd14	potassium channel tetramerisation domain	3.81	0.96	3.08	2.39	-1.29518324	-0.267283879
Ctnnal1	alpha-catulin	292.08	118.6	187.91	114.39	-1.293077131	-0.711180872
Hist1h2bb	histone H2B type 1-B	1.45	0	0.86	2.04	-1.292781749	0.708768702
Tpbg	trophoblast glycoprotein precursor	99.47	40.01	91.97	64.43	-1.292717133	-0.506812985
D18Ertd653e	hypothetical protein LOC52662	29.91	11.63	15.73	26.47	-1.291219015	0.715419465
Zfp72	zinc finger protein 72	9.52	3.31	3.9	3.18	-1.28737493	-0.229278807
Wdr93	WD repeat-containing protein 93	1.44	0	2.15	1.53	-1.286881148	-0.316214444
Arhgap26	rho GTPase-activating protein 26	12.79	4.66	1.91	2.73	-1.284748499	0.358156477
Ccdc125	coiled-coil domain-containing protein 125	5.94	1.85	5.14	4.11	-1.283973744	-0.264915364
Il22ra1	interleukin-22 receptor subunit alpha-1	48.59	19.4	38.36	26.28	-1.281480073	-0.528886576
Fras1	extracellular matrix protein FRAS1 precursor	3.35	0.8	19.63	23.54	-1.273018494	0.250391428
Upb1	beta-ureidopropionase	254.13	104.7	90.79	39.22	-1.271257175	-1.190423907
D630023F18Rik	hypothetical protein LOC98303	1.41	0	1.48	1.63	-1.269033146	0.084722679
Hmgcll1	probable 3-hydroxymethyl-3-methylglutaryl-CoA	2.9	0.62	3.15	0.77	-1.267480311	-1.229361976
C130079G13Rik	hypothetical protein LOC229333	17.17	6.57	12.13	6.86	-1.263193214	-0.740265699
Eps8	epidermal growth factor receptor kinase	88.99	36.57	59.26	51.45	-1.260183577	-0.2002579
Igfn1	immunoglobulin-like and fibronectin type III	3.15	0.74	0.36	0	-1.25402403	-0.443606651
Prss23	serine protease 23 precursor	778.23	326.1	88.42	100.49	-1.252317462	0.182668132
Ccdc13	coiled-coil domain containing 13	1.38	0	0.36	0	-1.250961574	-0.443606651
Crisp2	cysteine-rich secretory protein 2 precursor	1.38	0	0	0	-1.250961574	0
Plekhf1	pleckstrin homology domain-containing family F	38.08	15.49	24.04	9.2	-1.244839069	-1.29566541
Plekha2	pleckstrin homology domain-containing family A	47.19	19.34	52.09	37.63	-1.244414122	-0.458718464
Grtp1	growth hormone-regulated TBC protein 1	15.76	6.08	5.55	3.73	-1.243200884	-0.469654723
Nqo1	NAD(P)H dehydrogenase [quinone] 1	160.47	67.33	175.65	78.71	-1.240675115	-1.148061116
Arhgef16	rho guanine nucleotide exchange factor 16	65.84	27.3	68.95	37.38	-1.23990968	-0.865969346
Cacnb2	voltage-dependent L-type calcium channel subunit	6.65	2.24	1.52	0.81	-1.239465935	-0.477434036
Kcnb2	potassium voltage-gated channel subfamily B	3.22	0.79	0.83	0.66	-1.237283411	-0.140660407
Bmp6	bone morphogenetic protein 6 precursor	11.94	4.49	28.74	12.12	-1.236959563	-1.180636927
Ppil6	peptidyl-prolyl cis-trans isomerase-like 6	31.39	12.76	27.22	12.1	-1.235067998	-1.107151176
Cebpd	CCAAT/enhancer-binding protein delta	1129.44	479.25	356.52	357.58	-1.235026902	0.004271073
N4bp2l1	NEDD4-binding protein 2-like 1	97.86	41.04	39.63	36.06	-1.233624237	-0.132682483
Nkain1	sodium/potassium-transporting ATPase subunit	15.27	5.92	6.38	10.19	-1.233370308	0.600517315
Fam83d	hypothetical protein LOC71878	258.09	109.45	151.12	52.25	-1.230059915	-1.514356414
Cmtm8	CKLF-like MARVEL transmembrane domain-containing	58.54	24.4	44.96	35.1	-1.229030725	-0.348379961

Cdc42ep2	cdc42 effector protein 2	47.58	19.76	7.89	4	-1.226556046	-0.830255324
3110070M22Rik		1.34	0	0.69	1.51	-1.22650853	0.570664118
Zfp949	hypothetical protein LOC71640	49.88	20.8	27.33	16.1	-1.222770536	-0.728334277
Ephx2	epoxide hydrolase 2	139.9	59.4	101.87	95.15	-1.222051157	-0.097463547
Krt222	keratin-like protein KRT222	11.76	4.47	0.51	0.64	-1.222015591	0.119147265
Sh3rf2	putative E3 ubiquitin-protein ligase SH3RF2	101.21	42.94	61.87	39.36	-1.217929578	-0.639445589
Rem2	GTP-binding protein REM 2	8.63	3.14	6.99	6.49	-1.21790503	-0.093229784
6430527G18Rik	interferon regulatory factor 2-binding	93.85	39.8	113.36	101.77	-1.217078621	-0.154163342
Car7	carbonic anhydrase 7	1.32	0	0	0	-1.214124805	0
Gm4832	40S ribosomal protein S24-like	1.32	0	1.02	1.43	-1.214124805	0.266601021
Ugt1a6b	UDP glucuronosyltransferase 1 family,	15.72	6.21	12.58	12.2	-1.213503683	-0.04094555
Sardh	sarcosine dehydrogenase, mitochondrial	179.47	76.97	37.55	28.12	-1.210767994	-0.404720505
Thg1l	probable tRNA(His) guanylyltransferase	43.32	18.19	33.74	26.44	-1.20760317	-0.340317273
Fkbp11	peptidyl-prolyl cis-trans isomerase FKBP11	17.59	7.05	50.55	34.99	-1.207466082	-0.518376325
Nrg2	pro-neuregulin-2, membrane-bound isoform	5.88	1.98	0.92	2.55	-1.207096234	0.886712714
Krt14	keratin, type I cytoskeletal 14	7330.89	3177.41	10731.8	8723.41	-1.205879904	-0.298897024
Dock8	dedicator of cytokinesis protein 8	17.19	6.9	22.58	14.62	-1.203220985	-0.594169265
Ntn4	netrin-4 precursor	48.09	20.33	37.35	48.42	-1.202545201	0.365868433
1700048O20Rik		1.3	0	2.49	1.66	-1.201633861	-0.391800791
Fam180a	hypothetical protein LOC208164 precursor	183.5	79.36	59.25	31.55	-1.199071347	-0.888303698
Ak1	adenylate kinase isoenzyme 1 isoform 2	161.62	69.87	15.9	25.09	-1.198257746	0.626473698
Ttyh2	protein tweety homolog 2	20.09	8.24	21.92	13.53	-1.190594338	-0.657572341
Lsm11	U7 snRNA-associated Sm-like protein LSm11	21.55	8.88	14.44	9.79	-1.190544487	-0.516977888
Ism1	isthmin-1 precursor	388.33	169.61	65.64	63.16	-1.190291306	-0.054714259
Mfsd9	major facilitator superfamily domain-containing	103.11	44.63	38.03	24.27	-1.190054091	-0.627157798
Adamtsl4	ADAMTS-like protein 4 precursor	404.65	176.82	65.17	31.3	-1.18981789	-1.034643115
Dll1	delta-like protein 1 precursor	33.58	14.16	69.97	47.48	-1.189668115	-0.549819608
Gm826	hypothetical protein LOC329554	1.28	0	2.12	2.23	-1.189033824	0.049988136
Rnase6	ribonuclease K6 precursor	1.28	0	0	0	-1.189033824	0
Zfp551	zinc finger protein 551	13.75	5.51	7.38	5.36	-1.179985506	-0.397923478
Il1rl2	interleukin-1 receptor-like 2 precursor	64.04	27.74	121.65	91.39	-1.178267196	-0.408738621
2410066E13Rik	hypothetical protein LOC68235	114.53	50.06	18.67	26.93	-1.178002086	0.505818616
Nup210	nuclear pore membrane glycoprotein 210	3.25	0.88	29.82	21.97	-1.176730179	-0.424116005
Usp50	putative ubiquitin carboxyl-terminal hydrolase	1.26	0	12.11	3.01	-1.176322773	-1.708993544
Vldlr	very low-density lipoprotein receptor isoform b	12.16	4.83	6.65	6.62	-1.174591701	-0.00566875
Aknad1	AKNA domain containing 1	11.02	4.33	8.87	5.88	-1.173229458	-0.52064152
Prkcq	protein kinase C theta type	13.92	5.62	8.21	3.74	-1.172344413	-0.958314097
Zfp389		1.25	0	0	0	-1.169925001	0
Zkscan14	zinc finger protein 394	31.72	13.56	17.73	13.38	-1.168162393	-0.381287224
Eda	ectodysplasin-A isoform 1	81.01	35.56	22.83	23.77	-1.165533767	0.055814917
AI848285	expressed sequence AI848285	1.24	0	0	0	-1.163498732	0
Igfbp5	insulin-like growth factor-binding protein 5	218.68	97.24	18.19	23.52	-1.161021065	0.353604267
Etaa1	ewing's tumor-associated antigen 1 homolog	52.11	22.8	26.11	16.35	-1.158021956	-0.64388945
Plcd4	1-phosphatidylinositol-4,5-bisphosphate	5.58	1.95	1.16	6.55	-1.157372629	1.805445332
Pfn4	profilin-4	1.23	0	0	0	-1.15704371	0
Dpy19l1	protein dpy-19 homolog 1	117.58	52.24	30.55	28.73	-1.155278225	-0.085720542
St6galnac6	alpha-N-acetylgalactosaminide	27.43	11.78	4.27	7.16	-1.153526263	0.63076619
Thbs2	thrombospondin-2 precursor	106.87	47.57	129.05	170.8	-1.151156298	0.401663637
Gca	grancalcin	1.22	0	1.19	0.98	-1.150559677	-0.14543044
Atp8a2	probable phospholipid-transporting ATPase IB	42.16	18.46	8.66	9.02	-1.149183155	0.052787414
Mab21l3	protein mab-21-like 3	21.68	9.25	20.22	13.63	-1.145796731	-0.536494887
Hivep3	transcription factor HIVEP3	22.95	9.83	15.74	8.84	-1.144992413	-0.766569307
Nup62-il4i1	Nup62-Il4i1 protein	9.39	3.7	3.57	6.51	-1.144462992	0.716618742
Zfp960	zinc finger protein 960 isoform 2	33.5	14.61	26.97	14.55	-1.144125825	-0.846965673
Pla1a	phospholipase A1 member A precursor	1.21	0	0	1	-1.14404637	1
Ncald	neurocalcin-delta	99	44.3	19.05	15.21	-1.142417045	-0.306718146
Odz4	teneurin-4	49.31	21.8	29.22	26.14	-1.141811365	-0.15508294
Zfp97	zinc finger protein 97	31.74	13.84	24.67	14.11	-1.14156323	-0.764579635
Zfp874b	regulator of sex-limitation candidate 16	45.12	19.91	25.52	17.24	-1.141199451	-0.539975046
Ear5	eosinophil cationic-type ribonuclease 5	33.11	14.47	24.25	11.08	-1.140721558	-1.063662933
Spock1	testican-1 isoform 4 precursor	2.02	0.37	0.47	0	-1.140372656	-0.555816155
Rasgef1b	ras-GEF domain-containing family member 1B	175.18	78.95	191.61	281.59	-1.13988022	0.553027806
Hamp2	hepcidin-2	8.44	3.29	5.19	0	-1.137809212	-2.629939409
Krt31	keratin, type I cuticular Ha1	1.2	0	1.43	3.34	-1.137503524	0.836738729
Ms4a10	membrane-spanning 4-domains subfamily A member	5.09	1.77	1.21	3.83	-1.136556252	1.127976819
Slc26a7	anion exchange transporter	9.55	3.8	13.01	3.8	-1.136136688	-1.545350645
9430020K01Rik	hypothetical protein LOC240185	27.39	11.95	31.44	12.26	-1.132430751	-1.290693044
Shisa2	protein shisa-2 homolog precursor	1288.8	587.94	285.99	227.6	-1.130954807	-0.328175064
Atp4a	potassium-transporting ATPase alpha chain 1	1.19	0	0.84	0.66	-1.13093087	-0.148522525
Ang	angiogenin precursor	153.81	69.69	145.85	55.53	-1.130920619	-1.377254664
Ttll7	tubulin polyglutamylase TTLL7	54.88	24.52	10.55	15.56	-1.130703692	0.519809821
Thbs1	thrombospondin-1	2119.56	968.95	2444.86	3348.76	-1.128463019	0.453715908
9930005F22Rik	hypothetical protein LOC100045778	9.34	3.73	4.3	4.76	-1.128324097	0.120076452
Pcolce2	procollagen C-endopeptidase enhancer 2	57.87	25.96	7.04	9.93	-1.126712131	0.443025994
BC096441	tumor necrosis factor (ligand) superfamily,	2.36	0.54	0.09	0.03	-1.125530882	-0.081683798
Mamstr	MEF2-activating motif and SAP domain-containing	16.3	6.95	2.34	2.78	-1.121745272	0.178538132
Arvcf	armadillo repeat protein deleted in	226.25	103.44	66.87	53.05	-1.121605932	-0.328479395
Mlkl	mixed lineage kinase domain-like protein	4.46	1.51	12.75	4.49	-1.121213587	-1.324553564
Phyhipl	phytanoyl-CoA hydroxylase-interacting	46.11	20.66	2.73	6.03	-1.121000089	0.914349059
4732416N19Rik		41.54	18.58	4.36	4.75	-1.119439268	0.101328955
Crym	mu-crystallin homolog	1.17	0	1.16	0	-1.117695043	-1.111031312
Igsf9b	immunoglobulin superfamily, member 9B isoform 1	1.17	0	0.59	0.56	-1.117695043	-0.027480736
Tgm5	protein-glutamine gamma-glutamyltransferase 5	3055.35	1409.32	323.43	247.11	-1.115787218	-0.386927348
Etv4	ETS translocation variant 4	43.24	19.42	79.76	60.21	-1.115368519	-0.399873543
Hist1h4i	histone H4	20.66	9	23.01	13.44	-1.115033243	-0.733564661
Thnsl2	threonine synthase-like 2	33.05	14.73	29.94	19.61	-1.114136127	-0.586128692
Fbxo16	F-box only protein 16	22.14	9.7	6.12	4.22	-1.112778068	-0.447827434
Krt74		1.16	0	0.6	0	-1.111031312	-0.678071905
Rasgrf1	ras-specific guanine nucleotide-releasing factor	2.67	0.7	31.23	7.6	-1.110245317	-1.905995623
Vamp4	vesicle-associated membrane protein 4	152.24	70.05	52.56	46.07	-1.108886376	-0.186348108
Nrtn	neurturin precursor	418.97	193.83	228.4	117.92	-1.108070433	-0.947874023
Zfp874a	zinc finger protein 874	39	17.59	22.44	14.88	-1.10547323	-0.561761657

Mir686		324.29	150.26	333.38	192.48	-1.104695948	-0.789304116
Tslp		4.03	1.34	4.48	0	-1.10404987	-2.454175893
Ugt1a7c	UDP-glucuronosyltransferase 1-7C precursor	2.37	0.57	6.18	8.62	-1.101984032	0.42205305
Zfp119b	zinc finger protein 119b	16.55	7.18	16.14	5.9	-1.101298282	-1.312698842
Fam134b	family with sequence similarity 134, member B	277.11	128.73	378.28	244.97	-1.10014348	-0.624780932
Lix1	protein limb expression 1 homolog	2.75	0.75	1.28	1.09	-1.099535674	-0.125530882
Tle2	transducin-like enhancer protein 2	55.53	25.39	34.24	25.18	-1.099025346	-0.428748827
Vgll4	transcription cofactor vestigial-like protein 4	399.8	186.21	269.49	338.15	-1.098225009	0.326348234
Bmf	bcl-2-modifying factor	20.94	9.27	18.36	13.03	-1.095127344	-0.464563944
Gm10416		10.68	4.48	5.37	4.56	-1.091792476	-0.19620849
Dact2	dapper homolog 2	11.52	4.88	10.95	3.66	-1.090346502	-1.358608758
9930021D14Rik	hypothetical protein LOC319259	3.47	1.1	3.8	4.65	-1.089885504	0.235216462
Cspg5	chondroitin sulfate proteoglycan 5 isoform b	3.51	1.12	1.33	0.59	-1.089063169	-0.551303189
Adck3	chaperone activity of bc1 complex-like,	168.56	78.78	73.38	52.82	-1.087696843	-0.466772357
Cdc42ep3	cdc42 effector protein 3	313.49	147.07	403.64	214.93	-1.086734773	-0.906075246
Tcea3	transcription elongation factor A protein 3	47.94	22.06	13.26	12.47	-1.085621588	-0.082224131
Cyp2r1	vitamin D 25-hydroxylase	3.41	1.08	6.57	4.68	-1.084195127	-0.41440237
Csgalnact1	chondroitin sulfate	24.81	11.18	41.96	69.44	-1.083416008	0.713400916
Dsc1	desmocollin-1	23.54	10.59	172.07	97.69	-1.082254683	-0.810379857
Kcns3	potassium voltage-gated channel subfamily S	3.36	1.06	8.07	4.03	-1.081683798	-0.850544151
Dpyd	dihydropyrimidine dehydrogenase [NADP+]	72.27	33.69	33.1	10.59	-1.078702775	-1.556891173
Slc6a2	sodium-dependent noradrenaline transporter	8.23	3.37	6.41	5.1	-1.078697368	-0.2806643
Gabre	gamma-aminobutyric acid (GABA-A) receptor,	3.77	1.26	1.66	1.04	-1.077666494	-0.382857094
4831426I19Rik	nesprin-3 isoform alpha	49.23	22.8	29.34	18.18	-1.077587701	-0.661618365
Pla2g16	group XVI phospholipase A2	21.6	9.71	26.47	12.96	-1.077364293	-0.976557969
Fbxo32	F-box only protein 32	50.79	23.55	88.83	44.96	-1.076950534	-0.966818536
Ldb2	LIM domain-binding protein 2 isoform 2	9.31	3.9	1.91	0.9	-1.073190678	-0.615019735
Acsbg1	long-chain-fatty-acid--CoA ligase ACSBG1	110.83	52.15	811.33	326.07	-1.073165667	-1.312466489
Abhd12b	abhydrolase domain-containing protein 12B	84.26	39.57	53.01	34.35	-1.071455753	-0.611516333
Colec11	collectin-11 precursor	1.1	0	0	0	-1.070389328	0
Krt84	keratin, type II cuticular Hb4	1.1	0	1.91	1.84	-1.070389328	-0.035128223
Phyhip	phytanoyl-CoA hydroxylase-interacting protein	606.27	288.24	398.78	198.9	-1.070071018	-0.999927827
Spns3	protein spinster homolog 3	4.03	1.4	0.84	0	-1.067523994	-0.879705766
Bnc1	zinc finger protein basonuclin-1	184.55	87.8	59.84	116.85	-1.063176419	0.9538597
Crip2	cysteine-rich protein 2	1114.88	533.19	986.76	514.04	-1.062757016	-0.939476065
Il17b	interleukin-17B precursor	7.02	2.84	3.74	0	-1.062495926	-2.244887059
Slc6a9	sodium- and chloride-dependent glycine	77.91	36.84	46.89	44.65	-1.060296051	-0.069109575
Atp2a3	sarcoplasmic/endoplasmic reticulum calcium	40.66	18.99	3.01	2.77	-1.059384367	-0.089037713
Dcun1d3	DCN1-like protein 3	79.43	37.6	89.31	52.52	-1.059132873	-0.75480763
Isg20	interferon-stimulated gene 20 kDa protein	24.59	11.29	9.85	12.05	-1.058095232	0.266354764
Zfp429	zinc finger protein 429	11.78	5.15	7.75	5.93	-1.055229521	-0.336427665
Tigd2	tigger transposable element-derived protein 2	77.9	37	37.19	36.37	-1.054025882	-0.031314356
Gt(ROSA)26Sor		34.86	16.29	37.2	14.42	-1.052437619	-1.308769873
2010109K11Rik	hypothetical protein LOC72123	64.8	30.73	13.49	17.52	-1.052240063	0.354026504
Celf5	CUG-BP- and ETR-3-like factor 5	2.71	0.79	0.62	0.33	-1.051459599	-0.284567567
Emb	embigin precursor	862.83	416.5	580.06	344.94	-1.048971223	-0.748165306
Myom3	myomesin-3	11.31	4.95	10.74	7.45	-1.048869188	-0.474409162
Phospho1	phosphoethanolamine/phosphocholine phosphatase	427.15	206.31	180.9	151.93	-1.046326616	-0.250274098
Rhpn2	rhophilin-2	18.31	8.35	7.52	4.69	-1.046309894	-0.582424778
Krt16	keratin, type I cytoskeletal 16	557.88	269.65	889.83	740.23	-1.04611016	-0.265228871
Xk	membrane transport protein XK	2.57	0.73	1.21	0.96	-1.045152036	-0.173192715
Gm6981		5	1.91	1.18	0.87	-1.043943348	-0.221289865
Mycn	N-myc proto-oncogene protein	10.38	4.52	12.56	22.43	-1.043760386	0.788999776
Ascl2	achaete-scute homolog 2	5.74	2.27	1.75	3.66	-1.043457956	0.760898336
Pnp	purine nucleoside phosphorylase	240.56	116.23	125.04	87.33	-1.043039765	-0.512906243
Fam131c	hypothetical protein LOC277743	1.06	0	2.06	1.57	-1.042644337	-0.251763293
Gadl1	glutamate decarboxylase-like protein 1	1.06	0	1.02	0	-1.042644337	-1.014355293
Nudt17	nucleoside diphosphate-linked moiety X motif 17	28.32	13.24	67.92	54.18	-1.041935957	-0.320777245
Zfp947	zinc finger protein 947	5.54	2.18	3.2	2.37	-1.04026387	-0.317640736
Ppap2b	lipid phosphate phosphohydrolase 3	289.49	140.4	169.62	123.14	-1.03870638	-0.458818718
Gpha2	glycoprotein hormone alpha-2 precursor	69.74	33.47	142.91	134.55	-1.03718492	-0.086341732
Adamts9	a disintegrin-like and metalloprotease	8.11	3.44	46.99	51.19	-1.036891377	0.121039589
Trpv4	transient receptor potential cation channel	359.81	175.04	22.32	38.54	-1.035336047	0.761745083
4931403G20Rik		9.1	3.93	2.72	6.28	-1.034695741	0.968635829
Kctd21	BTB/POZ domain-containing protein KCTD21	23.91	11.16	10.79	7.9	-1.034581793	-0.405686477
Acot1	acyl-coenzyme A thioesterase 1	338.27	164.68	253.44	173.72	-1.034034406	-0.54228073
Gm13178	hypothetical protein LOC546849	11.55	5.13	30.06	22.21	-1.033728385	-0.420311307
Fut10	alpha-(1,3)-fucosyltransferase 10	23.81	11.12	15.43	9.87	-1.033532036	-0.59598054
Gatsl3	GATS-like protein 3	292.98	142.78	68.58	90.84	-1.031855	0.400449963
Hmgcs2	hydroxymethylglutaryl-CoA synthase,	320.76	156.46	378.61	1104.9	-1.030999603	1.542631034
1700061I17Rik		2.33	0.63	3.69	1.36	-1.030650213	-0.990801063
Pycr1	pyrroline-5-carboxylate reductase 1,	4.41	1.65	2.04	3.04	-1.029636234	0.410283969
2010107G12Rik	hypothetical protein LOC243753	1.04	0	0	0	-1.028569152	0
Pla2g3	phospholipase A2, group III	8.87	3.84	4.09	2.7	-1.028043037	-0.460140386
2410004N09Rik		139.65	68.08	146.65	121.47	-1.025769565	-0.269752964
Scnn1g	amiloride-sensitive sodium channel subunit	40.79	19.56	25.78	19.81	-1.023317494	-0.363878996
Zfp748	zinc finger protein 748 isoform 1	39.35	18.86	20.97	20.41	-1.022703051	-0.037250074
Rnase10	ribonuclease-like protein 10 isoform 2	1.03	0	1.83	1.47	-1.021479727	-0.196291011
Il7	interleukin-7 precursor	4.55	1.74	48.1	9.75	-1.018311878	-2.191386365
Rab17	ras-related protein Rab-17	61.59	29.93	6.72	8.97	-1.016925343	0.368992657
Matn2	matrilin-2	207.42	102.01	76.67	42.83	-1.016709327	-0.825438787
Paqr8	membrane progestin receptor beta	9.9	4.39	3.64	3.39	-1.015970957	-0.079903866
Ugt1a6a	UDP-glucuronosyltransferase 1-6 precursor	11.58	5.23	8.99	8.68	-1.013827854	-0.045477631
Zfp456	zinc finger protein 456	4.81	1.88	2.72	1.65	-1.012469352	-0.489310262
Noxo1	NADPH oxidase organizer 1	29.94	14.34	7.59	8.65	-1.012174714	0.167870811
Lmo1	rhombotin-1	660.08	326.84	272.55	241.5	-1.011832979	-0.173819808
Selenbp1	selenium-binding protein 1	41.93	20.29	31.79	20.02	-1.011810223	-0.641493232
Ppp1r3d	protein phosphatase 1 regulatory subunit 3D	4.86	1.91	2.39	2.61	-1.009881512	0.090713564
Fam101a	hypothetical protein LOC73121	11.48	5.2	12.03	16.21	-1.009277814	0.401410013
BC021891	mitogen-activated protein kinase kinase kinase kinase	3.14	1.06	6.73	0.69	-1.00698643	-2.193445168
Gpsm1	G-protein-signaling modulator 1 isoform 2	20.31	9.61	16.78	20.13	-1.006105937	0.249037443
Adamts17	ADAM metallopeptidase with thrombospondin type 1	14.68	6.81	28.84	32.98	-1.005531106	0.187438317

Trim12a	tripartite motif-containing protein 12	27.43	13.19	23.5	12.79	-1.00253951	-0.829159292
Tmeff2	tomoregulin-2 precursor	2.22	0.61	0.46	0	-1	-0.545968369
1110020A21Rik		10.94	4.97	4.06	5.61	-1	0.385512887
Gm5779		2.3	0.65	1.37	1.37	-1	0
Olfr856-ps1		1	0	0	0	-1	0

HG Down

GENE	Description	WT Bulge	KO Bulge	WT HG	KO HG	Log2 KO Bulge/WT Bulge	Log2 KO HG/WT HG
Skint3	selection and upkeep of intraepithelial T-cells	8.72	0	214.86	0	-3.280956314	-7.753952119
Skint4	selection and upkeep of intraepithelial T-cells	86.55	0.44	142.39	0	-5.925966462	-7.163800604
Mir3074-1		80.19	93.07	51.02	0	0.21243266	-5.700994494
Skint9	selection and upkeep of intraepithelial T-cells	12.04	0	46.94	0	-3.704871964	-5.583158004
Mir1306		36.97	0	45.16	0	-5.246788094	-5.528571319
Pcp2	Purkinje cell protein 2 isoform 2	0	0	30.94	0	0	-4.997292408
Ear12	eosinophil-associated, ribonuclease A family,	0	0	28.86	0	0	-4.90014226
Mir671		27.61	0	25.04	0	-4.838447593	-4.702657543
Snora24		0	12.48	16.41	0	3.752748591	-4.121844298
Krt13	keratin, type I cytoskeletal 13	89.24	1.22	30.2	0.85	-5.345135486	-4.075948853
Snora75		0	39.71	15.14	0	5.347311316	-4.012568674
Ear10	eosinophil-associated, ribonuclease A family,	0	0	11.46	0	0	-3.639232163
Sval2	seminal vesicle antigen-like 2	21.01	0	11.13	0	-4.46008724	-3.600507645
Rptn	repetin	0.35	0	32.42	1.87	-0.432959407	-3.541589091
Btg3	protein BTG3	0.12	0.11	11.11	0.04	-0.012939056	-3.541543432
Amd1	S-adenosylmethionine decarboxylase proenzyme 1	0.85	1.22	29.16	1.76	0.263034406	-3.449896256
Gjc1	gap junction gamma-1 protein	2.04	1.97	9.05	0	-0.033608393	-3.329123596
Myoc	myocilin precursor	586.87	35.65	33.32	3.58	-4.003612053	-2.905630049
Grp	gastrin-releasing peptide precursor	0	0	28.57	3.03	0	-2.8752825
Ear2	eosinophil cationic protein 2 precursor	0	1.73	27.83	3.09	1.448900951	-2.817398089
Hmga1-rs1	high mobility group protein HMG-I/HMG-Y isoform	10.83	15.36	20.64	2.12	0.467722675	-2.794082565
Syn1	synapsin-1 isoform b	0	0	5.93	0	0	-2.792855352
H60b	histocompatibility 60b	2.06	0	5.75	0	-1.613531653	-2.754887502
Lgals2	galectin-2	2.63	2.28	5.22	0	-0.146273733	-2.63691458
Hamp2	hepcidin-2	8.44	3.29	5.19	0	-1.137809212	-2.629939409
BC090627		13.39	12.47	5.06	0	-0.095316741	-2.599317794
Klk10	kallikrein-10	6.89	10.69	201.36	32.42	0.567177725	-2.598140506
Skint11	selection and upkeep of intraepithelial T-cells	5.29	1.12	4.84	0	-1.568995752	-2.545968369
Col8a1	collagen alpha-1(VIII) chain precursor	6.4	4.1	32.21	5.02	-0.537028024	-2.463782331
Tslp		4.03	1.34	4.48	0	-1.10404987	-2.454175893
Gngt2	guanine nucleotide-binding protein	2.28	7.64	4.32	0	1.397335498	-2.411426246
Cd72	B-cell differentiation antigen CD72 isoform 4	16.28	34.26	22.16	3.44	1.028929257	-2.383003672
Il18r1	interleukin-18 receptor 1 isoform a	2.5	2.34	43.43	7.67	-0.067506819	-2.357430243
Cyp1b1	cytochrome P450 1B1	88.63	33.55	338.56	66.29	-1.375295986	-2.335202494
1700028B04Rik		0	0	3.94	0	0	-2.304511042
Acox2	peroxisomal acyl-coenzyme A oxidase 2	0.94	1.88	17.85	2.84	0.570012159	-2.295386307
Riiad1	RIIa domain-containing protein 1	3.01	4.58	3.9	0	0.476662885	-2.292781749
Dmrta1	doublesex- and mab-3-related transcription	0	0	3.88	0	0	-2.286881148
Galnt6	polypeptide N-acetylgalactosaminyltransferase 6	0.9	0.79	22.52	3.85	-0.086039831	-2.277831408
E030003E18Rik		1.59	0	15.87	2.49	-1.372952098	-2.273161032
Col6a6	collagen alpha-6(VI) chain isoform 1	0	0.16	3.77	0	0.214124805	-2.253989266
Il17b	interleukin-17B precursor	7.02	2.84	3.74	0	-1.062495926	-2.244887059
Ifitm5	interferon-induced transmembrane protein 5	0	4.02	3.71	0	2.327687364	-2.23572706
Crb2	crumbs homolog 2 precursor	0.36	0	3.66	0	-0.443606651	-2.220329955
Col9a2	collagen alpha-2(IX) chain precursor	0.35	0	3.65	0	-0.432959407	-2.217230716
BC021891	mitogen-activated protein kinase kinase kinase	3.14	1.06	6.73	0.69	-1.00698643	-2.193445168
Il7	interleukin-7 precursor	4.55	1.74	48.1	9.75	-1.018311878	-2.191386365
Npbwr1	neuropeptides B/W receptor type 1	0.8	0	3.56	0	-0.847996907	-2.189033824
Mrgprb3	mas-related G-protein coupled receptor member	5.01	2.78	3.54	0	-0.668978756	-2.182692298
Tmem190	transmembrane protein 190 precursor	0	0	3.42	0	0	-2.14404637
1700016C15Rik	hypothetical protein LOC69428	0	0	3.38	0	0	-2.13093087
Gm14005		0	3.25	3.2	0	2.087462841	-2.070389328
Acoxl	acyl-coenzyme A oxidase-like protein	1.95	1.96	30.95	6.75	0.004882221	-2.043547716
Slc22a3	solute carrier family 22 member 3	51.5	36.19	38.12	8.55	-0.497402675	-2.034333732
Il3ra	interleukin-3 receptor subunit alpha precursor	19.46	2.24	14.9	2.89	-2.658740427	-2.031184705
4930415O20Rik	hypothetical protein LOC73863	2.21	3.44	3.08	0	0.467986379	-2.028569152
Grem1	gremlin-1 precursor	755.7	273.5	279.66	68.27	-1.462915296	-2.018520885
Dgkh	diacylglycerol kinase eta	1.03	0.64	10.77	1.93	-0.307783913	-2.006141751
Tox2	TOX high mobility group box family member 2	0	0	2.99	0	0	-1.996388746
Fut4-ps1		2.55	0	2.94	0	-1.827819025	-1.97819563
Gjd3	gap junction delta-3 protein	2.03	0	2.91	0	-1.599317794	-1.967168608
Fads6	fatty acid desaturase 6	5.97	1.17	2.87	0	-1.683463613	-1.952333566
Cyb5r2	NADH-cytochrome b5 reductase 2 isoform 1	0.6	0.56	7.54	1.22	-0.036525876	-1.943676393
Eda2r	tumor necrosis factor receptor superfamily	2.51	0	22.69	5.16	-1.811471031	-1.943275943
Gsdma2	gasdermin-A2	0.65	0.67	18.25	4.04	0.017382078	-1.933362807
Tnfrsf14	tumor necrosis factor receptor superfamily	0	0	2.81	0	0	-1.929790998
Il33	interleukin-33 precursor	18.82	11.39	157.04	40.5	-0.677780775	-1.92910651
Krtap3-2	keratin-associated protein 3-2	2.26	0	2.8	0	-1.704871964	-1.925999419
Serpina4-ps1		0	0	2.77	0	0	-1.914564523
Dbil5	diazepam-binding inhibitor-like 5	2.77	3.55	2.76	0	0.271302022	-1.910732662
C1qtnf1	complement C1q tumor necrosis factor-related	71.09	43.87	63.91	16.27	-0.684047965	-1.910172673
Rasgrf1	ras-specific guanine nucleotide-releasing factor	2.67	0.7	31.23	7.6	-1.110245317	-1.905995623
Slain1	SLAIN motif-containing protein 1	0.63	0.66	9.31	1.78	0.026311277	-1.890887545
1700030C10Rik		5.32	1.22	8.3	1.58	-1.509364882	-1.849859651
Orm1	alpha-1-acid glycoprotein 1 precursor	24.42	8.79	65.81	17.61	-1.376583265	-1.843986003
Chac1	cation transport regulator-like protein 1	8.84	2.2	2.59	0	-1.62058641	-1.843983844
Ptprcap	protein tyrosine phosphatase receptor type	1.37	5.26	2.59	0	1.401275598	-1.843983844
Cdo1	cysteine dioxygenase type 1	1.31	2.35	14.06	3.2	0.536268244	-1.842260537
Pyy	peptide YY precursor	0	0	2.58	0	0	-1.839959587
Rwdd2a	RWD domain-containing protein 2A	4.7	2.78	2.58	0	-0.592575685	-1.839959587
Arhgap40	rho GTPase-activating protein 18-like	1.25	1.75	22.11	5.5	0.289506617	-1.830005637
Gjb6	gap junction beta-6 protein	6.68	1.8	81.6	22.37	-1.455679484	-1.821484048
Stmn1-rs1		1.9	1.93	2.53	0	0.014847764	-1.819668183
Dab1	disabled homolog 1 isoform 2	1.55	0.82	8.27	1.64	-0.486558797	-1.812031409
Cyp2b10	cytochrome P450 2B10 isoform 2	36.86	20.49	273.47	77.19	-0.817008928	-1.811592456
Adora2a	adenosine receptor A2a	31.78	4.36	9.39	1.96	-2.612510949	-1.811526573
Pla2g2a	phospholipase A2, membrane associated precursor	0	0	2.5	0	0	-1.807354922

Adamts7	A disintegrin and metalloproteinase with	6.46	5.29	27.34	7.26	-0.246115613	-1.778626071
Klk12	kallikrein-12	0	0	2.43	0	0	-1.778208576
Ccrl1	C-C chemokine receptor type 11	857.26	109.4	518.48	150.46	-2.95867459	-1.778131373
Gdf5	growth/differentiation factor 5 precursor	1.88	0	6.24	1.12	-1.526068812	-1.771925433
Hist3h2bb-ps	histone H2B type 3-B	0	0	2.41	0	0	-1.769771739
Timp1	metalloproteinase inhibitor 1	1.99	2.86	2.4	0	0.368455363	-1.765534746
Npy	pro-neuropeptide Y precursor	0	0	2.39	0	0	-1.761285273
Pkib	cAMP-dependent protein kinase inhibitor beta	4.03	3.14	54.34	15.36	-0.280927632	-1.758149896
Krt27	keratin, type I cytoskeletal 27	123.6	2.32	42.75	11.95	-5.229977017	-1.756330919
Guca1a	guanylyl cyclase-activating protein 1	5.76	5.01	2.35	0	-0.169658256	-1.744161096
Gm2506	chemokine (C-C motif) ligand 27b isoform 3	4.37	3.73	8.12	1.75	-0.183081905	-1.729602206
Dpysl4	dihydropyrimidinase-related protein 4	6.77	0	2.29	0	-2.957914599	-1.718087584
Usp50	putative ubiquitin carboxyl-terminal hydrolase	1.26	0	12.11	3.01	-1.176322773	-1.708993544
Bcl2l15	bcl-2-like protein 15 isoform 2	2.93	2.48	36.1	10.35	-0.175442006	-1.708726889
Slc24a3	sodium/potassium/calcium exchanger 3	6.59	5.37	19.56	5.31	-0.252806513	-1.704128354
Bglap-rs1	osteocalcin-related protein precursor	0	0	2.25	0	0	-1.700439718
Rgn	regucalcin	0	0	2.24	0	0	-1.695993813
4930538K18Rik	hypothetical protein LOC75180	5.87	3.23	13.36	3.45	-0.699652436	-1.690178508
Bik	bcl-2-interacting killer	1.3	2.5	2.2	0	0.605721061	-1.678071905
Slc7a2	low affinity cationic amino acid transporter 2	16.59	3.66	172.68	53.29	-1.916353623	-1.677673242
Cited4	cbp/p300-interacting transactivator 4	8.08	7.77	27.75	8.04	-0.050115455	-1.669167278
Dcdc2b	doublecortin domain-containing protein 2B	1.91	3.85	2.18	0	0.736965594	-1.669026766
Lgr6	leucine-rich repeat-containing G-protein coupled	143.02	55.05	338.88	106.7	-1.361482894	-1.65800722
Enpp6	ectonucleotide pyrophosphatase/phosphodiesterase	0	0.65	2.13	0	0.722466024	-1.646162657
Fam71e1	hypothetical protein LOC75538	2.58	1.95	2.13	0	-0.279244633	-1.646162657
Gata6	transcription factor GATA-6	5.67	4.88	230.72	73.61	-0.181870606	-1.634941657
Rapsn	43 kDa receptor-associated protein of the	0	0	2.1	0	0	-1.632268215
Ch25h	cholesterol 25-hydroxylase	41.85	31.13	173.03	55.2	-0.415374224	-1.63069399
Kcnj2	inward rectifier potassium channel 2	17.53	9.88	19.15	5.51	-0.768184325	-1.63005039
Fam57b	hypothetical protein LOC68952 isoform 3	1.88	1.05	16.43	4.65	-0.490444902	-1.625249797
Aqp5	aquaporin-5	0.77	0	2.08	0	-0.82374936	-1.622930351
Folr2	folate receptor beta precursor	3.77	2.55	2.08	0	-0.426170242	-1.622930351
Ltbp1	latent-transforming growth factor beta-binding	121.23	82.26	144.8	46.45	-0.553902959	-1.619510727
Gm6644		8.84	7.14	6.85	1.58	-0.273629521	-1.605321588
Actn2	alpha-actinin-2	0.35	0	2.04	0	-0.432959407	-1.604071324
Fgfbp1	fibroblast growth factor-binding protein 1	349.74	130.09	1887.26	622.55	-1.419844336	-1.598480273
Slc41a2	solute carrier family 41 member 2	2.63	1.14	6.77	1.58	-0.762358752	-1.590543533
Ephx4	epoxide hydrolase 4	0	0	2.01	0	0	-1.589763487
Dclk1	serine/threonine-protein kinase DCLK1 isoform 7	30.3	8.45	50.88	16.33	-1.727776423	-1.581906825
Rnase12	ribonuclease-like protein 12 precursor	0	0	23.69	7.26	0	-1.57971315
5033406O09Rik		0.93	0	1.96	0	-0.948600847	-1.565597176
Dpyd	dihydropyrimidine dehydrogenase [NADP+]	72.27	33.69	33.1	10.59	-1.078702775	-1.556891173
Aspn	asporin preproprotein	176.48	184.36	313.96	106.71	0.062673491	-1.548016419
Mtag2		0	0	1.92	0	0	-1.545968369
Slc26a7	anion exchange transporter	9.55	3.8	13.01	3.8	-1.136136688	-1.545350645
Emid1	EMI domain-containing protein 1 precursor	13.79	6.77	13.92	4.12	-0.928635549	-1.54303182
Gdf15	growth/differentiation factor 15 precursor	1.68	3.08	1.91	0	0.606336152	-1.541019153
2210407C18Rik	epithelial progenitor 1	0	0	1.9	0	0	-1.5360529
Prr15	proline-rich protein 15	0	0	1.9	0	0	-1.5360529
Ptk6	protein-tyrosine kinase 6	1.97	1.76	18.72	5.8	-0.105794664	-1.5360529
Sv2b	synaptic vesicle glycoprotein 2B	0.44	0.41	1.9	0	-0.030373649	-1.5360529
Gas7	growth arrest-specific protein 7 isoform b	134.3	53.24	337.48	115.91	-1.318732756	-1.533672253
Lyn	tyrosine-protein kinase Lyn isoform A	4.61	2.64	3.95	0.71	-0.62406232	-1.5334322
Dnm3	dynamin-3 isoform 1	2.71	0.89	7.45	1.93	-0.973032952	-1.528050677
Crispld1	cysteine-rich secretory protein LCCL	107.14	76.12	70.18	23.78	-0.487723305	-1.522295745
Rep15	rab15 effector protein	0	1.46	1.86	0	1.298658316	-1.516015147
Fam83d	hypothetical protein LOC71878	258.09	109.45	151.12	52.25	-1.230059915	-1.514356414
Fmo5	dimethylaniline monooxygenase [N-oxide-forming]	53.27	27.02	110.47	38.03	-0.953697953	-1.514000121
Foxq1	forkhead box protein Q1	5.54	3.65	92.81	32.04	-0.49205992	-1.505528033
Prss22	brain-specific serine protease 4	1.35	1.64	26.84	8.82	0.167877173	-1.503364282
Slc5a11	sodium/myo-inositol cotransporter 2	0	0	9.4	2.67	0	-1.50273156
Cyp2j8	cytochrome P450, family 2, subfamily j,	1.04	1.19	1.83	0	0.102361718	-1.500802053
Ly6g5b	lymphocyte antigen 6 complex locus protein G5b	0	1.94	1.83	0	1.555816155	-1.500802053
Hsd17b13	17-beta-hydroxysteroid dehydrogenase 13 isoform	0	1.06	61.86	21.22	1.042644337	-1.500283455
Otoa	otoancorin precursor	0	0	1.82	0	0	-1.495695163
Sds	L-serine dehydratase/L-threonine deaminase	0	0	1.82	0	0	-1.495695163
Prr5	proline-rich protein 5	1.28	0.77	1.81	0	-0.365284464	-1.49057013
Btc	betacellulin preproprotein	2.58	1.11	13.54	4.2	-0.762716589	-1.483443741
Pdk4	pyruvate dehydrogenase kinase, isozyme 4	13.93	12.44	319.49	113.81	-0.151681027	-1.481031035
Cyp2b13	cytochrome P450, family 2, subfamily b,	2.63	1.43	8.67	2.47	-0.579013234	-1.478580227
BC048355	deoxyribonucleoside 5'-monophosphate	108.6	82.22	176.35	63.24	-0.397245605	-1.465055532
Cpxm2	inactive carboxypeptidase-like protein X2	8.35	8.61	25.61	8.65	0.039570066	-1.463367663
Ntf3	neurotrophin-3 isoform a	36.19	41.55	157.29	56.41	0.194244384	-1.463196155
Chrm3	muscarinic acetylcholine receptor M3	2.18	0	1.74	0	-1.669026766	-1.454175893
Sdsl	serine dehydratase-like	0	0	1.74	0	0	-1.454175893
Fbln7	fibulin-7 precursor	1.97	1.34	21.88	7.37	-0.343954401	-1.450787524
Fzd9	frizzled-9 precursor	10.31	2.99	1.72	0	-1.503138278	-1.443606651
Rufy4	RUN and FYVE domain-containing protein 4 isoform	20.5	7.47	11.25	3.51	-1.343902785	-1.441582411
Hist2h2aa2	histone H2A type 2-A	7.34	6.49	7.2	2.05	-0.155081665	-1.426814667
Eml1	echinoderm microtubule-associated protein-like 1	21.66	14.2	34.84	12.35	-0.576076537	-1.424730895
Guca2a	guanylin precursor	16.31	11.24	28.3	9.97	-0.500002167	-1.417337139
Hlx	H2.0-like homeobox protein	1.99	3.74	1.67	0	0.664741575	-1.416839742
Faah	fatty-acid amide hydrolase 1	10.17	4.81	79.58	29.24	-0.943019117	-1.413963666
Skint2	selection and upkeep of intraepithelial T-cells	2.39	4.16	49.86	18.15	0.606085792	-1.40918707
BC026439	prostaglandin-specific organic anion	32.17	11.79	8.11	2.44	-1.374862748	-1.405042489
Mogat1	2-acylglycerol O-acyltransferase 1	2.54	2.82	1.64	0	0.109823278	-1.40053793
Gm5084		11.47	2.71	17.1	5.88	-1.748970373	-1.395509227
Nt5e	5'-nucleotidase precursor	883.96	326.67	352.42	133.83	-1.433368655	-1.390242149
Fam3b	cytokine-like protein 2-21 precursor	0	0	1.62	0	0	-1.389566812
Pvt1		22.44	4.26	13.41	4.51	-2.155837865	-1.386946112
Nxph1	neurexophilin-1 precursor	2.25	0.9	1.61	0	-0.7744403	-1.384049807
Steap4	metalloreductase STEAP4	615.44	201.56	371.58	142.06	-1.60561117	-1.380929886

Sdr16c5	epidermal retinol dehydrogenase 2	44.12	21.89	347.39	132.82	-0.979049605	-1.380409465
Abcb1b	multidrug resistance protein 1	23.35	3.01	14.33	4.89	-2.602247631	-1.380018158
Cxcr4	C-X-C chemokine receptor type 4	63.59	42.32	56.48	21.09	-0.576277577	-1.379666643
Ang	angiogenin precursor	153.81	69.69	145.85	55.53	-1.130920619	-1.377254664
Cxcl9	C-X-C motif chemokine 9 precursor	17.14	15.62	43.3	16.08	-0.126254074	-1.374998724
Tsc22d3	TSC22 domain family protein 3 isoform 1	505.75	158.74	537.46	207.35	-1.665548565	-1.369830077
Msl3l2	male-specific lethal 3-like 2	9.16	5.19	8.12	2.53	-0.714889088	-1.369365641
Lrrn1	leucine-rich repeat neuronal protein 1	0.41	0.38	1.58	0	-0.031026896	-1.367371066
Foxc1	forkhead box protein C1	134.87	97.63	288.57	111.31	-0.462128506	-1.366425754
Elf5	ETS-related transcription factor Elf-5	0	0	15.94	5.6	0	-1.359895945
Dact2	dapper homolog 2	11.52	4.88	10.95	3.66	-1.090346502	-1.358608758
Sema3a	semaphorin-3A precursor	2.18	1.32	5.43	1.51	-0.45490196	-1.357131373
Klhl8	kelch-like protein 8	41.71	24.9	159.12	61.6	-0.7216218	-1.354918959
Crip3	cysteine-rich protein 3 isoform TLP-A	17.55	10.37	18.98	6.85	-0.706186933	-1.347792024
H2-M2	histocompatibility 2, M region locus 2	8.15	12.71	15	5.29	0.583384923	-1.346939983
Myl4	myosin light chain 4	2.15	2.55	1.54	0	0.172467196	-1.344828497
Steap1	metalloreductase STEAP1	1.67	1.74	1.54	0	0.037336151	-1.344828497
Tmigd1	transmembrane and immunoglobulin	0	0	1.54	0	0	-1.344828497
Napepld	N-acyl-phosphatidylethanolamine-hydrolyzing	17.88	14.5	51.83	19.84	-0.284590549	-1.342002132
Cyp27a1	sterol 26-hydroxylase, mitochondrial	22.89	12.54	257.99	101.35	-0.819179115	-1.339385292
Tmem171	transmembrane protein 171	2.35	0	1.53	0	-1.744161096	-1.339137385
Lipk	lipase member K isoform 1 precursor	3.6	2.42	23.79	8.8	-0.427637536	-1.338904617
B930059L03Rik		1.62	2.22	1.52	0	0.297493877	-1.333423734
Tnfsf13b	tumor necrosis factor ligand superfamily member	0.66	0	1.52	0	-0.731183242	-1.333423734
Ptn	pleiotrophin	2676.71	1626.29	1360.33	540.95	-0.718528346	-1.328785172
2310042E22Rik	hypothetical protein LOC66561	1.58	1.27	33.16	12.62	-0.184678768	-1.326581272
Sectm1b	secreted and transmembrane protein 1b precursor	8.2	4.75	68.77	26.84	-0.678071905	-1.325447622
Mlkl	mixed lineage kinase domain-like protein	4.46	1.51	12.75	4.49	-1.121213587	-1.324553564
Hist1h3a	histone H3.1	1.27	0.92	2.25	0.3	-0.241585987	-1.321928095
Lipn	lipase member N precursor	0	0	1.5	0	0	-1.321928095
Dach1	dachshund homolog 1 isoform 2	28.44	14.05	68.33	26.74	-0.968014184	-1.321511973
Cish	cytokine-inducible SH2-containing protein	349.56	90.48	463.92	185.62	-1.938133119	-1.316878882
Spata9	spermatogenesis-associated protein 9	0	0	1.49	0	0	-1.316145742
Zdhhc12	probable palmitoyltransferase ZDHHC12 isoform b	13.56	35.39	30.89	11.81	1.321531696	-1.315833622
Zfp119b	zinc finger protein 119b	16.55	7.18	16.14	5.9	-1.101298282	-1.312698842
Acsbg1	long-chain-fatty-acid--CoA ligase ACSBG1	110.83	52.15	811.33	326.07	-1.073165667	-1.312466489
Dnajb7	dnaJ homolog subfamily B member 7	0	0	1.48	0	0	-1.310340121
Olfr99	olfactory receptor 99	0	0	1.48	0	0	-1.310340121
Smcp	sperm mitochondrial-associated cysteine-rich	0	0	1.48	0	0	-1.310340121
Gt(ROSA)26Sor		34.86	16.29	37.2	14.42	-1.052437619	-1.308769873
Klk6	kallikrein related-peptidase 6 precursor	0	2.17	16.83	6.2	1.66448284	-1.308237891
Clec4n	C-type lectin domain family 6 member A isoform	1.92	1.37	1.47	0	-0.30108131	-1.304511042
Vpreb1	immunoglobulin iota chain precursor	1.16	2.6	1.47	0	0.736965594	-1.304511042
Nkpd1	NTPase KAP family P-loop domain-containing	0.74	0.9	6.8	2.16	0.126912112	-1.303549566
Spink5	serine protease inhibitor Kazal-type 5	33.7	24.07	227.03	91.52	-0.468973667	-1.301386469
Mecom	MDS1 and EVI1 complex locus protein EVI1 isoform	0.27	0.42	1.46	0	0.161062433	-1.298658316
Zbp1	Z-DNA-binding protein 1 isoform 2	1.63	1.54	1.46	0	-0.050234303	-1.298658316
Plekhf1	pleckstrin homology domain-containing family F	38.08	15.49	24.04	9.2	-1.244839069	-1.29566541
Efhd1	EF-hand domain-containing protein D1	2.03	2.12	1.45	0	0.042228235	-1.292781749
Chrna4	neuronal acetylcholine receptor subunit alpha-4	0.47	0	3.92	1.01	-0.555816155	-1.291462814
9430020K01Rik	hypothetical protein LOC240185	27.39	11.95	31.44	12.26	-1.132430751	-1.290693044
Cryab	alpha-crystallin B chain	226.26	176.29	209.79	85.27	-0.358232614	-1.288875565
Liph	lipase member H isoform 1	2.17	1.94	28.42	11.06	-0.108666685	-1.286567339
H2-Q7	H-2 class I histocompatibility antigen, Q7 alpha	30	30.43	333.68	136.38	0.019874057	-1.284610351
Ifi47	interferon gamma inducible protein 47	3.8	5.04	12	4.34	0.331514144	-1.283599976
Lrrc18	leucine-rich repeat-containing protein 18	18.74	1.61	4.89	1.42	-2.919000278	-1.283260587
1700001G17Rik		0	0	1.43	0	0	-1.280956314
4930505A04Rik	hypothetical protein LOC75087	6.19	4.05	1.43	0	-0.509708383	-1.280956314
Chst7	carbohydrate sulfotransferase 7	1.14	0.71	1.43	0	-0.323614472	-1.280956314
Hes7	transcription factor HES-7	0	0	1.43	0	0	-1.280956314
Cdsn	corneodesmosin precursor	45.76	35.39	319.77	131.11	-0.361732879	-1.279799545
H2-Q6	histocompatibility 2, Q region locus 6	109.67	90.49	556.79	229.94	-0.274578227	-1.272203993
Cacna2d2	voltage-dependent calcium channel subunit	11.18	3.39	7.05	2.34	-1.472221288	-1.269140681
Cd209f	CD209f antigen	1.98	2.51	1.41	0	0.2361587	-1.269033146
Kcnj16	inward rectifier potassium channel 16	1.5	0.54	3.24	0.76	-0.698997744	-1.268488836
Cd5	T-cell surface glycoprotein CD5 precursor	2.14	2.66	9.65	3.43	0.221079089	-1.265474827
Sema3d	semaphorin-3D precursor	14.03	20.14	33.33	13.28	0.492130367	-1.265473878
Tns1	tensin 1	448	125.41	165.48	68.25	-1.828604849	-1.265462894
Mesp2	mesoderm posterior protein 2	12.07	2.8	15.3	5.79	-1.782187817	-1.263388485
Dtx4	protein deltex-4	2.72	3.08	46.58	18.85	0.133266531	-1.261216264
Pglyrp3	peptidoglycan recognition protein 3 precursor	1.11	1.48	24.67	9.71	0.233097122	-1.261124816
Atp1b1	sodium/potassium-transporting ATPase subunit	22.56	27.48	31	12.39	0.273609607	-1.256915944
St8sia2	alpha-2,8-sialyltransferase 8B	2.21	2.18	5.93	1.9	-0.013546532	-1.256802452
Ccl1	C-C motif chemokine 1 precursor	3.16	3.82	20.33	7.98	0.212449618	-1.248096616
Tead4	transcriptional enhancer factor TEF-3 isoform a	28.38	13.97	20.08	7.88	-0.972760174	-1.247243285
2200002D01Rik	HAI-2 related small protein	4.28	6.86	19.53	7.65	0.573991383	-1.24696159
Ccdc64b	bicaudal D-related protein 2	8.07	5.55	47.17	19.32	-0.469607644	-1.245234522
Gm13306	chemokine (C-C motif) ligand 27b isoform 2	495.12	172.29	731.31	307.99	-1.517500714	-1.244894348
Ptchd3	patched domain-containing protein 3	5.59	0	1.37	0	-2.720278465	-1.244887059
Zglp1	GATA-type zinc finger protein 1	0	1.65	1.37	0	1.40599236	-1.244887059
2810403D21Rik		13.96	7.98	13.62	5.17	-0.736322825	-1.244600917
Il13ra2	interleukin-13 receptor subunit alpha-2	1.32	1.14	12.7	4.79	-0.116514009	-1.24254064
Syngr4	synaptogyrin-4	0	0	1.36	0	0	-1.23878686
Orm2	alpha-1-acid glycoprotein 2 precursor	1.81	1.44	4.87	1.49	-0.203688983	-1.237214761
Gm14047		0	0	9.23	3.34	0	-1.237039197
Iigp1	interferon-inducible GTPase 1	7.14	12.07	8.07	2.86	0.683158442	-1.232501703
Fam111a	hypothetical protein LOC107373	44.13	38.85	59.67	24.86	-0.179507054	-1.230261036
Hmgcll1	probable 3-hydroxymethyl-3-methylglutaryl-CoA	2.9	0.62	3.15	0.77	-1.267480311	-1.229361976
Avpr1a	vasopressin V1a receptor	4.43	3.9	115.63	48.78	-0.148170449	-1.228300796
Cd274	programmed cell death 1 ligand 1 precursor	5.8	6.01	16.11	6.32	0.043879698	-1.224924206
Tmprss11e	transmembrane protease serine 11E	0	0	5.49	1.78	0	-1.223133595
Gal3st1	galactosylceramide sulfotransferase	59.06	36.97	15.15	5.92	-0.661544476	-1.222690222

Serpinb1a	leukocyte elastase inhibitor A	51.91	34.64	37.94	15.74	-0.570043081	-1.217953356
Csf1	macrophage colony-stimulating factor 1 isoform 2	19.42	14.29	31.24	12.87	-0.41739446	-1.216883956
Gm6034	H2-GS14-2 antigen	0	0	1.32	0	0	-1.214124805
Irf5	interferon regulatory factor 5	13.25	10.12	55.39	23.35	-0.357805131	-1.211517571
Tmem45a	transmembrane protein 45A	305.27	201.03	1323.41	570.97	-0.600234519	-1.211338425
Gdpd1	glycerophosphodiester phosphodiesterase	3.05	1.65	44.38	18.6	-0.611929548	-1.211202955
Slc2a12	solute carrier family 2, facilitated glucose	33.92	19.08	27.58	11.35	-0.79829429	-1.210494875
Dab2	disabled homolog 2 isoform c	198.72	99.37	21.05	8.54	-0.992650691	-1.208717484
Gcnt4	glucosaminyl transferase 4, core 2	1.04	0.9	18.38	7.39	-0.102569734	-1.207825855
Sipa1l2	signal-induced proliferation-associated 1-like	21.68	15.24	88.26	37.79	-0.481869008	-1.202329031
Pik3r5	phosphoinositide 3-kinase regulatory subunit 5	0.74	1.38	2.29	0.43	0.451874267	-1.202072437
Cd209b	CD209 antigen-like protein B isoform a	1.27	2.58	1.3	0	0.65726729	-1.201633861
Clec4a3	dendritic cell inhibitory receptor 3	1.43	1.11	1.3	0	-0.203713315	-1.201633861
Rgl3	ral guanine nucleotide dissociation	0.48	0.75	4.45	1.37	0.241757746	-1.201369171
Ecm1	extracellular matrix protein 1 precursor	2342.99	500.06	379.66	164.88	-2.225911139	-1.198363026
Casp12	caspase-12 precursor	2.81	5.22	15.45	6.17	0.707123583	-1.19804256
Clec2d	C-type lectin domain family 2 member D	627.29	209.41	512.72	222.92	-1.578227346	-1.197998849
BB123696		5.95	0	1.29	0	-2.797012978	-1.195347598
C1ql1	C1q-related factor precursor	0	0	1.29	0	0	-1.195347598
Slc16a14	monocarboxylate transporter 14	19.1	5.8	49.51	21.1	-1.56358885	-1.192522672
Cyp4b1	cytochrome P450 4B1	243.35	87.84	355.9	155.16	-1.459667807	-1.192494943
Slc46a2	thymic stromal cotransporter protein	4.21	6.88	87.3	37.64	0.596912257	-1.192318344
Upb1	beta-ureidopropionase	254.13	104.7	90.79	39.22	-1.271257175	-1.190423907
S100b	protein S100-B	1.72	1.19	1.28	0	-0.312675782	-1.189033824
Ror1	tyrosine-protein kinase transmembrane receptor	21.16	13.88	23.5	9.75	-0.574583355	-1.188445089
Loxl4	lysyl oxidase homolog 4 isoform 1	6.17	7.05	10.16	3.9	0.167015664	-1.187483373
Fam83c	family with sequence similarity 83, member C	10.21	5.81	44.13	18.85	-0.719059575	-1.184947771
Cwh43	PGAP2-interacting protein	123.91	98.84	214.96	94.03	-0.323199141	-1.184309187
Ttpa	alpha-tocopherol transfer protein	26.45	9.85	15.03	6.06	-1.339111107	-1.183034337
Mmp27	matrix metalloproteinase-27	5.09	4.31	1.27	0	-0.197730367	-1.182692298
Defb6	beta-defensin 6 precursor	198.48	274.88	13738.1	6057.41	0.467796764	-1.181276381
Apobec3	DNA dC->dU-editing enzyme APOBEC-3 isoform 1	2.34	2.11	7.07	2.56	-0.102933522	-1.180691432
Bmp6	bone morphogenetic protein 6 precursor	11.94	4.49	28.74	12.12	-1.236959563	-1.180636927
Krt32	keratin, type I cuticular Ha2	23.85	12.09	41.84	17.9	-0.924780755	-1.180572246
Thsd1	thrombospondin type-1 domain-containing protein	471.84	393.09	144.82	63.41	-0.262826944	-1.17883201
C630043F03Rik		24.23	30.37	91.96	40.14	0.314245323	-1.176068275
Clca2	chloride channel calcium activated 2	77.43	76.44	1652.32	731.27	-0.018326648	-1.174918388
Oip5	protein Mis18-beta	3.72	4.51	15.91	6.49	0.223265459	-1.174839036
Sphk1	sphingosine kinase 1 isoform 1	36.09	21.17	77.78	33.9	-0.742421498	-1.174602381
Upp1	uridine phosphorylase 1	22.11	4.65	7.69	2.85	-2.032194487	-1.174497731
Nexn	nexilin	5.4	3.78	9.49	3.65	-0.421061287	-1.173712057
Slc46a3	solute carrier family 46 member 3 precursor	3.15	2.56	15.22	6.19	-0.221234095	-1.173710144
Vsnl1	visinin-like protein 1	79.41	59.68	137.74	60.64	-0.406153844	-1.170445023
Clca1	chloride channel calcium activated 1	15.41	16.64	344.9	152.7	0.104275322	-1.170237849
Gpr141	probable G-protein coupled receptor 141	1.94	2.88	1.25	0	0.400240497	-1.169925001
Rnd1	rho-related GTP-binding protein Rho6 precursor	30.6	9.74	32.79	14.04	-1.556930565	-1.167791783
Slco2b1	solute carrier organic anion transporter family	7.58	8.62	91.91	40.45	0.165059246	-1.164461782
1700101E01Rik	hypothetical protein LOC329375 isoform 2	0	0	1.24	0	0	-1.163498732
Ces1e	liver carboxylesterase 22 precursor	0	0	1.24	0	0	-1.163498732
Zbtb46	zinc finger and BTB domain-containing protein 46	0.79	0.8	1.24	0	0.008037319	-1.163498732
D0H4S114	neuronal protein 3.1	446.02	233.28	293.58	130.58	-0.932105581	-1.162719267
Fam190a	hypothetical protein LOC232035	2.21	1.45	5.8	2.04	-0.389791548	-1.161463423
H2-Q8	H-2 class I histocompatibility antigen, Q8 alpha	70.77	63.23	291.09	129.69	-0.160133624	-1.160264212
Ccnd2	G1/S-specific cyclin-D2	149.3	166.86	546.85	244.13	0.159413477	-1.160233883
Gm4980	hypothetical protein LOC100503386	1.17	0.64	7.41	2.77	-0.403999228	-1.157541277
Areg	amphiregulin preproprotein	23.65	22.06	295.39	132.16	-0.096195134	-1.154335997
F2r	proteinase-activated receptor 1 precursor	17.62	8.38	62.76	27.65	-0.989193245	-1.15411649
X99384	paladin	14.6	12.32	40.71	17.77	-0.227951947	-1.151964662
Anpep	aminopeptidase N	88.48	20.29	243.89	109.22	-2.071389307	-1.151747831
Ncapg	non-SMC condensin I complex, subunit G	4.77	14.15	37.05	16.14	1.39267457	-1.150529344
Clspn	claspin	0.96	4.45	16.64	6.95	1.475402576	-1.149823795
Nqo1	NAD(P)H dehydrogenase [quinone] 1	160.47	67.33	175.65	78.71	-1.240675115	-1.148061116
Kcnd3	potassium voltage-gated channel subfamily D	2.86	2.19	5.31	1.85	-0.275044424	-1.146678086
Eri2	ERI1 exoribonuclease 2	16.06	11.21	24.14	10.37	-0.482554446	-1.144752396
Noxa1	NADPH oxidase activator 1 isoform 1	0	0	1.21	0	0	-1.14404637
Itpripl1	inositol 1,4,5-triphosphate receptor-interacting	55.77	34.09	71.81	31.95	-0.694068794	-1.143858144
Gm12839		34.36	13.28	56.09	24.92	-1.308122295	-1.139172344
Cldn8	claudin-8	52.53	35.73	303.92	137.52	-0.543388757	-1.138336489
Ccl22	C-C motif chemokine 22 precursor	2.04	1.48	1.2	0	-0.293731203	-1.137503524
Mmp25	matrix metalloproteinase-25 precursor	0.46	0.64	2.21	0.46	0.167727446	-1.136604928
Psapl1	proactivator polypeptide-like 1	107.21	103.84	942.26	428.21	-0.04564457	-1.135971801
Bdnf	brain-derived neurotrophic factor isoform 2	39.09	40.47	15.29	6.42	0.04882563	-1.134495512
2810417H13Rik	PCNA-associated factor	4.08	17.75	71.63	32.1	1.883990193	-1.133734363
Fzd7	frizzled-7 precursor	509.44	323.81	635.37	289.45	-0.652145339	-1.131575995
Aadac	arylacetamide deacetylase	22.91	18.33	764.84	349.05	-0.306772493	-1.129482008
Pcdh18	protocadherin 18 precursor	2.53	4.48	7.2	2.75	0.63450771	-1.128733314
Tnfaip8l1	tumor necrosis factor alpha-induced protein	1.35	3.25	10.93	4.46	0.854802084	-1.127621187
Arhgap44	rho GTPase-activating protein 44 isoform 1	239.22	152.37	144.03	65.41	-0.647339959	-1.126878954
Cyp3a13	cytochrome P450 3A13	1.74	2.62	10.09	4.08	0.401813804	-1.126358963
Slc39a4	zinc transporter ZIP4 precursor	1.42	0.95	4.32	1.44	-0.311532924	-1.124545098
Clca4	chloride channel calcium activated 4	1.14	1.28	31.94	14.11	0.091423028	-1.124336895
Col2a1	collagen alpha-1(II) chain isoform 2 precursor	0.34	0	1.18	0	-0.422233001	-1.124328135
Cpeb1	cytoplasmic polyadenylation element-binding	20.14	7.05	11.84	4.89	-1.392914688	-1.124305663
Kcnk5	potassium channel subfamily K member 5	0.74	1.14	7.13	2.73	0.298523491	-1.124079722
Paqr7	membrane progestin receptor alpha	105.96	77.59	190.55	87.2	-0.444653714	-1.118870465
Snx20	sorting nexin-20	1.17	2.11	1.17	0	0.519219538	-1.117695043
Rpp25	ribonuclease P protein subunit p25	0	1.38	10.91	4.49	1.250961574	-1.117295359
Gfra1	GDNF family receptor alpha-1 precursor	238.92	38.03	29.12	12.89	-2.619898059	-1.116675171
Tm4sf1	transmembrane 4 L6 family member 1	24.16	58.93	449.12	206.75	1.252146452	-1.115461192
Ces1d	carboxylesterase 3 precursor	12.31	7.16	81.08	36.89	-0.705869514	-1.115213591
Ank	progressive ankylosis protein	745.23	515.29	845.13	390.24	-0.531438706	-1.112825459
Crym	mu-crystallin homolog	1.17	0	1.16	0	-1.117695043	-1.111031312

Apobec1	C->U-editing enzyme APOBEC-1 isoform 2	11.87	3.01	28.75	12.79	-1.682337912	-1.109267212
Adrb3	beta-3 adrenergic receptor	2.59	1.46	11.01	4.57	-0.545325528	-1.108486918
Trim72	tripartite motif-containing protein 72	1.52	1.39	9.19	3.73	-0.076413116	-1.107241963
Ppil6	peptidyl-prolyl cis-trans isomerase-like 6	31.39	12.76	27.22	12.1	-1.235067998	-1.107151176
Rarres1	retinoic acid receptor responder (tazarotene	34.53	23.11	92.5	42.41	-0.559406038	-1.106938942
Cst6	cystatin-M	43.68	57.8	1999.6	928.46	0.396186969	-1.105968059
2310007B03Rik	hypothetical protein LOC71874	1.7	1.41	30.89	13.83	-0.163926261	-1.1045855
Uchl1	ubiquitin carboxyl-terminal hydrolase isozyme	0	0	1.15	0	0	-1.10433666
Spns2	protein spinster homolog 2	4.11	5.05	22.39	9.89	0.243611851	-1.102887908
Angpt2	angiopoietin-2 precursor	0.71	2.29	4.9	1.75	0.944091259	-1.101283336
Grik1	glutamate receptor, ionotropic kainate 1 isoform	24.91	6.95	2.74	0.75	-1.70448225	-1.095683348
Irgm2	interferon inducible GTPase 2	23.59	20.03	25.48	11.42	-0.225622885	-1.092237949
Piwil2	piwi-like protein 2	26.32	13.26	34.62	15.71	-0.937983502	-1.091975783
Syt16	synaptotagmin-16	0.46	0	1.13	0	-0.545968369	-1.09085343
Tc2n	tandem C2 domains nuclear protein	2.11	2.22	1.13	0	0.050146108	-1.09085343
Alpk1	alpha-protein kinase 1	1.03	1.38	6.19	2.38	0.229481846	-1.088968524
Smagp	small cell adhesion glycoprotein	21.66	19.03	83.86	39.01	-0.17798544	-1.08472405
Cd163l1	CD163 molecule-like 1	1.06	0.54	1.12	0	-0.419713986	-1.084064265
Rgs18	regulator of G-protein signaling 18	1.14	1.65	1.12	0	0.308381563	-1.084064265
Hephl1	hephaestin-like protein 1	2.34	0.73	10.67	4.51	-0.949076065	-1.082680337
Rnase1	ribonuclease pancreatic precursor	5.13	5.14	24.9	11.23	0.002351582	-1.082527694
Irx3	iroquois-class homeodomain protein IRX-3	234.7	153.93	260.51	122.5	-0.60533523	-1.082355074
2210020M01Rik	hypothetical protein LOC66528	26.85	19.05	56.25	26.04	-0.474075091	-1.082180542
Chrm5	muscarinic acetylcholine receptor M5	0	0.78	1.11	0	0.831877241	-1.077242999
Krtap3-3	keratin-associated protein 3-2	0	0	1.11	0	0	-1.077242999
Maob	amine oxidase [flavin-containing] B	6.08	7.2	23.75	10.73	0.211874549	-1.077225512
Hist1h4c	histone H4	5.25	0	2.27	0.55	-2.64385619	-1.07702242
Fam26e	hypothetical protein LOC103511	68.83	78.31	83.57	39.09	0.18365581	-1.076903561
Adh7	alcohol dehydrogenase class 4 mu/sigma chain	526.18	145.22	473.24	223.87	-1.850154982	-1.076526149
1600029D21Rik	placenta-expressed transcript 1 protein	160.71	130.03	1230.67	584.34	-0.303511734	-1.073268992
Card10	caspase recruitment domain-containing protein	27.4	23.45	74.38	34.87	-0.216056465	-1.07140405
Rab11fip1	rab11 family-interacting protein 1 isoform 1	12.16	7.91	28.06	12.83	-0.562662152	-1.071233546
Cldn4	claudin-4	30.62	33.37	338.44	160.62	0.120312484	-1.070550845
3930402G23Rik		0	0	1.1	0	0	-1.070389328
Tspan15	tetraspanin 15	0.99	1.34	13.61	5.96	0.233740099	-1.069796967
LOC547349	MHC class I family member	0.03	0.06	1.18	0.04	0.041419927	-1.067744607
Als2cl	ALS2 C-terminal-like protein	21.06	17.77	27.27	12.49	-0.233004141	-1.067381535
Aldh3a1	aldehyde dehydrogenase, dimeric NADP-preferring	126.64	77.75	1185.89	565.54	-0.696728685	-1.066936509
Chit1	chitotriosidase-1 precursor	31.39	32.22	109.31	51.72	0.036503605	-1.065141307
Art3	ecto-ADP-ribosyltransferase 3	10.17	8.61	50.1	23.43	-0.21702085	-1.064669428
Zfp365	protein ZNF365	38.87	11.99	55.67	26.11	-1.617902175	-1.063760089
Ear5	eosinophil cationic-type ribonuclease 5	33.11	14.47	24.25	11.08	-1.140721558	-1.063662933
Mtmr7	myotubularin-related protein 7	3.96	1.64	25.38	11.63	-0.909802191	-1.062589925
Arhgap25	rho GTPase-activating protein 25 isoform a	1.3	1.6	3.49	1.15	0.176877762	-1.062378785
Dlk2	protein delta homolog 2	21.07	18.99	87.52	41.43	-0.142808158	-1.060918773
Sulf1	extracellular sulfatase Sulf-1 precursor	1.75	2.45	19.49	8.83	0.327164743	-1.059656663
Reil1	RELT-like protein 1 precursor	108.86	116.81	348.08	166.49	0.100795807	-1.05948274
Slc6a14	sodium- and chloride-dependent neutral and basic	2.76	2.04	20.69	9.41	-0.306661338	-1.059059984
Gm11202		7.86	12.61	5.04	1.9	0.619288463	-1.058495649
5730469M10Rik	hypothetical protein LOC70564 precursor	300.17	179.36	650.47	312.63	-0.739698653	-1.054635179
Tmprss2	transmembrane protease serine 2	0.83	0.76	8.49	3.57	-0.05626822	-1.054213922
Gpr111	G protein-coupled receptor 111	2.34	2.5	44.2	20.82	0.067506819	-1.050671671
Amz1	archaemetzincin-1	1.03	2.23	3.93	1.38	0.670054438	-1.050626073
Pcsk9	proprotein convertase subtilisin/kexin type 9	0	0	1.07	0	0	-1.049630768
Ptpn22	tyrosine-protein phosphatase non-receptor type	0.58	2.09	1.07	0	0.96768228	-1.049630768
Ube2t	ubiquitin-conjugating enzyme E2 T	12.51	18.43	47.67	22.54	0.524258226	-1.047918454
Bend4	BEN domain-containing protein 4	1.09	0.83	1.93	0.42	-0.191659294	-1.045009735
2010110P09Rik	calcineurin B homologous protein 2	2.04	3.15	1.06	0	0.449040013	-1.042644337
Arhgap15	rho GTPase-activating protein 15 isoform 2	0.89	1.68	1.06	0	0.503846766	-1.042644337
Card9	caspase recruitment domain-containing protein 9	1.57	1.56	1.06	0	-0.005624549	-1.042644337
Clec4a1	C-type lectin domain family 4, member a1	2.84	2.38	1.06	0	-0.184083064	-1.042644337
Frem3	FRAS1-related extracellular matrix protein 3	0	0	1.06	0	0	-1.042644337
Ncf4	neutrophil cytosol factor 4	0	1.28	1.06	0	1.189033824	-1.042644337
Slc9a7	sodium/hydrogen exchanger 7	0	0	4.54	1.69	0	-1.042279803
Crtac1	cartilage acidic protein 1 precursor	0	0	2.17	0.54	0	-1.041552489
Podn	podocan precursor	12.94	9.63	7.87	3.31	-0.391088964	-1.041246235
Tnfrsf4	tumor necrosis factor receptor superfamily	65.95	40.65	83.58	40.22	-0.68476756	-1.036972055
Orm3	alpha-1-acid glycoprotein 3 precursor	0	1.48	1.05	0	1.310340121	-1.03562391
Ngef	ephexin-1 isoform 1	85.59	10.71	13.49	6.07	-2.886459347	-1.035275475
Grb7	growth factor receptor-bound protein 7	36.26	24.1	76.02	36.58	-0.56994031	-1.035268056
Hist1h4b	histone H4	1.89	0	1.91	0.42	-1.531069493	-1.035128223
Adamtsl4	ADAMTS-like protein 4 precursor	404.65	176.82	65.17	31.3	-1.18981789	-1.034643115
Dusp26	dual specificity protein phosphatase 26	0.84	0	9.42	4.09	-0.879705766	-1.033617716
Sec14l4	SEC14-like protein 4	80.15	39.94	111.11	53.92	-0.987079992	-1.029511439
Ccna1	cyclin-A1	0	0	1.04	0	0	-1.028569152
Il1f9	interleukin-1 family member 9	1.18	1.93	1.04	0	0.42657253	-1.028569152
Nrgn	neurogranin	0	0	1.04	0	0	-1.028569152
Panx3	pannexin-3	4.7	2.22	15.29	6.99	-0.823901231	-1.027719196
Oxtr	oxytocin receptor	24.29	29.1	32.52	15.48	0.25119645	-1.024305907
Crabp2	cellular retinoic acid-binding protein 2	21.18	34.56	340.28	167	0.680995959	-1.022494638
Omp	olfactory marker protein	0.74	0.71	1.03	0	-0.025090981	-1.021479727
Ociad2	OCIA domain-containing protein 2	73.63	38.62	97.14	47.41	-0.913526806	-1.019536177
Ccnf	cyclin-F	5.95	8.83	22.29	10.52	0.500178439	-1.015569923
Ccl27a	C-C motif chemokine 27 isoform 1	734.29	388.84	1611.94	797.21	-0.915431237	-1.014852514
Gadl1	glutamate decarboxylase-like protein 1	1.06	0	1.02	0	-1.042644337	-1.014355293
Kcne3	potassium voltage-gated channel subfamily E	0.94	0	1.02	0	-0.956056652	-1.014355293
Rasal1	rasGAP-activating-like protein 1	0.74	0.84	2.17	0.57	0.08061846	-1.013718281
Ncaph	condensin complex subunit 2	7.34	16.78	53.52	26.02	1.092136035	-1.012757887
Depdc1b	DEP domain-containing protein 1B	1.07	3.48	8.24	3.58	1.113867965	-1.012545253
Itga4	integrin alpha-4	4.55	4.16	7.39	3.16	-0.105116706	-1.012087282
Tmem56	transmembrane protein 56	16.33	5.68	33.72	16.23	-1.375351647	-1.010844246
Tgfb3	transforming growth factor beta-3 preproprotein	75.36	94.82	163.91	80.88	0.327509711	-1.010095878

Krt77	keratin, type II cytoskeletal 1b	746.97	382.17	1522.06	755.47	-0.964995796	-1.009618003
BC006965		3.35	2.5	6.65	2.8	-0.313660479	-1.009460329
Tifa	TRAF-interacting protein with FHA	1.86	2.68	7.43	3.19	0.363690619	-1.008582387
Mmp17	matrix metalloproteinase-17 precursor	8.11	3.86	5.92	2.44	-0.90649474	-1.008363473
Was	wiskott-Aldrich syndrome protein homolog	1.05	0.76	1.01	0	-0.220048481	-1.007195501
Tec	tyrosine-protein kinase Tec isoform a	34.95	29.07	63.19	30.98	-0.257666903	-1.005178622
Gm13363		2.22	8.62	29.53	14.22	1.578976206	-1.004259231
Ifngr1	interferon gamma receptor 1 precursor	79.35	61.82	184.51	91.52	-0.355074081	-1.003659787
Ptgs2	prostaglandin G/H synthase 2	167.04	223.32	131.64	65.2	0.416753564	-1.00261279
Acss1	acetyl-coenzyme A synthetase 2-like,	11.6	3.32	21.72	10.34	-1.544320516	-1.002542195
Elovl6	elongation of very long chain fatty acids	58.84	34.78	335.27	167.07	-0.741956788	-1.000557845
Arg1	arginase-1	4.89	6.18	19.5	9.25	0.28571621	-1
Arhgef26	Rho guanine nucleotide exchange factor (GEF) 26	6.1	2.94	13.02	6.01	-0.849623395	-1
BB019430		0	0	1	0	0	-1
Cftr	cystic fibrosis transmembrane conductance	0	0	4.18	1.59	0	-1
Sash3	SAM and SH3 domain-containing protein 3	0.79	0	1	0	-0.839959587	-1
Uts2r	urotensin-2 receptor	0	0	1	0	0	-1

Table 3-2. Gene list from NFIB ChIP-seq analysis. Genes are sorted according to NFIB bound peak distribution relative to functional structure of a gene.

PROMOTERS(±2kb)

Transcript Name	Gene name	Gene Description
NM_172505	A730008H23Rik	Holliday junction recognition protein
NM_030210	Aacs	acetoacetyl-CoA synthetase
NM_022419	Abhd8	abhydrolase domain-containing protein 8
NM_001033606	Acsl3	long-chain-fatty-acid--CoA ligase 3 isoform a
NM_027827	Afmid	probable arylformamidase
NM_026375	Ahctf1	protein ELYS
NM_009667	Ampd3	AMP deaminase 3
NM_024213	Anapc4	anaphase-promoting complex subunit 4
NM_011923	Angptl2	angiopoietin-related protein 2 precursor
NR_030781	Ankrd10	
NM_013473	Anxa8	annexin A8
NM_023631	Aox4	aldehyde oxidase 4
NM_001080819	Arid1a	AT-rich interactive domain-containing protein
NM_001172205	Arid5a	AT-rich interactive domain-containing protein 5A
NM_023066	Asph	aspartyl/asparaginyl beta-hydroxylase isoform 1
NM_001039939	Asxl1	putative Polycomb group protein ASXL1
NM_007498	Atf3	cyclic AMP-dependent transcription factor ATF-3
NM_146065	Atf7	cyclic AMP-dependent transcription factor ATF-7
NM_153389	Atp10d	probable phospholipid-transporting ATPase VD
NM_001081182	Atp8b2	probable phospholipid-transporting ATPase ID
NM_175183	Atxn7l2	ataxin-7-like protein 2
NM_198423	Bahcc1	BAH and coiled-coil domain-containing protein 1
NM_025833	Baiap2l1	brain-specific angiogenesis inhibitor
NM_001033284	BC026585	quinone oxidoreductase-like protein 2
NR_015528	BC029722	
NM_001003910	BC030307	tetratricopeptide repeat protein GNN isoform 3
NM_172295	BC037703	hypothetical protein LOC242125
NM_016778	Bok	bcl-2-related ovarian killer protein
NM_009770	Btg3	protein BTG3
NR_029450	C530005A16Rik	
NM_009795	Capns1	calpain small subunit 1
NM_007616	Cav1	caveolin-1
NM_016900	Cav2	caveolin-2
NM_001033238	Cblb	E3 ubiquitin-protein ligase CBL-B
NM_001037916	Ccdc17	coiled-coil domain-containing protein 17
NM_013654	Ccl7	C-C motif chemokine 7
NM_001033342	Cdc42bpg	serine/threonine-protein kinase MRCK gamma
NM_007665	Cdh3	cadherin-3 isoform b
NM_007668	Cdk5	cell division protein kinase 5
NM_177270	Cdkl2	cyclin-dependent kinase-like 2 isoform 2
NM_177224	Chd9	chromodomain-helicase-DNA-binding protein 9
NM_001136240	Chdh	choline dehydrogenase, mitochondrial precursor
NM_134078	Chmp7	charged multivesicular body protein 7
NM_022890	Cldn12	claudin-12
NM_007713	Clk3	dual specificity protein kinase CLK3
NM_028266	Col16a1	collagen alpha-1(XVI) chain precursor
NM_009929	Col18a1	collagen alpha-1(XVIII) chain isoform 2
NM_001161854	Csde1	cold shock domain-containing protein E1 isoform
NM_028836	Ctbs	di-N-acetylchitobiase
NM_001113470	Ctdsp2	carboxy-terminal domain RNA polymerase II
NM_007795	Ctf1	cardiotrophin-1
NM_001165902	Ctnnb1	catenin beta-1
NM_001085449	Ctnnd1	catenin delta-1 isoform 3
NM_030560	Cwc22	pre-mRNA-splicing factor CWC22 homolog
NM_010010	Cyp46a1	cholesterol 24-hydroxylase
NM_010516	Cyr61	protein CYR61 precursor
NM_010015	Dad1	dolichyl-diphosphooligosaccharide--protein
NM_001037999	Dbi	acyl-CoA-binding protein isoform 1
NM_010024	Dct	L-dopachrome tautomerase precursor
NM_007837	Ddit3	DNA damage-inducible transcript 3 protein
NM_177564	Dhrs11	dehydrogenase/reductase SDR family member 11
NM_011303	Dhrs3	short-chain dehydrogenase/reductase 3 isoform 1
NM_027287	Dnajb4	dnaJ homolog subfamily B member 4
NM_172338	Dnajc16	dnaJ homolog subfamily C member 16 precursor
NM_007882	Dsc3	desmocollin-3
NM_001081316	Dsel	dermatan-sulfate epimerase-like protein
NM_013642	Dusp1	dual specificity protein phosphatase 1
NR_029447	E130317F20Rik	
NM_026598	Ebpl	emopamil-binding protein-like
NM_007902	Edn2	endothelin-2 precursor
NM_010109	Efna5	ephrin-A5 isoform 2
NM_010112	Efs	embryonal Fyn-associated substrate
NM_007913	Egr1	early growth response protein 1
NM_182840	Emilin3	EMILIN-3
NM_007680	Ephb6	ephrin type-B receptor 6
NM_010145	Ephx1	epoxide hydrolase 1
NM_176838	Esrp2	epithelial splicing regulatory protein 2
NM_028731	Esyt2	extended synaptotagmin-2
NM_008815	Etv4	ETS translocation variant 4
NM_145359	Fam100a	hypothetical protein LOC207740
NM_153782	Fam20a	family with sequence similarity 20, member A
NM_134087	Fam83h	family with sequence similarity 83, member H
NM_001122603	Fcgbp	Fc fragment of IgG binding protein
NM_057172	Fubp1	far upstream element-binding protein 1
NM_008059	G0s2	putative lymphocyte G0/G1 switch protein 2
NR_029457	G530011O06Rik	
NM_030166	Galntl2	polypeptide
NM_001113345	Gatad2a	transcriptional repressor p66 alpha isoform b
NM_028022	Gatsl3	GATS-like protein 3
NM_008112	Gdi2	rab GDP dissociation inhibitor beta
NM_145929	Gga1	ADP-ribosylation factor-binding protein GGA1
NR_002700	Gm7334	

NM_175193	Golim4	Golgi integral membrane protein 4
NM_026672	Gstm7	glutathione S-transferase Mu 7
NM_145546	Gtf2b	transcription initiation factor IIB
NM_172810	Gucy1b2	guanylate cyclase soluble subunit beta-2
NM_001166633	Gyltl1b	glycosyltransferase-like protein LARGE2 isoform
NM_027168	Hddc2	HD domain-containing protein 2
NM_019479	Hes6	transcription cofactor HES-6
NM_198652	Hjurp	Holliday junction recognition protein
NM_021877	Hr	protein hairless
NM_001130444	Hras1	GTPase HRas isoform 2
NM_011631	Hsp90b1	endoplasmin
NM_008300	Hspa4	heat shock 70 kDa protein 4
NM_030704	Hspb8	heat shock protein beta-8
NM_010499	Ier2	immediate early response gene 2 protein
NM_030694	Ifitm2	interferon-induced transmembrane protein 2
NM_019583	Il17rb	interleukin-17 receptor B precursor
NM_146152	Ipo13	importin-13
NM_022655	Ireb2	iron-responsive element-binding protein 2
NM_018826	Irx5	iroquois-class homeodomain protein IRX-5
NM_027534	Kdsr	3-ketodihydrosphingosine reductase precursor
NM_001166651	Klhl33	kelch-like 33
NM_027011	Krt5	keratin, type II cytoskeletal 5
NM_028770	Krt80	keratin, type II cytoskeletal 80
NM_001113406	Krtap11-1	keratin associated protein 11-1
NM_008484	Lamb3	laminin subunit beta-3 precursor
NM_025622	Lgals2	galectin-2
NM_010710	Lhx2	LIM/homeobox protein Lhx2
NM_010720	Lipg	endothelial lipase precursor
NM_001081109	Lmtk2	serine/threonine-protein kinase LMTK2 precursor
NR_028378	LOC100034739	
NM_177152	Lrig3	leucine-rich repeats and immunoglobulin-like
NM_001172064	Lrrc56	leucine-rich repeat-containing protein 56
NM_001111311	Lrrfip1	leucine-rich repeat flightless-interacting
NM_010771	Matr3	matrin-3
NM_033072	Mbd6	methyl-CpG binding domain protein 6
NM_175341	Mbnl2	muscleblind-like protein 2 isoform 1
NM_008617	Mdh2	malate dehydrogenase, mitochondrial precursor
NM_008587	Mertk	tyrosine-protein kinase Mer precursor
NM_001045489	Mfge8	lactadherin isoform 2
NM_172499	Mfsd9	major facilitator superfamily domain-containing
NR_029822	Mir125b-1	
NR_029739	Mir22	
NR_030494	Mir715	
NM_027973	Mlf1ip	centromere protein U
NM_008608	Mmp14	matrix metalloproteinase-14
NM_024431	Morf4l1	mortality factor 4-like protein 1 isoform b
NM_053162	Mrpl34	39S ribosomal protein L34, mitochondrial
NM_013602	Mt1	metallothionein-1
NM_181409	Mtmr11	myotubularin-related protein 11
NM_138656	Mvd	diphosphomevalonate decarboxylase
NM_016662	Mxd3	max dimerization protein 3
NM_008681	Ndrg1	protein NDRG1
NR_003513	Neat1	
NM_010907	Nfkbia	NF-kappa-B inhibitor alpha
NM_008738	Nrtn	neurturin precursor
NM_027289	Nt5dc2	5'-nucleotidase domain containing 2
NM_198190	Ntf5	neurotrophin-4 precursor
NM_175749	Nup153	nucleoporin 153
NM_010956	Ogdh	2-oxoglutarate dehydrogenase, mitochondrial
NM_153122	Oplah	5-oxoprolinase
NM_025661	Ormdl3	ORM1-like protein 3
NM_008772	P2ry1	P2Y purinoceptor 1
NM_023245	Palmd	palmdelphin
NM_033581	Pcdhgc3	protocadherin gamma subfamily C, 3
NM_008808	Pdgfa	platelet-derived growth factor subunit A
NM_011066	Per2	period circadian protein homolog 2
NR_028114	Pex16	
NM_021453	Pga5	pepsinogen 5, group I
NR_003519	Pisd-ps2	
NM_144859	Pja2	E3 ubiquitin-protein ligase Praja-2 isoform b
NM_019762	Pkp3	plakophilin-3 isoform 1
NM_016915	Pla2g6	85 kDa calcium-independent phospholipase A2
NM_024413	Plekhf1	pleckstrin homology domain-containing family F
NM_146030	Plekhh3	pleckstrin homology domain-containing family H
NM_001033225	Pnrc1	proline-rich nuclear receptor coactivator 1
NM_001081247	Polr3a	DNA-directed RNA polymerase III subunit RPC1
NM_001034085	Ppp2r1b	serine/threonine-protein phosphatase 2A 65 kDa
NM_008913	Ppp3ca	serine/threonine-protein phosphatase 2B
NM_001161111	Pqlc3	PQ-loop repeat-containing protein 3 isoform 2
NM_011104	Prkce	protein kinase C epsilon type
NM_175249	Psapl1	proactivator polypeptide-like 1
NM_008956	Ptbp1	polypyrimidine tract-binding protein 1 isoform
NM_008973	Ptn	pleiotrophin
NM_009009	Rad21	double-strand-break repair protein rad21
NM_027933	Ranbp3	ran-binding protein 3
NM_001146174	Rangap1	ran GTPase-activating protein 1
NM_028712	Rap2b	ras-related protein Rap-2b precursor
NM_009030	Rbbp4	histone-binding protein RBBP4
NM_001045807	Rbm15	RNA binding motif protein 15
NM_001029938	Rilp	rab-interacting lysosomal protein
NM_028810	Rnd3	rho-related GTP-binding protein RhoE precursor
NM_001099632	Rnf39	ring finger protein 39
NM_031248	Robld3	mitogen-activated protein-binding
NM_001013376	Rpp38	ribonuclease P protein subunit p38
NM_026467	Rps27l	40S ribosomal protein S27-like

NM_011305	Rxra	retinoic acid receptor RXR-alpha
NM_025393	S100a14	protein S100-A14 isoform a
NM_011310	S100a3	protein S100-A3
NM_011311	S100a4	protein S100-A4
NM_138665	Sardh	sarcosine dehydrogenase, mitochondrial
NM_007644	Scarb2	lysosome membrane protein 2
NM_198885	Scx	basic helix-loop-helix transcription factor
NM_013657	Sema3c	semaphorin-3C precursor
NM_001160307	Serpinb10	serpin B10 isoform 2
NM_009257	Serpinb5	serpin B5
NM_009825	Serpinh1	serpin H1 precursor
NM_030109	Sf3b2	splicing factor 3b, subunit 2
NM_028148	Sfrs2ip	splicing factor, arginine/serine-rich 2,
NM_172276	Sfrs8	splicing factor, arginine/serine-rich 8
NM_025858	Shisa5	protein shisa-5 isoform 1
NM_029415	Slc10a6	solute carrier family 10 member 6
NM_144893	Slc35c2	solute carrier family 35 member C2
NM_153142	Slc35e4	solute carrier family 35 member E4
NM_026721	Slc39a13	zinc transporter ZIP13
NM_001081349	Slc43a1	large neutral amino acids transporter small
NM_027872	Slc46a3	solute carrier family 46 member 3 precursor
NM_009207	Slc4a2	anion exchange protein 2
NM_033314	Slco2a1	solute carrier organic anion transporter family
NM_008541	Smad5	mothers against decapentaplegic homolog 5
NM_026003	Smarca2	probable global transcription activator SNF2L2
NM_025891	Smarcd3	SWI/SNF-related matrix-associated
NM_153115	Spag11a	sperm-associated antigen 11
NM_172561	Spag7	sperm-associated antigen 7 isoform 1
NM_025287	Spop	speckle-type POZ protein
NM_009272	Srm	spermidine synthase
NM_009179	St3gal2	CMP-N-acetylneuraminate-beta-galactosamide-
NM_011488	Stat5a	signal transducer and activator of transcription
NM_013515	Stom	erythrocyte band 7 integral membrane protein
NM_175162	Stox2	storkhead-box protein 2 isoform 2
NM_029659	Styxl1	serine/threonine/tyrosine-interacting-like
NM_194342	Sun2	SUN domain-containing protein 2
NM_153484	Tef	thyrotroph embryonic factor isoform 2
NM_009369	Tgfbi	transforming growth factor-beta-induced protein
NM_029431	Them4	thioesterase superfamily member 4
NM_025372	Tipin	TIMELESS-interacting protein
NM_009387	Tk1	thymidine kinase, cytosolic
NM_026669	Tmbim6	bax inhibitor 1
NM_026734	Tmem126b	transmembrane protein 126B
NM_001098271	Tmem176a	transmembrane protein 176A
NM_023056	Tmem176b	transmembrane protein 176B
NM_020588	Tmem183a	transmembrane protein 183 isoform a
NM_178625	Tmem209	transmembrane protein 209
NM_144794	Tmem63a	transmembrane protein 63A
NM_001033535	Tnfaip8l3	tumor necrosis factor alpha-induced protein
NM_013837	Tpst1	protein-tyrosine sulfotransferase 1 isoform 2
NM_001081055	Trappc10	trafficking protein particle complex subunit 10
NM_023910	Tsc22d4	TSC22 domain family protein 4
NM_146116	Tubb2c	tubulin beta-2C chain
NM_019803	Ube2g2	ubiquitin-conjugating enzyme E2 G2
NM_001039157	Ube2j2	ubiquitin-conjugating enzyme E2 J2 isoform a
NM_033526	Ubqln4	ubiquilin-4
NM_001136226	Utp14b	U3 small nucleolar RNA-associated protein 14
NM_175158	Utp20	small subunit processome component 20 homolog
NM_023054	Utp3	something about silencing protein 10
NM_013933	Vapa	vesicle-associated membrane protein-associated
NM_147776	Vwa1	von Willebrand factor A domain-containing
NM_028875	Xrcc3	DNA repair protein XRCC3
NM_025970	Zbtb8os	protein archease
NM_178404	Zc3h6	zinc finger CCCH domain-containing protein 6
NM_175160	Zdhhc1	probable palmitoyltransferase ZDHHC1
NM_001039198	Zfhx2	zinc finger homeobox protein 2
NM_013866	Zfp385a	zinc finger protein 385A
NM_146183	Zfp428	zinc finger protein 428
NM_030074	Zfp687	zinc finger protein 687
NM_146202	Zfp768	zinc finger protein 768
NM_026752	Zfyve21	zinc finger FYVE domain-containing protein 21
NM_183208	Zmiz1	zinc finger MIZ domain-containing protein 1
NM_001017955	Zscan18	zinc finger and SCAN domain containing 18
NM_029821	1190003J15Rik	5-hydroxyisourate hydrolase
NM_028166	1600014C10Rik	hypothetical protein LOC72244
NR_030711	2210403K04Rik	
NM_026629	2410066E13Rik	hypothetical protein LOC68235
NR_028428	2610005L07Rik	
NR_015483	2610203C20Rik	
NM_029366	2810422J05Rik	hypothetical protein LOC75620
NM_001172074	3110009E18Rik	hypothetical protein LOC73103 isoform 2
NM_025699	3230401D17Rik	oxidative stress responsive 1
NM_001080709	4930402F06Rik	hypothetical protein LOC74854
NM_177265	6330512M04Rik	CD225 family protein FLJ76511 homolog
NM_175521	6430598A04Rik	neuronal tyrosine phosphorylated adaptor for
NM_175398	6530418L21Rik	hypothetical protein LOC109050 isoform 1
NR_030708	6820431F20Rik	
NM_177205	9430015G10Rik	hypothetical protein LOC230996
NM_175417	9530008L14Rik	hypothetical protein LOC109254 isoform 1
NM_177003	9630033F20Rik	probable fructose-2,6-bisphosphatase TIGAR

DOWNSTREAM (±2kb)

Transcript Name	Gene name	Gene Description
NM_016689	Aqp3	aquaporin-3
NM_025338	Aurkaip1	aurora kinase A-interacting protein
NM_146082	BC027072	hypothetical protein LOC225004
NM_153544	BC030867	hypothetical protein LOC217216
NM_001122683	Bdh1	D-beta-hydroxybutyrate dehydrogenase,
NM_178116	Camta2	calmodulin-binding transcription activator 2
NM_027112	Capns2	calpain small subunit 2
NM_001033455	Ccdc27	coiled-coil domain-containing protein 27
NM_021339	Cdon	cell adhesion molecule-related/down-regulated by
NM_015734	Col5a1	collagen alpha-1(V) chain precursor
NM_019877	Copz2	coatomer subunit zeta-2
NM_001042611	Cp	ceruloplasmin isoform a
NM_153679	Cpt1c	carnitine O-palmitoyltransferase 1, brain
NM_153287	Csrnp1	cysteine/serine-rich nuclear protein 1
NM_153088	Ctdsp1	carboxy-terminal domain RNA polymerase II
NM_009983	Ctsd	cathepsin D precursor
NM_010055	Dlx3	homeobox protein DLX-3
NM_010100	Edar	tumor necrosis factor receptor superfamily
NM_153068	Ehd2	EH domain-containing protein 2
NM_010579	Eif6	eukaryotic translation initiation factor 6
NM_207706	Elmo2	engulfment and cell motility protein 2 isoform
NM_029001	Elovl7	elongation of very long chain fatty acids
NM_144866	Etf1	eukaryotic peptide chain release factor subunit
NM_194345	Fam160b2	family with sequence similarity 160, member B2
NM_015795	Fbxo16	F-box only protein 16
NM_008655	Gadd45b	growth arrest and DNA damage-inducible protein
NM_010815	Grap2	GRB2-related adaptor protein 2
NM_001013385	Grm4	metabotropic glutamate receptor 4
NM_010451	Hoxa2	homeobox protein Hox-A2
NM_010458	Hoxb3	homeobox protein Hox-B3
NM_138646	Hps4	Hermansky-Pudlak syndrome 4 protein homolog
NM_019508	Il17b	interleukin-17B precursor
NM_178257	Il22ra1	interleukin-22 receptor subunit alpha-1
NM_008916	Inpp5k	inositol polyphosphate 5-phosphatase K
NM_001163528	Itpripl1	inositol 1,4,5-triphosphate receptor-interacting
NM_008416	Junb	transcription factor jun-B
NM_021342	Kcne4	potassium voltage-gated channel subfamily E
NM_199364	Lzts1	leucine zipper putative tumor suppressor 1
NM_183195	Marveld1	putative MARVEL domain-containing protein 1
NM_010797	Mid1	midline-1
NM_010798	Mif	macrophage migration inhibitory factor
NM_021462	Mknk2	MAP kinase-interacting serine/threonine-protein
NM_010808	Mmp24	matrix metalloproteinase-24
NM_010849	Myc	myc proto-oncogene protein isoform a
NM_153136	Nudt18	nucleoside diphosphate-linked moiety X motif 18
NM_001025614	Otud7b	zinc finger, A20 domain containing 1
NM_148917	Pabpc4	polyadenylate-binding protein 4 isoform 2
NM_027995	Paqr7	membrane progestin receptor alpha
NM_011563	Prdx2	peroxiredoxin-2
NM_138659	Prpf8	pre-mRNA-processing-splicing factor 8
NM_175022	Prr12	proline rich 12
NM_177721	Ranbp6	ran-binding protein 6
NM_177572	Rimkla	ribosomal protein S6 modification-like protein
NM_030112	Rtf1	Paf1/RNA polymerase II complex component
NM_009113	S100a13	protein S100-A13
NM_009162	Scg5	neuroendocrine protein 7B2
NM_010831	Sik1	serine/threonine-protein kinase SIK1
NM_172892	Slc13a4	solute carrier family 13, member 4
NM_177243	Slc26a9	solute carrier family 26 member 9
NM_011988	Slc27a3	long-chain fatty acid transport protein 3
NM_031183	Sp6	transcription factor Sp6
NM_020564	Sult5a1	sulfotransferase family 5A, member 1
NM_008596	Sypl2	synaptophysin-like protein 2
NM_134023	Tbc1d10a	TBC1 domain family member 10A
NM_198020	Trmt1	N(2),N(2)-dimethylguanosine tRNA
NM_001077591	Tsks	testis-specific serine kinase substrate isoform
NM_011656	Tuft1	tuftelin
NM_019392	Tyro3	tyrosine-protein kinase receptor TYRO3
NM_198899	Uggt1	UDP-glucose:glycoprotein glucosyltransferase 1
NM_025407	Uqcrc1	cytochrome b-c1 complex subunit 1, mitochondrial
NM_011756	Zfp36	tristetraprolin
NM_028601	Zmiz2	zinc finger MIZ domain-containing protein 2
NM_026150	4921536K21Rik	hypothetical protein LOC67430
NR_029475	4930581F22Rik	
NM_001166394	4931428F04Rik	hypothetical protein LOC74356
NR_015459	4933431E20Rik	
NR_015497	9330133O14Rik	

EXONS

Transcript Name	Gene name	Gene Description
NM_033474	Arvcf	armadillo repeat protein deleted in
NM_030561	BC004004	hypothetical protein LOC80748
NM_020486	Bcam	basal cell adhesion molecule
NM_010238	Brd2	bromodomain-containing protein 2 isoform a
NM_017392	Celsr2	cadherin EGF LAG seven-pass G-type receptor 2
NM_012018	Cep110	centriolin
NM_013811	Dnahc8	dynein heavy chain 8, axonemal
NM_015794	Fbxl17	F-box/LRR-repeat protein 17
NM_001033312	Fbxl18	F-box and leucine-rich repeat protein 18
NM_001085549	Gm12824	UPF0632 protein A precursor
NM_001039472	Kif21b	kinesin-like protein KIF21B
NM_016693	Map3k6	mitogen-activated protein kinase kinase kinase
NM_001085373	Mcc	mutated in colorectal cancers isoform 1
NM_177855	Med12l	mediator of RNA polymerase II transcription
NM_011424	Ncor2	nuclear receptor corepressor 2
NM_030152	Nol3	nucleolar protein 3
NM_133947	Numa1	nuclear mitotic apparatus protein 1
NM_021512	Nup160	nuclear pore complex protein Nup160
NM_026936	Oxa1l	mitochondrial inner membrane protein OXA1L
NM_144920	Plekha5	phosphoinositol 3-phosphate-binding protein-2
NM_019688	Rapgef4	rap guanine nucleotide exchange factor 4
NM_146042	Rnf144b	E3 ubiquitin-protein ligase RNF144B
NM_028182	Sh2d4a	SH2 domain-containing protein 4A
NM_009195	Slc12a4	solute carrier family 12 member 4
NM_152808	Slc44a2	choline transporter-like protein 2 isoform 2
NM_001004468	Tacc2	transforming acidic coiled-coil-containing
NM_011547	Tcfap2a	transcription factor AP-2-alpha isoform a
NM_001081664	4833423E24Rik	fatty acid desaturase 2-like protein

INTRONS

Transcript Name	Gene name	Gene Description
NR_028376	A930004D18Rik	
NM_007378	Abca4	retinal-specific ATP-binding cassette
NM_008576	Abcc1	multidrug resistance-associated protein 1
NM_001103177	Ablim1	actin-binding LIM protein 1 isoform 2
NM_001164491	Ablim3	actin-binding LIM protein 3
NM_198895	Abr	active breakpoint cluster region-related protein
NM_175324	Acad11	acyl-CoA dehydrogenase family member 11
NM_207668	Acpp	prostatic acid phosphatase long isoform
NM_053178	Acsbg1	long-chain-fatty-acid--CoA ligase ACSBG1
NM_027976	Acsl5	long-chain-fatty-acid--CoA ligase 5
NM_134156	Actn1	alpha-actinin-1
NM_021895	Actn4	alpha-actinin-4
NR_021486	Adarb1	
NM_139153	Agap3	arf-GAP with GTPase, ANK repeat and PH
NM_146155	Ahdc1	AT-hook DNA-binding motif-containing protein 1
NM_198111	Akap6	A kinase (PRKA) anchor protein 6
NM_177859	Aknad1	AKNA domain containing 1
NM_178655	Ank2	ankyrin-2 isoform 2
NM_001081379	Ankrd11	ankyrin repeat domain 11
NM_001081139	Ankrd35	ankyrin repeat domain-containing protein 35
NM_007585	Anxa2	annexin A2
NM_001110211	Anxa6	annexin A6 isoform b
NM_175164	Arhgap26	rho GTPase-activating protein 26
NM_001130152	Arhgef1	rho guanine nucleotide exchange factor 1 isoform
NM_027871	Arhgef3	rho guanine nucleotide exchange factor 3
NM_001034858	Armc2	armadillo repeat-containing protein 2
NM_010026	Asap1	arf-GAP with SH3 domain, ANK repeat and PH
NM_025770	Atg10	ubiquitin-like-conjugating enzyme ATG10
NM_080640	Baalc	brain and acute leukemia cytoplasmic protein
NM_007521	Bach2	
NM_013800	Barx2	homeobox protein BarH-like 2
NM_172378	BC026439	prostaglandin-specific organic anion
NM_009954	Bcar1	breast cancer anti-estrogen resistance protein 1
NM_016707	Bcl11a	B-cell lymphoma/leukemia 11A isoform 1
NM_001079883	Bcl11b	B-cell lymphoma/leukemia 11B isoform a
NM_001081412	Bcr	breakpoint cluster region protein
NM_001039179	Bicd2	protein bicaudal D homolog 2 isoform 1
NM_172506	Boc	brother of CDO precursor
NM_028709	Btbd11	ankyrin repeat and BTB/POZ domain-containing
NM_025295	Btd	biotinidase
NM_181344	C1rl	complement C1r subcomponent-like protein
NM_020263	Cacna2d2	voltage-dependent calcium channel subunit
NM_001037099	Cacnb4	voltage-dependent L-type calcium channel subunit
NM_018883	Camkk1	calcium/calmodulin-dependent protein kinase
NM_007602	Capn5	calpain-5
NM_027195	Casz1	zinc finger protein castor homolog 1 isoform 2
NM_001161458	Cbfb	core-binding factor subunit beta isoform 4
NM_029212	Ccdc33	coiled-coil domain-containing protein 33 isoform
NM_029586	Ccdc46	coiled-coil domain-containing protein 46 isoform
NM_025689	Ccdc51	coiled-coil domain-containing protein 51
NM_001039150	Cd44	CD44 antigen isoform b precursor
NM_183016	Cdc42bpb	serine/threonine-protein kinase MRCK beta
NM_027219	Cdc42ep1	cdc42 effector protein 1
NM_009864	Cdh1	cadherin-1
NM_153599	Cdk8	cell division protein kinase 8
NM_173370	Cds1	phosphatidate cytidylyltransferase 1
NM_009886	Celsr1	cadherin EGF LAG seven-pass G-type receptor 1
NM_146019	Chd3	chromodomain helicase DNA binding protein 3
NM_027979	Chit1	chitotriosidase-1 precursor
NM_027928	Chst13	carbohydrate sulfotransferase 13
NM_019765	Clip1	CAP-Gly domain-containing linker protein 1
NM_030179	Clip4	CAP-Gly domain-containing linker protein 4
NM_029556	Clybl	citrate lyase subunit beta-like protein,
NM_001160211	Cnih3	protein cornichon homolog 3 isoform 2
NM_146105	Cnst	consortin
NM_139001	Cspg4	chondroitin sulfate proteoglycan 4 precursor
NM_198013	Cuedc1	CUE domain-containing protein 1 isoform 1
NM_009999	Cyp2b10	cytochrome P450 2B10 isoform 2
NM_007823	Cyp4b1	cytochrome P450 4B1
NM_001114125	Dab2ip	disabled homolog 2-interacting protein isoform
NM_010019	Dapk2	death-associated protein kinase 2
NM_027030	Dcps	scavenger mRNA-decapping enzyme DcpS
NM_007584	Ddr1	epithelial discoidin domain-containing receptor
NM_001159361	Dip2b	disco-interacting protein 2 homolog B isoform 1
NM_027712	Dlgap1	disks large-associated protein 1 isoform 2
NM_001163537	Dnajc5b	dnaJ homolog subfamily C member 5B
NM_027878	Dram1	DNA damage-regulated autophagy modulator protein
NM_023842	Dsp	desmoplakin
NM_019819	Dusp14	dual specificity protein phosphatase 14
NM_199307	Ece1	endothelin-converting enzyme 1
NM_001162425	Efna1	ephrin-A1 isoform 2
NM_007912	Egfr	epidermal growth factor receptor isoform 2
NM_172813	Enox1	ecto-NOX disulfide-thiol exchanger 1
NM_177304	Enpp6	ectonucleotide pyrophosphatase/phosphodiesterase
NM_007940	Ephx2	epoxide hydrolase 2
NM_001003817	Erbb2	receptor tyrosine-protein kinase erbB-2
NM_026170	Ergic1	endoplasmic reticulum-Golgi intermediate
NM_177775	Esyt3	extended synaptotagmin-3
NM_010162	Ext1	exostosin-1
NM_146119	Fam129b	niban-like protein 1
NM_153574	Fam13a	family with sequence similarity 13, member A1
NM_024244	Fam13c	hypothetical protein LOC71721 isoform 1

NM_177628	Fam167a	hypothetical protein LOC219148
NM_145570	Fam176a	transmembrane protein 166
NM_026062	Fam69a	family with sequence similarity 69, member A
NM_025850	Fank1	fibronectin type 3 and ankyrin repeat domains 1
NM_025386	Fbxo36	F-box only protein 36
NM_010206	Fgfr1	basic fibroblast growth factor receptor 1
NM_175276	Fhod3	FH1/FH2 domain-containing protein 3
NM_030163	Filip1l	
NM_021899	Foxj2	forkhead box protein J2
NM_199068	Foxk1	forkhead box protein K1
NM_019740	Foxo3	forkhead box protein O3
NM_053202	Foxp1	forkhead box protein P1 isoform 1
NM_145148	Frmd4b	FERM domain-containing protein 4B
NM_172887	Fry	furry homolog
NM_028194	Fryl	protein furry homolog-like
NM_173739	Galntl4	putative polypeptide
NM_011820	Ggt5	gamma-glutamyltransferase 5
NM_001081125	Gli2	GLI-Kruppel family member GLI2
NM_023120	Gnb1l	guanine nucleotide-binding protein subunit
NM_027694	Golga7b	Golgin subfamily A member 7B
NM_001081126	Gpr161	G-protein coupled receptor 161
NM_146072	Grik1	glutamate receptor, ionotropic kainate 1 isoform
NM_001145897	Gse1	genetic suppressor element 1 isoform 3
NM_207225	Hdac4	histone deacetylase 4
NM_010412	Hdac5	histone deacetylase 5 isoform 2
NM_010657	Hivep3	transcription factor HIVEP3
NM_001024720	Hmcn1	hemicentin 1
NM_001146323	Hps3	Hermansky-Pudlak syndrome 3 protein homolog
NM_183148	Iffo2	intermediate filament family orphan 2
NM_010513	Igf1r	insulin-like growth factor 1 receptor
NM_029646	Il34	interleukin-34 isoform 2
NM_001008700	Il4ra	interleukin-4 receptor subunit alpha precursor
NM_198411	Inf2	inverted formin-2
NM_001134383	Iqsec1	IQ motif and SEC7 domain-containing protein 1
NM_001126490	Ism1	isthmin-1 precursor
NM_013565	Itga3	integrin alpha-3
NM_001159564	Itgb6	integrin beta-6 precursor
NM_172471	Itih5	inter-alpha-trypsin inhibitor heavy chain H5
NM_022417	Itm2c	integral membrane protein 2C
NM_001081175	Itpkb	inositol-trisphosphate 3-kinase B
NM_181593	Itpkc	inositol-trisphosphate 3-kinase C
NM_010586	Itpr2	inositol 1,4,5-trisphosphate receptor type 2
NM_080553	Itpr3	inositol 1,4,5-trisphosphate receptor type 3
NM_021878	Jarid2	protein Jumonji
NM_010590	Jub	protein ajuba
NM_010593	Jup	junction plakoglobin
NM_020005	Kat2b	histone acetyltransferase KAT2B isoform 1
NM_001039056	Kcnj15	ATP-sensitive inward rectifier potassium channel
NM_029911	Kcnk10	potassium channel subfamily K member 10
NM_130867	Kirrel	kin of IRRE-like protein 1 precursor
NM_021366	Klf13	Krueppel-like factor 13
NM_008453	Klf3	Krueppel-like factor 3
NM_032396	Kremen1	kremen protein 1 precursor
NM_010680	Lama3	laminin subunit alpha-3
NM_008485	Lamc2	laminin subunit gamma-2
NM_173379	Leprel1	prolyl 3-hydroxylase 2 precursor
NM_008494	Lfng	beta-1,3-N-acetylglucosaminyltransferase lunatic
NM_010195	Lgr5	leucine-rich repeat-containing G-protein coupled
NM_172589	Lhfpl2	lipoma HMGIC fusion partner-like 2 protein
NM_010718	Limk2	LIM domain kinase 2 isoform a
NM_001111102	Lmna	prelamin-A/C isoform C
NM_022983	Lpar3	lysophosphatidic acid receptor 3
NM_001033439	Lrch1	leucine-rich repeat and calponin homology
NM_008377	Lrig1	leucine-rich repeats and immunoglobulin-like
NM_001170788	Lrrc36	leucine-rich repeat-containing protein 36
NM_175641	Ltbp4	latent-transforming growth factor beta-binding
NR_033304	Lypd6	
NM_009600	Macf1	microtubule-actin cross-linking factor 1
NM_001004176	Maml3	mastermind-like 3
NM_010789	Meis1	homeobox protein Meis1 isoform A
NM_027756	Mfap3l	microfibrillar-associated protein 3-like
NM_153396	Mical3	protein MICAL-3
NM_001113198	Mitf	microphthalmia-associated transcription factor
NM_029797	Mnd1	meiotic nuclear division protein 1 homolog
NM_001081100	Morn1	MORN repeat-containing protein 1
NM_021509	Moxd1	DBH-like monooxygenase protein 1 precursor
NM_080456	Mrps6	28S ribosomal protein S6, mitochondrial
NM_001043355	Mtap6	microtubule-associated protein 6 isoform 3
NM_008635	Mtap7	ensconsin isoform 1
NM_001008542	Mxi1	max-interacting protein 1 isoform b
NM_028021	Myh14	myosin-14
NM_181072	Myo1e	myosin IE
NM_010865	Myoc	myocilin precursor
NM_001113204	Ncam1	neural cell adhesion molecule 1 isoform 3
NM_178772	Nceh1	neutral cholesterol ester hydrolase 1
NM_019681	Ncs1	neuronal calcium sensor 1
NM_001111324	Nedd9	enhancer of filamentation 1 isoform 1
NM_021605	Nek7	serine/threonine-protein kinase Nek7
NM_001081656	Neurl1B	E3 ubiquitin-protein ligase NEURL1B
NM_001113210	Nfib	nuclear factor 1 B-type isoform 2
NM_008688	Nfic	nuclear factor 1 C-type isoform a
NM_010906	Nfix	nuclear factor 1 X-type isoform 2
NM_001112698	Ngf	beta-nerve growth factor isoform B
NM_001163592	Nhsl1	NHS-like protein 1 isoform 2
NM_001008421	Nol10	nucleolar protein 10

NM_008719	Npas2	neuronal PAS domain-containing protein 2
NM_001167891	Nrg2	pro-neuregulin-2, membrane-bound isoform
NM_001004363	Nuak1	NUAK family SNF1-like kinase 1
NM_028778	Nuak2	NUAK family SNF1-like kinase 2 isoform B
NM_008750	Nxn	nucleoredoxin
NM_008751	Nxph1	neurexophilin-1 precursor
NM_011856	Odz2	teneurin-2
NM_001033254	Pak6	serine/threonine-protein kinase PAK 6
NM_053117	Pard6g	partitioning defective 6 homolog gamma
NM_054056	Pawr	PRKC apoptosis WT1 regulator protein
NM_029357	Pcdh1	protocadherin-1
NM_001174154	Pcdha4-g	protocadherin alpha 4-gamma
NM_033584	Pcdhga1	protocadherin gamma-A1
NM_033593	Pcdhga10	protocadherin gamma-A10
NM_033594	Pcdhga11	protocadherin gamma-A11
NM_033595	Pcdhga12	protocadherin gamma subfamily A, 12
NM_033585	Pcdhga2	protocadherin gamma-A2
NM_033586	Pcdhga3	protocadherin gamma-A3
NM_033587	Pcdhga4	protocadherin gamma-A4
NM_033588	Pcdhga5	protocadherin gamma-A5
NM_033589	Pcdhga6	protocadherin gamma-A6
NM_033590	Pcdhga7	protocadherin gamma subfamily A, 7
NM_033591	Pcdhga8	protocadherin gamma subfamily A, 8
NM_033592	Pcdhga9	protocadherin gamma subfamily A, 9
NM_033574	Pcdhgb1	protocadherin gamma-B1
NM_033575	Pcdhgb2	protocadherin gamma-B2
NM_033576	Pcdhgb4	protocadherin gamma-B4
NM_033577	Pcdhgb5	protocadherin gamma-B5
NM_033578	Pcdhgb6	protocadherin gamma subfamily B, 6
NM_033579	Pcdhgb7	protocadherin gamma-B7
NM_033580	Pcdhgb8	protocadherin gamma subfamily B, 8
NM_011048	Pcsk6	paired basic amino acid cleaving system 4
NM_011057	Pdgfb	platelet-derived growth factor subunit B
NM_019417	Pdlim4	PDZ and LIM domain protein 4
NM_022554	Pdlim5	PDZ and LIM domain protein 5 isoform ENH3b
NM_001081064	Pdzd2	PDZ domain-containing protein 2
NM_001164594	Pdzrn4	PDZ domain containing RING finger 4 isoform 2
NM_019781	Pex14	peroxisomal membrane protein PEX14
NM_008841	Pik3r2	phosphatidylinositol 3-kinase regulatory subunit
NM_026880	Pink1	serine/threonine-protein kinase PINK1,
NM_145823	Pitpnc1	cytoplasmic phosphatidylinositol transfer
NM_013630	Pkd1	polycystin-1 precursor
NM_019645	Pkp1	plakophilin-1
NM_021280	Plcg1	1-phosphatidylinositol-4,5-bisphosphate
NM_172285	Plcg2	1-phosphatidylinositol-4,5-bisphosphate
NM_001114663	Plcl1	inactive phospholipase C-like protein 1
NM_008875	Pld1	phospholipase D1
NM_013738	Plek2	pleckstrin-2
NM_031257	Plekha2	pleckstrin homology domain-containing family A
NM_001033253	Plekhg1	pleckstrin homology domain containing, family G
NM_028199	Plxdc1	plexin domain-containing protein 1 isoform 2
NM_001039509	Pnkd	probable hydrolase PNKD isoform 3
NM_001034885	Pnpla1	patatin-like phospholipase domain-containing
NM_176833	Ppm1f	protein phosphatase 1F
NM_001135001	Ppp2r5c	serine/threonine-protein phosphatase 2A 56 kDa
NM_011155	Ppp5c	serine/threonine-protein phosphatase 5
NM_001134460	Prickle2	prickle-like protein 2 isoform b
NM_011101	Prkca	protein kinase C alpha type
NM_008856	Prkch	protein kinase C eta type
NM_008983	Ptprk	receptor-type tyrosine-protein phosphatase kappa
NM_011215	Ptprn2	receptor-type tyrosine-protein phosphatase N2
NM_011218	Ptprs	receptor-type tyrosine-protein phosphatase S
NR_003368	Pvt1	
NM_009014	Rad51l1	DNA repair protein RAD51 homolog 2
NM_001166408	Rai14	ankycorbin
NM_001145834	Ralgds	ral guanine nucleotide dissociation stimulator
NM_001039087	Rapgef1	Rap guanine nucleotide exchange factor (GEF) 1
NM_001080925	Rapgefl1	rap guanine nucleotide exchange factor-like 1
NM_001172122	Rbms3	RNA-binding motif, single-stranded-interacting
NM_001081549	Rcan1	calcipressin-1 isoform 1
NM_007874	Reep5	receptor expression-enhancing protein 5
NM_001085492	Rere	arginine-glutamic acid dipeptide repeats
NM_028713	Rftn2	raftlin-2
NM_177740	Rgma	repulsive guidance molecule A precursor
NM_173402	Rgs12	regulator of G-protein signalling 12 isoform A
NM_013646	Rora	nuclear receptor ROR-alpha
NM_146246	Rp1l1	retinitis pigmentosa 1-like 1 protein
NM_026830	Rreb1	ras-responsive element-binding protein 1 isoform
NM_009821	Runx1	runt-related transcription factor 1 isoform 4
NM_177225	Samd12	sterile alpha motif domain-containing protein
NM_175021	Samd4b	protein Smaug homolog 2
NM_175155	Sash1	SAM and SH3 domain-containing protein 1
NM_022886	Scel	sciellin
NM_013883	Scmh1	polycomb protein SCMH1 isoform 1
NM_011519	Sdc1	syndecan-1 precursor
NM_011521	Sdc4	syndecan-4 precursor
NM_172800	Sdk2	protein sidekick-2 precursor
NM_011349	Sema3f	semaphorin-3F
NM_009154	Sema5a	semaphorin-5A
NM_001113486	Septin9	septin-9 isoform a
NM_026535	Serpina12	serpin A12 precursor
NM_198247	Sertad4	SERTA domain-containing protein 4
NM_001162908	Sesn1	sestrin-1 isoform 1
NM_053099	Setbp1	SET-binding protein
NM_028385	Setd5	SET domain-containing protein 5

NM_013834	Sfrp1	secreted frizzled-related protein 1 precursor
NM_133220	Sgk3	serine/threonine-protein kinase Sgk3
NM_011893	Sh3bp2	SH3 domain-binding protein 2 isoform a
NM_133816	Sh3bp4	SH3 domain-binding protein 4
NM_177364	Sh3pxd2b	SH3 and PX domain-containing protein 2B
NM_001146299	Sh3rf2	putative E3 ubiquitin-protein ligase SH3RF2
NM_001113373	Shank2	SH3 and multiple ankyrin repeat domains protein
NM_011385	Ski	ski oncogene
NM_207651	Slc14a2	urea transporter 2 isoform a
NM_026244	Slc39a9	zinc transporter ZIP9
NM_009209	Slc6a2	sodium-dependent noradrenaline transporter
NM_178798	Slc7a6	Y+L amino acid transporter 2
NM_008542	Smad6	mothers against decapentaplegic homolog 6
NM_022315	Smoc2	SPARC-related modular calcium-binding protein 2
NM_178362	Sorbs1	sorbin and SH3 domain-containing protein 1
NM_030889	Sorcs2	VPS10 domain-containing receptor SorCS2
NM_001025560	Sox6	transcription factor SOX-6 isoform 3
NM_001144987	Spg20	spartin isoform a
NM_001166463	Spock1	testican-1 isoform 3 precursor
NM_145134	Spsb4	SPRY domain-containing SOCS box protein 4
NM_009177	St3gal1	CMP-N-acetylneuraminate-beta-galactosamide-
NM_145465	Stk24	serine/threonine-protein kinase 24
NM_029858	Ston1	stonin-1
NM_028072	Sulf2	extracellular sulfatase Sulf-2 precursor
NM_178046	Svil	
NM_018802	Syt8	synaptotagmin-8
NM_001166584	Tead1	transcriptional enhancer factor TEF-1 isoform 1
NM_011566	Tead3	transcriptional enhancer factor TEF-5 isoform 2
NM_001080979	Tead4	transcriptional enhancer factor TEF-3 isoform b
NM_001113464	Tec	tyrosine-protein kinase Tec isoform a
NM_001099275	Tekt5	tektin-5
NM_031199	Tgfa	protransforming growth factor alpha
NM_178060	Thra	thyroid hormone receptor alpha
NM_009384	Tiam1	T-lymphoma invasion and metastasis-inducing
NM_011594	Timp2	metalloproteinase inhibitor 2 precursor
NM_027154	Tmbim1	transmembrane BAX inhibitor motif-containing
NM_178874	Tmcc2	transmembrane and coiled-coil domains protein 2
NM_019631	Tmem45a	transmembrane protein 45A
NM_011609	Tnfrsf1a	tumor necrosis factor receptor superfamily
NM_027884	Tns1	tensin 1
NM_001083587	Tns3	tensin-3
NM_172564	Tns4	tensin-4 precursor
NM_175165	Tprg	tumor protein p63-regulated gene 1 protein
NM_013718	Trappc3	trafficking protein particle complex subunit 3
NM_023655	Trim29	tripartite motif-containing protein 29
NM_001127262	Trp63	tumor protein 63 isoform f
NM_022017	Trpv4	transient receptor potential cation channel
NM_175414	Tspan9	tetraspanin-9
NM_026132	Txndc8	thioredoxin domain-containing protein 8
NM_001160319	Ubr4	E3 ubiquitin-protein ligase UBR4
NM_016808	Usp2	ubiquitin carboxyl-terminal hydrolase 2 isoform
NM_030180	Usp54	inactive ubiquitin carboxyl-terminal hydrolase
NM_177387	Ust	uronyl 2-sulfotransferase
NM_020505	Vav3	guanine nucleotide exchange factor VAV3 isoform
NM_009504	Vdr	vitamin D3 receptor
NM_177683	Vgll4	transcription cofactor vestigial-like protein 4
NM_026664	Vps53	vacuolar protein sorting-associated protein 53
NM_012038	Vsnl1	visinin-like protein 1
NM_028640	Whrn	whirlin isoform 1
NM_212438	Wiz	protein Wiz isoform 1
NM_009523	Wnt4	protein Wnt-4 precursor
NM_019573	Wwox	WW domain-containing oxidoreductase
NM_207255	Zfp532	zinc finger protein 532
NM_177086	Zmat4	zinc finger matrin-type protein 4
NM_027230	Zmynd8	protein kinase C-binding protein 1
NM_001168622	Znrf1	E3 ubiquitin-protein ligase ZNRF1 isoform b
NM_028275	1700112E06Rik	leucine-rich repeat-containing protein C10orf11
NM_025599	2610528E23Rik	hypothetical protein LOC66497
NM_172884	2900026A02Rik	hypothetical protein LOC243219
NM_028473	3110079O15Rik	hypothetical protein LOC73234 precursor
NM_028732	4632428N05Rik	platelet receptor Gi24 isoform 1 precursor
NM_026359	4930578I06Rik	hypothetical protein LOC67750
NM_178682	4933426M11Rik	hypothetical protein LOC217684
NM_178801	6030446N20Rik	transmembrane protein C18orf45 homolog
NM_145448	9030617O03Rik	hypothetical protein LOC217830 precursor

PROXIMAL (2-50kb)

Transcript Name	Gene name	Gene Description
NM_183188	A2bp1	fox-1 homolog A isoform alpha
NM_145415	AA408296	digestive organ expansion factor homolog
NM_013454	Abca1	ATP-binding cassette sub-family A member 1
NM_172678	Acad9	acyl-CoA dehydrogenase family member 9,
NM_023735	Actr3	actin-related protein 3
NM_144899	Adamtsl4	ADAMTS-like protein 4 precursor
NM_133919	Aff1	AF4/FMR2 family member 1 isoform 2
NM_145566	Agfg2	arf-GAP domain and FG repeats-containing protein
NR_024189	AI837181	
NM_172645	AI848100	AI848100
NM_172393	Aim1	absent in melanoma 1 protein
NM_029332	Akap13	A kinase (PRKA) anchor protein 13
NM_007436	Aldh3a1	aldehyde dehydrogenase, dimeric NADP-preferring
NM_009663	Alox5ap	arachidonate 5-lipoxygenase-activating protein
NM_019764	Amotl2	angiomotin-like protein 2
NM_144524	Angel1	protein angel homolog 1
NM_009670	Ank3	ankyrin 3, epithelial isoform g
NM_153589	Ano2	anoctamin-2
NM_133237	Apcdd1	protein APCDD1 precursor
NM_007473	Aqp7	aquaporin-7
NM_013476	Ar	androgen receptor
NM_133674	Arhgef5	Rho guanine nucleotide exchange factor (GEF) 5
NM_001085355	Arid1b	AT rich interactive domain 1B (Swi1 like)
NM_007494	Ass1	argininosuccinate synthase
NM_026402	Atg3	ubiquitin-like-conjugating enzyme ATG3
NM_053069	Atg5	autophagy protein 5
NM_144900	Atp1a1	sodium/potassium-transporting ATPase subunit
NM_213616	Atp2b4	plasma membrane calcium ATPase 4 isoform x/e
NM_026468	Atp5g2	ATP synthase lipid-binding protein,
NM_016843	Atxn10	ataxin-10
NR_028382	B230319C09Rik	
NM_177897	B4galnt4	N-acetyl-beta-glucosaminyl-glycoprotein
NM_007520	Bach1	transcription regulator protein BACH1
NM_013863	Bag3	BAG family molecular chaperone regulator 3
NM_001044750	Banf2	barrier-to-autointegration factor-like protein
NR_027893	BB123696	
NR_024085	BC006965	
NM_145601	BC016201	cDNA sequence BC016201 isoform 2
NM_145972	BC027231	hypothetical protein LOC212547
NM_173022	BC048403	hypothetical protein LOC270802
NM_001164369	Bcas1	breast carcinoma-amplified sequence 1 homolog
NM_207681	Bcl2l11	bcl-2-like protein 11 isoform 2
NM_030256	Bcl9l	B-cell CLL/lymphoma 9-like protein
NM_199028	Bend3	BEN domain-containing protein 3
NM_007556	Bmp6	bone morphogenetic protein 6 precursor
NM_007559	Bmp8b	bone morphogenetic protein 8B precursor
NM_009758	Bmpr1a	bone morphogenetic protein receptor type-1A
NM_007562	Bnc1	zinc finger protein basonuclin-1
NM_172870	Bnc2	zinc finger protein basonuclin-2
NM_027453	Btf3l4	transcription factor BTF3 homolog 4
NM_177584	Btla	B- and T-lymphocyte attenuator isoform 2
NR_015546	C130026L21Rik	
NM_198037	Cachd1	VWFA and cache domain-containing protein 1
NM_001008706	Calm5	calmodulin 5
NM_027416	Calml3	calmodulin-like protein 3
NM_144817	Camk1g	calcium/calmodulin-dependent protein kinase type
NM_001039139	Camk2g	calcium/calmodulin-dependent protein kinase type
NM_145595	Cbr4	carbonyl reductase family member 4
NM_175369	Ccdc122	coiled-coil domain-containing protein 122
NM_007631	Ccnd1	G1/S-specific cyclin-D1
NM_007635	Ccng2	cyclin-G2
NM_019937	Ccnl1	cyclin-L1
NM_007719	Ccr7	C-C chemokine receptor type 7 precursor
NM_153098	Cd109	CD109 antigen precursor
NM_010818	Cd200	OX-2 membrane glycoprotein precursor
NM_001111059	Cd34	hematopoietic progenitor cell antigen CD34
NM_001033122	Cd69	early activation antigen CD69
NM_009856	Cd83	CD83 antigen precursor
NM_007657	Cd9	CD9 antigen
NM_007658	Cdc25a	M-phase inducer phosphatase 1
NM_001033373	Cdk15	cell division protein kinase 15
NM_008795	Cdk18	cell division protein kinase 18
NM_001111099	Cdkn1a	cyclin-dependent kinase inhibitor 1
NM_009884	Cebpg	CCAAT/enhancer-binding protein gamma
NM_145475	Cerk	ceramide kinase
NM_172759	Ces5	carboxylesterase 5
NM_001081345	Chd2	chromodomain helicase DNA binding protein 2
NM_001081417	Chd7	chromodomain-helicase-DNA-binding protein 7
NM_027882	Cic	protein capicua homolog isoform a
NM_010828	Cited2	cbp/p300-interacting transactivator 2
NM_175451	Ckap4	cytoskeleton-associated protein 4
NM_171826	Cldnd1	claudin domain-containing protein 1
NM_013748	Clnk	cytokine-dependent hematopoietic cell linker
NM_027294	Cmtm8	CKLF-like MARVEL transmembrane domain-containing
NM_033570	Cnnm4	metal transporter CNNM4
NM_009931	Col4a1	collagen alpha-1(IV) chain precursor
NM_027904	Cpn2	carboxypeptidase N subunit 2
NM_007759	Crabp2	cellular retinoic acid-binding protein 2
NM_015800	Crim1	cysteine-rich motor neuron 1 protein precursor
NM_024223	Crip2	cysteine-rich protein 2
NM_146087	Csnk1a1	casein kinase I isoform alpha
NM_007791	Csrp1	cysteine and glycine-rich protein 1

NM_133710	Ctdspl	CTD small phosphatase-like protein
NM_023465	Ctnnbip1	beta-catenin-interacting protein 1
NM_019568	Cxcl14	C-X-C motif chemokine 14 precursor
NM_007722	Cxcr7	C-X-C chemokine receptor type 7
NM_025558	Cyb5b	cytochrome b5 type B precursor
NM_029787	Cyb5r3	NADH-cytochrome b5 reductase 3
NM_007814	Cyp2b19	cytochrome P450 2B19
NM_001101478	D3Ertd254e	hypothetical protein LOC241944
NM_026102	Daam1	disheveled-associated activator of morphogenesis
NM_029723	Dapl1	death-associated protein-like 1
NM_207533	Dbx2	developing brain homeobox 2
NM_178896	Dcun1d4	DCN1-like protein 4 isoform B
NM_026993	Ddah1	N(G),N(G)-dimethylarginine
NM_007916	Ddx19a	ATP-dependent RNA helicase DDX19A
NM_007853	Degs1	sphingolipid delta(4)-desaturase DES1
NM_024440	Derl3	derlin-3
NM_015814	Dkk3	dickkopf-related protein 3 precursor
NM_007865	Dll1	delta-like protein 1 precursor
NM_001081371	Dmxl1	dmX-like protein 1
NM_018808	Dnajb1	dnaJ homolog subfamily B member 1
NM_020266	Dnajb2	dnaJ homolog subfamily B member 2 isoform 1
NM_019759	Dpt	dermatopontin precursor
NM_181680	Dsg1c	desmoglein-1-gamma precursor
NR_015511	E030011O05Rik	
NR_015614	E230029C05Rik	
NM_010332	Ednra	endothelin-1 receptor precursor
NM_007910	Efna4	ephrin-A4 precursor
NM_178444	Egfl7	epidermal growth factor-like protein 7 isoform 1
NM_145139	Eif3l	eukaryotic translation initiation factor 3
NM_145625	Eif4b	eukaryotic translation initiation factor 4B
NM_023479	Elac2	zinc phosphodiesterase ELAC protein 2
NM_148941	Elovl4	elongation of very long chain fatty acids
NM_134255	Elovl5	elongation of very long chain fatty acids
NM_023119	Eno1	alpha-enolase
NM_019427	Epb4.1l4b	band 4.1-like protein 4B
NM_010143	Ephb3	ephrin type-B receptor 3 precursor
NM_026067	Eri1	3'-5' exoribonuclease 1
NM_133753	Errfi1	ERBB receptor feedback inhibitor 1
NM_011809	Ets2	protein C-ets-2
NM_010165	Eya2	eyes absent homolog 2
NM_172647	F11r	junctional adhesion molecule A precursor
NM_010171	F3	tissue factor precursor
NM_178764	Fam168a	hypothetical protein LOC319604
NM_175514	Fam171b	family with sequence similarity 171, member B
NM_138746	Fam50b	DNA segment, human D6S2654E
NM_026143	Far1	fatty acyl-CoA reductase 1
NM_175127	Fbxo28	F-box only protein 28
NM_010193	Fem1b	protein fem-1 homolog B
NM_010197	Fgf1	heparin-binding growth factor 1 precursor
NM_008010	Fgfr3	fibroblast growth factor receptor 3 isoform 1
NM_001033301	Fhdc1	FH2 domain-containing protein 1
NM_018881	Fmo2	dimethylaniline monooxygenase [N-oxide-forming]
NM_010234	Fos	proto-oncogene c-Fos
NM_008037	Fosl2	fos-related antigen 2
NM_183298	Foxe1	forkhead box protein E1
NM_194060	Foxo6	forkhead box protein O6
NM_013522	Frg1	protein FRG1
NM_028127	Frmd6	FERM domain-containing protein 6
NM_016893	Fut8	alpha-(1,6)-fucosyltransferase
NM_020510	Fzd2	frizzled-2 precursor
NM_008086	Gas1	growth arrest-specific protein 1
NM_008091	Gata3	trans-acting T-cell-specific transcription
NM_153564	Gbp5	guanylate-binding protein 5
NM_010276	Gem	GTP-binding protein GEM
NM_010279	Gfra1	GDNF family receptor alpha-1 precursor
NM_020014	Gfra4	GDNF family receptor alpha-4 isoform 2
NM_008130	Gli3	zinc finger protein GLI3
NR_027829	Gm10638	
NR_026944	Gm10941	
NR_015474	Gm14047	
NM_001127576	Gm1564	hypothetical protein LOC268491
NM_201366	Gm1631	hypothetical protein LOC381371
NM_001033403	Gm1968	hypothetical protein LOC328657
NR_028424	Gm2176	
NM_001033333	Gm239	hypothetical protein LOC237558
NM_198657	Gm5148	hypothetical protein LOC381438
NM_001101609	Gm9376	hypothetical protein LOC668814
NM_001042672	Gpcpd1	putative glycerophosphocholine phosphodiesterase
NM_133776	Gpr110	G-protein coupled receptor 110 precursor
NM_001033493	Gpr111	G protein-coupled receptor 111
NM_019925	Gpr132	probable G-protein coupled receptor 132
NM_177366	Gpr157	probable G-protein coupled receptor 157
NM_181444	Gprc5a	retinoic acid-induced protein 3
NM_183209	Gprin2	G protein-regulated inducer of neurite outgrowth
NM_001033498	Gramd2	GRAM domain-containing protein 2
NM_019518	Grasp	general receptor for phosphoinositides
NM_001033426	Grxcr2	glutaredoxin domain-containing cysteine-rich
NM_146120	Gsn	gelsolin precursor
NM_001080746	Gtf2i	general transcription factor II-I isoform 1
NM_010376	H13	minor histocompatibility antigen H13 isoform 2
NM_175000	Hbq1	hemoglobin, theta T2
NM_145567	Hibadh	3-hydroxyisobutyrate dehydrogenase,
NM_010431	Hif1a	hypoxia-inducible factor 1-alpha
NM_025812	Hmg20a	high mobility group protein 20A
NM_010439	Hmgb1	high mobility group protein B1

NM_053263	Hnrnpa3	heterogeneous nuclear ribonucleoprotein A3
NM_175606	Hopx	homeodomain-only protein
NM_008266	Hoxb1	homeobox protein Hox-B1
NM_016677	Hpcal1	hippocalcin-like protein 1
NM_021429	Hs1bp3	HCLS1-binding protein 3
NM_010480	Hsp90aa1	heat shock protein HSP 90-alpha
NM_010479	Hspa1a	heat shock 70 kDa protein 1A
NM_031166	Id4	DNA-binding protein inhibitor ID-4
NM_008329	Ifi204	interferon-activable protein 204
NM_009879	Ift81	intraflagellar transport protein 81 homolog
NM_001122737	Igf2	insulin-like growth factor II isoform 2
NM_010518	Igfbp5	insulin-like growth factor-binding protein 5
NM_010550	Il11ra2	interleukin-11 receptor subunit alpha-2
NM_001127363	Inpp5a	inositol polyphosphate-5-phosphatase A isoform
NM_016721	Iqgap1	ras GTPase-activating-like protein IQGAP1
NM_001164598	Irf2bp2	interferon regulatory factor 2 binding protein
NM_015783	Isg15	ubiquitin-like protein ISG15 precursor
NM_008410	Itm2b	integral membrane protein 2B
NM_001033380	Itpripl2	inositol 1,4,5-triphosphate receptor-interacting
NM_027391	Iyd	iodotyrosine dehalogenase 1 precursor
NM_010592	Jund	transcription factor jun-D
NM_001081140	Kcna10	potassium voltage-gated channel subfamily A
NM_025734	Kcng4	potassium voltage-gated channel subfamily G
NR_027627	Kcnk2	
NM_001097621	Kif26a	kinesin-like protein KIF26A
NM_178357	Klf11	Krueppel-like factor 11
NM_023184	Klf15	Krueppel-like factor 15
NM_010637	Klf4	Krueppel-like factor 4
NM_011803	Klf6	Krueppel-like factor 6
NM_010638	Klf9	Krueppel-like factor 9
NM_001039042	Klk13	kallikrein 13 precursor
NM_001159374	Krt32	keratin, type I cuticular Ha2
NM_212483	Krt42	keratin, type I cytoskeletal 42
NM_008476	Krt6a	keratin, type II cytoskeletal 6A
NM_212487	Krt78	keratin Kb40
NM_031170	Krt8	keratin, type II cytoskeletal 8
NM_008477	Ktn1	kinectin
NM_008640	Laptm4a	lysosomal-associated transmembrane protein 4A
NM_010691	Lbx1	transcription factor LBX1
NM_010699	Ldha	L-lactate dehydrogenase A chain isoform 1
NM_001081272	Ldlrad1	low-density lipoprotein receptor class A
NM_178886	Ldlrad3	low-density lipoprotein receptor class A
NM_145554	Ldlrap1	low density lipoprotein receptor adapter protein
NM_027042	Lelp1	late cornified envelope-like proline-rich
NM_001083188	Lig1	DNA ligase 1
NM_019980	Litaf	lipopolysaccharide-induced tumor necrosis
NM_001081150	Lonrf1	LON peptidase N-terminal domain and RING finger
NM_178665	Lpp	lipoma-preferred partner homolog isoform 1
NM_153542	Lrrc20	leucine-rich repeat-containing protein 20
NM_026309	Lsm3	U6 snRNA-associated Sm-like protein LSm3
NM_026915	Lyzl4	lysozyme-like protein 4 precursor
NM_001013813	Maml2	mastermind like 2 isoform 1
NM_145569	Mat2a	S-adenosylmethionine synthase isoform type-2
NM_001081160	Mdga1	MAM domain-containing
NM_172424	Med13l	mediator of RNA polymerase II transcription
NM_026039	Med18	mediator of RNA polymerase II transcription
NM_026119	Med4	mediator of RNA polymerase II transcription
NM_153749	Mill1	MHC I like leukocyte 1
NR_029567	Mir129-1	
NR_029587	Mir200b	
NR_029592	Mir205	
NR_029773	Mir345	
NR_030491	Mir710	
NR_030439	Mir760	
NM_008626	Mrc2	C-type mannose receptor 2 precursor
NM_025796	Mrpl33	39S ribosomal protein L33, mitochondrial
NM_025927	Mrpl45	39S ribosomal protein L45, mitochondrial
NM_023331	Mrpl46	39S ribosomal protein L46, mitochondrial
NM_001024917	N4bp2	Nedd4 binding protein 2
NM_194335	Naif1	nuclear apoptosis-inducing factor 1
NM_008675	Nbl1	neuroblastoma suppressor of tumorigenicity 1
NM_025424	Nenf	neudesin precursor
NM_001047159	Net1	neuroepithelial cell-transforming gene 1 protein
NM_010903	Nfe2l3	nuclear factor erythroid 2-related factor 3
NM_017373	Nfil3	nuclear factor interleukin-3-regulated protein
NM_008689	Nfkb1	nuclear factor NF-kappa-B p105 subunit
NM_001109985	Nos1ap	carboxyl-terminal PDZ ligand of neuronal nitric
NM_001163504	Nr1h4	bile acid receptor isoform 2
NM_008173	Nr3c1	glucocorticoid receptor
NM_001036293	Nrbf2	nuclear receptor-binding factor 2
NM_019761	Nxt1	NTF2-related export protein 1
NM_145153	Oas1f	2'-5'oligoadenylate synthetase 1F
NM_175360	Obfc1	CST complex subunit STN1
NM_008757	Odf1	outer dense fiber protein 1
NM_172143	Ofcc1	orofacial cleft 1 candidate gene 1 protein
NM_052976	Ophn1	oligophrenin-1
NM_007538	Opn1sw	blue-sensitive opsin
NM_144500	Osbpl2	oxysterol-binding protein-related protein 2
NM_027950	Osgin1	oxidative stress-induced growth inhibitor 1
NM_001159509	Pacsin2	protein kinase C and casein kinase substrate in
NM_145962	Pank3	pantothenate kinase 3
NM_029595	Pbp2	phosphatidylethanolamine-binding protein 2
NM_018814	Pcnx	pecanex-like protein 1
NM_016798	Pdlim3	PDZ and LIM domain protein 3
NM_018884	Pdzrn3	E3 ubiquitin-protein ligase PDZRN3

NM_033602	Peli2	protein pellino homolog 2
NM_011065	Per1	period circadian protein homolog 1
NM_001042407	Pex10	peroxisome biogenesis factor 10
NM_133232	Pfkfb3	6-phosphofructo-2-kinase/fructose-2,
NM_019703	Pfkp	6-phosphofructokinase type C
NM_008831	Phb	prohibitin
NM_007905	Phc1	polyhomeotic-like protein 1 isoform a
NM_013750	Phlda3	pleckstrin homology-like domain family A member
NM_133821	Phlpp1	PH domain leucine-rich repeat-containing protein
NM_026078	Pigc	phosphatidylinositol
NM_013784	Pign	GPI ethanolamine phosphate transferase 1
NM_029094	Pik3cb	phosphatidylinositol-4,5-bisphosphate 3-kinase
NM_001146200	Pik3cg	phosphatidylinositol-4,5-bisphosphate 3-kinase
NM_177905	Piwil4	piwi-like protein 4
NM_001164203	Plec	plectin isoform 1hij
NM_153804	Plekhg3	pleckstrin homology domain-containing family G
NM_008882	Plxna2	plexin-A2 precursor
NM_011141	Pou3f1	POU domain, class 3, transcription factor 1
NM_008904	Ppargc1a	peroxisome proliferator-activated receptor gamma
NM_008909	Ppl	periplakin
NM_133485	Ppp1r14c	protein phosphatase 1 regulatory subunit 14C
NM_133819	Ppp1r15b	protein phosphatase 1 regulatory subunit 15B
NM_016854	Ppp1r3c	protein phosphatase 1 regulatory subunit 3C
NM_001161362	Ppp2r3a	protein phosphatase 2, regulatory subunit B",
NM_011103	Prkcd	protein kinase C delta type
NM_008859	Prkcq	protein kinase C theta type
NM_011170	Prnp	major prion protein precursor
NM_001128605	Psen2	presenilin-2
NM_011968	Psma6	proteasome subunit alpha type-6
NM_022415	Ptges	prostaglandin E synthase
NM_001130409	Ptk2	focal adhesion kinase 1 isoform 2
NM_008977	Ptpn2	tyrosine-protein phosphatase non-receptor type 2
NM_001160221	Pum2	pumilio homolog 2 isoform 2
NM_001033206	Pwwp2b	PWWP domain containing 2 isoform 2
NM_001033267	Qrich2	glutamine rich 2
NM_153559	Qsox2	sulfhydryl oxidase 2
NM_016676	Rab10	ras-related protein Rab-10
NM_009003	Rab4a	ras-related protein Rab-4A
NM_145510	Rabif	guanine nucleotide exchange factor MSS4
NM_009021	Rai1	retinoic acid-induced protein 1
NM_022327	Ralb	ras-related protein Ral-B precursor
NM_011244	Rarg	retinoic acid receptor gamma isoform 1
NM_138956	Rassf3	ras association domain-containing protein 3
NM_009826	Rb1cc1	RB1-inducible coiled-coil protein 1
NM_145923	Rell1	RELT-like protein 1 precursor
NM_026380	Rgs8	regulator of G-protein signaling 8
NM_139228	Rhbdl3	rhomboid-related protein 3
NM_007483	Rhob	rho-related GTP-binding protein RhoB precursor
NM_026357	Ribc2	RIB43A-like with coiled-coils protein 2
NM_177158	Rinl	ras and Rab interactor-like protein
NM_024242	Riok1	serine/threonine-protein kinase RIO1
NM_001162863	Rnase10	ribonuclease-like protein 10 isoform 2
NM_013846	Ror2	tyrosine-protein kinase transmembrane receptor
NM_026533	Rps13	40S ribosomal protein S13
NM_019924	Rps6ka4	ribosomal protein S6 kinase alpha-4
NM_028040	Rpusd4	RNA pseudouridylate synthase domain-containing
NM_009104	Rrm2	ribonucleoside-diphosphate reductase subunit M2
NM_019743	Rybp	RING1 and YY1-binding protein
NM_016741	Scarb1	scavenger receptor class B member 1
NM_011325	Scnn1b	amiloride-sensitive sodium channel subunit beta
NM_011348	Sema3e	semaphorin-3E precursor
NM_023475	Serhl	serine hydrolase-like protein
NM_008458	Serpina3c	serine protease inhibitor A3C precursor
NM_018754	Sfn	14-3-3 protein sigma
NM_001136080	Sgca	alpha-sarcoglycan isoform 1
NM_001161845	Sgk1	serine/threonine-protein kinase Sgk1 isoform a
NM_027921	Slc16a14	monocarboxylate transporter 14
NM_011395	Slc22a3	solute carrier family 22 member 3
NM_018824	Slc23a2	solute carrier family 23 member 2
NM_022880	Slc29a1	equilibrative nucleoside transporter 1 isoform
NM_011400	Slc2a1	solute carrier family 2, facilitated glucose
NM_009579	Slc30a1	zinc transporter 1
NM_028123	Slc37a3	sugar phosphate exchanger 3
NM_027052	Slc38a4	sodium-coupled neutral amino acid transporter 4
NM_009320	Slc6a6	sodium- and chloride-dependent taurine
NM_007513	Slc7a1	high affinity cationic amino acid transporter 1
NM_029949	Snapc3	snRNA-activating protein complex subunit 3
NM_175483	Snx33	sorting nexin-33
NM_007707	Socs3	suppressor of cytokine signaling 3
NM_011434	Sod1	superoxide dismutase [Cu-Zn]
NM_172752	Sorbs2	sorbin and SH3 domain-containing protein 2
NM_025312	Sostdc1	sclerostin domain-containing protein 1
NM_009242	Sparc	SPARC precursor
NM_027609	Speer4f	spermatogenesis associated glutamate (E)-rich
NM_001164140	Spert	spermatid-associated protein isoform 4
NM_183284	Spink2	serine protease inhibitor Kazal-type 2
NM_029012	Sppl3	signal peptide peptidase-like 3
NM_001025395	Src	neuronal proto-oncogene tyrosine-protein kinase
NM_012058	Srp9	signal recognition particle 9 kDa protein
NM_021403	Srrm3	serine/arginine repetitive matrix protein 3
NM_010656	Sspn	sarcospan
NM_009182	St8sia3	sia-alpha-2,3-Gal-beta-1,4-GlcNAc-R:alpha
NM_025288	Stfa3	stefin-3
NM_138649	Syt17	synaptotagmin-17
NM_031394	Sytl2	synaptotagmin-like protein 2 isoform 3

NM_001040435	Tacc3	transforming acidic coiled-coil-containing
NM_011530	Tap2	antigen peptide transporter 2
NM_001159907	Tarbp1	TAR (HIV-1) RNA binding protein 1
NM_172310	Tarsl2	probable threonyl-tRNA synthetase 2,
NM_175225	Tasp1	threonine aspartase 1 isoform a
NM_019636	Tbc1d1	TBC1 domain family member 1
NM_001163455	Tbck	TBC domain-containing protein kinase-like
NM_011544	Tcf12	transcription factor 12
NM_031182	Tcfap4	transcription factor AP-4
NM_023755	Tcfcp2l1	transcription factor CP2-like protein 1
NM_172605	Tdrd3	tudor domain-containing protein 3
NM_011902	Tekt2	tektin-2
NM_009357	Tex261	protein TEX261
NM_177588	Thnsl1	threonine synthase-like 1 isoform a
NM_011597	Tjp2	tight junction protein ZO-2 isoform 2
NM_019725	Tle2	transducin-like enhancer protein 2
NM_025453	Tm4sf20	transmembrane 4 L6 family member 20
NM_172051	Tmcc3	transmembrane and coiled-coil domains protein 3
NM_028336	Tmem107	transmembrane protein 107 isoform 2
NM_018872	Tmem131	transmembrane protein 131
NM_177260	Tmem154	transmembrane protein 154 precursor
NM_001081283	Tmem28	transmembrane protein FAM155B
NM_001163172	Tmem92	transmembrane protein 92 isoform 1
NM_198967	Tmtc1	transmembrane and TPR repeat-containing protein
NM_011607	Tnc	tenascin
NM_009397	Tnfaip3	tumor necrosis factor alpha-induced protein 3
NM_001159503	Tnfsf12-Tnfsf13	tumor necrosis factor (ligand) superfamily,
NM_001110147	Tnk2	activated CDC42 kinase 1 isoform 2
NM_001130180	Tnnt2	troponin T, cardiac muscle isoform e
NM_178242	Tnrc18	trinucleotide repeat-containing gene 18 protein
NM_020507	Tob2	protein Tob2
NM_011906	Tpra1	transmembrane protein adipocyte-associated 1
NM_194343	Trim45	tripartite motif-containing protein 45 isoform
NM_178110	Trim62	tripartite motif-containing protein 62
NM_001160412	Triml2	tripartite motif family-like 2
NM_001085421	Tspyl5	testis-specific Y-encoded-like protein 5
NM_027238	Ttc39b	tetratricopeptide repeat protein 39B
NM_029264	Ttll10	protein polyglycylase TTLL10
NM_017379	Tuba8	tubulin alpha-8 chain
NM_019913	Txn2	thioredoxin, mitochondrial precursor
NM_010633	Uhmk1	serine/threonine-protein kinase Kist
NM_026031	Utp11l	probable U3 small nucleolar RNA-associated
NM_011694	Vdac1	voltage-dependent anion-selective channel
NM_172255	Wdr11	WD repeat-containing protein 11
NM_145514	Wdr26	WD repeat-containing protein 26
NM_030215	Wrnip1	ATPase WRNIP1
NM_019653	Wsb1	WD repeat and SOCS box-containing protein 1
NM_011724	Xirp1	xin actin-binding repeat-containing protein 1
NM_001005341	Ypel2	protein yippee-like 2
NM_011740	Ywhaz	14-3-3 protein zeta/delta
NM_001122676	Zcchc2	zinc finger CCHC domain-containing protein 2
NM_001033261	Zfc3h1	proline/serine-rich coiled-coil 2
NM_199029	Zfp395	zinc finger protein 395
NM_172867	Zfp462	zinc finger protein 462
NM_201609	Zfp652	zinc finger protein 652
NM_001146000	Zfp710	zinc finger protein 710 isoform b
NM_153194	Zfp740	zinc finger protein 740
NM_172919	Zfp846	zinc finger protein 846
NM_145456	Zswim6	zinc finger SWIM domain-containing protein 6
NM_001045536	Zzef1	zinc finger ZZ-type and EF-hand
NM_025319	0610009B22Rik	hypothetical protein LOC66050
NM_001164210	1110032A04Rik	small subunit of serine palmitoyltransferase B
NM_001081005	1500012F01Rik	hypothetical protein LOC68949
NM_024283	1500015O10Rik	augurin precursor
NM_027063	1700013G24Rik	hypothetical protein LOC69380
NM_027966	1700019O17Rik	hypothetical protein LOC71863
NR_003953	1700022A21Rik	
NM_027970	1700023E05Rik	hypothetical protein LOC71868
NR_027909	1700029M20Rik	
NM_028851	1700080O16Rik	hypothetical protein LOC74279
NM_133998	1810008A18Rik	hypothetical protein LOC108707
NM_027129	2310035K24Rik	hypothetical protein LOC69596
NM_025621	2310050C09Rik	hypothetical protein LOC66533
NM_001007581	2810408M09Rik	hypothetical protein LOC381406
NR_015489	2900041M22Rik	
NR_030715	3930402G23Rik	
NR_015510	4632427E13Rik	
NM_172500	4831426I19Rik	nesprin-3 isoform beta
NM_029440	4930434E21Rik	hypothetical protein LOC381693
NR_015535	4930567H12Rik	
NM_001145759	4930571K23Rik	hypothetical protein LOC75861
NR_027879	4930583K01Rik	
NM_001081063	4933401F05Rik	serine protease 55 precursor
NM_028908	4933403G14Rik	hypothetical protein LOC74393
NM_001081101	4933407H18Rik	hypothetical protein LOC71101
NR_027843	4933432I09Rik	
NM_176921	6030419C18Rik	hypothetical protein LOC319477
NM_172859	6330439K17Rik	ankyrin repeat-containing protein C20orf12
NM_026377	6330577E15Rik	hypothetical protein LOC67788
NM_145836	6430527G18Rik	enhanced at puberty protein 1
NR_015553	9430076C15Rik	

DISTAL(>50kb)

Transcript Name	Gene name	Gene Description
NM_001081067	A1bg	alpha-1B-glycoprotein precursor
NM_177039	A530016L24Rik	transmembrane protein C14orf180 homolog
NM_025271	Actl7b	actin-like protein 7B
NM_007396	Acvr2a	activin receptor type-2A precursor
NM_009623	Adcy8	adenylate cyclase type 8
NM_020332	Ank	progressive ankylosis protein
NM_001080933	Ankfn1	ankyrin repeat and fibronectin type-III
NM_001167883	Ankrd50	ankyrin repeat domain 50
NM_007481	Arf6	ADP-ribosylation factor 6
NM_183019	Arhgef4	rho guanine nucleotide exchange factor 4
NM_007487	Arl4a	ADP-ribosylation factor-like protein 4A
NM_001042592	Arrdc4	arrestin domain containing 4 isoform 1
NM_176999	Atp10b	probable phospholipid-transporting ATPase VB
NM_007502	Atp1b3	sodium/potassium-transporting ATPase subunit
NM_175015	Atp5g3	ATP synthase lipid-binding protein,
NM_001001488	Atp8b1	probable phospholipid-transporting ATPase IC
NM_015732	Axin2	axin-2
NM_001102458	Azin1	antizyme inhibitor 1
NM_001033350	Bank1	B-cell scaffold protein with ankyrin repeats
NM_016812	Banp	protein BANP isoform 2
NM_130452	Bbox1	gamma-butyrobetaine dioxygenase
NM_013867	Bcar3	breast cancer anti-estrogen resistance protein
NM_007553	Bmp2	bone morphogenetic protein 2 precursor
NM_007557	Bmp7	bone morphogenetic protein 7 precursor
NM_028472	Bmper	BMP-binding endothelial regulator protein
NM_009782	Cacna1e	voltage-dependent R-type calcium channel subunit
NM_018770	Cadm1	cell adhesion molecule 1 isoform c
NM_001160399	Ccdc112	coiled-coil domain-containing protein 112
NM_201362	Ccdc68	coiled-coil domain-containing protein 68
NM_009866	Cdh11	cadherin-11 preproprotein
NM_198656	Cdh26	cadherin-like protein 26 precursor
NM_009868	Cdh5	cadherin-5 precursor
NM_144536	Cdkal1	CDK5 regulatory subunit-associated protein
NM_001024624	Cdkl5	cyclin-dependent kinase-like 5
NM_029976	Cdkn2aipnl	CDKN2AIP N-terminal-like protein
NM_028850	Chic2	cysteine-rich hydrophobic domain 2 protein
NM_009893	Chrd	chordin precursor
NM_027998	Cldn23	claudin-23
NM_173422	Colec10	collectin-10 precursor
NM_133805	Cops8	COP9 signalosome complex subunit 8
NM_025815	Cpne8	copine-8 isoform 1
NM_001080809	Cps1	carbamoyl-phosphate synthase [ammonia],
NM_010217	Ctgf	connective tissue growth factor precursor
NM_021704	Cxcl12	stromal cell-derived factor 1 isoform alpha
NM_144853	Cyyr1	cysteine and tyrosine-rich protein 1 precursor
NM_001109990	D0H4S114	neuronal protein 3.1
NM_001008702	Dab2	disabled homolog 2 isoform b
NM_029653	Dapk1	death-associated protein kinase 1
NM_019967	Dbc1	deleted in bladder cancer protein 1 homolog
NM_173419	Dleu7	leukemia-associated protein 7 homolog
NM_007862	Dlg1	disks large homolog 1
NM_029297	Dynlrb2	dynein light chain roadblock-type 2
NM_001014390	Dyrk2	dual specificity
NM_021469	Dysf	dysferlin isoform 1
NM_010104	Edn1	endothelin-1 precursor
NM_001001932	Eea1	early endosome antigen 1
NM_025769	Efcab1	EF-hand calcium-binding domain-containing
NM_010111	Efnb2	ephrin-B2 precursor
NM_025829	Eif4e3	eukaryotic translation initiation factor 4E type
NM_007930	Enc1	ectoderm-neural cortex protein 1
NM_013511	Epb4.1l2	band 4.1-like protein 2
NM_007961	Etv6	transcription factor ETV6
NM_010164	Eya1	eyes absent homolog 1
NM_173426	Fam110b	hypothetical protein LOC242297
NM_134096	Fam19a5	TAFA5 protein
NM_019995	Fam48a	family with sequence similarity 48, member A
NM_178390	Fam53a	dorsal neural-tube nuclear protein
NM_201361	Fam82a1	regulator of microtubule dynamics protein 2
NM_001045518	Fam83b	hypothetical protein LOC208994
NM_001033980	Fam92b	hypothetical protein LOC436062
NM_183221	Fat4	protocadherin Fat 4 precursor
NM_198029	Fermt1	fermitin family homolog 1
NM_201601	Fgfr2	fibroblast growth factor receptor 2 isoform
NM_001113412	Fggy	FGGY carbohydrate kinase domain-containing
NM_201518	Flrt2	fibronectin leucine rich transmembrane protein
NM_207636	Fndc3a	fibronectin type-III domain-containing protein
NM_019739	Foxo1	forkhead box protein O1
NM_008239	Foxq1	forkhead box protein Q1
NM_008057	Fzd7	frizzled-7 precursor
NM_011817	Gadd45g	growth arrest and DNA damage-inducible protein
NM_008082	Galr1	galanin receptor type 1
NM_030719	Gatsl2	GATS-like protein 2
NM_010267	Gdap1	ganglioside-induced differentiation-associated
NM_008115	Gfra2	GDNF family receptor alpha-2
NM_008131	Glul	glutamine synthetase
NM_001005422	Gm1574	hypothetical protein LOC380842
NM_001005420	Gm347	hypothetical protein LOC241289
NM_001033266	Gm525	hypothetical protein LOC217071 precursor
NM_001033411	Gm826	hypothetical protein LOC329554
NM_008149	Gpam	glycerol-3-phosphate acyltransferase 1,
NM_001002268	Gpr126	G-protein coupled receptor 126 precursor
NM_025325	Haao	3-hydroxyanthranilate 3,4-dioxygenase

NM_008216	Has2	hyaluronan synthase 2
NM_010437	Hivep2	transcription factor HIVEP2
NM_010481	Hspa9	stress-70 protein, mitochondrial
NM_019960	Hspb3	heat shock protein beta-3
NM_008316	Hus1	checkpoint protein HUS1
NM_010496	Id2	DNA-binding protein inhibitor ID-2
NM_008343	Igfbp3	insulin-like growth factor-binding protein 3
NM_008381	Inhbb	inhibin beta B chain precursor
NM_133748	Insig2	insulin-induced gene 2 protein isoform 1
NM_010573	Irx1	iroquois-class homeodomain protein IRX-1
NM_010574	Irx2	iroquois-class homeodomain protein IRX-2
NM_008393	Irx3	iroquois-class homeodomain protein IRX-3
NM_013822	Jag1	protein jagged-1 precursor
NM_001102670	Kbtbd8	kelch repeat and BTB domain-containing protein 8
NM_013692	Klf10	Krueppel-like factor 10
NM_001166659	Lekr1	leucine, glutamate and lysine rich 1 isoform 1
NM_001081298	Lphn2	latrophilin-2
NM_178725	Lrrc4c	leucine-rich repeat-containing protein 4C
NM_001025577	Maf	transcription factor Maf
NM_008548	Man1a	mannosyl-oligosaccharide 1,2-alpha-mannosidase
NM_011945	Map3k1	mitogen-activated protein kinase kinase kinase
NM_016700	Mapk8	mitogen-activated protein kinase 8
NM_001146176	Max	protein max isoform 2
NM_020007	Mbnl1	muscleblind-like protein 1
NM_008560	Mc2r	adrenocorticotropic hormone receptor
NM_001024703	Mctp2	multiple C2 and transmembrane domain-containing
NR_029540	Mir125b-2	
NR_029719	Mir148a	
NM_008604	Mme	neprilysin
NM_001113374	Mocs2	molybdopterin synthase sulfur carrier subunit
NM_010820	Mpdz	multiple PDZ domain protein
NM_016804	Mtx2	metaxin-2
NM_153789	Mylip	E3 ubiquitin-protein ligase MYLIP isoform 1
NM_001166030	Mylk4	myosin light chain kinase family member 4
NM_176957	Nckap5	Nck-associated protein 5 isoform 3
NM_022996	Ndfip1	NEDD4 family-interacting protein 1
NM_028757	Nebl	nebulette
NM_010894	Neurod1	neurogenic differentiation factor 1
NM_153079	Nmur2	neuromedin-U receptor 2
NM_023456	Npy	neuropeptide Y precursor
NM_011851	Nt5e	5'-nucleotidase precursor
NM_172290	Ntm	neurotrimin precursor
NM_027722	Nudt4	diphosphoinositol polyphosphate phosphohydrolase
NM_028696	Obfc2a	SOSS complex subunit B2
NM_011857	Odz3	teneurin-3 isoform 1
NM_011019	Osmr	oncostatin-M-specific receptor subunit beta
NM_001081164	Otud4	OTU domain-containing protein 4
NM_011033	Pabpc2	poly A binding protein, cytoplasmic 2
NM_181402	Parp11	poly [ADP-ribose] polymerase 11
NM_008781	Pax3	paired box protein Pax-3 isoform a
NM_008783	Pbx1	pre-B-cell leukemia transcription factor 1
NM_009344	Phlda1	pleckstrin homology-like domain family A member
NM_001024955	Pik3r1	phosphatidylinositol 3-kinase regulatory subunit
NR_003202	Pinc	
NM_011097	Pitx1	pituitary homeobox 1
NM_001083110	Pja1	E3 ubiquitin-protein ligase Praja-1 isoform 1
NM_153179	Pkhd1	polyductin
NM_008869	Pla2g4a	cytosolic phospholipase A2
NM_018797	Plxnc1	plexin-C1 precursor
NM_080555	Ppap2b	lipid phosphate phosphohydrolase 3
NM_177741	Ppp1r3b	protein phosphatase 1 regulatory subunit 3B
NM_177698	Psd3	PH and SEC7 domain-containing protein 3 isoform
NM_019550	Ptbp2	polypyrimidine tract-binding protein 2
NM_008960	Pten	phosphatidylinositol-3,4,5-trisphosphate
NM_008966	Ptgfr	prostaglandin F2-alpha receptor
NM_011201	Ptpn1	tyrosine-protein phosphatase non-receptor type
NM_001081432	Ptprq	phosphotidylinositol phosphatase PTPRQ
NM_021424	Pvrl1	poliovirus receptor-related protein 1 precursor
NM_001163303	Pxmp3	peroxisome biogenesis factor 2
NM_027455	Qpct	glutaminyl-peptide cyclotransferase precursor
NM_011246	Rasgrp1	RAS guanyl-releasing protein 1
NM_001080928	Rbpj	recombining binding protein suppressor of
NM_178606	Reep3	receptor expression-enhancing protein 3
NM_009061	Rgs2	regulator of G-protein signaling 2
NM_178779	Rnf152	RING finger protein 152
NM_025974	Rpl14	60S ribosomal protein L14
NM_011297	Rps24	40S ribosomal protein S24 isoform 1
NM_017475	Rragc	ras-related GTP-binding protein C
NM_172769	Sc5d	lathosterol oxidase
NM_030261	Sesn3	sestrin-3
NM_009144	Sfrp2	secreted frizzled-related protein 2 precursor
NM_013665	Shox2	short stature homeobox protein 2
NM_181590	Shq1	protein SHQ1 homolog
NM_015829	Slc25a13	calcium-binding mitochondrial carrier protein
NM_001033286	Slc30a10	zinc transporter 10
NM_022885	Slc30a5	zinc transporter 5
NM_175121	Slc38a2	sodium-coupled neutral amino acid transporter 2
NM_009208	Slc4a3	anion exchange protein 3
NM_011415	Snai2	zinc finger protein SNAI2
NM_028874	Snx19	sorting nexin-19
NM_025696	Sorcs3	VPS10 domain-containing receptor SorCS3
NM_011436	Sorl1	sortilin-related receptor
NM_001098425	Sp3	transcription factor Sp3 isoform 2
NR_001582	Speer5-ps1	
NM_033523	Spred2	sprouty-related, EVH1 domain-containing protein

NM_011372	St6galnac3	alpha-N-acetylgalactosaminide
NM_027399	Steap1	metalloreductase STEAP1
NM_054098	Steap4	metalloreductase STEAP4
NM_138667	Tab2	TGF-beta-activated kinase 1 and MAP3K7-binding
NM_177089	Tacc1	transforming acidic coiled-coil-containing
NM_030732	Tbl1xr1	F-box-like/WD repeat-containing protein TBL1XR1
NM_013685	Tcf4	transcription factor 4 isoform a
NM_207176	Tes	testin
NM_009371	Tgfbr2	TGF-beta receptor type-2 isoform 1
NM_001164074	Tgif1	homeobox protein TGIF1 isoform c
NM_011580	Thbs1	thrombospondin-1
NM_011581	Thbs2	thrombospondin-2 precursor
NM_178413	Thnsl2	threonine synthase-like 2
NM_012033	Tinag	tubulointerstitial nephritis antigen
NM_001163574	Tjp1	tight junction protein ZO-1 isoform 2
NM_001083928	Tle3	transducin-like enhancer protein 3 isoform 3
NM_178056	Tm2d3	TM2 domain-containing protein 3 isoform 2
NM_015775	Tmprss2	transmembrane protease serine 2
NM_177368	Tmtc2	transmembrane and TPR repeat-containing protein
NM_028339	Tmx1	thioredoxin-related transmembrane protein 1
NM_183391	Tnfsf18	tumor necrosis factor (ligand) superfamily,
NM_009408	Top1	DNA topoisomerase 1
NM_144549	Trib1	tribbles homolog 1
NM_030706	Trim2	tripartite motif-containing protein 2
NM_001039104	Trpm1	transient receptor potential cation channel
NM_001081300	Tshz1	teashirt homolog 1
NM_029321	Ttc32	tetratricopeptide repeat protein 32
NM_028283	Uaca	uveal autoantigen with coiled-coil domains and
NM_183225	Usp24	ubiquitin carboxyl-terminal hydrolase 24
NM_144826	Utp6	U3 small nucleolar RNA-associated protein 6
NM_027614	Wdr20b	WD repeat-containing protein 20
NM_080848	Wdr5	WD repeat-containing protein 5
NM_001014981	Wdr7	WD repeat-containing protein 7
NM_028599	Wdr75	WD repeat-containing protein 75
NM_026858	Xrcc6bp1	mitochondrial inner membrane protease ATP23
NM_023311	Yipf5	protein YIPF5
NM_022985	Zfand6	AN1-type zinc finger protein 6
NM_146224	Zfp280d	zinc finger protein 280D
NM_001001806	Zfp36l2	zinc finger protein 36, C3H1 type-like 2
NM_183033	Zfp516	zinc finger protein 516
NM_145492	Zfp521	zinc finger protein 521
NM_175751	Zfp608	zinc finger protein 608
NM_134054	1110002B05Rik	small subunit of serine palmitoyltransferase A
NM_001145198	1500009L16Rik	hypothetical protein LOC69784
NM_177718	1600021P15Rik	hypothetical protein LOC239796
NR_027968	1700020N01Rik	
NM_026931	1810011O10Rik	thyroid cancer-1
NM_001081236	2410131K14Rik	hypothetical protein LOC76792 precursor
NR_015556	2610035D17Rik	
NR_015579	2810032G03Rik	
NR_015605	2900052N01Rik	
NM_027637	4931428L18Rik	
NR_015512	4933406K04Rik	
NM_027668	4933412E24Rik	hypothetical protein LOC71088
NM_001081963	9430020K01Rik	hypothetical protein LOC240185

References

Adachi, S., Morii, E., Kim, D.K., Ogihara, H., Jippo, T., Ito, A., Lee, Y.M., and Kitamura, Y. (2000). Involvement of mi-transcription factor in expression of alpha-melanocyte-stimulating hormone receptor in cultured mast cells of mice. J. Immunol. *164*, 855–860.

Adameyko, I., Lallemend, F., Aquino, J.B., Pereira, J.A., Topilko, P., MUller, T., Fritz, N., Beljajeva, A., Mochii, M., Liste, I., et al. (2009). Schwann Cell Precursors from Nerve Innervation Are a Cellular Origin of Melanocytes in Skin. Cell *139*, 366–379.

Adur, J., Takizawa, S., Uchide, T., Casco, V., and Saida, K. (2007). High doses of ultraviolet-C irradiation increases vasoactive intestinal contractor/endothelin-2 expression in keratinocytes of the newborn mouse epidermis. Peptides *28*, 1083–1094.

Andl, T., Ahn, K., Kairo, A., Chu, E.Y., Wine-Lee, L., Reddy, S.T., Croft, N.J., Cebra-Thomas, J.A., Metzger, D., Chambon, P., et al. (2004). Epithelial Bmpr1a regulates differentiation and proliferation in postnatal hair follicles and is essential for tooth development. Development *131*, 2257–2268.

Aoki, H., Yamada, Y., Hara, A., and Kunisada, T. (2009). Two distinct types of mouse melanocyte: differential signaling requirement for the maintenance of non-cutaneous and dermal versus epidermal melanocytes. Development *136*, 2511–2521.

Aoki, H., Hara, A., Motohashi, T., and Kunisada, T. (2013). Keratinocyte stem cells but not melanocyte stem cells are the primary target for radiation-induced hair graying. J Investig Dermatol *133*, 2143–2151.

Aoki, H., Motohashi, T., Yoshimura, N., Yamazaki, H., Yamane, T., Panthier, J., and Kunisada, T. (2005). Cooperative and indispensable roles of endothelin 3 and KIT signalings in melanocyte development. Dev Dyn *233*, 407–417.

Asher, J.H., and Friedman, T.B. (1990). Mouse and hamster mutants as models for Waardenburg syndromes in humans. J. Med. Genet. *27*, 618–626.

Attié, T., Till, M., Pelet, A., Amiel, J., Edery, P., Boutrand, L., Munnich, A., and Lyonnet, S. (1995). Mutation of the endothelin-receptor B gene in Waardenburg-Hirschsprung disease. Human Molecular Genetics *4*, 2407–2409.

Aubin-Houzelstein, G., Djian-Zaouche, J., Bernex, F., Gadin, S., Delmas, V., Larue, L., and Panthier, J.-J. (2008). Melanoblasts' Proper Location and Timed Differentiation Depend on Notch/RBP-J Signaling in Postnatal Hair Follicles. J Investig Dermatol *128*, 2686–2695.

Baldwin, C.T., Lipsky, N.R., Hoth, C.F., Cohen, T., Mamuya, W., and Milunsky, A. (1994). Mutations in PAX3 associated with Waardenburg syndrome type I. Hum. Mutat. *3*, 205–211.

Baynash, A.G., Hosoda, K., Giaid, A., Richardson, J.A., Emoto, N., Hammer, R.E., and Yanagisawa, M. (1994). Interaction of endothelin-3 with endothelin-B receptor is essential for development of epidermal melanocytes and enteric neurons. Cell *79*, 1277–1285.

Beronja, S., Livshits, G., Williams, S., and Fuchs, E. (2010). Rapid functional dissection of genetic networks via tissue-specific transduction and RNAi in mouse embryos. Nat Med *16*, 821–827.

Bertolotto, C., Abbe, P., Hemesath, T.J., Bille, K., Fisher, D.E., ORTONNE, J.-P., and Ballotti, R. (1998). Microphthalmia gene product as a signal transducer in cAMP-induced differentiation of melanocytes. The Journal of Cell Biology *142*, 827–835.

Bertolotto, C., Bille, K., ORTONNE, J.-P., and Ballotti, R. (1996). Regulation of tyrosinase gene expression by cAMP in B16 melanoma cells involves two CATGTG motifs surrounding the TATA box: implication of the microphthalmia gene product. The Journal of Cell Biology *134*, 747–755.

Blanpain, C., and Fuchs, E. (2006). Epidermal stem cells of the skin. Annu. Rev. Cell. Dev. Biol. *22*, 339–373.

Blanpain, C., Lowry, W.E., Geoghegan, A., Polak, L., and Fuchs, E. (2004). Self-renewal, multipotency, and the existence of two cell populations within an epithelial stem cell niche. Cell *118*, 635–648.

Blume-Jensen, P., Jiang, G., Hyman, R., Lee, K.F., O'Gorman, S., and Hunter, T. (2000). Kit/stem cell factor receptor-induced activation of phosphatidylinositol 3'-kinase is essential for male fertility. Nature Genetics *24*, 157–162.

Bondurand, N., Pingault, V., Goerich, D.E., Lemort, N., Sock, E., Le Caignec, C., Wegner, M., and Goossens, M. (2000). Interaction among SOX10, PAX3 and MITF, three genes altered in Waardenburg syndrome. Human Molecular Genetics *9*, 1907–1917.

Botchkarev, V.A., Botchkareva, N.V., Roth, W., Nakamura, M., Chen, L.H., Herzog, W., Lindner, G., Mcmahon, J.A., Peters, C., Lauster, R., et al. (1999). Noggin is a mesenchymally derived stimulator of hair-follicle induction. Nat Cell Biol *1*, 158–164.

Botchkarev, V.A., BOTCHKAREVA, N.V., NAKAMURA, M., HUBER, O., Funa, K., LAUSTER, R., Paus, R., and Gilchrest, B.A. (2001). Noggin is required for induction of the hair follicle

Botchkarev, V.A., Botchkareva, N.V., Nakamura, M., Huber, O., Funa, K., Lauster, R., Paus, R., and Gilchrest, B.A. (2001). Noggin is required for induction of the hair follicle growth phase in postnatal skin. FASEB J *15*, 2205–2214.

Botchkareva, N.V., Khlgatian, M., Longley, B.J., Botchkarev, V.A., and Gilchrest, B.A. (2001). SCF/c-kit signaling is required for cyclic regeneration of the hair pigmentation unit. FASEB J *15*, 645–658.

Bray, S.J. (2006). Notch signalling: a simple pathway becomes complex. Nat Rev Mol Cell Biol *7*, 678–689.

Burchill, S.A., Virden, R., and Thody, A.J. (1989). Regulation of tyrosinase synthesis and its processing in the hair follicular melanocytes of the mouse during eumelanogenesis and phaeomelanogenesis. J Invest Dermatol *93*, 236–240.

Cable, J., Jackson, I.J., and Steel, K.P. (1995). Mutations at the W locus affect survival of neural crest-derived melanocytes in the mouse. Mechanisms of Development *50*, 139–150.

Campbell, C.E., Piper, M., Plachez, C., Yeh, Y.-T., Baizer, J.S., Osinski, J.M., Litwack, E.D., Richards, L.J., and Gronostajski, R.M. (2008). The transcription factor Nfix is essential for normal brain development. BMC Dev Biol *8*, 52.

Carreira, S., Liu, B., and Goding, C.R. (2000). The gene encoding the T-box factor Tbx2 is a target for the microphthalmia-associated transcription factor in melanocytes. The Journal of Biological Chemistry *275*, 21920–21927.

Carreira, S., Goodall, J., Aksan, I., La Rocca, S.A., Galibert, M.-D., Denat, L., Larue, L., and Goding, C.R. (2005). Mitf cooperates with Rb1 and activates p21Cip1 expression to regulate cell cycle progression. Nature *433*, 764–769.

Celso, Lo, C., Prowse, D.M., and Watt, F.M. (2004). Transient activation of beta-catenin signalling in adult mouse epidermis is sufficient to induce new hair follicles but continuous activation is required to maintain hair follicle tumours. Development *131*, 1787–1799.

Chabot, B., Stephenson, D.A., Chapman, V.M., Besmer, P., and Bernstein, A. (1988). The proto-oncogene c-kit encoding a transmembrane tyrosine kinase receptor maps to the mouse W locus. Nature *335*, 88–89.

Chang, I., Bramall, A.N., Baynash, A.G., Rattner, A., Rakheja, D., Post, M., Joza, S., McKerlie, C., Stewart, D.J., McInnes, R.R., et al. (2013). Endothelin-2 deficiency causes growth retardation, hypothermia, and emphysema in mice. J. Clin. Invest. *123*, 2643–2653.

Chou, W.C., Takeo, M., Rabbani, P., Hu, H., Lee, W., Chung, Y.R., Carucci, J., Overbeek, P., and Ito, M. (2013). Direct migration of follicular melanocyte stem cells to the epidermis after wounding or UVB irradiation is dependent on Mc1r signaling. Nat Med *19*, 924–929.

Colombo, S., Berlin, I., Delmas, V.É.R., and Larue, A.L. (2011). Classical and Nonclassical Melanocytes in Vertebrates. Melanins and Melanosomes: Biosynthesis, Biogenesis, Physiological, and Pathological Functions 1–41.

Commo, S., Gaillard, O., and Bernard, B.A. (2004). Human hair greying is linked to a specific depletion of hair follicle melanocytes affecting both the bulb and the outer root

sheath. Br. J. Dermatol. *150*, 435–443.

Copeland, N.G., Gilbert, D.J., Cho, B.C., Donovan, P.J., Jenkins, N.A., Cosman, D., Anderson, D., Lyman, S.D., and Williams, D.E. (1990). Mast cell growth factor maps near the steel locus on mouse chromosome 10 and is deleted in a number of steel alleles. Cell *63*, 175–183.

Costin, G.-E., and Hearing, V.J. (2007). Human skin pigmentation: melanocytes modulate skin color in response to stress. The FASEB Journal *21*, 976–994.

Cotsarelis, G., Sun, T.T., and Lavker, R.M. (1990). Label-retaining cells reside in the bulge area of pilosebaceous unit: implications for follicular stem cells, hair cycle, and skin carcinogenesis. Cell *61*, 1329–1337.

Cui, J., Shen, L.Y., and Wang, G.C. (1991). Role of hair follicles in the repigmentation of vitiligo. J Invest Dermatol *97*, 410–416.

Cui, R., Widlund, H.R., Feige, E., Lin, J.Y., Wilensky, D.L., Igras, V.E., D'Orazio, J., Fung, C.Y., Schanbacher, C.F., Granter, S.R., et al. (2007). Central Role of p53 in the Suntan Response and Pathologic Hyperpigmentation. Cell *128*, 853–864.

D'Orazio, J.A., Nobuhisa, T., Cui, R., Arya, M., Spry, M., Wakamatsu, K., Igras, V., Kunisada, T., Granter, S.R., Nishimura, E.K., et al. (2006). Topical drug rescue strategy and skin protection based on the role of Mc1r in UV-induced tanning. Nature *443*, 340–344.

Daniely, Y., Liao, G., Dixon, D., Linnoila, R.I., Lori, A., Randell, S.H., Oren, M., and Jetten, A.M. (2004). Critical role of p63 in the development of a normal esophageal and tracheobronchial epithelium. Am. J. Physiol., Cell Physiol. *287*, C171–C181.

Davis, R.L., Weintraub, H., and Lassar, A.B. (1987). Expression of a single transfected cDNA converts fibroblasts to myoblasts. Cell *51*, 987–1000.

Dooley, A.L., Winslow, M.M., Chiang, D.Y., Banerji, S., Stransky, N., Dayton, T.L., Snyder, E.L., Senna, S., Whittaker, C.A., Bronson, R.T., et al. (2011). Nuclear factor I/B is an oncogene in small cell lung cancer. Genes & Development *25*, 1470–1475.

Dorsky, R.I., Moon, R.T., and Raible, D.W. (1998). Control of neural crest cell fate by the Wnt signalling pathway. Nature *396*, 370–373.

Dorsky, R.I., Raible, D.W., and Moon, R.T. (2000). Direct regulation of nacre, a zebrafish MITF homolog required for pigment cell formation, by the Wnt pathway. Genes & Development *14*, 158–162.

Dottori, M., Gross, M.K., Labosky, P., and Goulding, M. (2001). The winged-helix transcription factor Foxd3 suppresses interneuron differentiation and promotes neural crest cell fate. Development *128*, 4127–4138.

Driller, K., Pagenstecher, A., Uhl, M., Omran, H., Berlis, A., Gründer, A., and Sippel, A.E. (2007). Nuclear factor I X deficiency causes brain malformation and severe skeletal defects. Molecular and Cellular Biology *27*, 3855–3867.

Du, J., Miller, A.J., Widlund, H.R., Horstmann, M.A., Ramaswamy, S., and Fisher, D.E. (2003). MLANA/MART1 and SILV/PMEL17/GP100 are transcriptionally regulated by MITF in melanocytes and melanoma. The American Journal of Pathology *163*, 333–343.

Du, J., Widlund, H.R., Horstmann, M.A., Ramaswamy, S., Ross, K., Huber, W.E., Nishimura, E.K., Golub, T.R., and Fisher, D.E. (2004). Critical role of CDK2 for melanoma growth linked to its melanocyte-specific transcriptional regulation by MITF. Cancer Cell *6*, 565–576.

Dutton, K.A., Pauliny, A., Lopes, S.S., Elworthy, S., Carney, T.J., Rauch, J., Geisler, R., Haffter, P., and Kelsh, R.N. (2001). Zebrafish colourless encodes sox10 and specifies non-ectomesenchymal neural crest fates. Development *128*, 4113–4125.

Dynek, J.N., Chan, S.M., Liu, J., Zha, J., Fairbrother, W.J., and Vucic, D. (2008). Microphthalmia-associated transcription factor is a critical transcriptional regulator of melanoma inhibitor of apoptosis in melanomas. Cancer Research *68*, 3124–3132.

Edery, P., Attié, T., Amiel, J., Pelet, A., Eng, C., Hofstra, R.M., Martelli, H., Bidaud, C., Munnich, A., and Lyonnet, S. (1996). Mutation of the endothelin-3 gene in the Waardenburg-Hirschsprung disease (Shah-Waardenburg syndrome). Nature Genetics *12*, 442–444.

Elemento, O., Slonim, N., and Tavazoie, S. (2007). A universal framework for regulatory element discovery across all genomes and data types. Molecular Cell *28*, 337–350.

Epstein, D.J., Vekemans, M., and Gros, P. (1991). Splotch (Sp2H), a mutation affecting development of the mouse neural tube, shows a deletion within the paired homeodomain of Pax-3. Cell *67*, 767–774.

Erickson, C.A., and Weston, J.A. (1983). An SEM analysis of neural crest migration in the mouse. J Embryol Exp Morphol *74*, 97–118.

Ezhkova, E., Pasolli, H.A., Parker, J.S., Stokes, N., Su, I.-H., Hannon, G., Tarakhovsky, A., and Fuchs, E. (2009). Ezh2 orchestrates gene expression for the stepwise differentiation of tissue-specific stem cells. Cell *136*, 1122–1135.

Falabella, R. (2009). Vitiligo and the melanocyte reservoir. Indian J Dermatol *54*, 313–318.

Festa, E., Fretz, J., Berry, R., Schmidt, B., Rodeheffer, M., Horowitz, M., and Horsley, V. (2011). Adipocyte lineage cells contribute to the skin stem cell niche to drive hair cycling. Cell *146*, 761–771.

Fitch, K.R., McGowan, K.A., van Raamsdonk, C.D., Fuchs, H., Lee, D., Puech, A.,

Hérault, Y., Threadgill, D.W., Hrabé de Angelis, M., and Barsh, G.S. (2003). Genetics of dark skin in mice. Genes & Development *17*, 214–228.

Fitzpatrick, T.B., and Breathnach, A.S. (1963). The epidermal melanin unit system. Dermatol Wochenschr *147*, 481–489.

Folgueras, A.R., Guo, X., Pasolli, H.A., Stokes, N., Polak, L., Zheng, D., and Fuchs, E. (2013). Architectural Niche Organization by LHX2 Is Linked to Hair Follicle Stem Cell Function. Cell Stem Cell *13*, 314–327.

Gammill, L.S., and Bronner-Fraser, M. (2003). Neural crest specification: migrating into genomics. Nat. Rev. Neurosci. *4*, 795–805.

Garcia, R.J., Ittah, A., Mirabal, S., Figueroa, J., Lopez, L., Glick, A.B., and Kos, L. (2008). Endothelin 3 induces skin pigmentation in a keratin-driven inducible mouse model. J Investig Dermatol *128*, 131–142.

García-Castro, M.I., Marcelle, C., and Bronner-Fraser, M. (2002). Ectodermal Wnt function as a neural crest inducer. Science *297*, 848–851.

Garraway, L.A., Widlund, H.R., Rubin, M.A., Getz, G., Berger, A.J., Ramaswamy, S., Beroukhim, R., Milner, D.A., Granter, S.R., Du, J., et al. (2005). Integrative genomic analyses identify MITF as a lineage survival oncogene amplified in malignant melanoma. Nature *436*, 117–122.

Geissler, E.N., Ryan, M.A., and Housman, D.E. (1988). The dominant-white spotting (W) locus of the mouse encodes the c-kit proto-oncogene. Cell *55*, 185–192.

Geurts, J.M., Schoenmakers, E.F., Röijer, E., Aström, A.K., Stenman, G., and van de Ven, W.J. (1998). Identification of NFIB as recurrent translocation partner gene of HMGIC in pleomorphic adenomas. Oncogene *16*, 865–872.

Giannopoulou, E.G., and Elemento, O. (2011). An integrated ChIP-seq analysis platform with customizable workflows. BMC Bioinformatics *12*, 277.

Giebel, L.B., and Spritz, R.A. (1991). Mutation of the KIT (mast/stem cell growth factor receptor) protooncogene in human piebaldism. Proc Natl Acad Sci USA *88*, 8696–8699.

Gilbert, S.F. (2006). Developmental Biology, Eighth Edition. Sinauer Associates Inc.

Goodarzi, H., Elemento, O., and Tavazoie, S. (2009). Revealing global regulatory perturbations across human cancers. Molecular Cell *36*, 900–911.

Govender, D., Davids, L.M., and Kidson, S.H. (2006). Immunofluorescent Identification of Melanocytes in Murine Hair Follicles. J Mol Hist *37*, 1–3.

Greco, V., Chen, T., Rendl, M., Schober, M., Pasolli, H.A., Stokes, N., Cruz-Racelis, dela, J., and Fuchs, E. (2009). A Two-Step Mechanism for Stem Cell Activation during

Hair Regeneration. Cell Stem Cell *4*, 155–169.

Gronostajski, R.M., Adhya, S., Nagata, K., Guggenheimer, R.A., and Hurwitz, J. (1985). Site-specific DNA binding of nuclear factor I: analyses of cellular binding sites. Molecular and Cellular Biology *5*, 964–971.

Gronostajski, R.M. (2000). Roles of the NFI/CTF gene family in transcription and development. Gene 1–15.

Gründer, A., Ebel, T.T., Mallo, M., Schwarzkopf, G., Shimizu, T., Sippel, A.E., and Schrewe, H. (2002). Nuclear factor I-B (Nfib) deficient mice have severe lung hypoplasia. Mechanisms of Development *112*, 69–77.

Halder, G., Callaerts, P., and Gehring, W.J. (1995). Induction of ectopic eyes by targeted expression of the eyeless gene in Drosophila. Science *267*, 1788–1792.

Hardman, M.J., Sisi, P., Banbury, D.N., and Byrne, C. (1998). Patterned acquisition of skin barrier function during development. Development *125*, 1541–1552.

Hardy, M.H. (1992). The secret life of the hair follicle. Trends Genet. *8*, 55–61.

Hari, L., Brault, V., Kléber, M., Lee, H.-Y., Ille, F., Leimeroth, R., Paratore, C., Suter, U., Kemler, R., and Sommer, L. (2002). Lineage-specific requirements of beta-catenin in neural crest development. The Journal of Cell Biology *159*, 867–880.

Hari, L., Miescher, I., Shakhova, O., Suter, U., Chin, L., Taketo, M., Richardson, W.D., Kessaris, N., and Sommer, L. (2012). Temporal control of neural crest lineage generation by Wnt/β-catenin signaling. Development *139*, 2107–2117.

Hata, A., Lo, R.S., Wotton, D., Lagna, G., and Massagué, J. (1997). Mutations increasing autoinhibition inactivate tumour suppressors Smad2 and Smad4. Nature *388*, 82–87.

Hearing, V.J., and Tsukamoto, K. (1991). Enzymatic control of pigmentation in mammals. Faseb J *5*, 2902–2909.

Hearing, V.J. (2011). Determination of melanin synthetic pathways. J Invest Dermatol *131*, E8-E11.

Heintz, N. (2004). Gene expression nervous system atlas (GENSAT). Nat. Neurosci. *7*, 483.

Hemesath, T.J., Price, E.R., Takemoto, C., Badalian, T., and Fisher, D.E. (1998). MAP kinase links the transcription factor Microphthalmia to c-Kit signalling in melanocytes. Nature *391*, 298–301.

Hemesath, T.J., Steingrimsson, E., Mcgill, G., Hansen, M.J., Vaught, J., Hodgkinson, C.A., Arnheiter, H., Copeland, N.G., Jenkins, N.A., and Fisher, D.E. (1994). microphthalmia, a critical factor in melanocyte development, defines a discrete

transcription factor family. Genes & Development *8*, 2770–2780.

Hennighausen, L., Siebenlist, U., Danner, D., Leder, P., Rawlins, D., Rosenfeld, P., and Kelly, T. (1985). High-affinity binding site for a specific nuclear protein in the human IgM gene. Nature *314*, 289–292.

Hertwig, P. (1942). Neue mutationen und kopplungsgruppen bei der hausmaus. Z. Indukt. Abstammungs-Vererbungsl.

Hirobe, T. (1984). Histochemical survey of the distribution of the epidermal melanoblasts and melanocytes in the mouse during fetal and postnatal periods. Anat. Rec. *208*, 589–594.

Hirobe, T. (2011). How are proliferation and differentiation of melanocytes regulated? Pigment Cell & Melanoma Research *24*, 462–478.

Hnisz, D., Abraham, B.J., Lee, T.I., Lau, A., Saint-André, V., Sigova, A.A., Hoke, H.A., and Young, R.A. (2013). Super-enhancers in the control of cell identity and disease. Cell *155*, 934–947.

Ho, A.S., Kannan, K., Roy, D.M., Morris, L.G.T., Ganly, I., Katabi, N., Ramaswami, D., Walsh, L.A., Eng, S., Huse, J.T., et al. (2013). The mutational landscape of adenoid cystic carcinoma. Nature Genetics *45*, 791–798.

Hodgkinson, C.A., Moore, K.J., Nakayama, A., Steingrimsson, E., Copeland, N.G., Jenkins, N.A., and Arnheiter, H. (1993). Mutations at the mouse microphthalmia locus are associated with defects in a gene encoding a novel basic-helix-loop-helix-zipper protein. Cell *74*, 395–404.

Hofstra, R.M., Osinga, J., Tan-Sindhunata, G., Wu, Y., Kamsteeg, E.J., Stulp, R.P., van Ravenswaaij-Arts, C., Majoor-Krakauer, D., Angrist, M., Chakravarti, A., et al. (1996). A homozygous mutation in the endothelin-3 gene associated with a combined Waardenburg type 2 and Hirschsprung phenotype (Shah-Waardenburg syndrome). Nature Genetics *12*, 445–447.

Hong, K.U., Reynolds, S.D., Watkins, S., Fuchs, E., and Stripp, B.R. (2004a). Basal cells are a multipotent progenitor capable of renewing the bronchial epithelium. The American Journal of Pathology *164*, 577–588.

Hong, K.U., Reynolds, S.D., Watkins, S., Fuchs, E., and Stripp, B.R. (2004b). In vivo differentiation potential of tracheal basal cells: evidence for multipotent and unipotent subpopulations. Am. J. Physiol. Lung Cell Mol. Physiol. *286*, L643–L649.

Horsley, V., Aliprantis, A.O., Polak, L., Glimcher, L.H., and Fuchs, E. (2008). NFATc1 balances quiescence and proliferation of skin stem cells. Cell *132*, 299–310.

Horsley, V., O'Carroll, D., Tooze, R., Ohinata, Y., Saitou, M., Obukhanych, T., Nussenzweig, M., Tarakhovsky, A., and Fuchs, E. (2006). Blimp1 defines a progenitor

population that governs cellular input to the sebaceous gland. Cell *126*, 597–609.

Hosoda, K., Hammer, R.E., Richardson, J.A., Baynash, A.G., Cheung, J.C., Giaid, A., and Yanagisawa, M. (1994). Targeted and natural (piebald-lethal) mutations of endothelin-B receptor gene produce megacolon associated with spotted coat color in mice. Cell *79*, 1267–1276.

Hou, L., Panthier, J.J., and Arnheiter, H. (2000). Signaling and transcriptional regulation in the neural crest-derived melanocyte lineage: interactions between KIT and MITF. Development *127*, 5379–5389.

Hörstadius, S. (1950). The Neural Crest. Oxford University Press.

Hsu, Y.-C., Pasolli, H.A., and Fuchs, E. (2011a). Dynamics between stem cells, niche, and progeny in the hair follicle. Cell *144*, 92–105.

Hsu, Y.-C., Osinski, J., Campbell, C.E., Litwack, E.D., Wang, D., Liu, S., Bachurski, C.J., and Gronostajski, R.M. (2011b). Mesenchymal nuclear factor I B regulates cell proliferation and epithelial differentiation during lung maturation. Dev. Biol. *354*, 242–252.

Hughes, M.J., Lingrel, J.B., Krakowsky, J.M., and Anderson, K.P. (1993). A helix-loop-helix transcription factor-like gene is located at the mi locus. The Journal of Biological Chemistry *268*, 20687–20690.

Ikeya, M., Lee, S.M., Johnson, J.E., Mcmahon, A.P., and Takada, S. (1997). Wnt signalling required for expansion of neural crest and CNS progenitors. Nature *389*, 966–970.

Imokawa, G., Kobayasi, T., and Miyagishi, M. (2000). Intracellular signaling mechanisms leading to synergistic effects of endothelin-1 and stem cell factor on proliferation of cultured human melanocytes. Cross-talk via trans-activation of the tyrosine kinase c-kit receptor. The Journal of Biological Chemistry *275*, 33321–33328.

Imokawa, G., Miyagishi, M., and Yada, Y. (1995). Endothelin-1 as a new melanogen: coordinated expression of its gene and the tyrosinase gene in UVB-exposed human epidermis. J Invest Dermatol *105*, 32–37.

Imokawa, G., Yada, Y., and Miyagishi, M. (1992). Endothelins secreted from human keratinocytes are intrinsic mitogens for human melanocytes. The Journal of Biological Chemistry *267*, 24675–24680.

Inomata, K., Aoto, T., Binh, N.T., Okamoto, N., Tanimura, S., Wakayama, T., Iseki, S., Hara, E., Masunaga, T., and Shimizu, H. (2009). Genotoxic Stress Abrogates Renewal of Melanocyte Stem Cells by Triggering Their Differentiation. Cell *137*, 1088–1099.

Inoue-Narita, T., Hamada, K., Sasaki, T., Hatakeyama, S., Fujita, S., Kawahara, K., Sasaki, M., Kishimoto, H., Eguchi, S., Kojima, I., et al. (2008). Pten deficiency in

melanocytes results in resistance to hair graying and susceptibility to carcinogen-induced melanomagenesis. Cancer Research *68*, 5760–5768.

Ito, M., Liu, Y., Yang, Z., Nguyen, J., Liang, F., Morris, R.J., and Cotsarelis, G. (2005). Stem cells in the hair follicle bulge contribute to wound repair but not to homeostasis of the epidermis. Nat Med *11*, 1351–1354.

Jaks, V., Barker, N., Kasper, M., Van Es, J.H., Snippert, H.J., Clevers, H., and Toftgård, R. (2008). Lgr5 marks cycling, yet long-lived, hair follicle stem cells. Nature Genetics *40*, 1291–1299.

Jamora, C., DasGupta, R., Kocieniewski, P., and Fuchs, E. (2003). Links between signal transduction, transcription and adhesion in epithelial bud development. Nature *422*, 317–322.

Jones, K.A., Kadonaga, J.T., Rosenfeld, P.J., Kelly, T.J., and Tjian, R. (1987). A cellular DNA-binding protein that activates eukaryotic transcription and DNA replication. Cell *48*, 79–89.

Kamada, S., Shimono, A., Shinto, Y., Tsujimura, T., Takahashi, T., Noda, T., Kitamura, Y., Kondoh, H., and Tsujimoto, Y. (1995). bcl-2 deficiency in mice leads to pleiotropic abnormalities: accelerated lymphoid cell death in thymus and spleen, polycystic kidney, hair hypopigmentation, and distorted small intestine. Cancer Research *55*, 354–359.

Kissel, H., Timokhina, I., Hardy, M.P., Rothschild, G., Tajima, Y., Soares, V., Angeles, M., Whitlow, S.R., Manova, K., and Besmer, P. (2000). Point mutation in kit receptor tyrosine kinase reveals essential roles for kit signaling in spermatogenesis and oogenesis without affecting other kit responses. EMBO J *19*, 1312–1326.

Klipper, E., Levit, A., Mastich, Y., Berisha, B., Schams, D., and Meidan, R. (2010). Induction of endothelin-2 expression by luteinizing hormone and hypoxia: possible role in bovine corpus luteum formation. Endocrinology *151*, 1914–1922.

Knecht, A.K., and Bronner-Fraser, M. (2002). Induction of the neural crest: a multigene process. Nat. Rev. Genet. *3*, 453–461.

Kobielak, K., Pasolli, H.A., Alonso, L., Polak, L., and Fuchs, E. (2003). Defining BMP functions in the hair follicle by conditional ablation of BMP receptor IA. The Journal of Cell Biology *163*, 609–623.

Kobielak, K., Stokes, N., la Cruz, de, J., Polak, L., and Fuchs, E. (2007). Loss of a quiescent niche but not follicle stem cells in the absence of bone morphogenetic protein signaling. Proc Natl Acad Sci USA *104*, 10063–10068.

Kopan, R., and Weintraub, H. (1993). Mouse notch: expression in hair follicles correlates with cell fate determination. The Journal of Cell Biology *121*, 631–641.

Kos, R., Reedy, M.V., Johnson, R.L., and Erickson, C.A. (2001). The winged-helix

transcription factor FoxD3 is important for establishing the neural crest lineage and repressing melanogenesis in avian embryos. Development *128*, 1467–1479.

Kruse, U., and Sippel, A.E. (1994). Transcription factor nuclear factor I proteins form stable homo- and heterodimers. FEBS Letters *348*, 46–50.

Kulessa, H., Turk, G., and Hogan, B.L. (2000). Inhibition of Bmp signaling affects growth and differentiation in the anagen hair follicle. Embo J *19*, 6664–6674.

Kunisada, T., Yamazaki, H., Hirobe, T., Kamei, S., Omoteno, M., Tagaya, H., Hemmi, H., Koshimizu, U., Nakamura, T., and Hayashi, S.I. (2000). Keratinocyte expression of transgenic hepatocyte growth factor affects melanocyte development, leading to dermal melanocytosis. Mechanisms of Development *94*, 67–78.

Kunisada, T., Lu, S.-Z., Yoshida, H., Nishikawa, S., Nishikawa, S.-I., Mizoguchi, M., Hayashi, S.-I., Tyrrell, L., Williams, D.A., Wang, X., et al. (1998a). Murine cutaneous mastocytosis and epidermal melanocytosis induced by keratinocyte expression of transgenic stem cell factor. J. Exp. Med. 1–9.

Kunisada, T., Yoshida, H., Yamazaki, H., Miyamoto, A., Hemmi, H., Nishimura, E., Shultz, L.D., and Hayashi, S.-I.N.S.-I. (1998b). Transgene expression of steel factor in the basal layer of epidermis promotes survival, proliferation, differentiation and migration of melanocyte precursors. Development 1–9.

Kurihara, Y., Kurihara, H., Suzuki, H., Kodama, T., Maemura, K., Nagai, R., Oda, H., Kuwaki, T., Cao, W.H., and Kamada, N. (1994). Elevated blood pressure and craniofacial abnormalities in mice deficient in endothelin-1. Nature *368*, 703–710.

LaBonne, C., and Bronner-Fraser, M. (1998). Neural crest induction in Xenopus: evidence for a two-signal model. Development *125*, 2403–2414.

Lahav, R., Ziller, C., Dupin, E., and Le Douarin, N.M. (1996). Endothelin 3 promotes neural crest cell proliferation and mediates a vast increase in melanocyte number in culture. Proc Natl Acad Sci USA *93*, 3892–3897.

Langmead, B., Trapnell, C., Pop, M., and Salzberg, S.L. (2009). Ultrafast and memory-efficient alignment of short DNA sequences to the human genome. Genome Biol *10*, R25.

Lechler, T., and Fuchs, E. (2005). Asymmetric cell divisions promote stratification and differentiation of mammalian skin. Nature *437*, 275–280.

Lee, H.-Y., Kléber, M., Hari, L., Brault, V., Suter, U., Taketo, M.M., Kemler, R., and Sommer, L. (2004). Instructive role of Wnt/beta-catenin in sensory fate specification in neural crest stem cells. Science *303*, 1020–1023.

Lee, H.-O., Levorse, J.M., and Shin, M.K. (2003). The endothelin receptor-B is required for the migration of neural crest-derived melanocyte and enteric neuron precursors. Dev.

Biol. *259*, 162–175.

Lee, M., Goodall, J., Verastegui, C., Ballotti, R., and Goding, C.R. (2000). Direct regulation of the Microphthalmia promoter by Sox10 links Waardenburg-Shah syndrome (WS4)-associated hypopigmentation and deafness to WS2. The Journal of Biological Chemistry *275*, 37978–37983.

Leegwater, P.A., van Driel, W., and van der Vliet, P.C. (1985). Recognition site of nuclear factor I, a sequence-specific DNA-binding protein from HeLa cells that stimulates adenovirus DNA replication. Embo J *4*, 1515–1521.

Leishman, E., Howard, J.M., Garcia, G.E., Miao, Q., Ku, A.T., Dekker, J.D., Tucker, H., and Nguyen, H. (2013). Foxp1 maintains hair follicle stem cell quiescence through regulation of Fgf18. Development *140*, 3809–3818.

Levy, C., Khaled, M., and Fisher, D.E. (2006). MITF: master regulator of melanocyte development and melanoma oncogene. Trends Mol Med *12*, 406–414.

Li, L., Rutlin, M., Abraira, V.E., Cassidy, C., Kus, L., Gong, S., Jankowski, M.P., Luo, W., Heintz, N., Koerber, H.R., et al. (2011). The functional organization of cutaneous low-threshold mechanosensory neurons. Cell *147*, 1615–1627.

Lien, W.-H., Guo, X., Polak, L., Lawton, L.N., Young, R.A., Zheng, D., and Fuchs, E. (2011). Genome-wide maps of histone modifications unwind in vivo chromatin states of the hair follicle lineage. Cell Stem Cell *9*, 219–232.

Loercher, A.E., Tank, E.M.H., Delston, R.B., and Harbour, J.W. (2005). MITF links differentiation with cell cycle arrest in melanocytes by transcriptional activation of INK4A. The Journal of Cell Biology *168*, 35–40.

Logan, C.Y., and Nusse, R. (2004). The Wnt signaling pathway in development and disease. Annu. Rev. Cell. Dev. Biol. *20*, 781–810.

Lowings, P., Yavuzer, U., and Goding, C.R. (1992). Positive and negative elements regulate a melanocyte-specific promoter. Molecular and Cellular Biology *12*, 3653–3662.

Lowry, W.E., Blanpain, C., Nowak, J.A., Guasch, G., Lewis, L., and Fuchs, E. (2005). Defining the impact of beta-catenin/Tcf transactivation on epithelial stem cells. Genes & Development *19*, 1596–1611.

Mackenzie, M.A., Jordan, S.A., Budd, P.S., and Jackson, I.J. (1997). Activation of the receptor tyrosine kinase Kit is required for the proliferation of melanoblasts in the mouse embryo. Dev. Biol. *192*, 99–107.

Mak, S.-S., Moriyama, M., Nishioka, E., OSAWA, M., and NISHIKAWA, S.-I. (2006). Indispensable role of Bcl2 in the development of the melanocyte stem cell. Dev. Biol. *291*, 144–153.

Martynoga, B., Mateo, J.L., Zhou, B., Andersen, J., Achimastou, A., Urbán, N., van den Berg, D., Georgopoulou, D., Hadjur, S., Wittbrodt, J., et al. (2013). Epigenomic enhancer annotation reveals a key role for NFIX in neural stem cell quiescence. Genes & Development *27*, 1769–1786.

Mayor, R., Guerrero, N., and Martínez, C. (1997). Role of FGF and noggin in neural crest induction. Dev. Biol. *189*, 1–12.

McDade, S.S., Henry, A.E., Pivato, G.P., Kozarewa, I., Mitsopoulos, C., Fenwick, K., Assiotis, I., Hakas, J., Zvelebil, M., Orr, N., et al. (2012). Genome-wide analysis of p63 binding sites identifies AP-2 factors as co-regulators of epidermal differentiation. Nucleic Acids Res *40*, 7190–7206.

McGill, G.G., Haq, R., Nishimura, E.K., and Fisher, D.E. (2006). c-Met expression is regulated by Mitf in the melanocyte lineage. The Journal of Biological Chemistry *281*, 10365–10373.

McGill, G.G., Horstmann, M., Widlund, H.R., Du, J., Motyckova, G., Nishimura, E.K., Lin, Y.-L., Ramaswamy, S., Avery, W., Ding, H.-F., et al. (2002). Bcl2 regulation by the melanocyte master regulator Mitf modulates lineage survival and melanoma cell viability. Cell *109*, 707–718.

Meisterernst, M., Gander, I., Rogge, L., and Winnacker, E.L. (1988). A quantitative analysis of nuclear factor I/DNA interactions. Nucleic Acids Res *16*, 4419–4435.

Meisterernst, M., Rogge, L., Foeckler, R., Karaghiosoff, M., and Winnacker, E.L. (1989). Structural and functional organization of a porcine gene coding for nuclear factor I. Biochemistry *28*, 8191–8200.

Mermod, N., ONeill, E.A., Kelly, T.J., and Tjian, R. (1989). The proline-rich transcriptional activator of CTF/NF-I is distinct from the replication and DNA binding domain. Cell *58*, 741–753.

Messina, G., Biressi, S., Monteverde, S., Magli, A., Cassano, M., Perani, L., Roncaglia, E., Tagliafico, E., Starnes, L., Campbell, C.E., et al. (2010). Nfix Regulates Fetal-Specific Transcription in Developing Skeletal Muscle. Cell *140*, 554–566.

Meulemans, D., and Bronner-Fraser, M. (2004). Gene-Regulatory Interactions Review in Neural Crest Evolution and Development. Developmental Cell 1–9.

Milner, Y., Sudnik, J., Filippi, M., Kizoulis, M., Kashgarian, M., and Stenn, K. (2002). Exogen, shedding phase of the hair growth cycle: characterization of a mouse model. J Invest Dermatol *119*, 639–644.

Monsoro-Burq, A.-H., Fletcher, R.B., and Harland, R.M. (2003). Neural crest induction by paraxial mesoderm in Xenopus embryos requires FGF signals. Development *130*, 3111–3124.

Moore, K.J. (1995). Insight into the microphthalmia gene. Trends Genet. *11*, 442–448.

Moriyama, M., Osawa, M., Mak, S.-S., Ohtsuka, T., Yamamoto, N., Han, H., Delmas, V., Kageyama, R., Beermann, F., Larue, L., et al. (2006). Notch signaling via Hes1 transcription factor maintains survival of melanoblasts and melanocyte stem cells. The Journal of Cell Biology *173*, 333–339.

Morris, R.J., Liu, Y., Marles, L., Yang, Z., Trempus, C., Li, S., Lin, J.S., Sawicki, J.A., and Cotsarelis, G. (2004). Capturing and profiling adult hair follicle stem cells. Nat Biotechnol *22*, 411–417.

Müller-Röver, S., Handjiski, B., Van Der Veen, C., Eichmüller, S., Foitzik, K., McKay, I.A., STENN, K.S., and Paus, R. (2001). A comprehensive guide for the accurate classification of murine hair follicles in distinct hair cycle stages. J Invest Dermatol *117*, 3–15.

Nagata, K., Guggenheimer, R.A., Enomoto, T., Lichy, J.H., and Hurwitz, J. (1982). Adenovirus DNA replication in vitro: identification of a host factor that stimulates synthesis of the preterminal protein-dCMP complex. Proc Natl Acad Sci USA *79*, 6438–6442.

Nakayama, A., Nguyen, M.T., Chen, C.-C., Opdecamp, K., Hodgkinson, C.A., and Arnheiter, H. (1998). Mutations in microphthalmia, the mouse homolog of the human deafness gene MITF, affect neuroepithelial and neural crest-derived melanocytes differently. Mechanisms of Development *70*, 155–166.

Neves, das, L., Duchala, C.S., Tolentino-Silva, F., Haxhiu, M.A., Colmenares, C., Macklin, W.B., Campbell, C.E., Butz, K.G., Gronostajski, R.M., and Godinho, F. (1999). Disruption of the murine nuclear factor I-A gene (Nfia) results in perinatal lethality, hydrocephalus, and agenesis of the corpus callosum. Proc Natl Acad Sci USA *96*, 11946–11951.

Nieto, M.A., Sargent, M.G., Wilkinson, D.G., and Cooke, J. (1994). Control of cell behavior during vertebrate development by Slug, a zinc finger gene. Science *264*, 835–839.

Nishikawa, S., Kusakabe, M., Yoshinaga, K., Ogawa, M., Hayashi, S., Kunisada, T., Era, T., Sakakura, T., and Nishikawa, S. (1991). In utero manipulation of coat color formation by a monoclonal anti-c-kit antibody: two distinct waves of c-kit-dependency during melanocyte development. Embo J *10*, 2111–2118.

Nishimura, E.K. (2005). Mechanisms of Hair Graying: Incomplete Melanocyte Stem Cell Maintenance in the Niche. Science *307*, 720–724.

Nishimura, E.K., Jordan, S.A., Oshima, H., Yoshida, H., OSAWA, M., Moriyama, M., Jackson, I.J., Barrandon, Y., Miyachi, Y., and NISHIKAWA, S.-I. (2002). Dominant role of the niche in melanocyte stem-cell fate determination. Nature *416*, 854–860.

Nishimura, E.K., Suzuki, M., Igras, V., Du, J., Lonning, S., Miyachi, Y., Roes, J., Beermann, F., and Fisher, D.E. (2010). Key roles for transforming growth factor beta in melanocyte stem cell maintenance. Cell Stem Cell *6*, 130–140.

Nowak, J.A., Polak, L., Pasolli, H.A., and Fuchs, E. (2008). Hair Follicle Stem Cells Are Specified and Function in Early Skin Morphogenesis. Cell Stem Cell *3*, 33–43.

Nowock, J., Borgmeyer, U., Püschel, A.W., Rupp, R.A., and Sippel, A.E. (1985). The TGGCA protein binds to the MMTV-LTR, the adenovirus origin of replication, and the BK virus enhancer. Nucleic Acids Res *13*, 2045–2061.

Opdecamp, K., Kos, L., Arnheiter, H., and Pavan, W.J. (1998). Endothelin signalling in the development of neural crest-derived melanocytes. Biochem. Cell Biol. *76*, 1093–1099.

Opdecamp, K., Nakayama, A., Nguyen, M.T., Hodgkinson, C.A., Pavan, W.J., and Arnheiter, H. (1997). Melanocyte development in vivo and in neural crest cell cultures: crucial dependence on the Mitf basic-helix-loop-helix-zipper transcription factor. Development *124*, 2377–2386.

Orford, K.W., and Scadden, D.T. (2008). Deconstructing stem cell self-renewal: genetic insights into cell-cycle regulation. Nat. Rev. Genet. *9*, 115–128.

Ortonne, J.-P., MacDonald, D.M., Micoud, A., and Thivolet, J. (1979). PUVA-induced repigmentation of vitiligo: a histochemical (split-DOPA) and ultrastructural study. Br. J. Dermatol. *101*, 1–12.

Oshima, H., Rochat, A., Kedzia, C.C., Kobayashi, K., and Barrandon, Y. (2001). Morphogenesis and renewal of hair follicles from adult multipotent stem cells. Cell *104*, 233–245.

Oshimori, N., and Fuchs, E. (2012). Paracrine TGF-β signaling counterbalances BMP-mediated repression in hair follicle stem cell activation. Cell Stem Cell *10*, 63–75.

Panteleyev, A.A., Jahoda, C.A., and Christiano, A.M. (2001). Hair follicle predetermination. Journal of Cell Science *114*, 3419–3431.

Paus, R., Müller-Röver, S., Van Der Veen, C., Maurer, M., Eichmüller, S., Ling, G., Hofmann, U., Foitzik, K., Mecklenburg, L., and Handjiski, B. (1999). A comprehensive guide for the recognition and classification of distinct stages of hair follicle morphogenesis. J Invest Dermatol *113*, 523–532.

Pavan, W.J., and Tilghman, S.M. (1994). Piebald lethal (sl) acts early to disrupt the development of neural crest-derived melanocytes. Proc Natl Acad Sci USA *91*, 7159–7163.

Pingault, V., Bondurand, N., Kuhlbrodt, K., Goerich, D.E., Préhu, M.O., Puliti, A., Herbarth, B., Hermans-Borgmeyer, I., Legius, E., Matthijs, G., et al. (1998). SOX10

mutations in patients with Waardenburg-Hirschsprung disease. Nature Genetics *18*, 171–173.

Pjanic, M., Pjanic, P., Schmid, C., Ambrosini, G., Gaussin, A., Plasari, G., Mazza, C., Bucher, P., and Mermod, N. (2011). Nuclear factor I revealed as family of promoter binding transcription activators. BMC Genomics *12*, 181.

Pla, P., and Larue, L. (2003). Involvement of endothelin receptors in normal and pathological development of neural crest cells. Int. J. Dev. Biol. *47*, 315–325.

Plasari, G., Edelmann, S., Högger, F., Dusserre, Y., Mermod, N., and Calabrese, A. (2010). Nuclear factor I-C regulates TGF-{beta}-dependent hair follicle cycling. Journal of Biological Chemistry *285*, 34115–34125.

Plikus, M.V., Mayer, J.A., La Cruz, De, D., Baker, R.E., Maini, P.K., Maxson, R., and Chuong, C.-M. (2008). Cyclic dermal BMP signalling regulates stem cell activation during hair regeneration. Nature *451*, 340–344.

Potterf, S.B., Furumura, M., Dunn, K.J., Arnheiter, H., and Pavan, W.J. (2000). Transcription factor hierarchy in Waardenburg syndrome: regulation of MITF expression by SOX10 and PAX3. Hum. Genet. *107*, 1–6.

Price, E.R., and Fisher, D.E. (2001). Sensorineural deafness and pigmentation genes: melanocytes and the Mitf transcriptional network. Neuron *30*, 15–18.

Price, E.R., Ding, H.F., Badalian, T., Bhattacharya, S., Takemoto, C., Yao, T.P., Hemesath, T.J., and Fisher, D.E. (1998a). Lineage-specific signaling in melanocytes. C-kit stimulation recruits p300/CBP to microphthalmia. The Journal of Biological Chemistry *273*, 17983–17986.

Price, E.R., Horstmann, M.A., Wells, A.G., Weilbaecher, K.N., Takemoto, C.M., Landis, M.W., and Fisher, D.E. (1998b). alpha-Melanocyte-stimulating hormone signaling regulates expression of microphthalmia, a gene deficient in Waardenburg syndrome. The Journal of Biological Chemistry *273*, 33042–33047.

Puffenberger, E.G., Hosoda, K., Washington, S.S., Nakao, K., deWit, D., Yanagisawa, M., and Chakravart, A. (1994). A missense mutation of the endothelin-B receptor gene in multigenic Hirschsprung's disease. Cell *79*, 1257–1266.

Rabbani, P., Takeo, M., Chou, W., Myung, P., Bosenberg, M., Chin, L., Taketo, M.M., and Ito, M. (2011). Coordinated Activation of Wnt in Epithelial and Melanocyte Stem Cells Initiates Pigmented Hair Regeneration. Cell *145*, 941–955.

Raposo, G., and Marks, M.S. (2007). Melanosomes — dark organelles enlighten endosomal membrane transport. Nat Rev Mol Cell Biol *8*, 786–797.

Rawles, M.E. (1947). Origin of pigment cells from the neural crest in the mouse embryo. Physiological Zoology *20*, 248–266.

Reid, K., Nishikawa, S., Bartlett, P.F., and Murphy, M. (1995). Steel factor directs melanocyte development in vitro through selective regulation of the number of c-kit+ progenitors. Dev. Biol. *169*, 568–579.

Reid, K., Turnley, A.M., Maxwell, G.D., Kurihara, Y., Kurihara, H., Bartlett, P.F., and Murphy, M. (1996a). Multiple roles for endothelin in melanocyte development: regulation of progenitor number and stimulation of differentiation. Development *122*, 3911–3919.

Reid, K., Turnley, A.M., Maxwell, G.D., Kurihara, Y., Kurihara, H., and Murphy, P.F.B.M. (1996b). Multiple roles for endothelin in melanocyte development: regulation of

progenitor number and stimulation of differentiatio. Development 1–9.

Rendl, M., Lewis, L., and Fuchs, E. (2005). Molecular dissection of mesenchymal-epithelial interactions in the hair follicle. Plos Biol *3*, e331.

Rhee, H., Polak, L., and Fuchs, E. (2006). Lhx2 maintains stem cell character in hair follicles. Science *312*, 1946–1949.

Robbins, L.S., Nadeau, J.H., Johnson, K.R., Kelly, M.A., Roselli-Rehfuss, L., Baack, E., Mountjoy, K.G., and Cone, R.D. (1993). Pigmentation phenotypes of variant extension locus alleles result from point mutations that alter MSH receptor function. Cell *72*, 827–834.

Rock, J.R., Onaitis, M.W., Rawlins, E.L., Lu, Y., Clark, C.P., Xue, Y., Randell, S.H., and Hogan, B.L.M. (2009). Basal cells as stem cells of the mouse trachea and human airway epithelium. Proceedings of the National Academy of Sciences *106*, 12771–12775.

Rodeck, U., Bossler, A., Graeven, U., Fox, F.E., Nowell, P.C., Knabbe, C., and Kari, C. (1994). Transforming growth factor beta production and responsiveness in normal human melanocytes and melanoma cells. Cancer Research *54*, 575–581.

Rompolas, P., Mesa, K.R., and Greco, V. (2013). Spatial organization within a niche as a determinant of stem-cell fate. Nature 1–16.

Roulet, E., Bucher, P., Schneider, R., Wingender, E., Dusserre, Y., Werner, T., and Mermod, N. (2000). Experimental analysis and computer prediction of CTF/NFI transcription factor DNA binding sites. Journal of Molecular Biology *297*, 833–848.

Russell, E.S. (1979). Hereditary anemias of the mouse: a review for geneticists. Adv. Genet. *20*, 357–459.

Sakurai, T., Yanagisawa, M., and Masaki, T. (1992). Molecular characterization of endothelin receptors. Trends Pharmacol. Sci. *13*, 103–108.

Sasai, N., Mizuseki, K., and Sasai, Y. (2001). Requirement of FoxD3-class signaling for

neural crest determination in Xenopus. Development *128*, 2525–2536.

Sato-Jin, K., Nishimura, E.K., Akasaka, E., Huber, W., Nakano, H., Miller, A., Du, J., Wu, M., Hanada, K., Sawamura, D., et al. (2008). Epistatic connections between microphthalmia-associated transcription factor and endothelin signaling in Waardenburg syndrome and other pigmentary disorders. The FASEB Journal *22*, 1155–1168.

Schlake, T. (2007). Determination of hair structure and shape. Seminars in Cell and Developmental Biology *18*, 267–273.

Schmidt-Ullrich, R., and Paus, R. (2005). Molecular principles of hair follicle induction and morphogenesis. Bioessays *27*, 247–261.

Schouwey, K., Delmas, V., Larue, L., Zimber-Strobl, U., Strobl, L.J., Radtke, F., and Beermann, F. (2006). Notch1 and Notch2 receptors influence progressive hair graying in a dose-dependent manner. Dev Dyn *236*, 282–289.

Serbedzija, G.N., Fraser, S.E., and Bronner-Fraser, M. (1990). Pathways of trunk neural crest cell migration in the mouse embryo as revealed by vital dye labelling. Development *108*, 605–612.

Sharov, A., Tobin, D.J., Sharova, T.Y., Atoyan, R., and Botchkarev, V.A. (2005). Changes in different melanocyte populations during hair follicle involution (catagen). J Invest Dermatol *125*, 1259–1267.

Shen, C.N., Slack, J.M., and Tosh, D. (2000). Molecular basis of transdifferentiation of pancreas to liver. Nat Cell Biol *2*, 879–887.

Shi, Y., Wang, Y.F., Jayaraman, L., Yang, H., Massagué, J., and Pavletich, N.P. (1998). Crystal structure of a Smad MH1 domain bound to DNA: insights on DNA binding in TGF-beta signaling. Cell *94*, 585–594.

Shi, Y., and Massagué, J. (2003). Mechanisms of TGF-beta signaling from cell membrane to the nucleus. Cell *113*, 685–700.

Shin, M.K., Levorse, J.M., Ingram, R.S., and Tilghman, S.M. (1999). The temporal requirement for endothelin receptor-B signalling during neural crest development. Nature *402*, 496–501.

Siegel, P.M., and Massagué, J. (2003). Cytostatic and apoptotic actions of TGF-beta in homeostasis and cancer. Nat. Rev. Cancer *3*, 807–821.

Soeda, T., Deng, J.M., de Crombrugghe, B., Behringer, R.R., Nakamura, T., and Akiyama, H. (2010). Sox9-expressing precursors are the cellular origin of the cruciate ligament of the knee joint and the limb tendons. Genesis *48*, 635–644.

Sotiropoulou, P.A., Candi, A., and Blanpain, C. (2008). The Majority of Multipotent Epidermal Stem Cells Do Not Protect Their Genome by Asymmetrical Chromosome

Segregation. Stem Cells *26*, 2964–2973.

Southard-Smith, E.M., Kos, L., and Pavan, W.J. (1998). Sox10 mutation disrupts neural crest development in Dom Hirschsprung mouse model. Nature Genetics *18*, 60–64.

Spokony, R.F., Aoki, Y., Saint-Germain, N., Magner-Fink, E., and Saint-Jeannet, J.-P. (2002). The transcription factor Sox9 is required for cranial neural crest development in Xenopus. Development *129*, 421–432.

Srinivas, S., Watanabe, T., Lin, C.S., William, C.M., Tanabe, Y., Jessell, T.M., and Costantini, F. (2001). Cre reporter strains produced by targeted insertion of EYFP and ECFP into the ROSA26 locus. BMC Dev Biol *1*, 4.

Steel, K.P., Davidson, D.R., and Jackson, I.J. (1992). TRP-2/DT, a new early melanoblast marker, shows that steel growth factor (c-kit ligand) is a survival factor. Development *115*, 1111–1119.

Steele-Perkins, G., Butz, K.G., LYONS, G.E., Zeichner-David, M., Kim, H.-J., Cho, M.-I., and Gronostajski, R.M. (2003). Essential role for NFI-C/CTF transcription-replication factor in tooth root development. Molecular and Cellular Biology *23*, 1075–1084.

Steele-Perkins, G., Plachez, C., Butz, K.G., Yang, G., Bachurski, C.J., Kinsman, S.L., Litwack, E.D., Richards, L.J., and Gronostajski, R.M. (2005). The transcription factor gene Nfib is essential for both lung maturation and brain development. Molecular and Cellular Biology *25*, 685–698.

Sternberg, J., and Kimber, S.J. (1986a). The relationship between emerging neural crest cells and basement membranes in the trunk of the mouse embryo: a TEM and immunocytochemical study. J Embryol Exp Morphol *98*, 251–268.

Sternberg, J., and Kimber, S.J. (1986b). Distribution of fibronectin, laminin and entactin in the environment of migrating neural crest cells in early mouse embryos. J Embryol Exp Morphol *91*, 267–282.

Tachibana, M., Takeda, K., Nobukuni, Y., Urabe, K., Long, J.E., Meyers, K.A., Aaronson, S.A., and Miki, T. (1996). Ectopic expression of MITF, a gene for Waardenburg syndrome type 2, converts fibroblasts to cells with melanocyte characteristics. Nature Genetics *14*, 50–54.

Takahashi, K., and Yamanaka, S. (2006). Induction of Pluripotent Stem Cells from Mouse Embryonic and Adult Fibroblast Cultures by Defined Factors. Cell *126*, 663–676.

Takeda, K., Yasumoto, K., Takada, R., Takada, S., Watanabe, K., Udono, T., Saito, H., Takahashi, K., and Shibahara, S. (2000). Induction of melanocyte-specific microphthalmia-associated transcription factor by Wnt-3a. The Journal of Biological Chemistry *275*, 14013–14016.

Tanimura, S., Tadokoro, Y., Inomata, K., Binh, N.T., Nishie, W., Yamazaki, S.,

Nakauchi, H., Tanaka, Y., Mcmillan, J.R., Sawamura, D., et al. (2011). Hair follicle stem cells provide a functional niche for melanocyte stem cells. Cell Stem Cell *8*, 177–187.

Tassabehji, M., Newton, V.E., and Read, A.P. (1994). Waardenburg syndrome type 2 caused by mutations in the human microphthalmia (MITF) gene. Nature Genetics *8*, 251–255.

Tassabehji, M., Read, A.P., Newton, V.E., Harris, R., Balling, R., Gruss, P., and Strachan, T. (1992). Waardenburg's syndrome patients have mutations in the human homologue of the Pax-3 paired box gene. Nature *355*, 635–636.

Tassabehji, M., Read, A.P., Newton, V.E., Patton, M., Gruss, P., Harris, R., and Strachan, T. (1993). Mutations in the PAX3 gene causing Waardenburg syndrome type 1 and type 2. Nature Genetics *3*, 26–30.

Taylor, G., Lehrer, M.S., Jensen, P.J., Sun, T.T., and Lavker, R.M. (2000a). Involvement of follicular stem cells in forming not only the follicle but also the epidermis. Cell *102*, 451–461.

Taylor, G., Lehrer, M.S., Jensen, P.J., Sun, T.-T., and Lavker, R.M. (2000b). Involvement of Follicular Stem Cells in FormingNot Only the Follicle but Also the Epidermis. Cell 1–11.

Thomas, A.J., and Erickson, C.A. (2009). FOXD3 regulates the lineage switch between neural crest-derived glial cells and pigment cells by repressing MITF through a non-canonical mechanism. Development *136*, 1849–1858.

Tobin, D.J., Slominski, A., Botchkarev, V., and Paus, R. (1999). The fate of hair follicle melanocytes during the hair growth cycle. J Investig Dermatol Symp Proc *4*, 323–332.

Trapnell, C., Pachter, L., and Salzberg, S.L. (2009). TopHat: discovering splice junctions with RNA-Seq. Bioinformatics *25*, 1105–1111.

Trapnell, C., Williams, B.A., Pertea, G., Mortazavi, A., Kwan, G., Baren, M.J.V., Salzberg, S.L., Wold, B.J., and Pachter, L. (2010). Transcript assembly and quantification by RNA-Seq reveals unannotated transcripts and isoform switching during cell differentiation. Nat Biotechnol *28*, 516–520.

Trempus, C.S., Morris, R.J., Bortner, C.D., Cotsarelis, G., Faircloth, R.S., Reece, J.M., and Tennant, R.W. (2003). Enrichment for living murine keratinocytes from the hair follicle bulge with the cell surface marker CD34. J Invest Dermatol *120*, 501–511.

Tumbar, T., Guasch, G., Greco, V., Blanpain, C., Lowry, W.E., Rendl, M., and Fuchs, E. (2004). Defining the epithelial stem cell niche in skin. Science *303*, 359–363.

Valluet, A., Druillennec, S., Barbotin, C., Dorard, C., Monsoro-Burq, A.H., Larcher, M., Pouponnot, C., Baccarini, M., Larue, L., and Eychène, A. (2012). B-Raf and C-Raf are required for melanocyte stem cell self-maintenance. CellReports *2*, 774–780.

Valverde, P., Healy, E., Jackson, I., Rees, J.L., and Thody, A.J. (1995). Variants of the melanocyte-stimulating hormone receptor gene are associated with red hair and fair skin in humans. Nature Genetics *11*, 328–330.

Van Mater, D., Kolligs, F.T., Dlugosz, A.A., and Fearon, E.R. (2003). Transient activation of beta -catenin signaling in cutaneous keratinocytes is sufficient to trigger the active growth phase of the hair cycle in mice. Genes & Development *17*, 1219–1224.

Vance, K.W., Carreira, S., Brosch, G., and Goding, C.R. (2005). Tbx2 is overexpressed and plays an important role in maintaining proliferation and suppression of senescence in melanomas. Cancer Research *65*, 2260–2268.

Vasioukhin, V., Degenstein, L., Wise, B., and Fuchs, E. (1999). The magical touch: genome targeting in epidermal stem cells induced by tamoxifen application to mouse skin. Proc Natl Acad Sci USA *96*, 8551–8556.

Verastegui, C., Bille, K., ORTONNE, J.-P., and Ballotti, R. (2000). Regulation of the microphthalmia-associated transcription factor gene by the Waardenburg syndrome type 4 gene, SOX10. The Journal of Biological Chemistry *275*, 30757–30760.

Vetrini, F., Auricchio, A., Du, J., Angeletti, B., Fisher, D.E., Ballabio, A., and Marigo, V. (2004). The microphthalmia transcription factor (Mitf) controls expression of the ocular albinism type 1 gene: link between melanin synthesis and melanosome biogenesis. Molecular and Cellular Biology *24*, 6550–6559.

Vidal, V.P.I., Chaboissier, M.-C., Lützkendorf, S., Cotsarelis, G., Mill, P., Hui, C.-C., Ortonne, N., Ortonne, J.-P., and Schedl, A. (2005). Sox9 is essential for outer root sheath differentiation and the formation of the hair stem cell compartment. Current Biology *15*, 1340–1351.

Waardenburg, P.J. (1951). A new syndrome combining developmental anomalies of the eyelids, eyebrows and nose root with pigmentary defects of the iris and head hair and with congenital deafness. Am. J. Hum. Genet. *3*, 195–253.

Waghmare, S.K., Bansal, R., Lee, J., Zhang, Y.V., Mcdermitt, D.J., and Tumbar, T. (2008). Quantitative proliferation dynamics and random chromosome segregation of hair follicle stem cells. Embo J *27*, 1309–1320.

Walker, G.J., Kimlin, M.G., Hacker, E., Ravishankar, S., Muller, H.K., Beermann, F., and Hayward, N.K. (2009). Murine neonatal melanocytes exhibit a heightened proliferative response to ultraviolet radiation and migrate to the epidermal basal layer. J Invest Dermatol *129*, 184–193.

Watanabe, A., Takeda, K., Ploplis, B., and Tachibana, M. (1998). Epistatic relationship between Waardenburg syndrome genes MITF and PAX3. Nature Genetics *18*, 283–286.

Wehrle-Haller, B., and Weston, J.A. (1995). Soluble and cell-bound forms of steel factor activity play distinct roles in melanocyte precursor dispersal and survival on the lateral

neural crest migration pathway. Development *121*, 731–742.

Weiner, L., Han, R., Scicchitano, B.M., Li, J., Hasegawa, K., Grossi, M., Lee, D., and Brissette, J.L. (2007). Dedicated Epithelial Recipient Cells

Determine Pigmentation Patterns. Cell *130*, 932–942.

Wilson, P.A., and Hemmati-Brivanlou, A. (1997). Vertebrate neural induction: inducers, inhibitors, and a new synthesis. Neuron *18*, 699–710.

Wu, M., Hemesath, T.J., Takemoto, C.M., Horstmann, M.A., Wells, A.G., Price, E.R., Fisher, D.Z., and Fisher, D.E. (2000). c-Kit triggers dual phosphorylations, which couple activation and degradation of the essential melanocyte factor Mi. Genes & Development *14*, 301–312.

Xiong, Y., Li, W., Shang, C., Chen, R.M., Han, P., Yang, J., Stankunas, K., Wu, B., Pan, M., Zhou, B., et al. (2013). Brg1 governs a positive feedback circuit in the hair follicle for tissue regeneration and repair. Developmental Cell *25*, 169–181.

Xu, W., Gong, L., Haddad, M.M., Bischof, O., Campisi, J., Yeh, E.T., and Medrano, E.E. (2000). Regulation of microphthalmia-associated transcription factor MITF protein levels by association with the ubiquitin-conjugating enzyme hUBC9. Experimental Cell Research *255*, 135–143.

Yada, Y., Higuchi, K., and Imokawa, G. (1991). Effects of endothelins on signal transduction and proliferation in human melanocytes. The Journal of Biological Chemistry *266*, 18352–18357.

Yamaguchi, Y., and Hearing, V.J. (2009). Physiological factors that regulate skin pigmentation. Biofactors *35*, 193–199.

Yamamura, K., Kamada, S., Ito, S., Nakagawa, K., Ichihashi, M., and Tsujimoto, Y. (1996). Accelerated disappearance of melanocytes in bcl-2-deficient mice. Cancer Research *56*, 3546–3550.

Yang, G., Li, Y., Nishimura, E.K., Xin, H., Zhou, A., Guo, Y., Dong, L., Denning, M.F., Nickoloff, B.J., and Cui, R. (2008). Inhibition of PAX3 by TGF-beta modulates melanocyte viability. Molecular Cell *32*, 554–563.

Yoshida, H., Kunisada, T., Kusakabe, M., Nishikawa, S., and Nishikawa, S.-I. (1996). Distinct stages of melanocyte differentiation revealed by anlaysis of nonuniform pigmentation patterns. Development *122*, 1207–1214.

Zaidi, M.R., Davis, S., Noonan, F.P., Graff-Cherry, C., Hawley, T.S., Walker, R.L., Feigenbaum, L., Fuchs, E., Lyakh, L., Young, H.A., et al. (2011). Interferon-γ links ultraviolet radiation to melanomagenesis in mice. Nature *469*, 548–553.

Zhang, J., He, X.C., Tong, W.-G., Johnson, T., Wiedemann, L.M., Mishina, Y., Feng,

J.Q., and Li, L. (2006). Bone morphogenetic protein signaling inhibits hair follicle anagen induction by restricting epithelial stem/progenitor cell activation and expansion. Stem Cells *24*, 2826–2839.

Zhang, Y.V., Cheong, J., Ciapurin, N., Mcdermitt, D.J., and Tumbar, T. (2009). Distinct Self-Renewal and Differentiation Phases in the Niche of Infrequently Dividing Hair Follicle Stem Cells. Cell Stem Cell *5*, 267–278.